



2

**SYNTHESIS AND STRUCTURAL CHARACTERIZATION OF
NEW HIGH-VALENT INORGANIC FLUORINE COMPOUNDS
AND THEIR OXIDIZING PROPERTIES:**

VOLUME 2.

Prof. G.J. Schrobilgen

**Mc Master University
Department of Chemistry
Hamilton, Ontario L8S 4M1
Canada**

February 1992

Final Report



APPROVED FOR PUBLIC RELEASE; DISTRIBUTION UNLIMITED.

92-15527



**PHILLIPS LABORATORY
Propulsion Directorate
AIR FORCE SYSTEMS COMMAND
EDWARDS AIR FORCE BASE CA 93523-5000**

NOTICE

When U.S. Government drawings, specifications, or other data are used for any purpose other than a definitely related Government procurement operation, the fact that the Government may have formulated, furnished, or in any way supplied the said drawings, specifications, or other data, is not to be regarded by implication or otherwise, or in any way licensing the holder or any other person or corporation, or conveying any rights or permission to manufacture, use or sell any patented invention that may be related thereto.

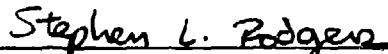
FOREWORD

This final report was prepared by McMaster University, Hamilton, Ontario, Canada under contract F49620-87-C-0049 for Operating Location AC, Phillips Laboratory (AFSC), Edwards AFB CA 93523-5000. OLAC PL Project Manager was 1Lt Robert A. mantz.

This report has been reviewed and is approved for release and distribution in accordance with the distribution statement on the cover and on the SF Form 298.

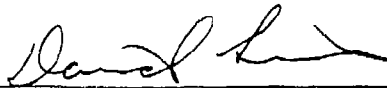


ROBERT A. MANTZ, 1Lt, USAF
Project Manager



STEPHEN L. RODGERS
Chief, Emerging Technologies Branch

FOR THE COMMANDER



DAVID W. LEWIS, Major, USAF
Acting Director,
Fundamental Technologies Division



RANNEY G. ADAMS
Public Affairs Director

REPORT DOCUMENTATION PAGE			Form Approved OMB No. 0704-0188	
Public reporting burden for this collection of information is estimated to average 1 hour per response, including the time for reviewing instructions, searching existing data sources, gathering and maintaining the data needed, and completing and reviewing the collection of information. Send comments regarding this burden estimate or any other aspect of this collection of information, including suggestions for reducing this burden, to Washington Headquarters Services, Directorate for Information Operations and Reports, 1215 Jefferson Davis Highway, Suite 1204, Arlington, VA 22202-4302, and to the Office of Management and Budget, Paperwork Reduction Project (0704-0188), Washington, DC 20503.				
1. AGENCY USE ONLY (Leave blank)		2. REPORT DATE February 1992	3. REPORT TYPE AND DATES COVERED Final-1 May 1987 to 30 April 1991	
4. TITLE AND SUBTITLE SYNTHESIS AND STRUCTURAL CHARACTERIZATION OF NEW HIGH-VALENT INORGANIC FLUORINE COMPOUNDS AND THEIR OXIDIZING PROPERTIES			5. FUNDING NUMBERS C - F49620-87-C-0049 PR- 5730 TA- 007G	
6. AUTHOR(S) G.J. Schrobilgen				
7. PERFORMING ORGANIZATION NAME(S) AND ADDRESS(ES) McMaster University Department of Chemistry Hamilton, Ontario L8S 4M1 Canada			8. PERFORMING ORGANIZATION REPORT NUMBER	
9. SPONSORING/MONITORING AGENCY NAME(S) AND ADDRESS(ES) Phillips Laboratory (AFSC) OLAC PL/RKFE Edwards AFB CA 93523-5000			10. SPONSORING/MONITORING AGENCY REPORT NUMBER PL-TR-91-3108 Volume 2	
11. SUPPLEMENTARY NOTES Phillips Laboratory, Edwards is the former Astronautics Laboratory. COSATI Code: 07/02				
12a. DISTRIBUTION/AVAILABILITY STATEMENT Approved for Public Release; Distribution is unlimited.			12b. DISTRIBUTION CODE	
13. ABSTRACT (Maximum 200 words) Noble gas fluorine oxidizers of Neon, Krypton, Argon, and Xenon have been synthesized and characterized. KrF^+ and XeF^+ cations have been made with neutral organic bases. Kr-N and Kr-O bonded molecules are also synthesized and characterized. The hypervalent compounds ClF_6^- and XeF_5^- are made. The anions IF_6O^- , TeF_6O^{2-} , TeF_7^- and TeF_8^{2-} anions are also made. Proof that the ClF_6^- anion exists is also presented. The photoelectron spectra of XeF_2 , XeF_4 , and XeF_6 are obtained using monochromatized synchrotron radiation. The synthesis and characterization of $Sb(OTeF_5)_6^- Et_4N^+$, and $Bi(OTeF_5)_6^- Et_4N^+$ salts is completed. Radiotracer experiments involving ^{18}F are also accomplished to show the inability to synthesize NF_5 is due to mainly steric reasons.				
14. SUBJECT TERMS fluorine, oxidizers, noble gas, NMR, photoelectron, HEDM.			15. NUMBER OF PAGES 130	
			16. PRICE CODE	
17. SECURITY CLASSIFICATION OF REPORT UNCLASSIFIED	18. SECURITY CLASSIFICATION OF THIS PAGE UNCLASSIFIED	19. SECURITY CLASSIFICATION OF ABSTRACT UNCLASSIFIED	20. LIMITATION OF ABSTRACT SAR	

PART II

SYNTHESES AND CHARACTERIZATION OF THE FIRST
KRYPTON-NITROGEN BONDS

Accession For	
NTIS CRA&I	<input checked="" type="checkbox"/>
DTIC TAB	<input type="checkbox"/>
Unannounced	<input type="checkbox"/>
Justification	
By	
Distribution /	
Availability Codes	
Dist	Avail & / or Special
A-1	



The Fluoro(hydrocyano)krypton(II) Cation $[\text{HC}\equiv\text{N}-\text{Kr}-\text{F}]^+$; the First Example of a Krypton-Nitrogen Bond

Gary J. Schrobilgen

Department of Chemistry, McMaster University, Hamilton, Ontario L8S 4M1, Canada

The first example of krypton bonded to an element other than fluorine has been provided by the synthesis of the novel $[\text{HC}\equiv\text{N}-\text{Kr}-\text{F}]^+$ cation, prepared as its AsF_6^- salt by low-temperature reaction of $\text{HC}\equiv\text{NH}^+\text{AsF}_6^-$ with KrF_2 in HF or BrF_3 as solvent, and characterized by low-temperature Raman spectroscopy and ^1H , ^{13}C , ^{15}N , and ^{19}F n.m.r. spectroscopy.

Numerous examples of xenon bonded to oxygen or fluorine and of xenon bonded to other highly electronegative inorganic ligands through oxygen are now known.¹ However, it is only within the last few years that the first examples of xenon bonded to an element other than fluorine or oxygen have been fully characterized. These are provided by the xenon-nitrogen bonded derivatives of the $-\text{N}(\text{SO}_2\text{F})_2^{2-6}$ and $-\text{N}(\text{SO}_2\text{CF}_3)_2^7$ groups, and two recent reports of the XeF^+ cation nitrogen-bonded to $\text{HC}\equiv\text{N}$ and organo-nitrogen ligands (nitriles and perfluoropyridines).^{8,9} Hitherto, no examples have been reported in which krypton is bonded to an element other than fluorine.

We have recently shown that XeF^+ forms relatively stable Lewis acid-base adduct cations with $\text{HC}\equiv\text{N}$,⁸ nitriles,⁸ and several perfluoropyridines⁹ which are resistant to oxidation by XeF^+ at low temperatures. On the basis of photoionization studies, $\text{HC}\equiv\text{N}$ is oxidatively the most resistant ligand among the pyridines and nitriles we have investigated thus far (first ionization potential 13.59 eV).¹⁰ In view of the estimated electron affinity of XeF^+ (10.9 eV) and our previous success in forming the xenon(II) cation $[\text{HC}\equiv\text{N}-\text{Xe}-\text{F}]^+$ as its AsF_6^- salt, the synthesis of the krypton(II) analogue was undertaken. The estimated electron affinity for KrF^+ (13.2 eV) suggested that $\text{HC}\equiv\text{N}$ might have at least a marginal resistance to oxidative attack by the KrF^+ cation and that $[\text{HC}\equiv\text{N}-\text{Kr}-\text{F}]^+$ might have sufficient thermal stability to permit its spectroscopic characterization.

Direct interaction of $\text{KrF}^+\text{AsF}_6^-$ with $\text{HC}\equiv\text{N}$ solutions in HF or BrF_3 solvent [as used for the xenon(II) analogue] was not attempted owing to the strongly oxidizing character of the KrF^+ cation towards $\text{HC}\equiv\text{N}$ and BrF_3 as well as its tendency to undergo autoredox reactions in both solvents. Instead, the interaction of less reactive KrF_2 with $\text{HC}\equiv\text{NH}^+\text{AsF}_6^-$ in HF was initially investigated. At -60°C reaction of sparingly soluble $\text{HC}\equiv\text{NH}^+\text{AsF}_6^-$ with KrF_2 in HF led to instantaneous

deposition of a white solid which, upon warming above -50°C , rapidly began to evolve Kr, NF_3 , and CF_4 gases. This was usually followed by a violent detonation and accompanying emission of white light. When these reactions were allowed to proceed at approximately -60°C , the mixtures could be periodically quenched to -196°C in order to study the development of the Raman spectrum of the product. Raman spectra were recorded for the solid under HF at -196°C with 541.5 nm excitation. ^{19}F n.m.r. spectra were obtained by briefly warming the samples to -60°C followed by rapid acquisition of the free induction decays with a high-field pulse instrument.

The Raman spectrum is consistent with the formation of the novel $[\text{HC}\equiv\text{N}-\text{Kr}-\text{F}]^+$ cation. In addition to strong lines arising from unreacted KrF_2 (465 and 122 cm^{-1}), an intense line at $560(100)\text{ cm}^{-1}$ attributable to a new Kr-F stretching mode was observed. The higher frequency of this line relative to that of the difluoride (465 cm^{-1}) is consistent with a more covalent Kr-F bond and parallels Xe-F stretching frequency increases observed for F-Xe-L compounds in general and those of the $\text{HC}\equiv\text{N}$ and nitrile cations in particular.⁸ Despite the lower mass of the krypton atom, the Kr-F stretching frequency of $[\text{HC}\equiv\text{N}-\text{Kr}-\text{F}]^+$ is only slightly lower than the factor-group-split Xe-F stretching frequency of the xenon analogue [559(100) and $569(94)\text{ cm}^{-1}$]⁸ and indicates that this Kr-F bond, like those of KrF_2 , KrF^+ , and Kr_2F_3^+ ,¹¹ is substantially weaker than in the xenon analogue. Two $\text{C}\equiv\text{N}$ stretching frequencies were observed, at $2116(8)$ and $2158(41)\text{ cm}^{-1}$. The former is assigned to unreacted $\text{HC}\equiv\text{NH}^+\text{AsF}_6^-$, by comparison with the Raman spectrum of the pure solid. The $\text{C}\equiv\text{N}$ stretch at $2158(41)\text{ cm}^{-1}$ is assigned to the $[\text{HC}\equiv\text{N}-\text{Kr}-\text{F}]^+$ cation and is similar to that of $[\text{HC}\equiv\text{N}-\text{Xe}-\text{F}]^+\text{AsF}_6^-$ (2161 cm^{-1}).⁸ Vibrational bands associated with $\nu(\text{Kr}-\text{N})$, $\nu(\text{H}-\text{C})$, and $\delta(\text{C}\equiv\text{N}-\text{Kr})$ are expected, by analogy with $[\text{HC}\equiv\text{N}-\text{Xe}-\text{F}]^+\text{AsF}_6^-$, to be weak and/or

Table 1. N.m.r. (^{19}F , ^{13}C , ^{15}N , and ^1H) parameters for the $[\text{HC}\equiv\text{N}-\text{Kr}-\text{F}]^+$ cation and related species.*

Species	$\delta(^{19}\text{F})/\text{p.p.m.}^{\text{b}}$	$\delta(^{13}\text{C})^{\text{b}}$	$\delta(^{15}\text{N})/\text{p.p.m.}^{\text{b}}$	$\delta(^1\text{H})/\text{p.p.m.}^{\text{b}}$	J/Hz^{c}
$[\text{HC}\equiv\text{N}-\text{Kr}-\text{F}]^+$	99.4 ^c (81.0)	98.5	-200.8	6.09 ^d	$^1J(^{13}\text{C}-^{15}\text{N})$ 312 $^2J(^{15}\text{N}-^{19}\text{F})$ 26 $^2J(^{15}\text{N}-^1\text{H})$ 12.2 $^3J(^{19}\text{F}-^{13}\text{C})$ 25.0 $^4J(^{19}\text{F}-^1\text{H})$ 4.2
KrF_2	63.9 (48.1)				
AsF_6^-	-62.6 (-69.1) ^f				
HF	-192.9 (-194.4)			6.71	$^1J(^1\text{H}-^{19}\text{F})$ 520(519)
BrF_3	134.7 ^g				$^2J(^{19}\text{F}-^{19}\text{F})$ 73
	271.9 ^h				

* Spectra were recorded in 4 mm (ext. diam.) FEP sample tubes at spectrometer frequencies (MHz): 235.36 (^{19}F), 50.70 (^{15}N), and 80.02 (^1H); BrF_3 solvent at -57°C ; values in parentheses are for spectra recorded with HF as solvent at -60°C . ^b Samples were referenced externally at 24°C with respect to the neat liquid references: CFCl_3 (^{19}F), MeNO_2 (^{15}N), and SiMe_4 (^{13}C , ^1H). A positive chemical shift denotes a resonance to high frequency of the reference. ^c Krypton isotopic shifts of 0.0138 p.p.m. p. a.m.u. were observed for this resonance, corresponding to fluorine directly bonded to ^{82}Kr , ^{84}Kr , and ^{86}Kr . ^d The corresponding resonance in $\text{HC}\equiv\text{NH}^+$ occurs at 5.20 p.p.m. in BrF_3 as solvent at -57°C . ^e Measured for samples containing 99.5% ^{15}N or 99.2% ^{13}C . ^f Linewidths at half-height were 1840 (HF) and 2190 Hz (BrF_3); the AsF_6^- resonance in BrF_3 exhibited the saddle-shaped structure of a partially quadrupole-collapsed 1:1:1:1 quartet arising from $^1J(^{75}\text{As}-^{19}\text{F})$. ^g Doublet. ^h Quintet.

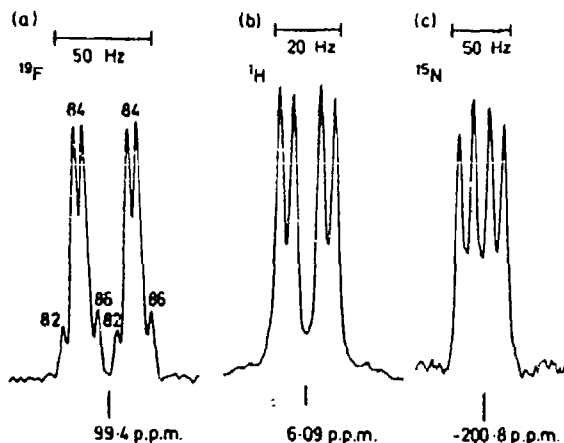


Figure 1. N.m.r. spectra of the $[\text{HC}\equiv\text{N}-\text{Kr}-\text{F}]^+$ cation enriched to 99.5% with ^{15}N , in BrF_3 as solvent at -57°C . (a) ^{19}F Spectrum (235.36 MHz) depicting $^2J(^{19}\text{F}-^{15}\text{N})$ and $^4J(^{19}\text{F}-^1\text{H})$ and krypton isotope shifts. Lines assigned to fluorine bonded to ^{82}Kr (11.56%), ^{84}Kr (56.90%), and ^{86}Kr (17.37%) are denoted by the krypton mass number. The innermost lines of the ^{82}Kr and ^{86}Kr doublets overlap their corresponding ^{84}Kr doublets. The isotopic shift arising from ^{82}Kr (11.53%) is not resolved; those of ^{78}Kr (0.35%) and ^{80}Kr (2.27%) are too weak to be observed. (b) ^1H Spectrum (80.02 MHz) depicting $^2J(^{15}\text{N}-^1\text{H})$ and $^4J(^{19}\text{F}-^1\text{H})$. (c) ^{15}N Spectrum (50.70 MHz) depicting $^2J(^{19}\text{F}-^{15}\text{N})$ and $^2J(^{15}\text{N}-^1\text{H})$.

broad and cannot yet be assigned with certainty. The doubly degenerate bending mode, $\delta(\text{F}-\text{Kr}-\text{N})$, is expected to be intense but is presumably obscured by the intense KrF_2 line at 122 cm^{-1} . Frequencies associated with the octahedral anion AsF_6^- were observed at 684 (36) [$\nu_1(a_{1g})$], 587 (16) [$\nu_2(e_g)$], and 370 (13) cm^{-1} [$\nu_3(t_{2g})$] (ν_2 and ν_3 overlap with the corresponding frequencies of unreacted $\text{HC}\equiv\text{NH}^+\text{AsF}_6^-$).

The interaction of $\text{HC}\equiv\text{NH}^+\text{AsF}_6^-$ and KrF_2 in BrF_3 led to a soluble product which was stable to at least -55°C in BrF_3 with only slight decomposition. The ^{19}F n.m.r. spectra of these solutions at -58°C and in HF at -60°C (Table 1) are consistent with equation (1). A new resonance in the

fluorine-on-krypton(II) region. [81.0 (HF) and 99.4 (BrF_3)] occurs to high frequency of unreacted KrF_2 [48.1 (HF) and 63.9 (BrF_3)] in both solvents. In BrF_3 this resonance is split into a doublet (4.2 Hz) attributable to the four-bond coupling $^4J(^{19}\text{F}-^1\text{H})$ [cf. $^4J(^{19}\text{F}-^1\text{H})$ 2.6 Hz for $[\text{HC}\equiv\text{N}-\text{Xe}-\text{F}]^+$ in HF solvent]. Like the terminal fluorine resonance of Kr_2F_3^+ [δ 73.6 p.p.m. (BrF_3)]¹¹ the fluorine-on-krypton resonance of $[\text{HC}\equiv\text{N}-\text{Kr}-\text{F}]^+$ lies to high frequency of the parent fluoride resonance. The chemical shift trend suggests that the Kr-N bond is more ionic than the Kr-F bridge bond of Kr_2F_3^+ . The ^1H spectrum recorded in BrF_3 solvent is also consistent with the formation of the $[\text{HC}\equiv\text{N}-\text{Kr}-\text{F}]^+$ cation. In addition to the doublet arising from HF in equation (1), a doublet (4.2 Hz) attributed to $^4J(^{19}\text{F}-^1\text{H})$ was observed at δ 6.09, to high frequency of the proton-on-carbon resonance of the $\text{HC}\equiv\text{NH}^+$ cation [δ 5.20 (BrF_3)].



The structure of the $[\text{HC}\equiv\text{N}-\text{Kr}-\text{F}]^+$ cation in solution has been confirmed by repetition of the reaction in BrF_3 with 99.5% ^{15}N -enriched $\text{HC}\equiv\text{NH}^+\text{AsF}_6^-$. The ^{19}F and ^1H resonances exhibit new doublet splittings attributed to ^{15}N coupling [Figure 1(a)]. The new splitting (26 Hz) of the ^{19}F resonance is attributed to the two-bond spin-spin coupling $^2J(^{19}\text{F}-^{15}\text{N})$ and is similar in magnitude to previously reported values for $\text{F}-\text{Xe}-\text{N}(\text{SO}_2\text{F})_2$ [$^2J(^{19}\text{F}-^{15}\text{N})$ 39.2 Hz] and $[\text{MeC}\equiv\text{N}-\text{Xe}-\text{F}]^+$ [$^2J(^{19}\text{F}-^{14}\text{N})$ 18 Hz; $^2J(^{19}\text{F}-^{15}\text{N})$ 25 Hz (calc.)]. Krypton isotopic shifts arising from ^{82}Kr (11.56%), ^{84}Kr (56.90%), and ^{86}Kr (17.37%) are well resolved on the ^{19}F resonance (0.0138 p.p.m. per a.m.u.). The value compared favourably with that measured for KrF_2 in BrF_3 solvent (0.0104 p.p.m. per a.m.u.)¹² and serves as an added confirmation that the fluorine resonance arises from fluorine directly bonded to krypton. The new doublet fine structure (12.2 Hz) on the ^1H resonance of the ^{15}N -enriched cation [Figure 1(b)] is attributed to $^2J(^{15}\text{N}-^1\text{H})$ [cf. $^2J(^{15}\text{N}-^1\text{H})$ 19.0 Hz for $\text{HC}\equiv\text{NH}^+$ in HF solvent]. The ^{15}N n.m.r. spectrum consists of a well resolved doublet of doublets [Figure 1(c)] arising from $^2J(^{19}\text{F}-^{15}\text{N})$ and $^2J(^{15}\text{N}-^1\text{H})$, which simplifies to a doublet (26 Hz) upon broad-band ^1H decoupling, confirming the aforementioned coupling constant assignments. A 99.2% ^{13}C

enriched sample resulted in additional doublet splittings in the ^1H and ^{13}C spectra arising from $^1J(^{13}\text{C}-^1\text{H})$ 312 Hz and $^3J(^{19}\text{F}-^{13}\text{C})$ 25.0 Hz.

It is noteworthy that the resonances of both solvents displayed well resolved spin-spin couplings (Table 1) indicating that fluorine exchange is slow under the stated conditions. This, coupled with the low concentration of NF_4^+ decomposition products in freshly prepared BrF_5 samples (<1%), has allowed reliable integrations of the ^1H and ^{19}F resonances. The following relative intensities were obtained and further support the cation structure and equation (1): ^{19}F , $[\text{HC}\equiv\text{N}-\text{Kr}-\text{F}]^+ : \text{HF} : \text{AsF}_6^-$ 1 : 1 : 6; ^1H , $[\text{HC}\equiv\text{N}-\text{Kr}-\text{F}]^+ : \text{HF}$ 1 : 1.

Solutions of $[\text{HC}\equiv\text{N}-\text{Kr}-\text{F}]^+ \text{AsF}_6^-$ in BrF_5 have withstood temperatures of -58 to -55°C for several hours with little sign of additional decomposition. Monitoring the ^{19}F spectra has shown that subsequent brief warmings of these solutions above -50°C lead to rapid formation of NF_4^+ [δ 218.9 p.p.m., $^1J(^{19}\text{F}-^{14}\text{N})$ 229 Hz, $^1J(^{19}\text{F}-^{15}\text{N})$ 320 Hz], CF_4 (-63.1 p.p.m.), and CF_3H (-79.3 p.p.m., $^2J(^{19}\text{F}-^1\text{H})$ 79 Hz] and exchange-broadening of both HF and AsF_6^- resonances arising from AsF_5 formation. The HF samples also displayed weak ^{19}F resonances attributable to NF_4^+ [δ 218.9 p.p.m., $^1J(^{19}\text{F}-^{14}\text{N})$ 229 Hz], NF_3 [142.9 p.p.m., $^1J(^{19}\text{F}-^{14}\text{N})$ 140 Hz], CF_3H [-81.5 p.p.m., $^2J(^{19}\text{F}-^1\text{H})$ 79 Hz], and CF_4 (-64.9 p.p.m.) as decomposition products.

Additional examples of inorganic and perfluoro-organic nitrogen bases are under investigation in this laboratory as potential electron-pair donors towards KrF^+ .

This research was sponsored by the United States Air Force Astronautics Laboratory, Edwards Air Force Base, California (Contract F49620-87-C-0049) and a Natural Sciences and Engineering Research Council of Canada operating grant.

Received, 1st March 1988; Com. 8100838H

References

- (a) N. Bartlett and F. O. Sladky, 'Comprehensive Inorganic Chemistry,' Pergamon, New York, 1973, vol. 1, ch. 6, pp. 213-330; (b) K. Seppelt and D. Lentz, *Progr. Inorg. Chem.*, 1982, 29, 167.
- D. D. DesMarteau, *J. Am. Chem. Soc.*, 1978, 100, 6270.
- D. D. DesMarteau, R. D. LeBlond, S. F. Hossain, and D. Nothe, *J. Am. Chem. Soc.*, 1981, 103, 7734.
- J. F. Sawyer, G. J. Schrobilgen, and S. J. Sutherland, *Inorg. Chem.*, 1982, 21, 4064.
- G. A. Schumacher and G. J. Schrobilgen, *Inorg. Chem.*, 1983, 22, 2178.
- R. Faggiani, D. K. Kennepohl, C. J. L. Lock, and G. J. Schrobilgen, *Inorg. Chem.*, 1986, 25, 563.
- J. Foropoulos, Jr., and D. D. DesMarteau, *J. Am. Chem. Soc.*, 1982, 104, 4260.
- A. A. A. Emara and G. J. Schrobilgen, *J. Chem. Soc., Chem. Commun.*, 1987, 1646.
- A. A. A. Emara and G. J. Schrobilgen, *J. Chem. Soc., Chem. Commun.*, 1988, 257.
- V. H. Dibeler and S. K. Liston, *J. Chem. Phys.*, 1968, 48, 4765.
- R. J. Gillespie and G. J. Schrobilgen, *Inorg. Chem.*, 1976, 15, 22.
- J. C. P. Sanders and G. J. Schrobilgen, unpublished work.

Best Available Copy

The Fluoro(perfluoroalkylnitrile)noble-gas(II) Cations, $R_F C \equiv N - NgF^+$ ($Ng = Kr$ or Xe ; $R_F = CF_3, C_2F_5, n-C_3F_7$), and the Fluoro(trifluoro-s-triazine)xenon(II) Cation, $s-C_3F_3N_2N - XeF^+$; Novel Noble Gas-Nitrogen Bonds

Gary J. Schrobilgen

Department of Chemistry, McMaster University, Hamilton, Ontario L8S 4M1, Canada

Three novel examples of Kr-N bonds derived from perfluoroalkylnitriles, the $R_F C \equiv N - KrF^+$ cations, and their xenon analogues $R_F C \equiv N - XeF^+$ ($R_F = CF_3, C_2F_5, n-C_3F_7$), have been prepared and characterized in BrF_5 solvent by ^{19}F and ^{129}Xe n.m.r. spectroscopy; the Xe-N bonded cation $s-C_3F_3N_2N - XeF^+$, synthesized as the AsF_6^- salt, is stable at room temperature and has been fully characterized by ^{129}Xe and ^{19}F n.m.r. and Raman spectroscopy.

We have previously reported that hydrogen cyanide and several classes of organic and fluoro-organic nitrogen bases are capable of forming Xe-N bonds with the hard acid XeF^+ .^{1,2} The bases include alkyl and fluoroalkyl nitriles¹ and perfluoropyridines.² We have also reported the first example of a Kr-N bond, $HC \equiv N - KrF^+ AsF_6^-$.³ All the nitrogen bases thus far found capable of bonding with NgF^+ are oxidatively resistant and possess first adiabatic ionization potentials (I.P.) close to, or exceeding, the estimated electron affinities of XeF^+ (10.9 eV) and KrF^+ (13.2 eV), e.g., the first I.P. of $HC \equiv N$ is 13.59 eV.⁴ The low basicity of the nitrogen atoms in these bases gives rise to noble gas-nitrogen bonds possessing

significant ionic character, an important criterion for thermal stability of the noble gas cation.

The measured value of the first adiabatic I.P. of $CF_3C \equiv N$ (13.90 eV)⁵ suggested that this and possibly related fluoroalkyl bases should be resistant to oxidative attack by KrF^+ and XeF^+ , and would be expected to possess nitrogen base centres conducive to the formation of correspondingly ionic noble gas-nitrogen bonds. The first I.P. (11.50 eV) for s-trifluoro-triazine, $s-C_3F_3N_3$,⁶ and the existence of $C_3F_3N - XeF^+ AsF_6^-$,⁷ where the first I.P. of pentathioropyridine is 10.08 eV,⁸ suggested that the $s-C_3F_3N_2N - XeF^+$ cation also ought to exist.

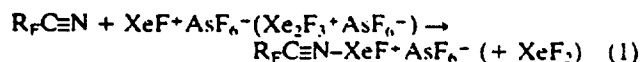
The interaction of equimolar amounts of $XeF^+ AsF_6^-$ or

Table 1. N.m.r. parameters for the $R_F C \equiv N-NgF^+$ ($R_F = CF_3, C_2F_5, n-C_3F_7$) cations^a

Cation	Chemical shift (p.p.m.) ^{b,c}		
	$\delta(^{129}Xe)$	$\delta(^{19}F)$	$J(^{129}Xe-^{19}F)/Hz$
$CF_3C \equiv N-KrF^+$		93.1 F-Kr- -53.9 F ₃ C-	
$CF_3CF_2C \equiv N-KrF^+$		91.1 F-Kr- -83.8 F ₃ C- ^d -108.6-CF ₂ - ^d	
$CF_3CF_2CF_2C \equiv N-KrF^+$		91.9 F-Kr- -81.1 F ₃ C- -105.7 F ₃ C-CF ₂ -CF ₂ - -125.2 F ₃ C-CF ₂ -CF ₂ -	
$CF_3C \equiv N-XeF^+$	-1337.1	-210.4 F-Xe- -54.8 F ₃ C-	6397
$CF_3CF_2C \equiv N-XeF^+$	-1293.7	-212.9 F-Xe- -83.9 F ₃ C- -109.3-CF ₂ -	6437
$CF_3CF_2CF_2C \equiv N-XeF^+$	-1294.2	-213.2 F-Xe- -81.9 F ₃ C- -106.6 F ₃ C-CF ₂ -CF ₂ - -125.7 F ₃ C-CF ₂ -CF ₂ -	6430

^a Spectra were recorded at 69.563 MHz (^{129}Xe) and 235.361 MHz (^{19}F) in BrF_3 solvent at -57 to $-61^\circ C$ for $R_F C \equiv N-KrF^+$ samples, and at -58 to $-68^\circ C$ (^{19}F) and $-64^\circ C$ (^{129}Xe) for $R_F C \equiv N-XeF^+$ samples. ^b Referenced externally at $24^\circ C$ with respect to the neat liquid references: $XeOF_4$ (^{129}Xe) and $CFCl_3$ (^{19}F); a positive sign denotes a chemical shift to high frequency of the reference. ^c With the exception of $C_2F_5C \equiv N-XeF^+$, no other $J(F-F)$ couplings could be observed owing to line broadening arising from slow chemical exchange and/or residual scalar coupling of the fluorine environments to ^{129}Xe . ^d $J(F-F) = 4.3$ Hz.

$Xe_2F_3^+AsF_6^-$ and $R_F C \equiv N$ ($R_F = CF_3, C_2F_5, n-C_3F_7$) in BrF_3 solvent according to equation (1) was initially studied. The syntheses of the krypton(II) analogues were also undertaken at low temperatures in BrF_3 solvent using the general synthetic approach given in equation (2).



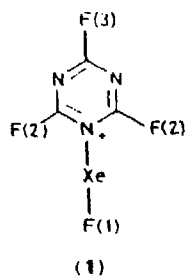
The $R_F C \equiv N-NgF^+$ cations have been characterized in BrF_3 by low-temperature (-57 to $-61^\circ C$) ^{19}F and ^{129}Xe n.m.r. spectroscopy and consist of two sets of new signals: a singlet in the F-on-Kr^{II} and in the F-on-Xe^{II} regions, and resonances in the F-on-C region with characteristic $J(FF)$ and $J(^{19}F-^{13}C)$ couplings having chemical shifts to high frequency of the parent base molecules (Table 1). In each case, the singlet assigned to F-on-Xe^{II} was flanked by natural abundance (26.44%) ^{129}Xe satellites arising from $J(^{129}Xe-^{19}F)$. The integrated relative intensities of the fluorine-on-noble gas environments and perfluoroalkyl group are consistent with the proposed formulations. Furthermore, the F-on-Kr^{II} resonance of $CF_3C \equiv N-KrF^+$ could be resolved to show the ^{82}Kr , ^{84}Kr , and ^{86}Kr isotopic shifts (0.0105 p.p.m. atomic mass unit, amu), which compare favourably with previously measured values for $HC \equiv N-KrF^+$ (0.0138 p.p.m./amu),³ and KrF_2 (0.0104 p.p.m./amu).⁷ In addition, the F-on-Kr^{II} resonances occur to high frequency of KrF_2 [$\delta(^{19}F)$ 68.0 p.p.m.; $-56^\circ C$; BrF_3 solvent] while the F-on-Xe^{II} resonances occur to low frequency of XeF_2 [$\delta(^{19}F)$ -184.3 p.p.m.; $\delta(^{129}Xe)$ -1685.2 p.p.m.; $J(^{129}Xe-^{19}F)$ 5621 Hz; $-52^\circ C$; BrF_3] (cf. Table 1). Similar, but slightly more positive ^{19}F chemical shifts have been observed for $HC \equiv N-KrF^+$ [$\delta(^{19}F)$ 99.4 p.p.m.; $-57^\circ C$; BrF_3 solvent]³ with respect to KrF_2 . This is in contrast to the $R_F C \equiv N-XeF^+$ series of cations which display significantly

more positive ^{19}F (F-on-Xe^{II}) and ^{129}Xe chemical shifts when compared with $HC \equiv N-XeF^+$ [$\delta(^{19}F)$ -198.4 p.p.m.; $\delta(^{129}Xe)$ -1552 p.p.m.; $J(^{129}Xe-^{19}F)$ 6150 Hz; $-10^\circ C$; HF solvent]¹ and XeF_2 . The ^{129}Xe and ^{19}F complexation shifts indicate that the Xe-N Bonds of the $R_F C \equiv N-XeF^+$ cations are significantly more ionic than in $HC \equiv N-XeF^+$ or $RC \equiv N-XeF^+$ (ref. 1) and this is further supported by significantly larger $J(^{129}Xe-^{19}F)$ values measured for the $R_F C \equiv N-XeF^+$ cations, which are known to increase with ionic character of the Xe-L bond in F-Xe-L type compounds.⁸ The $R_F C \equiv N-XeF^+$ cations represent the most ionic Xe-N bonded species presently known. In contrast, the analogous comparison of ^{19}F chemical shifts for $R_F C \equiv N-KrF^+$ cations indicates the Kr-N bonds are slightly more covalent than in $HC \equiv N-KrF^+$.

All three fluoro(perfluoroalkyl)nitrile)krypton(II) cations are thermally less stable with respect to redox decomposition than $HC \equiv N-KrF^+$ or their xenon(II) analogues, preventing their isolation and characterization in the solid state by Raman spectroscopy. Decompositions were monitored by ^{19}F n.m.r. and occurred over periods of ca. 1-2 h at -57 to $-61^\circ C$ with the assigned cation resonances decreasing while maintaining their relative intensity relationships. The major decomposition products consisted of Kr and the fluorinated products (^{19}F n.m.r. parameters listed in parentheses): CF_4 (-63.1 p.p.m.), C_2F_6 (-88.6 p.p.m.), and NF_4^+ [219.4 p.p.m., $J(^{19}F-^{14}N)$ 229 Hz] for all three $R_F C \equiv N-KrF^+$ cations studied, and $n-C_3F_8$ (-83.8 p.p.m.), F_3C- (-132.8 p.p.m., -CF₂-) for $C_2F_5C \equiv N-KrF^+$, and $n-C_3F_8$, $n-C_4F_{10}$ (-82.8 p.p.m.), F_3C- (-129.2 p.p.m., -CF₂-) for $n-C_3F_7C \equiv N-KrF^+$.



The interaction of liquid trifluoro-s-triazine, $s-C_3F_7N_3$, with $XeF^+ AsF_6^-$ at room temperature for three hours followed by removal of excess of s-trifluoro-triazine *in vacuo* resulted in a white powder which is stable indefinitely at room tempera-



ture. The combining ratio $\text{XeF}^+ \text{AsF}_6^- : s\text{-C}_3\text{N}_3\text{F}_3 = 1.00 : 1.00$ is consistent with equation (3). Both the ^{19}F and ^{129}Xe n.m.r. findings for the salt dissolved in BrF_3 and HF solvents are consistent with the cation formulation given by structure (1). The ^{129}Xe n.m.r. spectrum recorded in BrF_3 at -50°C consists of a doublet [$\delta(^{129}\text{Xe}) -1862.4$ p.p.m.] arising from $^1J(^{129}\text{Xe}-^{19}\text{F}) = 5932$ Hz. The $^{129}\text{Xe}-^{14}\text{N}$ coupling is quadrupole collapsed, as has been observed previously for $4\text{-CF}_3\text{-C}_3\text{F}_4\text{N-XeF}^+ \text{AsF}_6^-$ and $\text{C}_3\text{F}_5\text{N-XeF}^+ \text{AsF}_6^-$ in BrF_3 at low temperatures.² In HF solvent, however, $^1J(^{129}\text{Xe}-^{14}\text{N})$ is observed at -5°C [$\delta(^{129}\text{Xe}) -1807.9$ p.p.m.; $^1J(^{129}\text{Xe}-^{14}\text{N}) 5909$ Hz]. The magnitude, 245 Hz, compares favourably with those reported previously for the related perfluoropyridine cations (235–238 Hz). The ^{19}F n.m.r. spectra show two F-on-C environments in the ratio of 1:2 [F(1), -154.9 ; F(2), -27.7 ; F(3), -13.5 p.p.m. in HF solvent at -5°C and F(1), -145.6 ; F(2), -26.2 ; F(3), -8.7 p.p.m. in BrF_3 solvent at -50°C] and a F-on-Xe^{II} environment with accompanying ^{129}Xe natural abundance (26.44%) satellites arising from $^1J(^{129}\text{Xe}-^{19}\text{F})$ and a 1:2:1 triplet arising from $^4J\{\text{F}(1)\text{-F}(2)\}$ 10.9 Hz [resolved at -50°C in BrF_3 solvent along with $^4J\{\text{F}(2)\text{-F}(3)\}$ 13.3 Hz]. The coupling, $^4J\{\text{F}(1)\text{-F}(2)\}$, has also been observed for the perfluoropyridine cations $4\text{-CF}_3\text{-C}_3\text{F}_4\text{N-XeF}^+$ (25.8 Hz) and $\text{C}_3\text{F}_5\text{N-XeF}^+$ (25.0 Hz).²

A comparison of ^{129}Xe chemical shift and $^1J(^{129}\text{Xe}-^{19}\text{F})$ coupling constant values for other Xe-N bonded species studied to date reveals the following order: $\text{R}_1\text{C}\equiv\text{N} > \text{HC}\equiv\text{N} > s\text{-C}_3\text{F}_4\text{N}_3 \approx 4\text{-CF}_3\text{-C}_3\text{F}_4\text{N} > \text{C}_3\text{F}_5\text{N} > (\text{FSO}_2)_2\text{N} > (\text{CF}_3\text{SO}_2)_2\text{N}$, where the ^{129}Xe chemical shift and $^1J(^{129}\text{Xe}-^{19}\text{F})$ decrease with increasing covalent character of the Xe-N bond.

The Raman spectrum of $s\text{-C}_3\text{F}_4\text{N}_3\text{N-XeF}^+ \text{AsF}_6^-$ was recorded at -196°C using 514.5 nm excitation. In addition to modes associated with the ring, the spectrum is consistent with an ionic formulation, structure (1). Some key frequencies and their assignments follow: $\nu(\text{Xe-F})$, 544 (100), 553 (53) cm^{-1} ; $\nu(\text{Xe-N})$, 313 (0.6) cm^{-1} (tentative assignment); $\delta(\text{F-Xe-N})$, 156 (23), 159 (sh) cm^{-1} ; $\tau(\text{C}_3\text{F}_4\text{N}_3\text{N-Xe})$, 108 (6) cm^{-1} (tentative assignment) and AsF_6^- modes $\nu_1(a_{1g})$ 684 (19) cm^{-1} ; $\nu_2(e_g)$ 588 (sh), 591 (4) cm^{-1} ; $\nu_3(t_{2g})$ 370 (5), 375 (4) cm^{-1} .

This research was sponsored by the United States Air Force Astronautics Laboratory, Edwards Air Force Base, California (Contract F49620-87-C-0049), and a Natural Sciences and Engineering Research Council of Canada (NSERC) operating grant.

Received, 2nd June 1988, Com. 8102198H

References

- 1 A. A. A. Emara and G. J. Schrobilgen, *J. Chem. Soc., Chem. Commun.*, 1987, 1644.
- 2 A. A. A. Emara and G. J. Schrobilgen, *J. Chem. Soc., Chem. Commun.*, 1988, 257.
- 3 G. J. Schrobilgen, *J. Chem. Soc., Chem. Commun.*, 1988, 863.
- 4 V. H. Dibelet and S. K. Liston, *J. Chem. Phys.*, 1968, **48**, 4765.
- 5 H. Bock, R. Dammel, and D. Lentz, *Inorg. Chem.*, 1984, **23**, 1535.
- 6 C. R. Brundle, M. B. Robin, and K. A. Kuebler, *J. Am. Chem. Soc.*, **94**, 1466.
- 7 J. C. P. Sanders and G. J. Schrobilgen, unpublished work.
- 8 G. J. Schrobilgen, in *NMR and the Periodic Table*,¹ eds. R. K. Harris and B. E. Mann, Academic Press, London, 1978; ch. 14, pp. 439–454.

Properties of Atoms in Molecules: Krypton and Xenon and Their Bonds to Nitrogen and Fluorine in $\text{HC}\equiv\text{N}-\text{NgF}^+$, NgF^+ , and NgF_2

Preston J. MacDougall,[†] Gary J. Schrobilgen, and Richard F. W. Bader*

Received August 17, 1988

The recent synthesis of a salt of $\text{FKr}-\text{NCH}^+$, together with the earlier preparation of its Xe analogue, makes possible a comparison of the experimental properties of the bonds formed by N and F to the noble-gas atoms (Ng) Kr and Xe. This experimental study is complemented by a theoretical investigation at the SCF level of the properties of molecules containing such bonds and by the determination of the properties of the atoms and bonds in these molecules using the theory of atoms in molecules. The exceptional ability of the NgF^+ ions to act as Lewis acids is related to the presence of holes in the valence shell charge concentrations of the Kr and Xe atoms that expose their cores. The mechanism of formation of the Ng-N bonds in the adducts of NgF^+ with HCN is similar to the formation of a hydrogen bond: the mutual penetration of the outer diffuse nonbonded densities of the Ng and N atoms is facilitated by their dipolar and quadrupolar polarizations, which remove density from along their axis of approach, to yield a final density in the interatomic surface that is only slightly greater than the sum of the unperturbed densities. The Ng-N interactions lie closer to the closed-shell limit than do the Ng-F bonds formed in the reaction of NgF^+ with F. The energies of formation of these adducts are dominated by the large stabilizations of the Ng atoms that result from the increase in the concentration of charge in their inner quantum shells.

Introduction

The compound $\text{FKr}-\text{N}\equiv\text{CH}^+\text{AsF}_6^-$, the first to contain a krypton-nitrogen bond, was recently synthesized at this university.¹ Prior to this, the only known compounds of krypton were the Kr-F bonded species KrF_2 , KrF^+ , and Kr_2F_3^+ ^{2a} as well as $\text{KrF}_2\cdot\text{WOF}_4$ and $\text{KrF}_2\cdot n(\text{MoOF})_4$ ($n = 1-3$).^{2b} The corresponding compound containing a Xe-N bond was synthesized earlier³ through the reaction of $\text{XeF}^+\text{AsF}_6^-$ or $\text{Xe}_2\text{F}_3^+\text{AsF}_6^-$ with HCN. The krypton compound was not prepared in such a direct manner because KrF^+ is too strong an oxidizing agent. Instead, its synthesis was obtained by allowing KrF^+ to react with the protonated HCN salt $\text{HCNH}^+\text{AsF}_6^-$. The Xe compound, $\text{FXe}-\text{N}\equiv\text{CH}^+\text{AsF}_6^-$, is stable up to -10°C while the corresponding limit for the Kr compound is around -50°C . It is the purpose of this paper to compare the properties of the bonds formed by F and N to Kr and Xe in terms of their experimental properties and by use of the theory of atoms in molecules.⁴⁻⁶

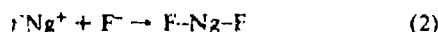
Energies and Geometries

Single determinantal SCF calculations with linearly constrained geometry optimizations using the program GAMESS⁷ were performed for ArF^+ , KrF^+ , XeF^+ , KrF_2 , XeF_2 , FKrNCH^+ , and FXeNCH^+ . Huzinaga's basis sets for Kr (432121s/42121p/311d) and Xe (4332121s/432121p/4211d)⁸ were employed while the other atoms were described by the 4-31G** basis⁹ augmented with diffuse s and p functions.¹⁰ Previous ab initio calculations on the diatomic NgF^+ species have been performed by Liebman and Allen (HeF^+ , NeF^+ , and ArF^+),^{11,12} Liu and Schaefer (KrF^+),¹³ Frenking et al. (HeF^+ , NeF^+ , and ArF^+),¹⁴ and Hottoka et al. (NeF^+).¹⁵ Basch et al.¹⁶ have included XeF_2 in a theoretical study of the neutral fluorides of xenon while Bagus et al.¹⁷ have performed a CI calculation for a portion of the potential energy surface for KrF_2 .

The minimum energy geometrical parameters and the total energies obtained here are given in Table I. The energies of the reaction between the closed-shell species HCN and FNg^+



are calculated to be -32.5 and -34.5 kcal/mol for $\text{Ng} = \text{Kr}$ and Xe , respectively, while the corresponding energies of the ion reaction



are -209.0 and -211.9 kcal/mol.

In spite of a lack of relativistic corrections, which tend to reduce the predicted bond distances to a heavy atom,¹⁸ the calculated

Table I. Energies and Geometries of Ng Compounds^a

species	energy, au	calcd (exptl) bond lengths, Å
ArF^+	-624.97477	1.628
KrF^+	-2848.47027	1.734
XeF^+	-7325.92011	1.886
KrF_2	-2948.13396	1.843 (1.875 ± 0.002) ^b
XeF_2	-7425.58845	1.985 (1.977 ± 0.0015) ^c
FKrNCH^+	-2941.31362	1.748 [Kr-F], 2.307 [Kr-N], 1.128 [N-C], 1.068 [C-H]
FXeNCH^+	-7418.76656	1.904 [Xe-F], 2.421 [Xe-N], 1.127 [N-C], 1.068 [C-H]
HCN	-92.79150	1.132 (1.156) [C-N], 1.060 (1.064) [C-H] ^d
F ⁻	-99.33059	

^a See text for basis sets. ^b Murchison, C.; Reichman, S.; Anderson, D.; Overend, J.; Schreiner, F. *J. Am. Chem. Soc.* 1968, 90, 5690. Gas-phase infrared data. ^c Agron, P. A.; Begun, G. M.; Levy, H. A.; Mason, A. A.; Jones, G.; Smith, D. F.; *Science* 1963, 139, 842. Smith, D. F. *J. Chem. Phys.* 1963, 38, 270. Gas-phase infrared data. ^d Herzberg, G. *Electronic Spectra of Polyatomic Molecules*; Van Nostrand: New York, 1966.

bond lengths for the two difluorides are in good agreement with the experimental results, with errors typical of SCF calculations

- (1) Schrobilgen, G. J. *J. Chem. Soc., Chem. Commun.* 1988, 863.
- (2) (a) Gillespie, R. J.; Schrobilgen, G. J. *Inorg. Chem.* 1976, 15, 22. (b) Holloway, J. H.; Schrobilgen, G. J. *Inorg. Chem.* 1981, 20, 3363.
- (3) Emara, A. A. A.; Schrobilgen, G. J. *J. Chem. Soc., Chem. Commun.* 1987, 1644.
- (4) Bader, R. F. W.; Beddall, P. M. *J. Chem. Phys.* 1972, 56, 3320.
- (5) Bader, R. F. W.; Nguyen-Dang, T. T. *Adv. Quantum Chem.* 1981, 14, 63.
- (6) Bader, R. F. W.; Nguyen-Dang, T. T.; Tal, Y. *Rep. Prog. Phys.* 1981, 44, 893. Srebrenik, S.; Bader, R. F. W. *J. Chem. Phys.* 1975, 63, 3945.
- (7) Dupius, M.; Spangler, D.; Wendoloski, J. J. *NRC Software Catalog* 1980, 1, QG01.
- (8) Huzinaga, S. *Gaussian Basis Sets for Molecular Calculations*; Elsevier: Amsterdam Publ. 1984.
- (9) Hehre, W. J.; Ditchfield, R.; Pople, J. A. *J. Chem. Phys.* 1972, 56, 2257.
- (10) Chandrasekar, J.; Andrade, J. G.; Schleyer, P. v. R. *J. Am. Chem. Soc.* 1981, 103, 5609.
- (11) Liebman, J. F.; Allen, L. C. *J. Am. Chem. Soc.* 1970, 92, 3539.
- (12) Liebman, J. F.; Allen, L. C. *J. Chem. Soc., Chem. Commun.* 1969, 1355.
- (13) Liu, B.; Schaefer, H. F. *J. Chem. Phys.* 1971, 55, 2369.
- (14) Frenking, G.; Koch, W.; Deakne, A.; Liebman, J. F.; Bartlett, N., in press.
- (15) Hottoka, M.; Roos, B.; Delos, J. B.; Srivastava, R.; Sharma, R. B.; Koski, W. S. *Phys. Rev. A* 1987, 45, 4515.
- (16) Basch, H.; Moskowitz, J. W.; Hollister, C.; Henkin, D. *J. Chem. Phys.* 1971, 55, 1922.
- (17) Bagus, P. S.; Liu, B.; Schaefer, H. F. *J. Am. Chem. Soc.* 1972, 94, 6635.

[†] Present address: Department of Chemistry, Texas A&M University, College Station, TX 77843.

Table II. Correlation of Physical Properties for Representative Ng-F Bonds

species ^a	$r(\text{Ng-F})$, Å	$\nu(\text{Ng-F})$, cm ⁻¹	NMR params ^c			T , °C	ref
			$^1J(^{129}\text{Xe}-^{19}\text{F})$, ^d Hz	$\delta(^{129}\text{Xe})$, ^{d,e} ppm	$\delta(^{19}\text{F})$, ^{d,e} ppm		
KrF ⁺	(1.740)						
KrF ⁺ Sb ₂ F ₁₁ ⁻		624					l
KrF ⁺ AsF ₆ ⁻		609					l, m
(FKr) ₂ F ^{+/2}		605			73.6	-65	l
HC≡N-KrF ⁺	(1.748)	560			99.4	-57	n
CF ₃ C≡N-KrF ⁺					93.1	-59	o-q
KrF ₂	1.875 (1.843)	462			68.0	-56	p, q
XeF ⁺	(1.886)						
XeF ⁺ Sb ₂ F ₁₁ ⁻	1.82 (3)	619	7230	-574	-290.2	23 ^e	l, r-t
XeF ⁺ AsF ₆ ⁻	1.873 (6)	610	6892	-869		-47	l, m, o, u
(FXe) ₂ F ^{+/2}	1.90 (3)	593	6740	-1051	-252.0	-62	l, s, t, v
CF ₃ C≡N-XeF ⁺			6397	-1337	-210.4	-63	o
HC≡N-XeF ⁺	(1.904)	564	6181	-1569	-198.4 ^k	-58	w
CH ₃ C≡N-XeF ⁺ ^h		565	6020	-1708	-185.5	-10	w
s-C ₃ F ₃ N ₂ N-XeF ⁺		548	5932	-1862	-145.6	-50	o
FO ₂ SO-XeF	1.940 (8)	528	5830	-1666		-40	s, t, x, y
cis/trans-F ₄ OIO-XeF		527	5803/5910	-1824/-1720	-161.7/-170.1 ^l	0	z
C ₃ F ₃ N-XeF ⁺		528	5926	-1922	-139.6	-30	aa
4-CF ₃ C ₃ F ₄ N-XeF ⁺		524	5977	-1853	-144.6	-50	aa
F ₂ TeO-XeF ^l		520		-2051	-151.0 ^k	26	bb, cc
(FO ₂ S) ₂ N-XeF	1.967 (3)	506	5586	-1977	-126.1	-58	dd, ee
			5664 ^l	-2009 ^l	-126.0 ^l	-40	
XeF ₂	1.977 (1.984)	496	5621	-1685	-184.3	-52	o, ff, gg

^a Unless otherwise indicated, all cations have AsF₆⁻ as the counterion. ^b Values in parentheses are calculated values determined in the present work. ^c Spectra were obtained in BrF₃ solvent unless otherwise indicated. ^d The NMR parameters of KrF and XeF groups are very sensitive to solvent and temperature conditions; it is therefore important to make comparisons in the same solvent medium at the same or nearly the same temperatures. ^e Referenced with respect to the neat liquids XeOF₄ (¹²⁹Xe) and CFCl₃ (¹⁹F) at 24 °C; a positive sign denotes the chemical shift of the resonance in question occurs to high frequency of (is more deshielded than) the resonance of the reference substance. ^f Table entries refer to the terminal fluorine on the noble-gas atom. ^g Recorded in SbF₅ solvent. ^h $\delta(^{19}\text{F})$ measured in anhydrous HF solvent at -10 °C. ⁱ $\delta(^{19}\text{F})$ measured in SO₂CIF solvent at -40 °C. ^j NMR parameters measured in SO₂CIF solvent. ^k NMR parameter measured in SO₂CIF solvent at -50 °C. ^l Gillespie, R. J.; Schrobilgen, G. J. *Inorg. Chem.* 1976, 15, 22. ^m Schrobilgen, G. J. Unpublished work. ⁿ Schrobilgen, G. J. *J. Chem. Soc., Chem. Commun.* 1988, 863. ^o Schrobilgen, G. J. *J. Chem. Soc., Chem. Commun.* 1988, 1506. ^p Murchison, C.; Reichman, S.; Anderson, D.; Overend, J.; Schreiner, F. *J. Am. Chem. Soc.* 1968, 90, 5680. ^q Claassen, H.; Goodman, G. L.; Malm, J. G.; Schreiner, F. *J. Chem. Phys.* 1965, 42, 1229. ^r Burgess, J.; et al. *J. Inorg. Nucl. Chem., Suppl.* 1976, 183. ^s Schrobilgen, G. J.; Holloway, J. H.; Granger, P.; Brevard, C. *Inorg. Chem.* 1978, 17, 980. ^t Gillespie, R. J.; Netzer, A.; Schrobilgen, G. J. *Inorg. Chem.* 1974, 13, 1455. ^u Zalkin, A.; et al. *Inorg. Chem.* 1978, 17, 1318. ^v Bartlett, N.; et al. *Inorg. Chem.* 1974, 12, 780. ^w Emara, A. A. A.; Schrobilgen, G. J. *J. Chem. Soc., Chem. Commun.* 1987, 1644. ^x Bartlett, N.; et al. *Inorg. Chem.* 1972, 11, 1124. ^y Landa, B.; Gillespie, R. J. *Inorg. Chem.* 1973, 12, 1383. ^z Syvret, R. G.; Schrobilgen, G. J. *Inorg. Chem.*, submitted for publication. ^{aa} Emara, A. A. A.; Schrobilgen, G. J. *J. Chem. Soc., Chem. Commun.* 1988, 257. ^{ab} Birchall, T.; Myers, R. D.; deWaard, H.; Schrobilgen, G. J. *Inorg. Chem.* 1982, 21, 1068. ^{ac} Sanders, J. C. P.; Schrobilgen, G. J. Unpublished work. ^{ad} Sawyer, J. F.; Schrobilgen, G. J.; Sutherland, S. J. *Inorg. Chem.* 1982, 21, 4064. ^{ae} Schumacher, G. A.; Schrobilgen, G. J. *Inorg. Chem.* 1983, 22, 2178. ^{af} Reichman, S.; Schreiner, F. *J. Chem. Phys.* 1969, 51, 2355. ^{ag} Agron, P. A.; Begun, G. M.; Levy, H. A.; Mason, A. A.; Jones, G.; Smith, D. F. *Science* 1963, 139, 842.

with extended basis sets, (compare the results for HCN). The reaction of the NgF⁺ ions with F⁻ to yield the difluorides results in increases in the Ng-F bond lengths of 0.1 Å, while their reaction with HCN causes the same bonds to lengthen on average by only 0.016 Å. There is a correlation of Ng-F bond length, as is also reflected in its vibrational frequency, with the base strength of the ligand attached to Ng-F⁺. This is illustrated by the examples shown in Table II. The NgF⁺ species are only weakly coordinated by a fluorine bridge to the anion Sb₂F₁₁⁻ while the interaction of NgF⁺ with N(SO₂F)₂⁻ is representative of a much stronger interaction. Thus as the strength of the base B increases and the Ng-B bond becomes progressively less ionic, the Ng-F bond is lengthened and weakened. The observed values of the Ng-F vibrational frequencies place the adducts with HCN toward the most ionic end of the scale. The same trends are reflected in the ¹⁹F and ¹²⁹Xe chemical shifts, which are also listed in Table II, if one accepts the correlation of increased shielding (more negative chemical shift) with a transfer of charge to Xe and hence with a reduced ionic character of the Ng-B interaction.

Quadrupolar nuclei in noncubic environments generally yield poorly resolved one-bond coupling patterns in their NMR spectra due to quadrupolar relaxation effects. In spite of the axial symmetry of the FXe-NCH⁺ cation the ¹⁴NMR spectrum showed well resolved and only partially quadrupole collapsed ¹J(¹²⁹Xe-

¹⁴N), ¹J(¹⁴N), and ¹J(¹³C) couplings.³ The extent of minimal quadrupolar relaxation via a reduced electric field gradient was examined theoretically by calculating this field gradient at the nitrogen nucleus and comparing it to that in isolated HCN. The principal component of the electric field gradient tensor, (∇E)_{zz} (+z is in the direction H → N), at the position of the nitrogen nucleus decreases from +1.02 au in HCN to +0.49 au in FXe-NCH⁺. The electric field gradient at the nitrogen nucleus is halved upon formation of the KrF⁺ adduct as well; thus, it may be possible to observe highly resolved ¹J(¹⁴N-¹³C) coupling in the ¹⁴N NMR of this adduct. As a further check of the accuracy of these calculations, we have calculated the electric field gradients at the Xe nucleus in XeF⁺ and FXe-NCH⁺ and find them to differ by less than 7%, a result in agreement with the experimental observation that the quadrupolar splitting observed in the ¹²⁹Xe Mössbauer spectra of FXe-NCH⁺ (40.2 ± 0.3 mm/s) is, within experimental error, the same as that obtained for the salt XeF⁺AsF₆⁻ (40.5 ± 0.1 mm/s).¹⁹

The C-N bond of HCN is calculated to shorten by ≈0.05 Å on forming the adducts, while the C-H bond is calculated to lengthen by 0.008 Å. These predicted changes in bond length are in agreement with the observed shifts in their corresponding stretching frequencies, $\nu(\text{CN})$ increasing by 70 cm⁻¹ for both compounds and $\nu(\text{C-H})$ decreasing by 171 cm⁻¹ in the Xe adduct.³

(18) Ziegler, T.; Sniijders, J. G.; Baerends, E. J. *J. Chem. Phys.* 1981, 74, 1271.

(19) Valsdóttir, J.; Frampton, C.; Birchall, T.; Schrobilgen, G. J. Unpublished results.

Table III. Bond Properties of HCN and of Ng Compounds (in au)

bond A-B	R	$r_b(A)$	$r_b(B)$	ρ_b	$\nabla^2\rho_b$	λ_{\parallel}	λ_{\perp}	$\Delta r(Ng)$	$\Delta r(N)$	ρ_b°
H-CN	2.002	0.681	1.321	0.302	-1.334	0.394	-0.864			
HC-N	2.138	0.734	1.404	0.497	+0.891	3.067	-1.088			
FKr-NCH ⁺	4.359	2.171	2.188	0.053	+0.169	0.268	-0.050	1.26	1.39	0.047
FXe-NCH ⁺	4.575	2.318	2.257	0.049	+0.150	0.224	-0.037	1.40	1.32	0.046
F-F	2.538	1.269	1.269	0.332	+0.353	2.209	-0.928			
Ar-F ⁺	3.076	1.612	1.464	0.266	+0.136	0.982	-0.423			
Kr-F ⁺	3.277	1.664	1.624	0.184	+0.134	0.664	-0.265			
Xe-F ⁺	3.565	1.813	1.752	0.141	+0.312	0.648	-0.168			
F-KrF	3.483	1.755	1.728	0.138	+0.274	0.619	-0.173			
F-XeF	3.752	1.847	1.905	0.109	+0.314	0.541	-0.114			

Table IV. Properties of Atoms in Ng-F⁺ and HCN

atom Ω	$q(\Omega)$	$\mu(\Omega)^a$	$Q_{ii}(\Omega)$	atom Ω	$q(\Omega)$	$\mu(\Omega)^a$	$Q_{ii}(\Omega)$
Ar	+0.928	+0.257	3.262	F	+0.072	-0.063	1.520
Kr	+1.148	+0.465	5.185	F	-0.148	+0.050	1.219
Xe	+1.406	+0.883	8.496	F	-0.406	+0.160	0.940
H	+0.193	+0.098	0.376	C	+1.260	+1.135	2.238
N	-1.454	+0.958	0.060				

^aWhen $\mu(\Omega) > 0$, the negative end of the dipole is directed away from F and toward Ng or away from N and toward H.

Table V. Changes in Atomic Properties in Formation of FNg-NCH⁺ and FNg-F ($\Delta E(\Omega)$ in kcal/mol; Other Properties in au)

	F	Kr	N	C	H
$\Delta q(\Omega)$	-0.169	+0.026	-0.102	+0.123	+0.123
$\Delta \mu(\Omega)$	-0.003	-0.075	+0.087	+0.083	-0.002
$\Delta Q_{ii}(\Omega)$	-0.143	+1.018	+0.471	-0.953	-0.091
	F	Xe	N	C	H
$\Delta q(\Omega)$	-0.132	+0.009	-0.133	+0.128	+0.128
$\Delta \mu(\Omega)$	-0.017	-0.246	+0.041	+0.088	-0.002
$\Delta Q_{ii}(\Omega)$	-0.091	+1.771	+0.330	-0.994	-0.094
	F ^a	Kr	F ^a	Xe	
$\Delta q(\Omega)$	-0.434	+0.016	-0.291	-0.012	
$\Delta \mu(\Omega)$	-0.035	-0.883	-0.088	-0.465	
$\Delta Q_{ii}(\Omega)$	-0.282	+2.085	-0.164	+3.511	
$\Delta E(\Omega)$	-129.2 (+98.8)	-178.6	-76.1 (+23.5)	-159.4	

^aThe energy differences in parentheses are calculated relative to the energy of F; the remaining values in these columns are calculated relative to the values for the F atoms in NgF⁺.

These experimental characterizations of the bonds are complemented with the theoretical results obtained from an investigation of the charge distributions and properties of the atoms in the reactants and the changes they undergo on forming the adducts.

Atoms and Bonds

The necessary and sufficient condition for two atoms to be bonded to one another is that their nuclei be joined by an atomic interaction line in an equilibrium geometry, i.e., that they be linked by a bond path.^{20,21} The presence of such a path indicates that electronic charge has been accumulated between the nuclei in an absolute sense, for it denotes the presence of a line linking the nuclei along which the charge density is a maximum with respect to any neighboring line.^{22,23} The charge distributions of the complexes exhibit such lines between the Ng and N nuclei, as illustrated in Figure 1 for the Kr adduct. The presence of a bond

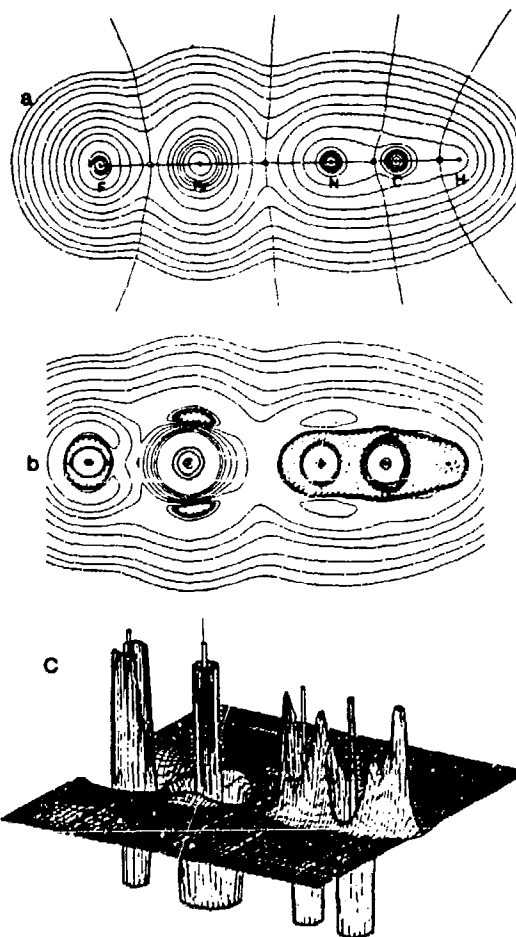


Figure 1. (a) Contour map of the charge density in the adduct FKrNCH⁺ showing the bond paths and the intersection of the interatomic surfaces. Bond critical points are denoted by black circles. Note the near planarity of the Kr-N interatomic surface, which is also a characteristic of a hydrogen bond. The outer contour value is 0.001 au. The remaining contours increase in value in the order 2×10^4 , 4×10^4 , 8×10^4 with n starting at -3 and increasing in steps of 1 to give a maximum contour value of 20. (b) Contour map of the Laplacian distribution for FKrNCH⁺. The positions of the nuclei are the same as in part a. Solid contours denote positive and dashed lines denote negative values of $\nabla^2\rho$. The magnitudes of the contour values are as in part a, without the initial value of 0.001 au. (c) A relief map of $-\nabla^2\rho$. A maximum in the relief map is a maximum in charge concentration. If the inner spikelike feature at its nucleus is counted, the Kr atom exhibits four alternating regions of charge concentration and charge depletion corresponding to the presence of four quantum shells. Note the absence of a lip on the N side of the Kr VSCC demonstrating the presence of a hole in its outer sphere of charge concentration. Contrast the localized, atomic-like nature of the Laplacian distribution for the F and Kr atoms with the continuous valence shell of charge concentration enveloping all three of the nuclei in HCN.

- (20) Bader, R. F. W.; Essén, H. *J. Chem. Phys.* 1984, 80, 1943.
 (21) Bader, R. F. W. *Acc. Chem. Res.* 1985, 18, 9.
 (22) Bader, R. F. W. In *International Review of Science: Physical Chemistry, Series 2*; Buckingham, A. D., Coulson, C. A., Eds.; Butterworths: London, 1975; Vol. 1. Runtz, G.; Bader, R. F. W.; Messer, R. R. *Can. J. Chem.* 1977, 55, 3040.
 (23) The presence of a line of maximum charge density linking bonded nuclei and its absence when no bond is present is graphically illustrated for the bridgehead carbon atoms in propellanes and their corresponding bicyclic analogues: Wiberg, K. B.; Bader, R. F. W.; Lau, C. D. H. *J. Am. Chem. Soc.* 1987, 109, 985.

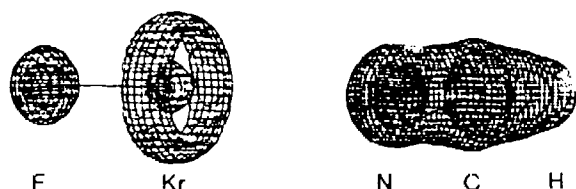


Figure 2. Zero envelopes of the Laplacian distributions ($\nabla^2\rho = 0$ for all points on the surface) for isolated KrF^+ and HCN shown aligned for adduct formation and shown to the same scale. The separation between the Kr and N nuclei is 5.0 Å. All that remains of the VSCC of the Kr atom is a belt of charge concentration, and the diagram clearly illustrates the exposure of its penultimate spherical shell of charge concentration—the core of the krypton atom. The diagram also contrasts the interatomic nature of the charge concentration in HCN with its pronounced intraatomic form in KrF^+ .

this point; along the bond path, it is a maximum with respect to directions perpendicular to this path. The lines of steepest descent through the three-dimensional charge distribution starting from the bond critical point define the interatomic surface (Figure 1). Such a surface is not crossed by any vectors $\nabla\rho$ —it is a “zero flux surface”.⁴ These surfaces partition the space of a molecule into atoms, and the properties of each atom, because this space is a region of space bounded by a zero flux surface, are defined and predicted by quantum mechanics.^{5,24} The bonds in the reactants and adducts are classified in terms of the properties of the charge density at the bond critical points (Table III). The formation of the adducts is discussed in terms of the properties of the atoms and their changes, Tables IV and V. Values of properties evaluated at a bond critical point are denoted by the subscript b. It has been shown²⁵ that in general, the properties of ρ at the bond critical points and its integrated averages over an atomic basin are relatively insensitive to electron correlation, the SCF values differing by small percentages relative to results obtained in CI calculations. The addition of correlation does not alter the classification of the bonds obtained by using SCF densities.

Bond Classification

The Laplacian of the charge density has the important property of determining where electronic charge is locally concentrated ($\nabla^2\rho < 0$) and locally depleted ($\nabla^2\rho > 0$),²⁰ information which is not evident in the topology of ρ itself. The local maxima in the concentrations of charge defined in this manner recover the Lewis model of localized electron pairs and the associated VSEPR model of molecular geometry,^{26,27} while the course of a generalized Lewis acid–base reaction is predicted by aligning a maximum of charge concentration on the base with a minimum corresponding to a region of charge depletion on the acid.^{26,28–30} The Laplacian distributions of the acids NgF^+ and the base HCN correctly predict the formation of the adducts described here. This is dramatically illustrated in Figure 2 where the plots of the zero envelope of $\nabla^2\rho$, which separates the valence shell of charge concentration (VSCC) from the valence shell of charge depletion, demonstrates the presence of a charge concentration (a maximum in $-\nabla^2\rho$) corresponding to the nonbonded electron pair on N of HCN and an axial hole in the valence shell of charge concentration of the Kr atom of KrF^+ . The alignment of the maximum in charge concentration of the base with the hole in the VSCC of the acid yields the linear adduct.

Frontier orbital theory describes the formation of these adducts in terms of the overlap of the HOMO, corresponding to the

nonbonded σ orbital localized on N, with the LUMO of the acid, the antibonding σ orbital localized on Ng. There is frequently a correspondence of HOMO and LUMO with the charge concentration in the VSCC of the base and the hole in the VSCC of the acid, respectively,^{28,31} as is again evident in the present examples. The LUMO's of both KrF^+ and XeF^+ have negative orbital energies (≈ -6.0 eV), a reflection of the strong acidic character of these ions. This same behavior is reflected by the presence of actual holes in the VSCC's of Kr and Xe in these molecular ions, which provide a base with direct access to the inner cores of these atoms. There is a sphere in the VSCC of a free Ng atom over which the electronic charge is maximally concentrated (the radial curvature of $-\nabla^2\rho$ is negative over the entire sphere). Usually upon chemical combination this sphere persists but is no longer uniform, as local maxima and minima are created on its surface. In the case of strong Lewis acids such as BH_3 and carbonium ions, however, this sphere of charge concentration is punctured and reduced to a beltlike structure as found here for Kr and Xe in NgF^+ . In ArF^+ , however, the sphere of charge concentration persists and $\nabla^2\rho$ is negative over the whole of its VSCC. This qualitative difference with KrF^+ and XeF^+ is reflected in the barely negative LUMO energy of ArF^+ , -0.6 eV. Thus the properties of the Laplacian distributions for these compounds, in addition to predicting the formation of the linear adducts, show the Kr and Xe molecular ions to be stronger Lewis acids than is ArF^+ . This conclusion lends credence to the calculations of Frenking et al.,¹⁴ which indicate that $\text{ArF}^+\text{AuF}_6^-$ should possess at least marginal stability in the solid state.

If $\nabla^2\rho(\mathbf{r}) < 0$, then the value of ρ at the point \mathbf{r} is greater than the value of ρ averaged over an infinitesimal sphere centered at \mathbf{r} . The corresponding statement is true in one dimension, and since the charge density is a minimum at the bond critical point along the bond path, the associated curvature of ρ_b , λ_1 , is positive and electronic charge is locally depleted at this point with respect to neighboring points along the bond path. The charge density is, however, a maximum at the critical point in the interatomic surface, the two curvatures of ρ_b perpendicular to the bond path, λ_{\perp} , being negative. Thus electronic charge is locally concentrated at the critical point with respect to the interatomic surface. The formation of a chemical bond and an interatomic surface is, therefore, the result of a competition between the perpendicular contractions of the charge density toward the bond path that lead to a concentration of electronic charge between the nuclei along the bond path and the parallel contraction of ρ that leads to its separate concentration in the basins of the neighboring atoms. The value of the Laplacian at the bond critical point, $\nabla^2\rho_b$, equals the sum of the three curvatures, $\nabla^2\rho_b = 2\lambda_{\perp} + \lambda_1$, and its sign determines which of the two competing effects is dominant in the formation of a given bond. The bonds in the adducts described here cover the spectrum of possible behavior.

When $\nabla^2\rho_b < 0$ and is large in magnitude as for the H–C bond in HCN (Table III), the perpendicular contractions in ρ dominate the interaction and electronic charge is concentrated between the nuclei along the bond path (see Figures 1 and 2) as is also reflected in the relatively large value of ρ_b . The result is a sharing of electronic charge between the nuclei as is found in covalent or slightly polar bonds as in NO , for example. The Laplacian of the charge density appears in the local expression of the virial theorem

$$\frac{1}{4}\nabla^2\rho(\mathbf{r}) = 2G(\mathbf{r}) + V(\mathbf{r}) \quad (3)$$

where $G(\mathbf{r})$, which is always positive, is the kinetic energy density (it yields the electronic kinetic energy $T(\Omega)$ when integrated over the basin of atom Ω) and $V(\mathbf{r})$, which is always negative, is the potential energy density (it yields the electronic potential energy $V(\Omega)$ when integrated over the basin of the atom). Because of the zero flux surface condition, the integration of the Laplacian over an atom vanishes and thus integration of eq 3 yields the virial theorem ($2T(\Omega) + V(\Omega) = 0$) for an atom, free or bound. The

(24) Bader, R. F. W. *Pure Appl. Chem.* 1988, 60, 145.

(25) Gatti, C.; MacDougall, P. J.; Bader, R. F. W. *J. Chem. Phys.* 1988, 88, 3792.

(26) Bader, R. F. W.; MacDougall, P. J.; Lau, C. D. H. *J. Am. Chem. Soc.* 1984, 106, 1594.

(27) Bader, R. F. W.; Gillespie, R. J.; MacDougall, P. J. *J. Am. Chem. Soc.* 1988, 110, 7329.

(28) Bader, R. F. W.; MacDougall, P. J. *J. Am. Chem. Soc.* 1985, 107, 6788.

(29) Carroll, M. T.; Chang, C.; Bader, R. F. W. *Mol. Phys.* 1988, 63, 387.

(30) Bader, R. F. W.; Chang, C. *J. Phys. Chem.*, in press.

(31) Tang, T.-H.; Bader, R. F. W.; MacDougall, P. J. *Inorg. Chem.* 1985, 24, 2041.

total energy density is given by $E(\mathbf{r}) = G(\mathbf{r}) + V(\mathbf{r})$,⁵ and one has another form of the virial theorem, $E(\Omega) = -T(\Omega)$. As a consequence of eq 3, it follows that the total energy density is most negative (most stabilizing) in those regions of space where $\nabla^2\rho < 0$, that is, where electronic charge is concentrated and the potential energy density dominates the local virial relationship. Thus in a shared interaction, the atoms are bound because of the lowering of the potential energy associated with the charge concentration and shared between the nuclei.

In a very polar bond such as CN of HCN, the perpendicular contractions of ρ , as measured by λ_{\perp} , are greater than those for the H-C bond and electronic charge is concentrated between the nuclei to an even greater extent, as demonstrated by the Laplacian distribution in Figure 1 and as reflected in a larger value of ρ_b . However, the electronic charge is unequally shared between the atoms and as a result, the bond critical point is shifted toward the carbon core where the density rises very rapidly and the Laplacian undergoes a change in sign. At the critical point its sign is dominated by λ_1 in spite of large negative values for λ_{\perp} .

These bond characteristics change little on formation of the adducts: ρ_b for C-H remains unchanged and $\nabla^2\rho_b$ decreases by 0.12 au while both quantities decrease by approximately 0.006 au for the C-N bond.

When $\nabla^2\rho_b > 0$ and ρ_b is small in value, one has the other extreme of bonding, one dominated by the contraction of each atomic density toward its own nucleus resulting in a depletion of charge at the critical point and in the interatomic surface. These are called closed-shell interactions as they typify interactions between closed-shell atoms as found in noble-gas repulsive states, ionic bonds, hydrogen bonds, and van der Waals molecules and in the relatively long bonds formed between what are formally closed-shell atoms, as between S atoms in S_4N_4 and S_8^{2+} .^{20,29,31} The depletion of electronic charge in the interatomic surface arises because of the demands of the Pauli principle, and hence these interactions are typified both by a positive value for $\nabla^2\rho_b$ and a low value for ρ_b . In closed-shell interactions the charge concentrations and the associated lowering of the potential energy are separately localized in the basins of each of the atoms.

Reference to Figures 1 and 2 shows that the valence shells of all three atoms in the HCN fragment form one contiguous region of charge concentration—the valence shells of charge concentration (VSCC) are linked together over the H-C and C-N bonds as is typical of shared interactions, polar and nonpolar. For the Ng-N bonds and also for the Ng-F bonds, however, the VSCC's of the individual atoms are not linked. Instead charge is concentrated separately in each atomic basin and there is no shared concentration of charge. The Ng-N bonds result from the interaction of the closed-shell reactants NgF^+ and NCH, and they are examples of the closed-shell type of interaction. The values of ρ_b are small, the same order as found in ionic systems such as KF and NaCl, and $\nabla^2\rho_b$ is positive with $\lambda_1 \gg \lambda_{\perp}$, and both components are relatively small in magnitude (Table III). The mechanism of formation of the relatively long adduct bond Ng-N is similar to the formation of a hydrogen bond.

A hydrogen bond results from a partial penetration of the van der Waals envelope of the H atom of the acid and the base atom B of the base molecule, the strength of the interaction increasing with the degree of mutual penetration. Electronic charge is not concentrated in the interatomic surface as is typical of a shared interaction. Instead, the densities of the H and B atoms are polarized so as to remove density along their line of approach to facilitate the penetration of their nonbonded envelopes with the result that the final density at the H-B bond critical point is approximately equal to the sum of the unperturbed densities of the H and B atoms at their points of penetration.³² These same features characterize the redistribution of charge found to accompany the formation of the Ng-N bonds.

A bonded radius of an atom is defined as the distance from its nucleus to the appropriate bond critical point and is denoted by $r_b(\Omega)$ (Table III). Its nonbonded radius is correspondingly defined

as the distance from the nucleus to some outer contour of the charge density, $r_n(\Omega)$.^{33,34} The contour shown in Figure 1 and used in the determination of the nonbonded radii, the 0.001 au contour, yields molecular sizes and atomic diameters in good agreement with gas-phase van der Waals radii.^{33,35} The bonded radii for the Ng-N bonds are considerably greater than those for the other reactant bonds, including the Ng-F bonds. They result from the partial penetration of the outer van der Waals envelopes of the Ng and N atoms. The extent of this penetration is given by the difference between the nonbonded radii of the Kr, Xe, and N atoms in the reactants, $r_n(\Omega)$ equaling 3.43, 3.72, and 3.58 au, respectively, and the corresponding bonded radii of the Ng-N bonds (Table III). These changes in radii are given in Table III. The strength of a hydrogen bond in general parallels the degree of penetration of the van der Waals envelopes.³² The total penetrations are 2.65 and 2.72 au for the Kr and Xe adducts, respectively. The greater penetration of the Xe atom and its greater total value are in agreement with its slightly greater energy of formation. The total penetration of 1.80 au encountered in the formation of the hydrogen-bonded complex FH-NCH is considerably less, as is its energy of formation of ≈ 6 kcal/mol. Also listed in Table III under ρ_b^0 is the sum of the values of the unperturbed densities of the isolated reactants at their points of penetration, i.e., at the positions determined by the values of the bonded radii in the adducts. It is a characteristic of bonds resulting from the penetration of closed-shell distributions that the value of ρ at the bond critical point differs little in value from the sum of the unperturbed reactant densities evaluated at the point of penetration, like the average value of 0.005 au found here. (The value of ρ_b^0 is 0.0177 au for the hydrogen bond in FH-NCH compared to a value of 0.0183 au for ρ_b .)

This analysis yields a picture of adduct or hydrogen-bond formation that corresponds to the mutual penetration of the outer diffuse nonbonded densities of the appropriate atoms of the base and acid molecules, with the final density at the bond critical point being only slightly greater than the sum of the unperturbed densities. Unlike a shared or covalent interaction, there is no concentration of charge density in the interatomic surface and along the bond path. The final density is instead determined primarily by the extent of penetration—the greater the penetration the larger the value of ρ_b and the stronger the resulting bond. The analysis of the atomic properties given below shows that both the Ng and N atoms of the reactants polarize in such a way as to facilitate this mutual penetration of their closed-shell density distributions.

The Ng-F bonds in the reactants NgF^+ , including ArF^+ for an extended comparison, are intermediate between the two extremes of bonding and are similar in their characteristics to the bond in the isoelectronic F_2 molecule (Table III). This is particularly true for the first member of the series ArF^+ in which the valence electrons are nearly equally shared between the two atoms (Table IV), the net charge on Ar being close to +1. The net charge of atom Ω , $q(\Omega)$, is defined as the difference between its nuclear charge and its average number of electrons, $N(\Omega)$, the latter being obtained by an integration of the charge density over the basin of the atom.

$$q(\Omega) = Z_0 - N(\Omega) = Z_0 - \int_{\Omega} \rho(\mathbf{r}) d\tau \quad (4)$$

The positive charge on the Ng atom increases in the order $Ar < Kr < Xe$, and their bond characteristics exhibit a corresponding shift toward the closed-shell limit. While the charge density is contracted toward the bond path, leading to a significant value for ρ_b for F_2 and ArF^+ , the interactions are increasingly dominated through the series by the separate localization of electronic charge in the basins of each of the atoms. Not only do the F and Ng

(32) Carroll, M. T.; Bader, R. F. W. *Mol. Phys.* 1988, 65, 695.

(33) Bader, R. F. W.; Henneker, W. H.; Cade, P. E. *J. Chem. Phys.* 1967, 46, 3341.

(34) Bader, R. F. W.; Boddall, P. M.; Cade, P. E. *J. Am. Chem. Soc.* 1971, 93, 3095.

(35) Bader, R. F. W.; Carroll, M. T.; Chiriacman, J. R.; Chang, C. J. *Am. Chem. Soc.* 1987, 109, 7968.

atoms bind their densities tightly but also the charge is physically localized within the boundaries of each atom.²⁰ Thus even in F₂ the intraatomic Fermi correlation is pronounced, the electrons are 93% localized within the basins of the separate atoms, compared to a value of 73% in a molecule such as C₂.³⁶ Such localization of charge, while providing the major source of binding in fluorides via a charge transfer to fluorine, is the antithesis of that required for the sharing of electronic charge through the mechanism of exchange as found in a homopolar bond such as F₂. Thus the bonds in F₂ and ArF⁺ are relatively weak. This analysis leads one to conclude that the bond strengths should increase with the degree of charge transfer in the order F₂ ≈ ArF⁺ < KrF⁺ < XeF⁺. This conclusion is supported by the known dissociation energies, which in kcal/mol are 37.0,³⁷ ≥38, ≥36.4, and 46.8,³⁸ respectively. Liu and Schaefer¹² have calculated a value of 43.8 kcal/mol for KrF⁺.

The Ng-F bonds of the molecular ions are only slightly perturbed on forming the adducts with HCN. Their bond lengths increase by 0.014 and 0.018 Å for Kr and Xe species, respectively, with corresponding small decreases in the values of ρ_b, of 0.005 and 0.008 au, and increases in the values of ∇²ρ_b to 0.195 and 0.348 au. These changes are consistent with a weakening of the Ng-F bond and to a slight shift in its characteristics toward the closed-shell limit on formation of the adduct. There is a small shift in electronic charge from Ng to F (Table V). The same changes are found for the H-A bond of an acid in the formation of a hydrogen bond.

These same bonds (Ng-F) are perturbed to a much greater extent on the formation of the adducts with F⁻ and so is the shift toward the closed-shell limit of bonding in agreement with the experimental characterization of these bonds. The values of ρ_b and ∇²ρ_b are decreased and increased, respectively. While the increase in the value of the Laplacian is quite small for the Xe adduct, the ratio of the parallel to the perpendicular contractions of ρ as measured by λ₁/λ_⊥, increases significantly for both adducts from 2.5 to 3.6 and from 3.9 to 4.8 for the Kr and Xe compounds, respectively. Except for XeF₂, the Ng atoms are predicted to undergo small decreases in electron population on formation of the adducts. While this might appear to be at variance with the general conclusion that the Ng atom becomes more shielded as the base strength increases, as exemplified by ¹²⁹Xe chemical shift data given in Table II, this is not the case because small changes in population do not necessarily reflect corresponding changes in the screening of a nucleus. A more direct indicator of nuclear shielding is the quantity V_{ao}(Ω), the attraction of a nucleus for the electronic charge density in its own basin. An increase in the magnitude of this quantity, in spite of a loss of charge for the atom, implies that the density is more contracted toward the nucleus and hence is bound more tightly—and provides greater shielding. The magnitudes of V_{ao}(Kr) relative to its value in KrF⁺ are greater by 20.1 and 52.0 kcal/mol for the HCN and F⁻ adducts, respectively, in accord with the trend established in Table II. The properties of ρ at the bond critical point and of the atoms clearly indicate that the Ng-F bonds in the HCN adducts are intermediate in character between those for Ng-F⁺ and for NgF₂.

Changes in Atomic Properties

In addition to the net charges on the atoms, Table IV lists the first and second moments of the atoms in the reactants and Table V gives the changes in the atomic properties on forming the adducts. The charge q(Ω) of atom Ω is defined in eq 4. The first moment μ(Ω) measures the dipolar polarization of the atomic density and is defined as

$$\mu(\Omega) = - \int_{\Omega} r_{i0} \rho(r) d\tau \quad (5)$$

where the position vector r_{i0} is centered at the nucleus of atom Ω. The diagonal element of the quadrupole moment of an atomic distribution for the z axis is

$$Q_{zz}(\Omega) = - \int_{\Omega} \rho(r) (3z^2 - r_{i0}^2) d\tau \quad (6)$$

with corresponding definitions for the other diagonal elements. Each of the diagonal elements, which sum to zero, has the form of the familiar d_{z²} orbital. For a spherical charge distribution, each equals zero. For the linear molecules considered here with z as the internuclear axis, -1/2 Q_{zz}(Ω) = Q_{xx}(Ω) = Q_{yy}(Ω). A positive value for Q_{zz}(Ω) implies that electronic charge is removed from along the internuclear axis and concentrated in a toruslike distribution about the axis. The quadrupole moment is the density complement of an orbital π population. Thus in acetylene, Q_{zz}(C) is large and positive, equal to +4.14 au, corresponding to an accumulation of π density in a torus about the z axis. In benzene and ethylene, with z perpendicular to the plane of the nuclei, Q_{zz}(C) is large and negative corresponding to the presence of one π electron per atom. The magnitude of Q_{zz}(C) for the para carbon atom in substituted benzenes varies in a linear manner with its integrated π population,³⁰ from a maximum value in phenoxide ion to a minimum in nitrobenzene.

The charge on the Ng atom in NgF⁺ increases from ≈+1 for Ar to +1.4 for Xe, and there is an accompanying increase in the polarizations of the density of the Ng atom away from the increasingly negatively charged F atom. It is a general result that atoms are polarized in a direction counter to the direction of charge transfer. Thus the N, C, and H atoms are all polarized in the direction N to H, because of the transfer of negative charge to N.

In forming a hydrogen bond AH-BX between an acid AH and a base BX, there is a small transfer of charge from the base to the acid. Within the acid itself, there is a still smaller loss of charge from H and a slightly larger gain in charge for the base atom B. There is thus a net transfer of charge from X to A. Both the H and B atoms polarize in such a way as to facilitate their mutual interpenetration: the polarization of H away from A is decreased, while the polarization of B toward X is increased. The quadrupolar polarizations of both H and B are increased, corresponding to a promotion of density from along the internuclear axis in the direction of approach to a torus of charge about the axis. This corresponds to a promotion of σ to π density. In the formation of FH-NCH, which has a relatively small energy of formation of ≈6 kcal/mol, the changes in populations of the acid atoms are Δq(F) = -0.038 and Δq(H) = +0.021 and in the atoms of the base are Δq(N) = -0.039 and Δq(C) = +0.056, while the changes in quadrupole for the HCN fragment are ΔQ_{zz}(N) = 0.220 au, ΔQ_{zz}(C) = -0.226 au, and ΔQ_{zz}(H) = -0.017 au.

Precisely the same changes in charge and polarizations accompany the formation of the rare-gas adducts, as can be seen from Table V. The F atom gains more electronic charge than the Ng atoms lose, and the N atom gains less electronic charge than the CH fragment loses. There is thus a net transfer of charge from the CH fragment to F as in the formation of a hydrogen bond. (The loss of charge from the CH fragment of the base is remarkably similar for the two adducts, as is the fact that both atoms lose the same amount of charge.) In both adducts the polarization of the Ng atoms away from F is decreased and the polarization of the N atom toward the CH fragment is increased. Finally, the value of Q_{zz}(Ω) is increased for both the Ng and N atoms and decreased for the remaining atoms, indicating that the dipolar and quadrupolar polarizations are such as to remove density from the Ng-N internuclear region and along their internuclear axis so as to facilitate the approach of two closed-shell systems.

These same polarizations are reflected in the changes of the Laplacian distributions upon adduct formation. The magnitude of the nonbonded charge concentration on the N atom is decreased from 3.4 au in HCN to 2.8 au in the adducts. The maximum magnitude attained in the vestigial belt of charge concentration in the VSCC's of the Ng atoms increases from 0.08 to 0.10 au for Kr and from 0.03 to 0.04 au for Xe, while the magnitude of the toroidal belt encompassing the axis on the N atom increases from 0.72 au in HCN to 0.89 au in the adducts. The same belt for the carbon atom, which loses π density on adduct formation¹²

(36) Bader, R. F. W.; Stephens, M. E. *J. Am. Chem. Soc.* 1975, 97, 7391.

(37) Darwent, B. de B. NBS Pub. NSRDS-NBS 31, 1970.

(38) Berkowitz, J.; Chupka, W. A. *Chem. Phys. Lett.* 1970, 7, 447.

and for which $\Delta Q_{zz}(C) < 0$, decreases in magnitude, from 0.72 au in HCN to 0.46 au in the adducts. Similar behavior is observed for the F atoms where the belt of charge concentration in its VSCC (see Figure 1) decreases in magnitude from 14.3 to 13.1 au for the Kr system, and from 12.9 to 11.8 for the Xe system.

The energy of an atom in a molecule is defined using the atomic statement of the virial theorem.^{4,5,24} These theoretical energies agree with the experimentally measurable additive energies of the methyl and methylene groups in the saturated hydrocarbons,^{39,40} thereby showing, together with their properties, that these atoms are the atoms of chemistry. Because the virial theorem is not satisfied to the same degree for HCN alone as it is for NgF^+ and their HCN adducts, the changes in the atomic energies cannot be discussed for reaction 1.³⁹ This difficulty is not encountered for the molecules involved in the formation of NgF_2 , and the changes in the energies of the Ng and F atoms for reaction 2 are listed in Table V.

The energies of reaction 2 are dominated by the changes in the energies of the Ng atoms, and the same qualitative result is obtained for the formation of the HCN adducts. The considerable increase in stability of these atoms is not a result of charge-transfer effects, which are small and correspond to a slight loss in charge for Kr, but rather are a result of a reorganization of the charge within the Ng atoms and their interaction with the base atoms. As noted above, the charge density of the Kr atom in KrF^+ is contracted toward the nucleus in forming an adduct. In the case of KrF_2 this results in a contribution of 52 kcal/mol to the stabilization of the Kr atom, in spite of its loss of charge. This contraction is also evident in the change in the volume of the Kr atom on adduct formation, from $187 a_0^3$ in KrF^+ to $169 a_0^3$ in KrF_2 .⁴¹ Further stabilization results from the interaction of the density on the Ng atom with the nucleus of the base atom. These increased attractive interactions outweigh the increased destabilizing effects, the interatomic electron repulsions being minimized by the dipolar and quadrupolar polarizations of the densities of the Ng atoms as described above.

The considerable decrease in the energies of the Ng atoms on formation of a Lewis acid-base adduct is predicted by the theory of atoms in molecules is the quantum equivalent of the classical description of the interaction in terms of a large polarizable atom in the negative field of the base atom. The reason why the adducts of HCN with KrF^+ and XeF^+ are considerably more stable than the adduct formed with the acid HF are quantitatively accounted for by comparing the properties of the Ng atoms with those of H. The net positive charge on H is only 0.75 compared to 1.15 and 1.41 for Kr and Xe, respectively, in the three fluorides. The

charge distribution of HF is dominated by the electronegative F, making the density on H difficult to polarize. The change in dipolar polarization of H on formation of FH-NCH is 0.02 au, 25–45 times smaller than that for the Ng atoms. The quadrupolar polarization of the H atom is similarly very slight, $\Delta Q_{zz}(\text{H}) = 0.07$ au, compared to a promotion of axial to toroidal density corresponding to changes of 1.0–2.0 au in the $Q_{zz}(\Omega)$ values of the Ng atoms. The H of HF is a much "harder" atom than the Ng atoms, as is also reflected in the relatively small value of 0.79 au for the penetration of its van der Waals envelope in its reaction with HCN. As a result, the energy change for the H atom on hydrogen bond formation is small and, since it is dominated by a loss in charge, destabilizing.³²

A comparison of the Laplacian distributions for the NgF^+ ions and HF^{20} also show that the Kr and Xe atoms in NgF^+ are stronger Lewis acids than H of HF. The Laplacian distribution for HF^{20} exhibits a single, continuous valence shell of charge concentration (VSCC) that encompasses the proton. There is a small local minimum in the valence shell of charge depletion located 0.72 au from the proton, as opposed to the presence of an actual hole in the VSCC of the Ng atoms, which, as discussed above and illustrated in Figures 1 and 2, lays bare to an approaching base the field of the central core of these atoms. Thus, in addition to the decrease in the magnitude of the nonbonded charge concentration on the nitrogen atom on adduct formation, there is an increase in the penultimate shell of charge concentration of the Ng atoms, corresponding to the third quantum shell in Kr (Figure 1) and to the fourth shell in Xe. These are the shells exposed by the holes in the valence shells of charge concentration in the Ng atoms (Figure 2). According to eq 3, which shows that the sign of the Laplacian determines the local departures of the kinetic and potential energy densities from their average ratio of 2:1, a Lewis acid-base reaction corresponds to the combination of a region with excess kinetic energy (the local charge depletion on the acid) with a region of excess potential energy (the local charge concentration on the base). It is the transfer of nonbonded charge from the VSCC on the N atom to the tightly bound inner quantum shell of charge concentration of the Kr or Xe atom as made possible by their dipolar and quadrupolar polarizations that results in the dramatic lowering in the energies of these atoms on adduct formation.

Acknowledgment is made to the donors of the Petroleum Research Fund, administered by the American Chemical Society, for partial support of this research (P.J.M. and R.F.W.B.). This research was also sponsored by the U.S. Air Force Astronautics Laboratory, Edwards Air Force Base, California, Contract 49620-87-C-0049 (G.J.S.), and a Natural Sciences and Engineering Research Council of Canada operating grant (G.J.S.).

Registry No. Kr, 7439-90-9; Xe, 7440-63-3; N₂, 7727-37-9; F₂, 7782-41-4; ArF⁺, 11089-94-4; KrF⁺, 11088-74-7; XeF⁺, 47936-70-9; KrF₂, 13773-81-4; XeF₂, 13709-36-9; FKrNCH⁺, 118494-40-9; FXeNCH⁺, 118494-41-0; HCN, 74-90-8; F⁻, 16984-48-8.

(39) Wiberg, K. B.; Bader, R. F. W.; Lau, C. D. H. *J. Am. Chem. Soc.* **1987**, *109*, 1001.

(40) Bader, R. F. W. *Can. J. Chem.* **1986**, *64*, 1036.

(41) The volume of an atom is a measure of the region of space enclosed by the union of the atom's interatomic surfaces and the 0.001 au density envelope.

Krypton Bis[pentafluoro-oxotellurate(vi)], $\text{Kr}(\text{OTeF}_5)_2$, the First Example of a Kr–O Bond

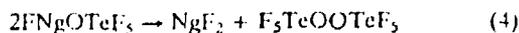
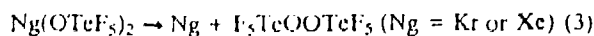
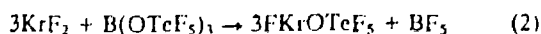
Jeremy C. P. Sanders and Gary J. Schrobilgen*

Department of Chemistry, McMaster University, Hamilton, Ontario L8S 4M1, Canada

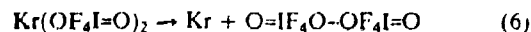
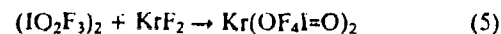
Krypton bis[pentafluoro-oxotellurate(vi)] provides the first example of a species containing a krypton–oxygen bond and has been prepared by the reaction of KrF_2 with natural abundance and ^{17}O -enriched $\text{B}(\text{OTeF}_5)_3$ at -90 to -112°C in SO_2ClF solvent; characterization of the thermally unstable $\text{Kr}(\text{OTeF}_5)_2$ and its decomposition products has been achieved using ^{19}F and ^{17}O n.m.r. spectroscopy.

It is only recently that the chemistry of krypton has been extended beyond the Kr–F bonded species KrF_2 ,¹ KrF^+ , and $\text{Kr}_2\text{F}_3^{+2}$ to include the Kr–N bonded cations $\text{HC}\equiv\text{N}-\text{KrF}^+$ ³ and $\text{R}_F\text{C}\equiv\text{N}-\text{KrF}^+$ ($\text{R}_F = \text{CF}_3$, C_2F_5 , $n\text{-C}_3\text{F}_7$)⁴ which are thermally unstable above -50°C . With the extension of the chemistry of Kr^{II} to Kr–N bonds, it seemed likely that a suitable strongly electron withdrawing oxygen ligand might afford a Kr–O bond, albeit thermally unstable.

A previous published attempt to form Kr–O bonds reports the reaction of KrF_2 with $\text{B}(\text{OTeF}_4)_3$ in ClO_3F at -100°C for 16 h followed by a further 3 h at -78°C .⁵ However, instead of the anticipated products being formed according to equations (1) and (2), the ^{19}F n.m.r. spectrum of the sample only revealed resonances attributable to $\text{F}_5\text{TeOOTeF}_5$ and the solvent. Similar results have been obtained in this laboratory for the reaction of KrF_2 with $\text{B}(\text{OTeF}_5)_3$ in SO_2ClF at -78°C for several minutes.⁶ In contrast, the reaction of XeF_2 with $\text{B}(\text{OTeF}_5)_3$ yields the thermally stable $\text{Xe}(\text{OTeF}_5)_2$.⁷ It was proposed that the $\text{F}_5\text{TeOOTeF}_5$ resulted from the decomposition of the intermediates, FKrOTeF_5 or $\text{Kr}(\text{OTeF}_5)_2$, according to equations (3) and (4).⁵



The interaction of KrF_2 and $(\text{IO}_2\text{F}_3)_2$ in SO_2ClF solvent has also been reported to lead to peroxide formation at -45°C by the route proposed in equations (5) and (6).⁸ The series of adducts $\text{XeF}_2 \cdot n\text{WOF}_4$ ($n > 2$) undergo bond isomerization to give equilibrium mixtures of $\text{FXeF} \cdots \text{WOF}_4(\text{WOF}_4)_{n-1}$ and $\text{FXe-O-WF}_5(\text{WOF}_4)_{n-1}$ in SO_2ClF solvent while the MoOF_4 adducts and their KrF_2 analogues only exist as the $\text{FNg-F} \cdots \text{MoOF}_4(\text{MoOF}_4)_{n-1}$ structures.⁹ While it was thought that the reaction between KrF_2 and WOF_4 might lead to Kr–O bonded species, these mixtures, unlike their F bridged Mo analogues, are remarkably unstable, decomposing above -100°C in SO_2ClF to Kr, O_2 , WF_6 , and WOF_4 .⁹ Again, it was proposed that a Kr–O bonded structure may be an intermediate in the decomposition.



The thermolyses of $\text{Xe}(\text{OTeF}_5)_2$ and FXeOTeF_5 have been reinvestigated in glass at 160°C in the present study and shown to yield almost quantitatively $\text{F}_5\text{TeOOTeF}_5$ and Xe, and $\text{F}_5\text{TeOOTeF}_5$ and XeF_2 , according to equations (3) and (4), respectively. Contrary to previous reports in which the thermolyses of the two xenon compounds had been carried out in a Monel vessel at 130°C ,^{10,11} only traces of $\text{F}_5\text{TeOOTeF}_5$ (<2%) and other members of the series $\text{TeF}_n(\text{OTeF}_5)_{6-n}$ were observed for the thermolyses in glass tubes. These findings suggested that analogous decompositions of

Table 1. ^{17}O and ^{19}F n.m.r. parameters for $\text{Kr}(\text{OTeF}_5)_2$ and related species.^a

Species	Chemical shifts ^b			$^2J_{\text{F-F}}$ /Hz	T/°C
	$\delta(^{17}\text{O})$	$\delta(^{19}\text{F})$			
		A	B ₄		
$\text{F}_5\text{TeOOTeF}_5^c$	314.5 (314.6)	-50.8 (-52.4)	-52.3 (-53.1)	(200)	-110 (30)
$\text{F}_5\text{TeOTeF}_5$	140.7	-49.1	-39.2	182	-70
$\text{Xe}(\text{OTeF}_5)_2^d$	152.1	-42.6	-45.3	183	-16
FXeOTeF_5^d	128.8	-40.8	-46.7	180	-16
$\text{Kr}(\text{OTeF}_5)_2$	95.2	-42.1	-47.2	181	-90

^a Recorded in SO_2ClF solvent. ^b Chemical shifts were referenced with respect to H_2O (^{17}O) and CFCl_3 (^{19}F). ^c Parentheses denote n.m.r. parameters obtained from a sample of the pure material in SO_2ClF . ^d N.m.r. parameters obtained from samples of the pure material in SO_2ClF .

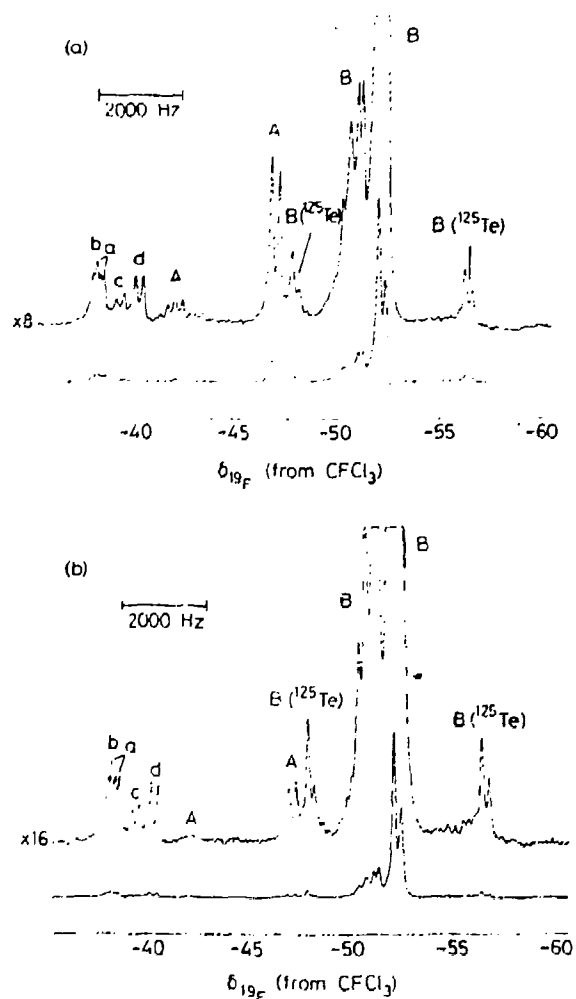


Figure 1. ^{19}F N.m.r. spectra (470.599 MHz) of KrF_2 (excess) and $\text{B}(\text{OTeF}_5)_3$ in SO_2ClF solution at -110°C . (a) Spectrum obtained immediately after placing sample in probe: (A) AB_4 spectrum of $\text{Kr}(\text{OTeF}_5)_2$; (B) AB_4 spectrum of $\text{F}_5\text{TeOOTeF}_5$ with accompanying ^{125}Te (6.99%, $I = 1/2$) satellites. (a,b,c,d) B_4 parts of AB_4 spectra arising from species in the series $\text{TeF}_n(\text{OTeF}_5)_{6-n}$. (b) Spectrum obtained at -110°C after warming sample to -78°C for 3 min depicting the substantially diminished intensity of the $\text{Kr}(\text{OTeF}_5)_2$ resonances (A).

FKrOTeF_5 and/or $\text{Kr}(\text{OTeF}_5)_2$, but at much lower temperatures, may be responsible for the formation of $\text{F}_5\text{TeOOTeF}_5$ resulting from the reaction of KrF_2 and $\text{B}(\text{OTeF}_5)_3$. These findings prompted the reinvestigation of reactions (1) and (2) at lower temperatures with the view to providing definitive evidence for FKrOTeF_5 and/or $\text{Kr}(\text{OTeF}_5)_2$.

The reaction of $\text{B}(\text{OTeF}_5)_3$ and 21% ^{17}O enriched $\text{B}(\text{OTeF}_5)_3$ with KrF_2 at -110°C was monitored in SO_2ClF by both high-field ^{19}F (470.599 MHz) and ^{17}O (67.801 MHz) n.m.r. spectroscopy. Owing to the increased dispersion afforded in the ^{19}F spectra at 11.744 T, it was possible to observe a new AB_4 pattern to high frequency of the AB_4 pattern of $\text{F}_5\text{TeOOTeF}_5$ (Figure 1) and this new pattern is assigned to $\text{Kr}(\text{OTeF}_5)_2$. The AB_4 pattern of this species resembles the corresponding AB_4 spectra of $\text{Xe}(\text{OTeF}_5)_2$ and FXeOTeF_5 in that the A part occurs to high frequency of the B_4 part and the A part is well separated from the B_4 part at an external field strength of 11.744 T (Table 1). Furthermore, the new AB_4 pattern cannot be attributed to any of the species in the $\text{BF}_n(\text{OTeF}_5)_{6-n}$ series, since the ^{19}F n.m.r. spectrum of a sample containing BF_3 and $\text{B}(\text{OTeF}_5)_3$ in a 1:1 mole ratio in SO_2ClF reveals that, although the AB_4 spectra of the mixed species occur in the region -45 to -48 p.p.m., the A parts of the spectra are almost coincident with the B_4 parts. The absence of these species in the $\text{KrF}_2/\text{B}(\text{OTeF}_5)_3$ reaction mixture is corroborated by the fact that the F-on-B region of the ^{19}F spectrum shows only a single resonance attributable to BF_3 (-126.8 p.p.m.). The signals ascribed to $\text{Kr}(\text{OTeF}_5)_2$ slowly diminished at -90°C and rapidly decreased upon warming to -78°C for 3 min, yielding Kr and additional $\text{F}_5\text{TeOOTeF}_5$ (Figure 1). However, a new F-on-Kr signal was not observed in these spectra, ruling out the formation of FKrOTeF_5 . The ^{19}F n.m.r. spectrum also showed four weak doublets in the region -38.2 to -40.3 p.p.m. These have been assigned to the B_4 parts of the AB_4 spectra arising from species in the series $\text{TeF}_n(\text{OTeF}_5)_{6-n}$, by comparison with ^{19}F n.m.r. data obtained at 470.599 MHz for solutions of $\text{TeF}_n(\text{OTeF}_5)_{6-n}$ in SO_2ClF and with the literature data for these species.^{12,13} The weaker A parts of the AB_4 patterns were not identified since they are obscured by the AB_4 pattern of $\text{F}_5\text{TeOOTeF}_5$. The formation of small amounts of the $\text{TeF}_n(\text{OTeF}_5)_{6-n}$ species is analogous to the results obtained for the high-temperature decompositions of FXeOTeF_5 and $\text{Xe}(\text{OTeF}_5)_2$. The ^{17}O n.m.r. spectrum of the $\text{KrF}_2/\text{B}(\text{OTeF}_5)_3$ reaction mixture also yielded a new ^{17}O resonance to low frequency of the $\text{F}_5\text{TeOOTeF}_5$ resonance (Table 1). The new resonance displayed analogous behaviour to the new ^{19}F resonance when the sample was warmed and is assigned to

$\text{Kr}(\text{OTeF}_5)_2$. The new ^{19}F and ^{17}O chemical shifts are consistent with the OTeF_5 ligands possessing more ionic character than in their FXeOTeF_5 and $\text{Xe}(\text{OTeF}_5)_2$ analogues, whose ^{17}O chemical shifts are reported here for the first time (Table I).¹² Thus, the ^{17}O resonance of $\text{Kr}(\text{OTeF}_5)_2$ appears at the lowest frequency in this series.

In contrast to the reaction of XeF_2 with one third the stoichiometric amount of $\text{B}(\text{OTeF}_5)_3$, which yields an equilibrium mixture of XeF_2 , FXeOTeF_5 , and $\text{Xe}(\text{OTeF}_5)_2$ in SO_2ClF , the reaction of a three-fold excess of KrF_2 with $\text{B}(\text{OTeF}_5)_3$ has failed to produce any direct evidence for FKrOTeF_5 formation. Instead, $\text{Kr}(\text{OTeF}_5)_2$, Kr , and $\text{F}_5\text{TeOOTeF}_5$ with traces of $\text{TeF}_n(\text{OTeF}_5)_{6-n}$ were observed when the reaction was allowed to proceed at -90 to -110°C in SO_2ClF . The high solubility of $\text{B}(\text{OTeF}_5)_3$ relative to KrF_2 in SO_2ClF at the low temperatures required to stabilize $\text{Kr}(\text{OTeF}_5)_2$ presumably serves to maintain $\text{B}(\text{OTeF}_5)_3$ in excess, preventing the formation and observation of FKrOTeF_5 .

The thermolysis of $\text{Kr}(\text{OTeF}_5)_2$ has been found to be analogous to that found for $\text{Xe}(\text{OTeF}_5)_2$, but occurs rapidly at considerably lower temperatures. It is therefore not surprising that the species was not observed under the previously reported reaction conditions and at the low dispersion field strengths used to observe the ^{19}F n.m.r. spectra.

In view of these findings further attempts to synthesize additional examples of $\text{Kr}-\text{O}$ bonded species are presently underway in this laboratory.

This research was sponsored by the United States Air Force Astronautics Laboratory, Edwards Air Force Base, California (Contract F49620-87-C-0049) and a Natural Sciences and Engineering Research Council of Canada (N.S.E.R.C.C.) operating grant.

Received, 14th June 1989; Com. 9102501D

References

- 1 F. Schreiner, J. G. Malin, and J. S. Hindman, *J. Am. Chem. Soc.*, 1965, **87**, 25.
- 2 R. J. Gillespie and G. J. Schrobilgen, *Inorg. Chem.*, 1976, **15**, 22.
- 3 G. J. Schrobilgen, *J. Chem. Soc., Chem. Commun.*, 1988, 863.
- 4 G. J. Schrobilgen, *J. Chem. Soc., Chem. Commun.*, 1988, 1506.
- 5 E. Jacob, D. Lentz, K. Seppelt, and A. Simon, *Z. Anorg. Allg. Chem.*, 1981, **472**, 7.
- 6 N. Keller and G. J. Schrobilgen, unpublished observations.
- 7 K. Seppelt, *Angew. Chem., Int. Ed. Engl.*, 1982, **21**, 877.
- 8 R. G. Syvret, Ph.D. Thesis, McMaster University, 1985.
- 9 J. H. Holloway and G. J. Schrobilgen, *Inorg. Chem.*, 1981, **20**, 3363.
- 10 F. Sladky, *Monatsh. Chem.*, 1970, **101**, 1559.
- 11 F. Sladky, *Monatsh. Chem.*, 1970, **101**, 1571.
- 12 D. Lentz, H. Pritzkow, and K. Seppelt, *Inorg. Chem.*, 1978, **17**, 1926.
- 13 R. Damerius, P. Huppmann, D. Lentz, and K. Seppelt, *J. Chem. Soc., Dalton Trans.*, 1984, 2821.
- 14 J. C. P. Sanders and G. J. Schrobilgen, *Inorg. Chem.*, to be submitted for publication.

PART V

XENON(II) ADDUCT-CATIONS OF $\text{N}\equiv\text{SF}_3$ AND THE SOLVOLYTIC
BEHAVIOR OF FXe-NSF_3^+ ; THE $\text{LXe-N}\equiv\text{SF}_3^+$ ($\text{L} = \text{F}, \text{OSeF}_3$),
 $\text{FXe-N(H}_2\text{)SF}_5^+$ and FXe-N(H)=SF_4^+ CATIONS

SECTION I. REACTIONS OF NOBLE-GAS CATIONS WITH THE LEWIS BASE $N\equiv SF_3$;

EXAMPLES OF NOVEL BONDING SITUATIONS IN NOBLE-GAS CHEMISTRY

INTRODUCTION

General Criteria Required for Ligands Bonded to Xenon

There are two general classes of ligands which are suitable for stabilizing noble gases in their positive oxidation states, those derived from protonic acids which also exist as stable anions, and neutral Lewis base species. An "anion-type" ligand must possess properties which renders it resistant to redox degradation if it is to withstand the high electron affinity associated with the positive formal oxidation state of the noble gas it is bonded to. Using the following criteria, a ligand of this class

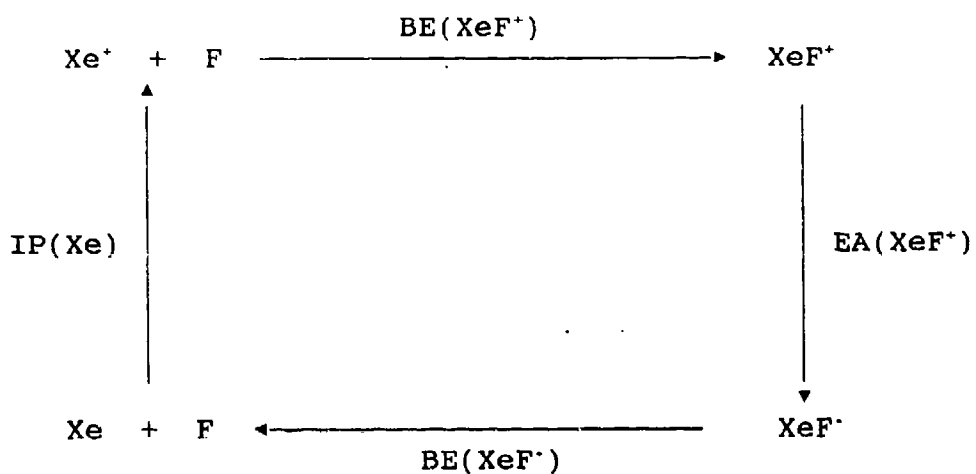
1. must have a high effective group electronegativity,
2. usually exists as a moderate to strong monoprotic acid,
3. should exist as a stable anion in alkali metal salts,
4. should form a positive chlorine derivative.

For example, in the case of $FXeOTeF_5$, $Xe(OTeF_5)_2$ and $Kr(OTeF_5)_2$, the precursor acid, $HOTeF_5$, its alkali metal salts $M^+OTeF_5^-$ and the chlorine derivative $ClOTeF_5$ are known.

Neutral Lewis base-type ligands must meet somewhat modified requirements in order to serve as a suitable noble-gas ligand

1. the base should possess a first adiabatic ionization potential greater than the electron affinity of the strongly oxidizing noble-gas cation, and
2. the ligand must be basic enough to donate a lone pair to the noble-gas cation.

The electron affinity of the cation XeF^+ has been estimated to be 10.9 eV¹ using a modified form of the Born-Haber cycle (Figure 1), while that of KrF^+ is estimated at 13.2 eV¹ using a similar approach.² In xenon(II) cations, their electron affinity decreases as the electronegativity of the stabilizing ligand decreases. Therefore, the electron affinity trend for these cations is $\text{KrF}^+ > \text{XeF}^+ > \text{XeOSeF}_5^+ > \text{XeOTeF}_5^+$. Using the estimated electron affinities, one can generate a list of ligands which, based solely on their first adiabatic ionization potentials, should serve as a guide for forecasting which ligands are stable to redox degradation by these noble-gas cations (Table 4).



$$\text{EA}(\text{XeF}^+) = \text{IP}(\text{Xe}) + \text{BE}(\text{XeF}^-) - \text{BE}(\text{XeF}^+)$$

$$\text{IP}(\text{Xe}) = 12.1 \text{ eV}$$

$$\text{BE}(\text{XeF}^+) \approx 2.1 \text{ eV} = 2.03 \text{ eV (gas phase)}$$

$$\text{BE}(\text{XeF}^-) \approx 0.86 \text{ eV}$$

$$\text{EA}(\text{XeF}^+) \approx 10.9 \text{ eV}$$

Figure 1. Estimation of the electron affinity of XeF^+ .

Table 4. Ionization Potentials of Some Organic and Inorganic Ligands (eV)

Compound	1 st IP	Ref.	Compound	1 st IP	Ref.
CF ₃ C≡N	13.90	a	ND ₃	11.52	j
(C≡N) ₂	13.80	b	s-C ₃ F ₃ N ₃	11.50	k
HC≡N	13.59	c	ND ₂ H	11.47	j
trans-N ₂ F ₂	13.10	d	NCC≡CCN	11.45	l
CH ₂ FC≡N	13.00	e	NCC≡CC≡CCN	11.40	l
CH ₂ ClC≡N	12.90	e	S(C≡N) ₂	11.32	m
CF ₃ N≡C	12.60	a	CH ₃ N≡C	11.30	a
N≡SF ₃	12.50	f	CH ₃ C≡CH	11.24	b
ClC≡N	12.49	g	IC≡N	10.98	g
CHF ₂ C≡N	12.40	e	H ₂ NC≡N	10.76	n
CD ₃ C≡N	12.24	h	B-B ₃ H ₃ F ₃ N ₃	10.46	k
CHCl ₂ C≡N	12.20	e	NH ₃	10.34	o
CH ₃ C≡N	12.19	h	C ₅ F ₅ N	10.08	k
N ₂ F ₄	12.04	i	C ₃ H ₆ N ₃	10.07	p
BrC≡N	11.95	g	C ₆ F ₅ H	10.00	q
C ₂ H ₅ C≡N	11.85	b	CF ₃	9.25	r
N≡SF	11.82	f			

* Bock, H; Dammel, R. and Lentz, D., Inorg. Chem., 1984, 23, 1535.

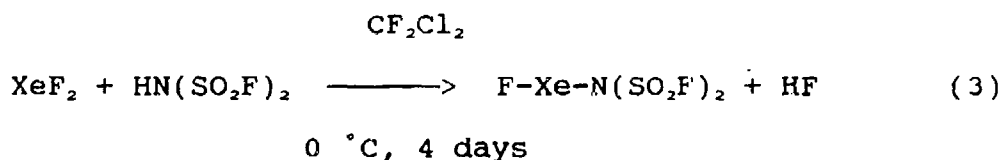
^b Field, F.H. and Franklin, J.L., "Electron Impact Phenomena and the Properties of Gaseous Ion", 1954.

^c Dibeler, V.H. and Liston, S.K., J. Chem. Phys., 1968, 48, 4765.

- ^a Herron, J.H. and Dibeler, V.H., J. Res. Nat. Bur. Standards, 1961, A 65, 405.
- ^a Van der Kelen, G.P. and DeBievre, P.J., Bull Soc. Chim., Belg., 1961, 64, 379.
- ^c Beach, D.B., Jolly, W.L., Mews, R. and Waterfeld A., Inorg. Chem., 1984, 23, 4080.
- ^g Herron, J.T. and Dibeler, V.H., J. Am. Chem. Soc., 1960, 82, 1555.
- ^h Rider, D.M., Ray, G.W. Darland, E.J. and Lero, G.E., J. Chem. Phys., 1981, 74, 1652.
- ⁱ Herron, J.H. and Dibeler, V.H., J. Chem. Phys., 1960, 33, 1595.
- ^j Neuert, H., Z. Naturforsch, 1952, A7, 293.
- ^k Brundle, C.R., Robin, M.B. and Kuebler, N.A., J. Am. Chem. Soc., 1972, 94, 1466.
- ^l Dibeler, V.H., Reese, R.M. and Franklin, J.L., J. Am. Chem. Soc., 1961, 83, 1813.
- ^m Rosums, P., Stafast, H. and Bock, H., Chem. Phys. Lett., 1975, 34, 275.
- ⁿ Prasad, S.R. and Singh, A.N., Indian J. Phys., 1985, 59B, 1.
- ^o Collin, J., Canad. J. Chem., 1959, 37, 1053.
- ^p Omura, I.; Baba, H and Higan, K., Bull. Chem. Soc. Japan, 1957, 30, 633.
- ^q Majer, J.R. and Patric, C.R., Trans. Far. Soc., 1962, 58, 1.
- ^r Lifshitz, C. and Chupka, W.A., J. Chem. Phys., 1967, 47, 3439.

Xenon-Nitrogen Chemistry

It was not until 1974 that the first xenon-nitrogen compound was prepared.³ The general approach was to use a ligand satisfying the criteria for "anion-type" ligands. For this purpose, a nitrogen ligand made highly electronegative by substitution with the electron withdrawing SO₂F groups was selected. The reaction was shown to proceed according to equation (3).³



The instability of the bis(fluorosulfonyl)imido derivative resulted in the product not being fully characterized until 1982 when definitive evidence for Xe-N bonding was obtained in the form of low-temperature crystal structure in this laboratory (Figure 2).⁴

Several other compounds containing N(SO₂X)₂ (X = F, CF₃) groups bonded to xenon(II) were also prepared (Table 5) with Xe[N(SO₂CF₃)₂]₂ being stable at room temperature.

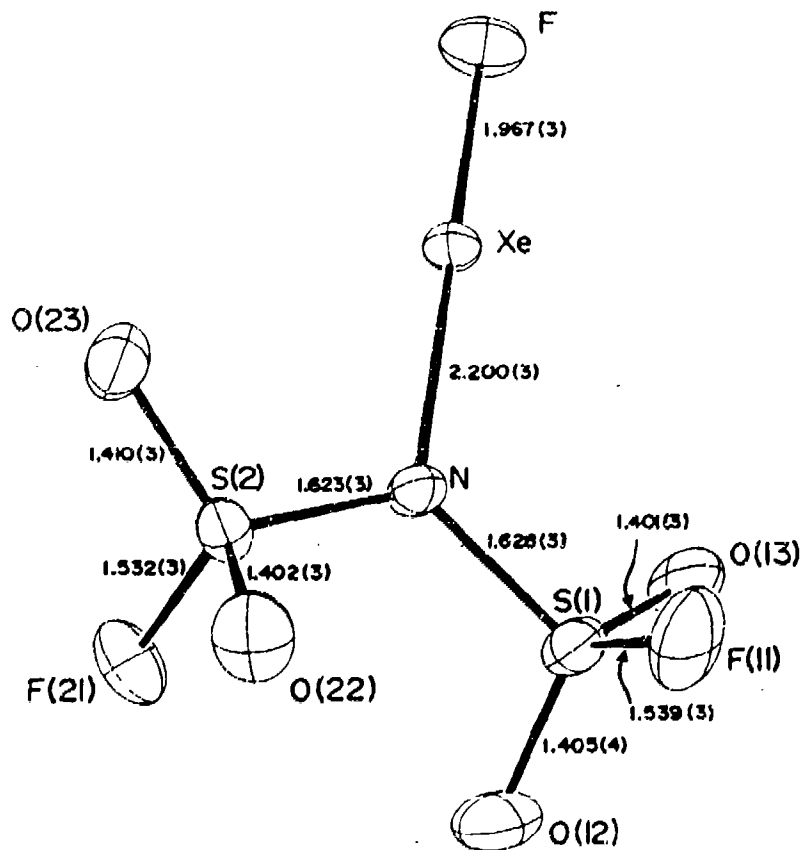


Figure 2. Crystal Structure of $\text{F-Xe-N(SO}_2\text{F)}_2$.

Table 5. Xe-N Derivatives of the $N(SO_2X)_2$ Group ($X = F, CF_3$)

<u>Compounds</u>	<u>Reference</u>
$FXeN(SO_2F)_2$	4
$[XeN(SO_2F)_2]^+AsF_6^-$	5
$[XeN(SO_2F)_2]^+Sb_2F_{11}^-$	5
$F[XeN(SO_2F)_2]_2^+AsF_6^-$	6
$Xe[N(SO_2F)_2]_2$	7
$Xe[N(SO_2CF_3)_2]_2$	3

Table 6. Physical Properties of Thiazyl Trifluoride

melting point, ° -72.6 °C

boiling point, ° -27.1 °C

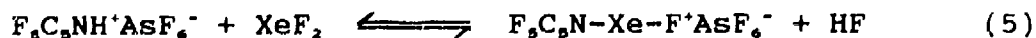
first adiabatic ionization potential⁹ 12.50 eV

<u>vapour pressure, Torr</u>	<u>temperature, °C</u>
78.4	-67.2
134.9	-59.2
206.8	-52.2
300.0	-45.6
400.1	-40.2
443.5	-38.3
548.6	-34.0

Lewis Acid Behavior of XeF⁺ and KrF⁺

In 1987, the scope of xenon-nitrogen chemistry and noble-gas chemistry in general was dramatically broadened by the discovery that XeF⁺ had significant Lewis acid properties and would, therefore, interact with nitrogen bases to form donor-acceptor type adducts.¹⁰ The XeF⁺ cation functions as an electron-pair acceptor towards the lone pair on a variety of oxidatively resistant nitrogen base ligands and can conveniently be classed as a "hard" Lewis acid.¹ Nitrogen containing ligands possessing first adiabatic ionization potentials in excess of 10.9 eV, the estimated electron affinity of XeF⁺, were sought out as suitable candidates for adduct formation.

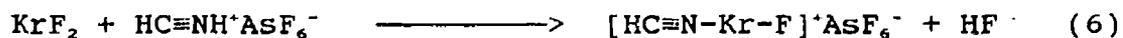
Adduct preparation involves the interaction of stoichiometric amounts of XeF⁺AsF₆⁻ and a suitable nitrogen base in anhydrous HF solvent (e.g., reaction 4), or a protonated base salt with XeF₂ in BrF₃ solvent (e.g., reaction 5). Both reactions



are followed by pumping off the HF and BrF₃ solvents and HF produced in the reaction. Brief warming to between -30 and -20 °C generally effects reaction and dissolution of the xenon(II) adduct cations in the solvent without significant decomposition. Pumping (in vacuo) at -50 to -30 °C

resulted in the isolation of white solids, many of which are not stable above -10 °C. This approach has led to the preparation of a large number of novel xenon-nitrogen compounds, including adducts with perfluoroalkyl-nitriles,¹¹ perfluoropyridines¹⁰ and s-trifluorotriazines.¹² Solutions of the adducts in HF and/or BrF₃ have been examined by ¹H, ¹³C, ¹⁹F, ¹²⁹Xe, ¹⁴N and ¹⁵N NMR spectroscopy, and solid samples of many of these compounds have been characterized by low-temperature laser Raman spectroscopy.

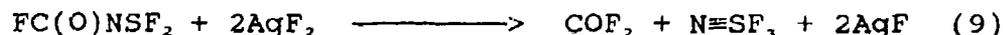
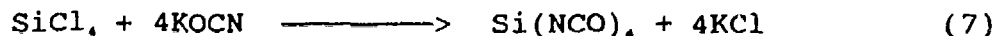
The KrF⁺ cation (estimated electron affinity, 13.2 eV),¹ has also been shown to exhibit Lewis acid properties, reacting with suitable oxidatively resistant ligands using the synthetic procedures outlined above. The KrF⁺ cation is, in its own right, a very potent oxidant, the most potent chemical oxidant known, and also undergoes autocatalytic redox reactions in HF solvent liberating Kr and F₂ gases. In order to overcome these difficulties, the interaction of neutral KrF₂ with HC≡NH⁺AsF₆⁻ (first IP of HC≡N, 13.59 eV)¹³ in BrF₃ was attempted. The reaction proceeded according to equation (6) and resulted in the formation of HC≡N-KrF⁺AsF₆⁻, the first known species containing a krypton-nitrogen bond.¹⁴ The HC≡N-Kr-F⁺ cation



is stable at -50 to -60 °C in BrF₃ solvent but detonates as a solid precipitated from HF solvent at ca. -60 °C. The cation has been unambiguously characterized by low-temperature Raman spectroscopy and ¹⁹F, ¹⁵N, ¹³C and ¹H NMR spectroscopy.

Thiazyl Trifluoride: a Lewis-Base for Adduct Formation

Thiazyl trifluoride, $N\equiv SF_3$, is synthesized in a three step process as shown by equations (7) - (9).^{15,16} Some of its physical



properties are given in Table 6. Crude $N\equiv SF_3$ gas is further purified by washing in water to remove COF_2 , but in the process, unreacted SF_4 is hydrolyzed to SOF_2 . Unfortunately, the vapour pressures of $N\equiv SF_3$ and SCF_2 are sufficiently similar so that their separation cannot be effected by simple trap to trap distillation. Therefore, chemical means were employed where SOF_2 was oxidized by an aqueous solution of potassium permanganate to SO_4^{2-} .¹⁶

The observed first adiabatic ionization potential (12.50 eV)⁹ ought to render the compound stable to redox degradation due to oxidative fluorination of the ligand by XeF^+ . Moreover, the known adduct behavior of $N\equiv SF_3$ with Lewis acids (e.g., MF_3 , $M = As, Sb$)¹⁷ suggests that $N\equiv SF_3$ possesses a significant basicity and it should form stable Xe-N bonds with XeF^+ , $XeOSeF_5^+$ and $XeOTeF_5^+$ and possibly even KrF^+ and the xenon(IV) cation, XeF_3^+ .

Nuclear Magnetic Resonance Spectroscopy

NMR spectroscopy is the single most powerful technique used in the structural characterization of noble gas species. This technique is especially useful in the structural verification of xenon-nitrogen compounds due to the presence of several naturally occurring, spin-active isotopes, e.g., ^{129}Xe , ^{14}N , ^1H , ^{13}C and ^{19}F . The one-bond coupling constants $^1J(^{129}\text{Xe}-^{19}\text{F})$ and, in some cases, $^1J(^{129}\text{Xe}-^{14}\text{N})$ can be used to characterize F-Xe-N linkages. Two-, three- and, sometimes, four-bond couplings can also be observed which provide additional structural information. Although ^{14}N is a quadrupolar nucleus with a small quadrupole moment ($Q = 1.67 \times 10^{-30}\text{m}^2$),¹⁸ couplings to it can be observed when the following conditions are met: a) the electric field gradient at the nucleus is zero or low as in tetrahedral or octahedral environments (e.g. AsF_6^-), or small as in axially symmetric species such as the $\text{HC}\equiv\text{N}-\text{XeF}^+$ cation and b) the rotational correlation time is small, such as in the low-viscosity solvent anhydrous HF. Spin-spin coupling constants can also be used to assess bonding trends in structurally-related species. The NMR-active isotopes relevant to the present work and some of their properties are listed in Table 7.

Table 7. NMR Properties of Nuclides Employed in This Work^{1a}

<u>Isotope</u>	<u>Spin</u>	<u>Natural Abundance (%)</u>	<u>NMR Frequency (MHz)^a</u>
¹⁹ F	1/2	100.00	94.094
¹²⁹ Xe	1/2	26.44	27.856
¹⁴ N	1	99.63	7.226
⁷⁷ Se	1/2	7.58	19.071

^a Frequencies are relative to the protons of TMS, which resonate at exactly 100 MHz ($B_0 = 2.349$ T).

Raman Spectroscopy

Raman spectroscopy is the preferred vibrational spectroscopic method employed for the characterization of the majority of reactive fluorides in the solid state. Because of their strong oxidant characters, noble-gas fluoride species are particularly problematic. These materials must be handled in inert sample containers composed of a transparent fluoroplastic such as FEP, glass or sapphire. This technique is especially useful for noble-gas species of the type L-Xe-F (e.g., L = $-\text{OTeF}_5^-$, $\text{HC}\equiv\text{N}-$). In particular, the Xe-F stretch is generally the most intense or one of the most intense lines in the Raman spectrum and can be used to assess the degree of covalency in the Xe-L bond, i.e., a shift to lower frequency for

the Xe-F stretch implies a more covalent Xe-L bond (see Table 8).

In the present study, Raman spectroscopy was the preferred vibrational method for several reasons. Raman spectroscopy provides more information about low-frequency vibrations which are common for the heavier, main-group elements and is a particularly sensitive technique owing to the strong Raman scattering character of vibrations involving heavy elements. Of the two containment materials used in this study, FEP does not produce a significant number of bands in the frequency range of interest and glass produces no interfering lines. However, both of these materials absorb strongly in the IR spectrum, rendering them useless for the latter studies. Moreover, noble-gas species studied in the course of the present work cannot be studied using conventional IR cell materials owing to the strongly oxidizing properties of these species which attack most IR window materials. Other advantages are that Raman spectra can be easily obtained, even at low temperature (-196°C), since the apparatus allows the sample to be suspended in an unsilvered Dewar containing liquid nitrogen (see Figure 10).

Table 8. Comparison of Xe-F Stretching Frequencies in F-Xe-L Derivatives

Compound/ Cation	$\nu(\text{Xe-F}), \text{cm}^{-1}$	Ref.
$\text{F-Xe}^+\cdots\text{F}\cdots\text{Sb}_2\text{F}_{11}^-$	619	a
$\text{F-Xe}^+\cdots\text{F}\cdots\text{AsF}_5^-$	610	a
$(\text{F-Xe})_2\text{F}^+$	596	a
$\text{CH}_3\text{C}\equiv\text{N-Xe-F}^+$	560	b
$\text{HC}\equiv\text{N-Xe-F}^+$	559	b,c
$\text{C}_3\text{F}_3\text{N}_2\text{N-Xe-F}^+$	544	d
F-XeOIOF_4	527	e
$\text{C}_5\text{F}_5\text{N-Xe-F}^+$	528	f
$4\text{-CF}_3\text{C}_3\text{F}_4\text{N-Xe-F}^+$	524	f
F-XeOTeF_5	516	g
$\text{F-XeN}(\text{SO}_2\text{F})_2$	506	h

^a R.J. Gillespie and B. Landa, *Inorg. Chem.*, 1973, 12, 1383.

^b A.A.A. Emara and G.J. Schrobilgen, *J. Chem. Soc., Chem. Commun.*, 1987, 1644.

^c A.A.A. Emara and G.J. Schrobilgen, unpublished work.

^d G.J. Schrobilgen, *J. Chem. Soc., Chem Commun.*, 1988, 1506.

^e R.G. Syvret and G.J. Schrobilgen, *Inorg. Chem.*, 1989, 28, 1564.

^f A.A.A. Emara and G.J. Schrobilgen, *J. Chem. Soc., Chem. Commun.*, 1988, 254.

^g F.O. Sladky, *Monatsh. Chem.*, 1970, 101, 1571.

^h G.A. Schumacher and G.J. Schrobilgen, *Inorg. Chem.*, 1983, 22, 2178.

Purpose and Scope of the Present Work

In the present work, $\text{N}\equiv\text{SF}_3$ was selected as a suitable candidate to form adducts with selected xenon(II) cations because of its high first adiabatic ionization potential (12.50 eV).⁹ Thiazyl trifluoride was studied in solvents used in noble-gas research to determine the stability and solubility of the ligand. The $\text{F}_3\text{S}=\text{N}-\text{AsF}_6$ adduct was prepared in order to confirm the base strength of the ligand. Based on the expected base strength of $\text{N}\equiv\text{SF}_3$, syntheses were attempted to form Lewis acid-base adducts with the noble-gas cations XeF^+ and XeOSeF_6^+ . Characterization by ^{19}F , ^{14}N and ^{129}Xe NMR spectroscopy was the primary spectroscopic technique employed with adducts in solvents deemed suitable for either the preparative work or the dissolution of the species. The isolated salts were studied in the solid state using low-temperature Raman spectroscopy.

EXPERIMENTAL

Apparatus and Materials

The air- and moisture-sensitive natures of the precursors and products required that all manipulations be carried out under anhydrous conditions. Air-sensitive samples of low volatility, e.g., $\text{XeF}^+\text{AsF}_6^-$, were transferred in a nitrogen-filled drybox (Vacuum Atmospheres Model DLX) equipped with cryogenic wells which were used to transfer samples that were thermally unstable under anhydrous conditions. Volatile reagents and

solvents were transferred on a metal vacuum line constructed from 316 stainless steel, nickel, Teflon, FEP and Kel-F (Figure 3). Pressures were measured at ambient temperature using an MKS Model PDR-5B power supply digital readout in conjunction with pressure transducers having inert, wetted surfaces constructed of inconel. Two transducers of different dynamic ranges were used, 0 to 1000 Torr and 0 to 1 Torr. The pressures were accurate to $\pm 0.5\%$ of scale.

NMR samples were prepared either in glass tubes (5 or 10 mm o.d.) and flame-sealed, or in FEP tubes (4 or 9 mm o.d.) heat-sealed at one end and flared (SAE 45°) at the other. Raman samples were prepared in FEP tubes (1/4 inch o.d.) heat-sealed at one end and flared (SAE 45°) at the other. Each tube was fitted with a Kel-F valve (see Figures 5 and 7).

The purification of the solvents SO_2ClF (Columbia Organic Chemicals),¹⁹ HF (Harshaw Chemical Co.),²⁰ and BrF_3 (Ozark Mahoning),²⁰ have been described previously. The preparation of the starting materials $\text{XeF}^+\text{AsF}_6^-$,²¹ and $\text{XeOSeF}_5^+\text{AsF}_6^-$ ²² has been described elsewhere.

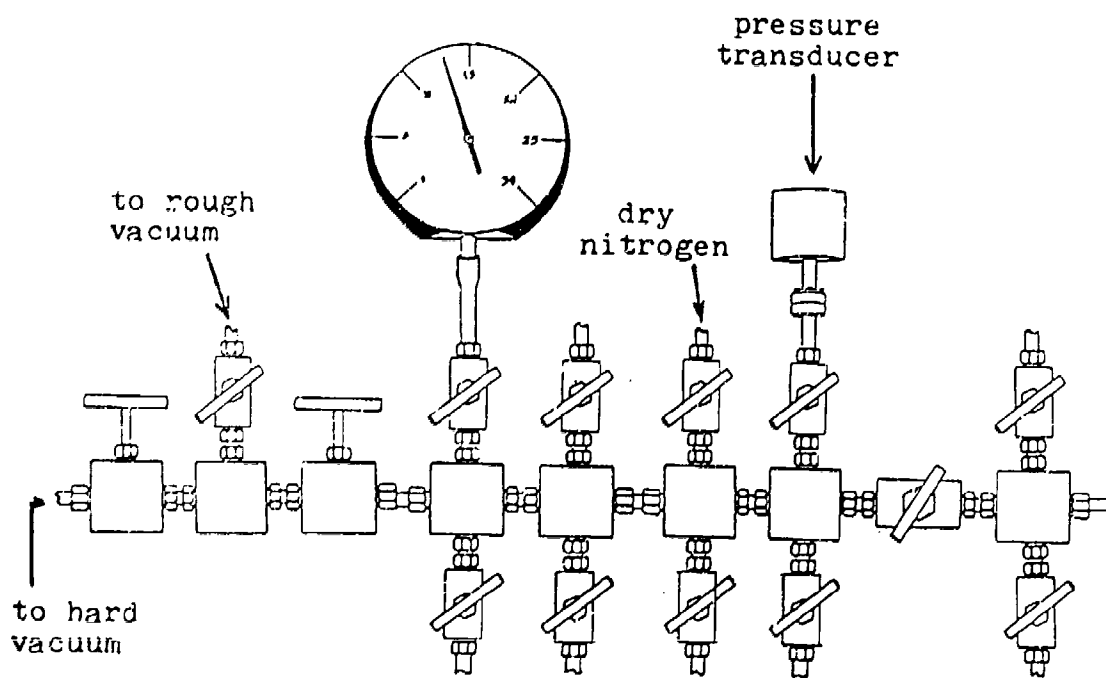


Figure 3. Metal vacuum line used for the preparation of $N\equiv SF_3$ derivatives and spectroscopic samples.

Purification of N≡SF₃

A sample of N≡SF₃, provided by Dr. J. Thrasher, University of Alabama, Tuscaloosa, was prepared by the standard literature method.^{15,16} A modified version of the literature method for purifying N≡SF₃ was employed,¹⁶ using the apparatus shown schematically in Figure 4. The apparatus was initially flushed with dry nitrogen for five minutes and was maintained at slightly over atmospheric (ca. 780 Torr). Impure N≡SF₃ was introduced into the flow at a very slow rate. The SOF₂ impurity,¹⁵ was oxidized by aqueous solutions of 5% KMnO₄ to SO₄²⁻ by dispersing the gas stream using a coarse sintered glass diffuser followed by passage through a second fine diffuser. The carrier-gas and N≡SF₃ were dried by passage through a column filled with granular P₂O₁₀. The dried gases were then passed through a U-tube cooled to -196 °C where the purified N≡SF₃ was collected.

The amount of pure N≡SF₃ recovered was 90.1%. The purity of N≡SF₃ was assessed using gas-phase infrared spectroscopy. The spectra were recorded in a glass cell (10 cm path) equipped with AgCl windows. The predominant impurity, SOF₂, displays a band at 1333 cm⁻¹ corresponding to the S=O symmetric stretch²³ which is not coincident with any peak in the infrared spectrum of N≡SF₃. The impure sample, at 10 Torr pressure in the IR cell, produced an intense peak at 1333 cm⁻¹, but no peak was observed for the pure sample even at 300 Torr.

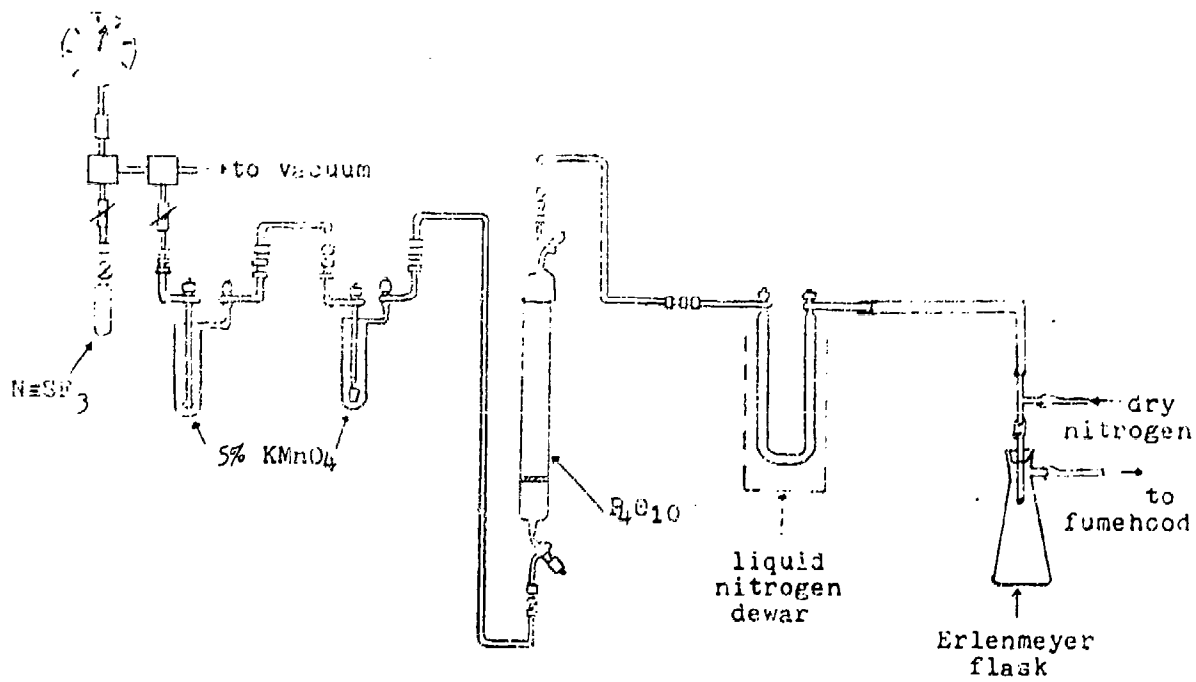


Figure 4. Schematic diagram of the apparatus used for the purification for $N\equiv SF_3$.

Preparation of $N\equiv SF_5$ Solutions for NMR Spectroscopy

Approximately 0.04 mL of $N\equiv SF_5$ was distilled into a 5 mm glass precision medium-wall NMR tube (Wilmad), or a 4 mm FEP tube (used for HF solvent). The appropriate solvent (SO_2ClF , BrF_3 , or anhydrous HF, ca. 0.4 mL) was then distilled onto the sample which was frozen at $-196^\circ C$ and the tube sealed under dynamic vacuum. Apparatus used for the preparation of solutions in each solvent are shown in Figures 5 - 7.

Preparation of $F_3S\equiv N-AsF_6$ for ^{19}F NMR Spectroscopy

Approximately 0.04 mL of $N\equiv SF_5$ was distilled into a 5 mm glass precision medium-wall NMR tube (Wilmad) and frozen, followed by a slight excess of AsF_5 . Under static vacuum, the sample was warmed to $-71^\circ C$ where reaction took place forming a white solid which dissociated upon warming to room temperature. After cooling to $-78^\circ C$, unreacted volatiles were pumped off and solvent (SO_2ClF , or BrF_3) was distilled into the tube at $-196^\circ C$ (Figure 8) and the tube was flame-sealed under vacuum at $-196^\circ C$.

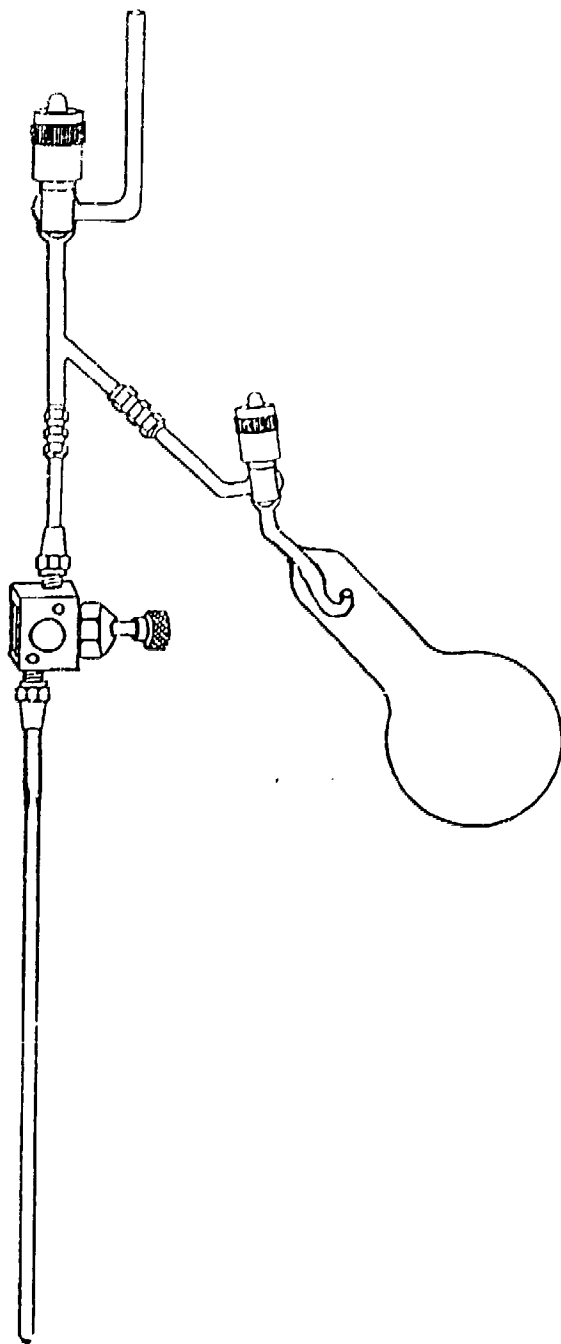


Figure 5. Apparatus used for the preparation of a solution of $\text{N}\equiv\text{SF}_3$ in SO_2ClF solvent for NMR spectroscopy.

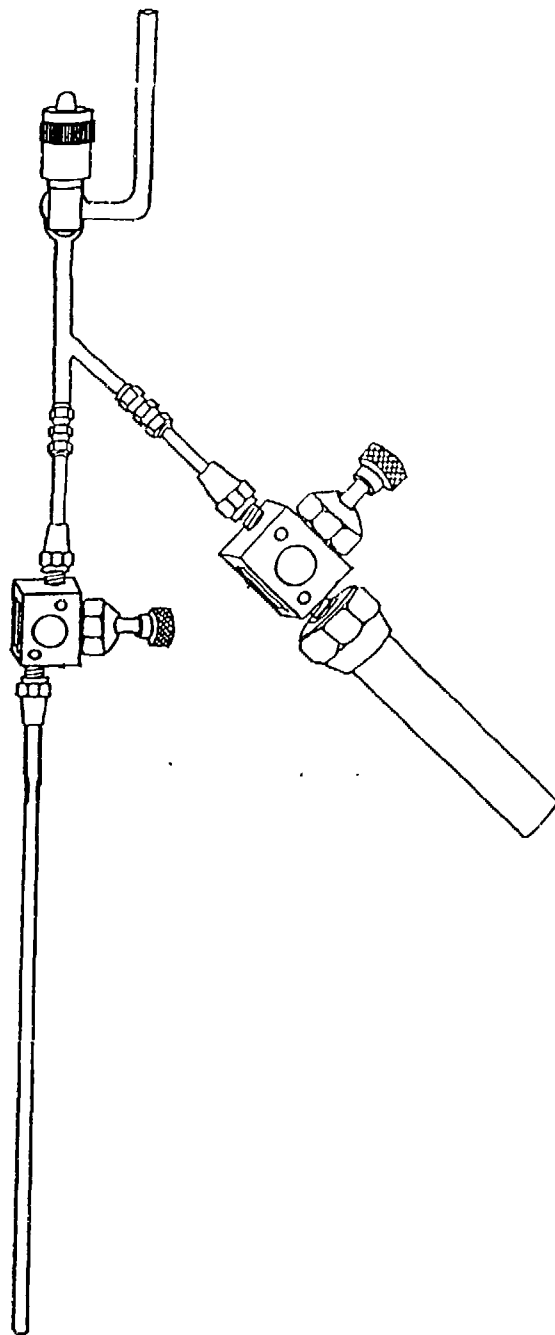


Figure 6. Apparatus used for the preparation of a solution of $\text{N}\equiv\text{SF}_3$ in BrF_3 solvent for NMR spectroscopy.

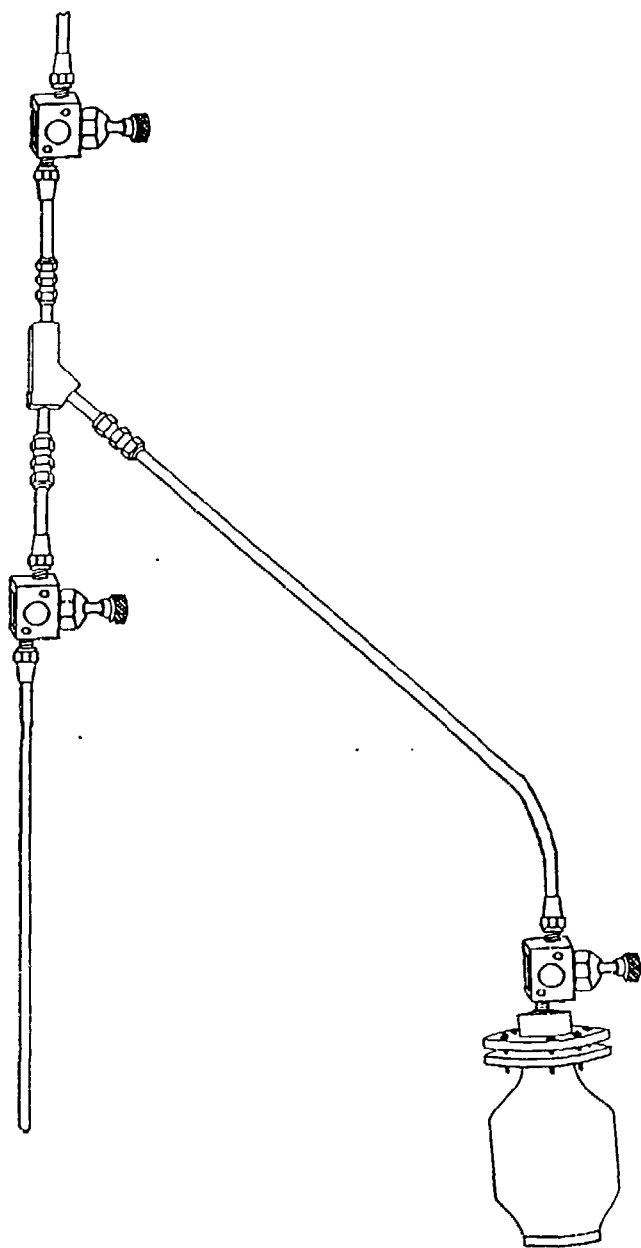


Figure 7. Apparatus used for the preparation of a solution of $\text{N}\equiv\text{SF}_6$ in anhydrous HF solvent or samples for NMR spectroscopy.

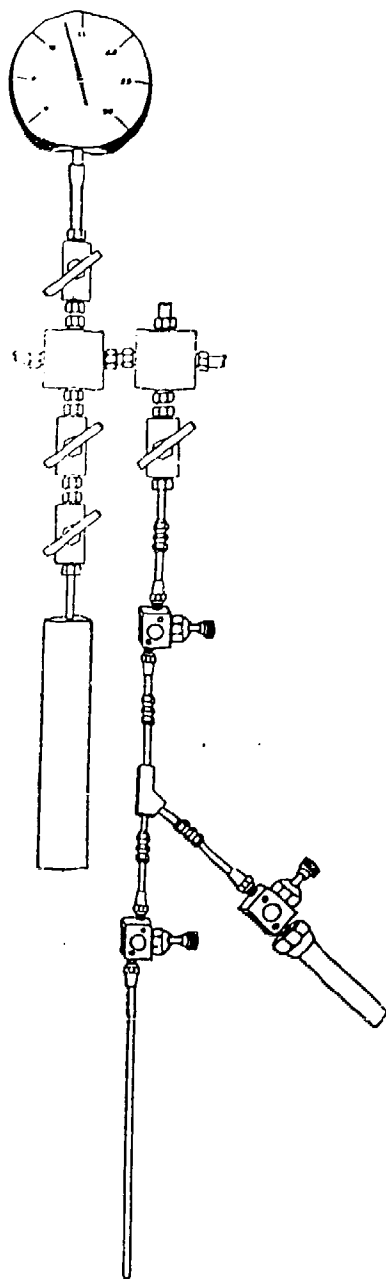


Figure 8. Apparatus used for the preparation of $F_3S=N-AsF_6$ in BrF_3 solvent or samples for NMR spectroscopy.

Preparation of $F_3S\equiv N-Xe-F^+AsF_6^-$ for ^{19}F and ^{129}Xe NMR Spectroscopy

In a typical preparation, $XeF^+AsF_6^-$ (0.0988 g, 0.291 mmol) was transferred in a drybox into a 5 mm glass precision medium-wall NMR tube (Wilmad). The solvent, BrF_5 (ca. 0.4 mL), was distilled onto the salt at $-196^\circ C$. The $XeF^+AsF_6^-$ was dissolved in the BrF_5 solvent at room temperature and then reprecipitated by chilling to give finely divided material. Thiazyl trifluoride was then distilled in at $-196^\circ C$ (295 Torr, 21.28 mL; 0.317 mmol), Figure 9. A pale yellow solution was observed as the reaction proceeded at $-65^\circ C$. The tube was then frozen at $-196^\circ C$ and flame-sealed under vacuum. The same synthesis was carried out in a 9 mm FEP NMR tube using 0.4304 g (1.269 mmol) of $XeF^+AsF_6^-$ and 1.377 mmol (1202 Torr, 21.28 mL) of $N\equiv SF_3$.

Preparation of $F_3S\equiv N-Xe-OSeF_5^+AsF_6^-$ for ^{19}F and ^{129}Xe NMR Spectroscopy

The sample was prepared in an analogous fashion to that used for the preparation of $F_3S\equiv N-XeF^+AsF_6^-$ in BrF_5 solvent using 0.1520 g (0.2979 mmol) of $XeOSeF_5^+AsF_6^-$ and a 15 mole % excess (319 Torr, 21.28 mL) of $N\equiv SF_3$. On warming to $-65^\circ C$, the BrF_5 solution turned pale brown in color. The solid adduct was not isolated from the solution. The same synthesis was carried out in a 9 mm FEP NMR tube using 0.5145 g (1.008 mmol) of $XeOSeF_5^+AsF_6^-$ and a 36 mole % excess (1200 Torr, 21.28 mL) of $N\equiv SF_3$.

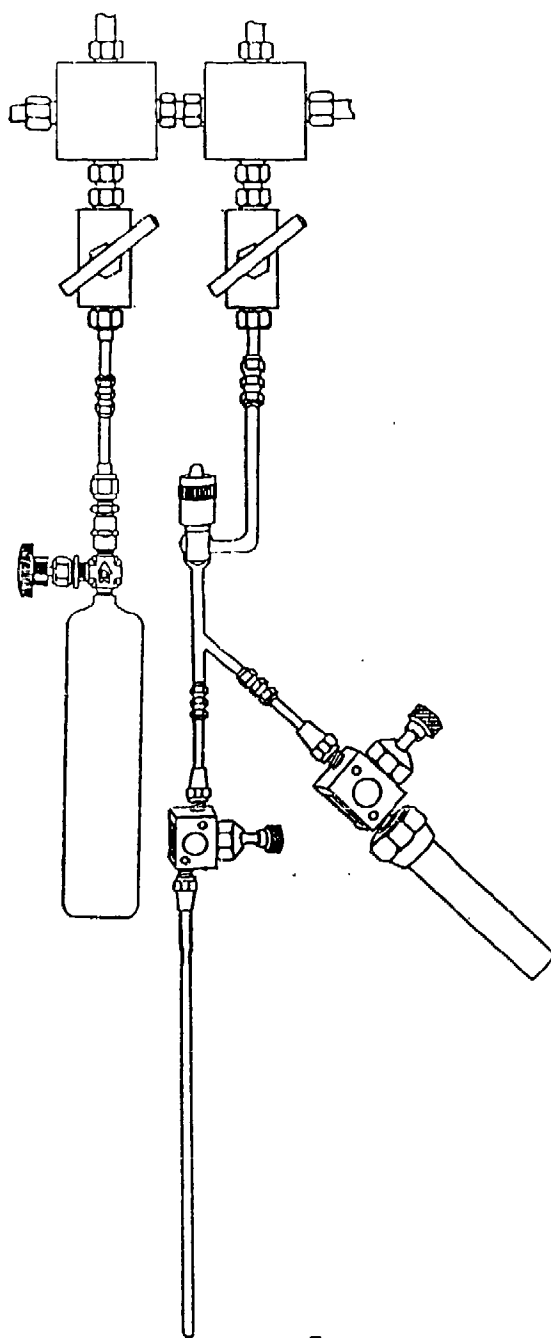


Figure 9. Apparatus used for the preparation of $F_3S \equiv N - Xe - L^+ AsF_6^-$ ($L = -F, -OSeF_5$) by the direct interaction of $Xe - L^+ AsF_6^-$ and $N \equiv SF_5$ in BrF_3 solvent.

Preparation of $F_3S\equiv N-XeF^+AsF_6^-$ for Raman Spectroscopy and for Solution in Anhydrous HF Solvent for NMR Spectroscopy

The title compound was prepared as described previously, except that a 1/4" o.d. x 3/16" i.d. FEP reaction tube was used, and larger scale samples were prepared. Typical quantities used were 0.4266 g (1.2577 mmol) of $XeF^+AsF_6^-$ and a 27 mole % excess (1365 Torr, 21.28 mL; 1.597 mmol) of $N\equiv SF_3$. The sample was not sealed, but warmed to ca. -40 °C, then warmed further to -15 °C, in an attempt to pump off the BrF_3 solvent used for these preparations. Even after several days of pumping, BrF_3 was still detected by condensation at -196 °C on the wall of the tube.

For the NMR sample, solid $F_3S\equiv N-XeF^+AsF_6^-$ from a Raman sample isolated from BrF_3 solvent (ca. 0.1 g) was transferred at low temperature in a drybox to a 4 mm FEP tube. Anhydrous HF solvent (ca. 0.4 mL) was distilled at -196 °C onto the salt, the tube was heat-sealed, and the sample warmed briefly to -78 °C to dissolve the salt before storing at -196 °C.

Neat Preparation of $F_3S\equiv N-XeF^+AsF_6^-$ for Raman Spectroscopy and for Solution in Anhydrous HF Solvent for NMR Spectroscopy

The salt, $XeF^+AsF_6^-$ (0.1481 g, .437 mmol), was transferred to a 1/4" o.d. x 3/16" FEP reaction tube and a two-fold excess (738 Torr, 21.28 mL; 0.793 mmol) of $N\equiv SF_3$ was distilled onto the salt. The tube was warmed to -25 °C for two hours while the reaction took place which produced a white powder.

For the NMR sample, the title compound was prepared as above on a similar scale, but in a 9 mm FEP NMR tube. Anhydrous HF (ca. 1.5 mL) was distilled onto the salt at $-196\text{ }^{\circ}\text{C}$ and the sample was heat-sealed and stored at $-196\text{ }^{\circ}\text{C}$.

Nuclear Magnetic Resonance Spectroscopy

Additional samples of the above systems were prepared as required depending on the nucleus under investigation and the solvent used as specified in Table 9.

The ^{19}F NMR spectra were recorded with the use of a Bruker AM-500 spectrometer equipped with a 11.7438-T cryomagnet and a Aspect 3000 computer. The ^{129}Xe and ^{14}N spectra were recorded with the use of a Bruker WM-250 spectrometer equipped with a 5.8719-T cryomagnet and an Aspect 2000 computer. Acquisition parameters for ^{19}F , ^{129}Xe and ^{14}N are listed in Table 10. For low-temperature measurements, the samples were usually warmed only sufficiently to liquify and solubilize or partially solubilize the compounds. Samples were placed in the precooled NMR probe and allowed to equilibrate in the probe for several minutes while spinning prior to data acquisition.

Table 9. Sample Tube Materials and Dimensions for NMR Samples

<u>Nucleus</u>	<u>Solvent</u>	<u>Sample Tube Materials and Dimensions</u>
¹⁹ F	SO ₂ ClF BrF ₃	Wilmad 5 mm o.d. medium wall glass tube
	HF	4 mm o.d. FEP tube for insertion into a Wilmad thin wall 5 mm o.d. precision glass tube ^a
¹²⁹ Xe	BrF ₃	9 mm o.d. FEP tube for insertion into a HF Wilmad thin wall 10 mm o.d. precision glass tube ^a
¹⁴ N	HF	9 mm o.d. FEP tube for insertion into a Wilmad thin wall 10 mm o.d. precision glass tube ^a

^a FEP tubes are made to fit inside an appropriate glass NMR tube which is precooled when necessary for obtaining low-temperature spectra.

Table 10. Acquisition Parameters for ¹⁹F, ¹²⁹Xe and ¹⁴N NMR Spectra

<u>Acquisition Parameter</u>	<u>¹⁹F</u>	<u>¹²⁹Xe</u>	<u>¹⁴N</u>
Reference Standard (24 °C, neat)	CFCl ₃	XeOF ₄	CH ₃ NO ₂
Resonance Frequency (MHz)	470.599	69.562	18.075
Data Point Resolution (Hz/data point)	0.2 to 3.6	1.5 to 12.0	4.9
Spectral Width (Hz)	2000 to 30000	25000	20000
Memory Size (Kb)	16 to 32	8 to 32	8
Pulse Width (μs)	1.00	35.00	49.00
Line Broadening (Hz)	0 to 5	3 to 15	1
Number of Transients	400 to 3000	2000 to 20000	2000

Raman Spectroscopy

A Coherent Nova 90-5 argon ion laser, providing up to 5 W at 514.5 nm was used as the excitation source in conjunction with a Spex Industries Model 14018 double monochromator equipped with 1800-grooves/mm holographic gratings. The spectra were accumulated using a RCA C 31034 phototube detector combined with a pulse count system (Hamner NA11) consisting of a pulse amplifier analyzer (Hamner NC-11), and a rate meter (Hamner N-708 A). Spectra were recorded using a Texas Instruments Model FSOZWBA strip chart recorder. Slit widths depended on the scattering efficiency of the sample but were typically set between 50 and 150 μm . The scanning rate used was 0.5 $\text{cm}^{-1}\text{s}^{-1}$. The typical laser power range used was between 0.4 and 0.9 W. All Raman shifts quoted are estimated to be accurate to $\pm 2 \text{ cm}^{-1}$. Cylindrical sample tubes were mounted vertically. The angle between the laser beam and sample tube was 45° , and Raman-scattered radiation was observed at 45° to the laser beam or 90° to the sample tube. Low-temperature spectra were recorded by mounting the sample vertically in an unsilvered Pyrex glass Dewar filled with liquid nitrogen (Figure 10). All spectra were obtained directly in FEP reaction vessels.

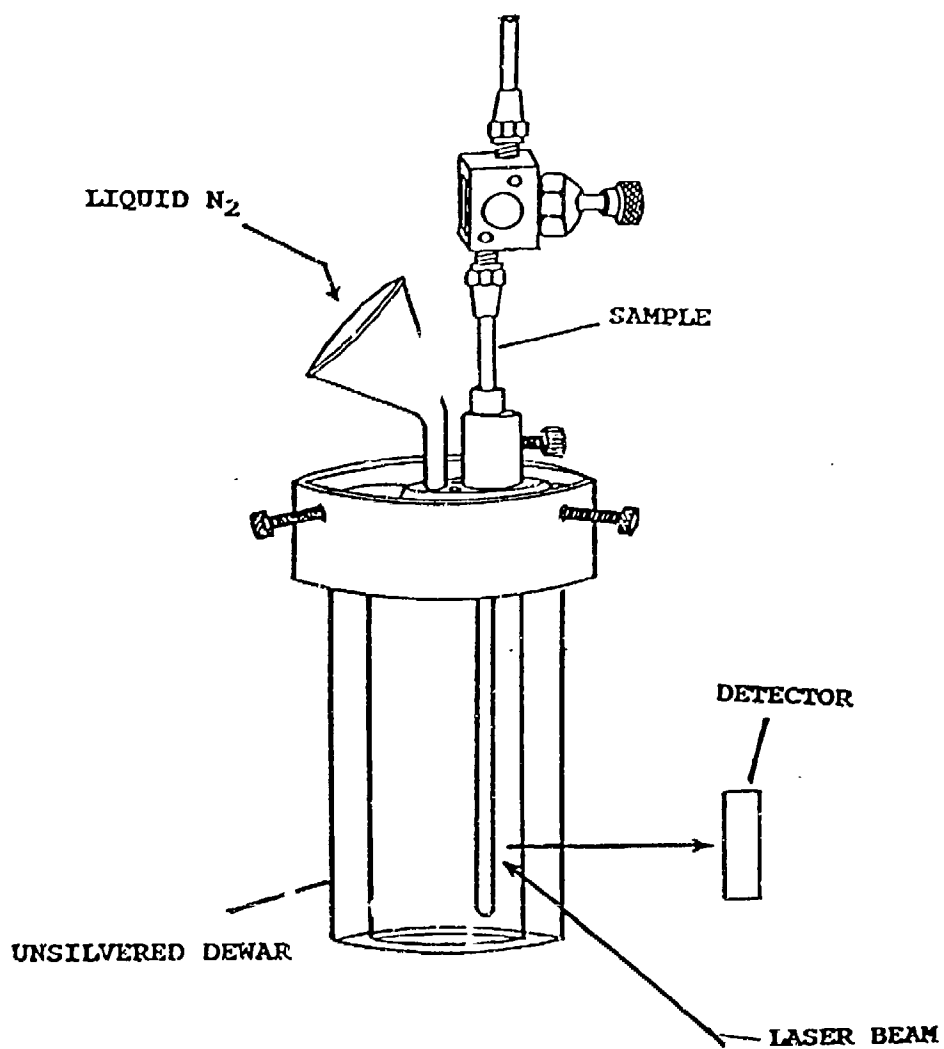


Figure 10. Unsilvered glass Pyrex dewar used to obtain low-temperature Raman spectra.

RESULTS AND DISCUSSION

Characterization of $N\equiv SF_3$ by ^{19}F NMR Spectroscopy

The characterization of $N\equiv SF_3$ by low-temperature ^{19}F NMR spectroscopy was carried out in SO_2ClF , BrF_3 , and anhydrous HF solvents, and served as the basis for the selection of appropriate solvents in subsequent synthetic work. Thiazyl trifluoride was expected to be stable in SO_2ClF and the spectrum of this sample was used primarily as an additional means to assess the purity of the compound. The strong oxidative fluorinating solvent, BrF_3 , may reasonably be expected to fluorinate $N\equiv SF_3$, thereby rendering the solvent unsuitable for further synthetic work. Moreover, $N\equiv SF_3$ was known to undergo solvolysis in anhydrous HF by addition of HF to the $N\equiv S$ bond forming SF_5-NH_2 as the product.²⁴ By monitoring the extent of solvent attack in both BrF_3 and HF at low temperature, the suitability of each solvent for the proposed synthetic work could be assessed.

The ^{19}F NMR parameters for $N\equiv SF_3$ in SO_2ClF , BrF_3 , and anhydrous HF solvents are given in Table 11. The ^{19}F NMR spectrum of $N\equiv SF_3$ in SO_2ClF solvent at 28 °C is shown in Figure 11. The scalar coupling, $^2J(^{19}F-^{14}N)$, between ^{19}F and ^{14}N is observed as a 1:1:1 triplet in the ^{19}F spectrum. In addition, the isotopic shift associated with ^{34}S (4.21 % natural abundance)²⁵ was observed for the first time at -0.060 ppm relative to $N\equiv^{32}SF_3$. The observation of coupling to the quadrupolar nucleus, ^{14}N , indicates that quadrupole relaxation is slow, presumably because the electric field gradient at nitrogen is small and the low viscosity of the solvent allows for rapid molecular tumbling, reducing the molecular correlation time

Table 11. ^{19}F Parameters for $\text{N}\equiv\text{SF}_3$ and Related Species^a

<u>Species</u>	<u>Solvent</u>	$\delta(^{19}\text{F}),^{\text{b}}$ <u>ppm</u>	$^2\text{J}(^{19}\text{F}-^{14}\text{N}),$ <u>Hz</u>	$^1\Delta^{19}\text{F}(^{34}/^{32})\text{S},$ <u>ppm</u>
$\text{F}_3\text{S}\equiv\text{N}:$	SO_2ClF	68.2	26.5	-0.060
$\text{F}_3\text{S}\equiv\text{N}:$	BrF_3	63.1	c	-0.060
$\text{F}_3\text{S}\equiv\text{N}:$	HF	56.3	c	d
$\text{F}_3\text{S}-\text{NH}_2$	HF	51.0, F_{ax} 71.3, F_{eq}	c c	-0.060 -0.057
$\text{F}_3\text{S}\equiv\text{N}-\text{AsF}_5^{\text{e}}$	SO_2ClF	49.7	c	-0.067
$\text{F}_3\text{S}\equiv\text{N}-\text{AsF}_5^{\text{f}}$	BrF_3	46.3	c	d

^a All spectra were recorded at $-56.5\text{ }^\circ\text{C}$ with the exception of the NSF₃ solution in SO_2ClF , which was recorded at $28\text{ }^\circ\text{C}$.

^b F-on-S(VI) region.

^c Spin-spin coupling not observed.

^d Isotopic shift not resolved.

^e Spectrum obtained at $28\text{ }^\circ\text{C}$; F-on-As(V) region: $\delta(^{19}\text{F}), -42.8$ ppm.

^f F-on-As(V) region: $\delta(\text{F}_{\text{ax}}), -80.6$ ppm; $\delta(\text{F}_{\text{eq}}), -32.7$ ppm;

$^2\text{J}(^{19}\text{F}_{\text{ax}}-^{19}\text{F}_{\text{eq}}), 121$ Hz.

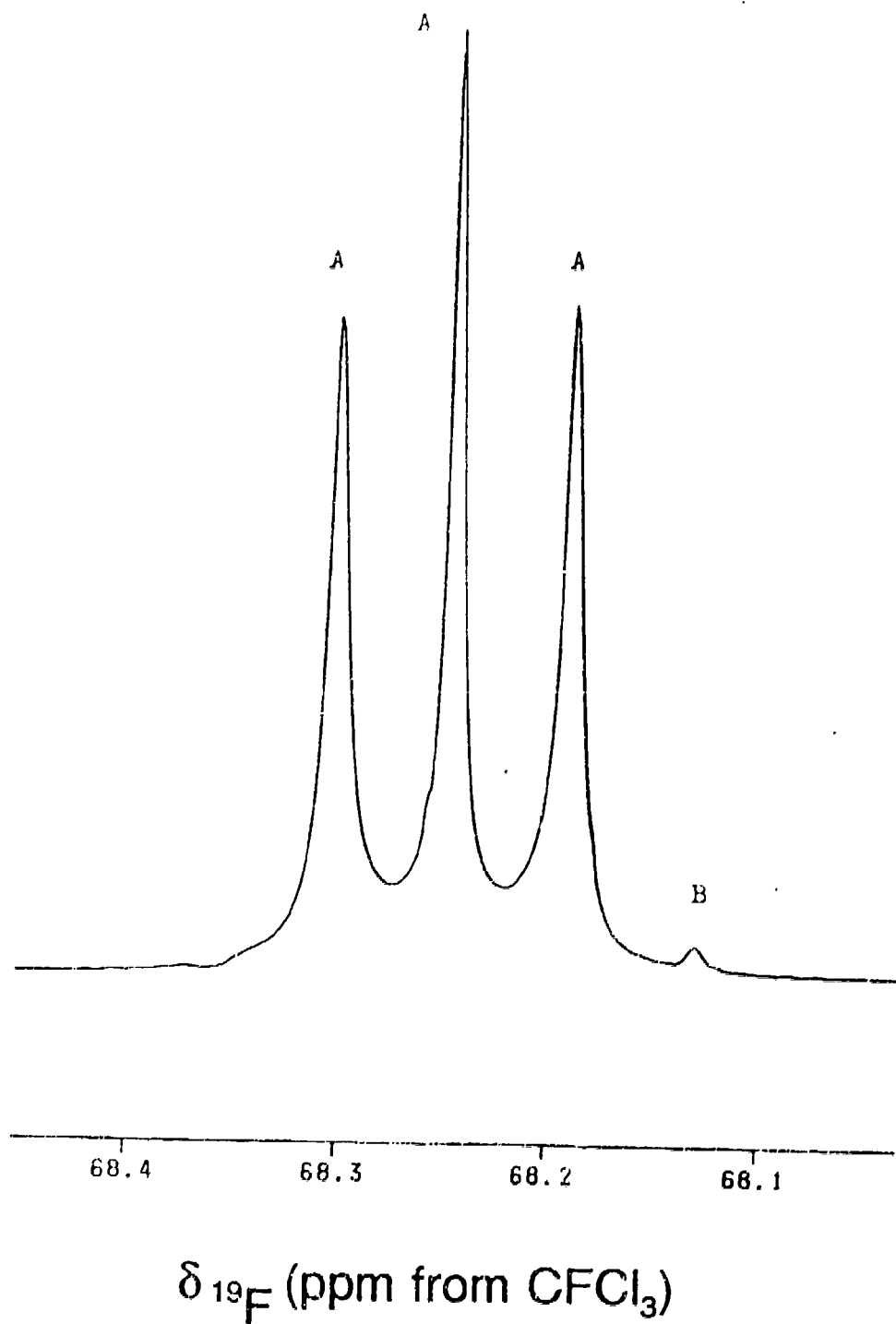


Figure 11. ^{19}F NMR spectrum of $\text{N}\equiv\text{SF}_6$ in SO_2ClF at 28 °C:

(A) F-on- ^{32}S (VI), (B) F-on- ^{34}S (VI).

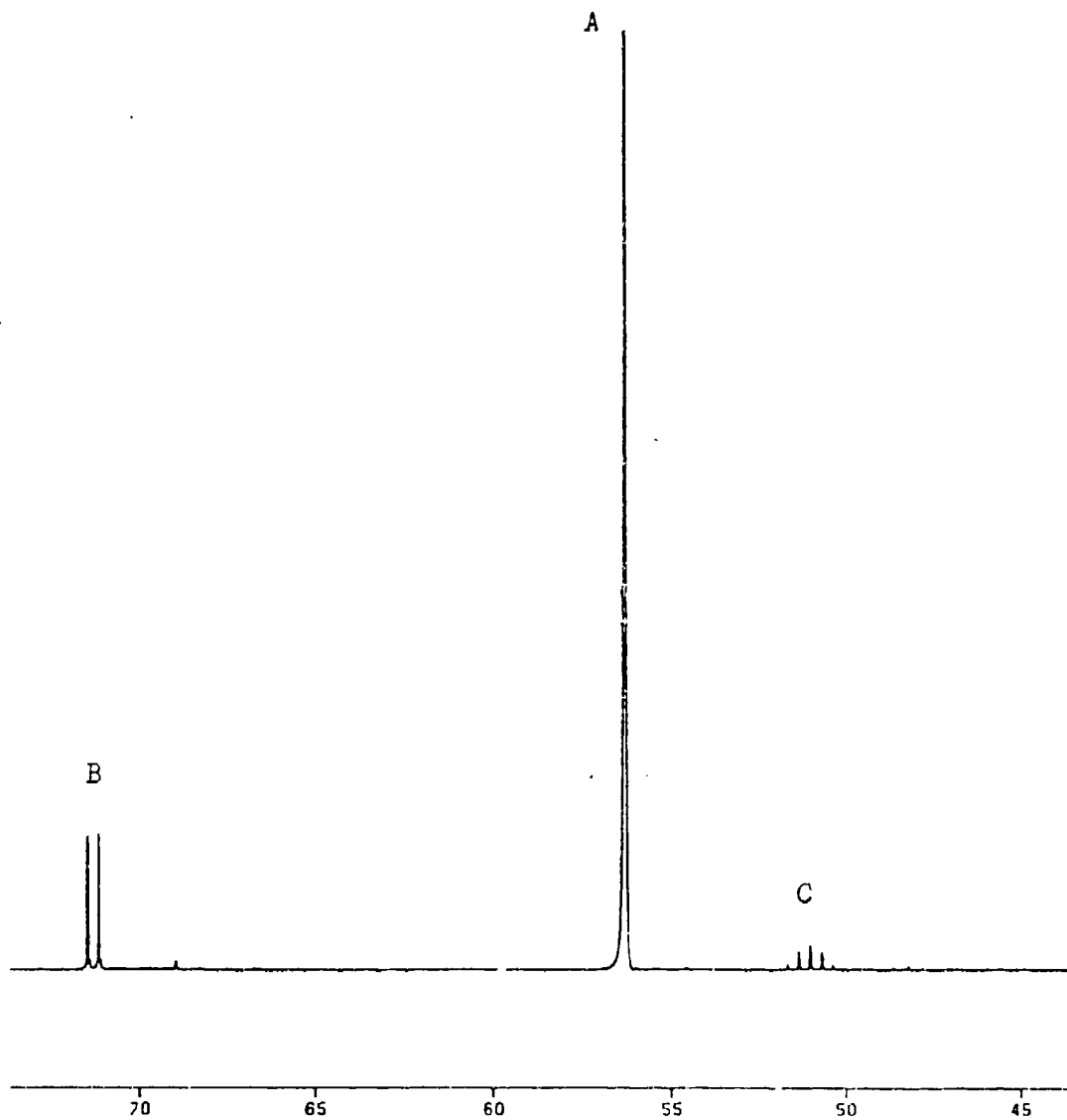
in the equation for quadrupole relaxation.²⁵

The ^{19}F NMR spectrum for $\text{N}=\text{SF}_3$ in BrF_3 at -56°C displayed no evidence for decomposition in BrF_3 solvent. The isotopic shift associated with ^{34}S was observed at -0.060 ppm relative to $\text{N}=\text{S}^{32}\text{SF}_3$, while the coupling to ^{14}N was no longer observed owing to the greater viscosity of the BrF_3 solvent which, in turn, increases the molecular tumbling rate, leading to quadrupole collapse of $^2\text{J}(^{19}\text{F}-^{14}\text{N})$.²⁶

The reported solvolysis of $\text{N}=\text{SF}_3$ in anhydrous HF ²⁴ was confirmed by recording its ^{19}F NMR spectrum at -56.5°C . The spectrum consisted of an intense singlet at 56.3 ppm assigned to $\text{N}=\text{SF}_3$ in the F-on-S(VI) region and was similar to that observed for $\text{N}=\text{SF}_3$ in BrF_3 solvent (63.1 ppm); however, the coupling to ^{14}N and the ^{34}S isotopic shift were not observed. A weaker set of signals at 51.0 and 71.3 ppm was also observed (Fig. 12) which could be associated with the solvolysis product $\text{F}_2\text{S}-\text{NH}_2$. A mechanism has been suggested which proceeds by the addition of polar species such as HF or ClF across the $\text{S}=\text{N}$ triple bond.²⁷ Upon warming to ambient temperature, the characteristic pattern for an AX₂ spin-system grew in with the concomitant loss of the $\text{N}=\text{SF}_3$ singlet, confirming the complete solvolysis of $\text{N}=\text{SF}_3$ by anhydrous HF at or near room temperature.

Characterization of $\text{F}_2\text{S}=\text{N}-\text{AsF}_6$ in SO_2ClF and BrF_3 Solvents by ^{19}F NMR Spectroscopy

The $\text{F}_2\text{S}=\text{N}-\text{AsF}_6$ adduct was prepared in order to confirm the base strength of the ligand, $\text{N}=\text{SF}_3$. The ^{19}F NMR parameters for this adduct in SO_2ClF and BrF_3 solvents are given in Table 11. The ^{19}F NMR



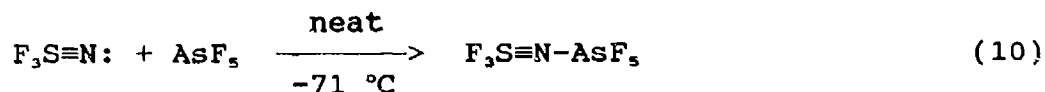
$\delta_{19}\text{F}$ (ppm from CFCl_3)

Figure 12. ^{19}F NMR spectrum of $\text{N}=\text{SF}_6$ in anhydrous HF at -56.5 °C:

(A) F-on-S(VI); (B) F_{ax} -on-S(VI), (C) F_{eq} -on-S(VI).

spectrum of $F_3S=N-AsF_6$ in BrF_3 solvent at -56.5 °C is shown in Figure 13.

Adduct formation was confirmed in both solvents as demonstrated by the lower frequencies of the F-on-S(VI) chemical shifts and proceeds according to equation (10). The ^{19}F chemical shift

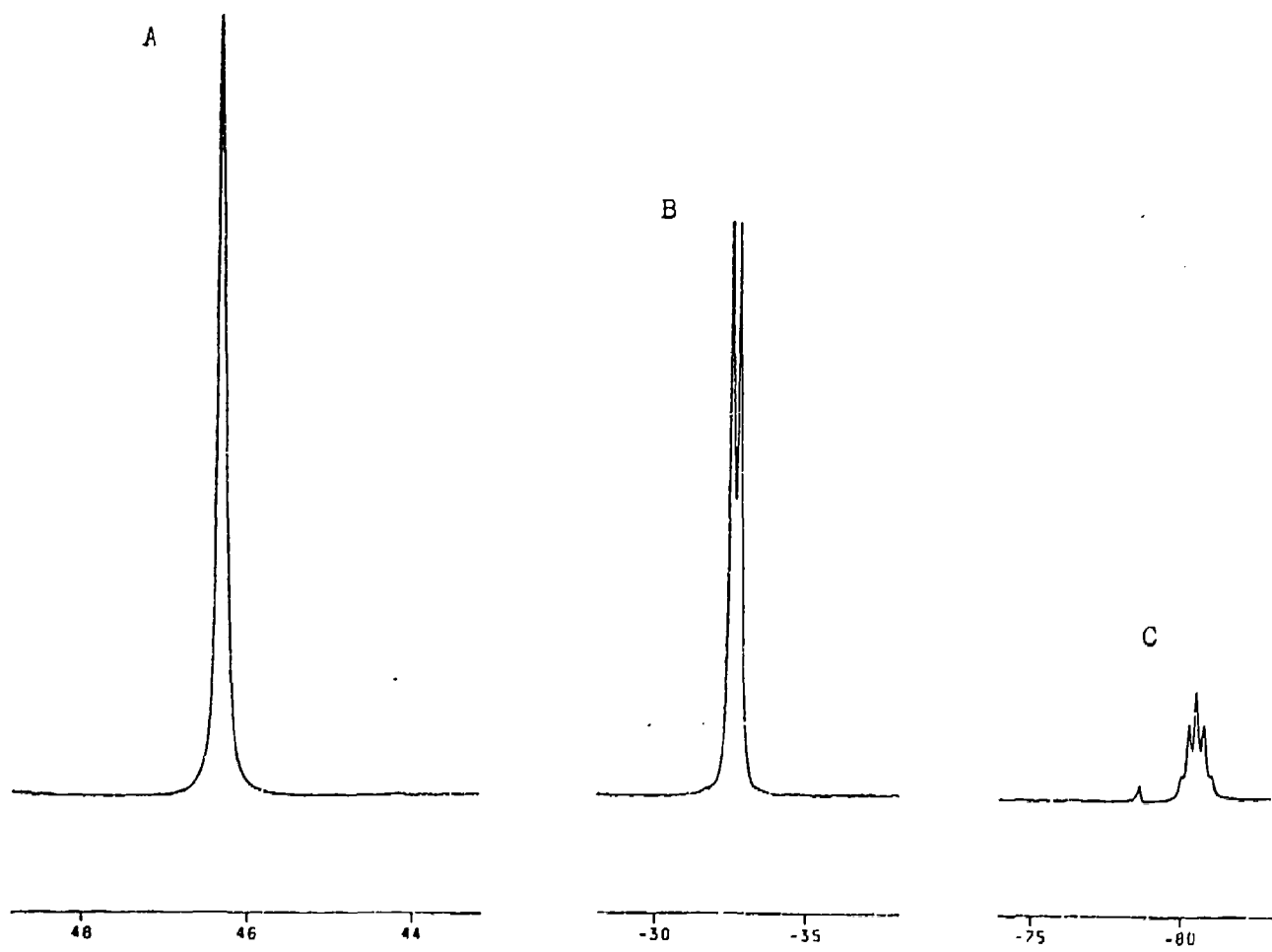


decreases from 68.2 to 49.7 ppm in SO_2ClF , and from 63.1 to 46.3 ppm in BrF_3 solvent. The isotopic shift, $^1\Delta^{19}F(^{34}/^{32})S$, increases in magnitude from 0.060 to 0.067 ppm as a result of adduct formation in SO_2ClF solvent, and is indicative of an increase in the S-F bond strength.¹⁵

Characterization of $F_3S=N-Xe-OSeF_6^+AsF_6^-$ in BrF_3 Solvent by ^{19}F and ^{129}Xe NMR Spectroscopy

The $F_3S=N-Xe-OSeF_6^+$ cation was prepared by the reaction of $XeOSeF_6^+AsF_6^-$ with $N\equiv SF_3$ in BrF_3 solvent at -60 °C, and was characterized at this temperature in BrF_3 solvent by ^{19}F and ^{129}Xe NMR spectroscopy. The NMR parameters are given in Table 12.

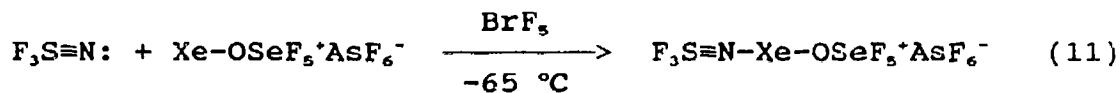
The ^{129}Xe NMR spectrum of $F_3S=N-Xe-OSeF_6^+AsF_6^-$ in BrF_3 at -60 °C displays a broad singlet ($\Delta\nu_q = 157$ Hz) at -1979 ppm compared with -1438 ppm for $Xe-OSeF_6^+$ in BrF_3 (-56 °C). The decrease in $\delta(^{129}Xe)$ results from an increase in shielding at xenon attributable to the formation of the Xe-N donor-acceptor bond according to equation (11).



$\delta_{19\text{F}}$ (ppm from CFCl_3)

Figure 13. ^{19}F NMR spectrum of $\text{F}_3\text{S}\equiv\text{N}-\text{AsF}_6$ in BrF_3 at -56.5°C :

(A) F-on-S(VI), (B) F_{ax} -on-As(V), (C) F_{eq} -on-As(V).



The ^{19}F NMR spectrum in the F-on-S(VI) region (Figure 14), displays a singlet at 53.5 ppm (cf., 63.1 ppm for free $\text{N}\equiv\text{SF}_3$) and an isotopic shift, $^1\Delta^{19}\text{F}(^{34}/^{32})\text{S}$, of -0.066 ppm (cf., -0.060 ppm for free $\text{N}\equiv\text{SF}_3$). Both parameters are similar to those of the $\text{F}_3\text{S}\equiv\text{N-AsF}_5$ adduct (see Table 11), indicating that the Xe-OSeF_5^+ cation forms a stable Lewis acid-base adduct with $\text{N}\equiv\text{SF}_3$. The doublet of $\text{F}_3^{32}\text{S}\equiv\text{N-Xe-F}^+$ and the isotopically shifted doublet associated with $\text{F}_3^{34}\text{S}\equiv\text{N-Xe-F}^+$ (see discussion in the following section) were also observed in this region and result from solvolysis of the $\text{F}_3\text{S}\equiv\text{N-Xe-OSeF}_5^+$ cation.

Evidence of the solvolysis of the $\text{F}_3\text{S}\equiv\text{N-Xe-OSeF}_5^+$ cation was observed in the F-on-Se(VI) region of the ^{19}F NMR spectrum (Figure 15). A multiplet at 59.0 ppm, with satellites corresponding to coupling to ^{77}Se ($^1J(^{77}\text{Se}-^{19}\text{F}) = 1428\text{ Hz}$) is observed and can be assigned to SeF_6 .²⁴ Under high resolution, the central line was clearly resolved into five lines in the ratio 2:12:29:55:10. The pattern arises from isotopic shifts corresponding to the non-magnetically active isotopes of natural abundance selenium.²⁵ The intensities are in good agreement with the natural isotopic abundances which occur in the ratio 1:10:27:57:10. The isotopic shift was -0.007 ppm/amu. It is likely that SeF_6 and $\text{F}_3\text{S}\equiv\text{N-XeF}^+$ could arise from the solvolysis reaction (equation 12), however, a peak in the region -150 to -160 ppm could not be observed for BrOF_3 .

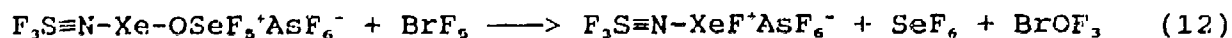


Table 12. NMR Parameters for $F_3S\equiv N-Xe-OSeF_5^+AsF_6^-$ in BrF_3 Solvent

Species	Solvent, T(°C)	Chemical Shift, ppm		
		$\delta(^{129}Xe)$	$\delta(^{19}F)^a$	$\delta(^{19}F)^b$
$Xe-OSeF_5^+AsF_6^-$ °	$BrF_3, -56$	-1438	d	62.4, F_{ax} 73.5, F_{aq}
$F_3S\equiv N-Xe-OSeF_5^+AsF_6^-$ *	$BrF_3, -60$	-1979	53.5	67.9, F_{ax} 70.4, F_{aq}

^a F-on-S(VI) region.

^b F-on-Se(VI) region.

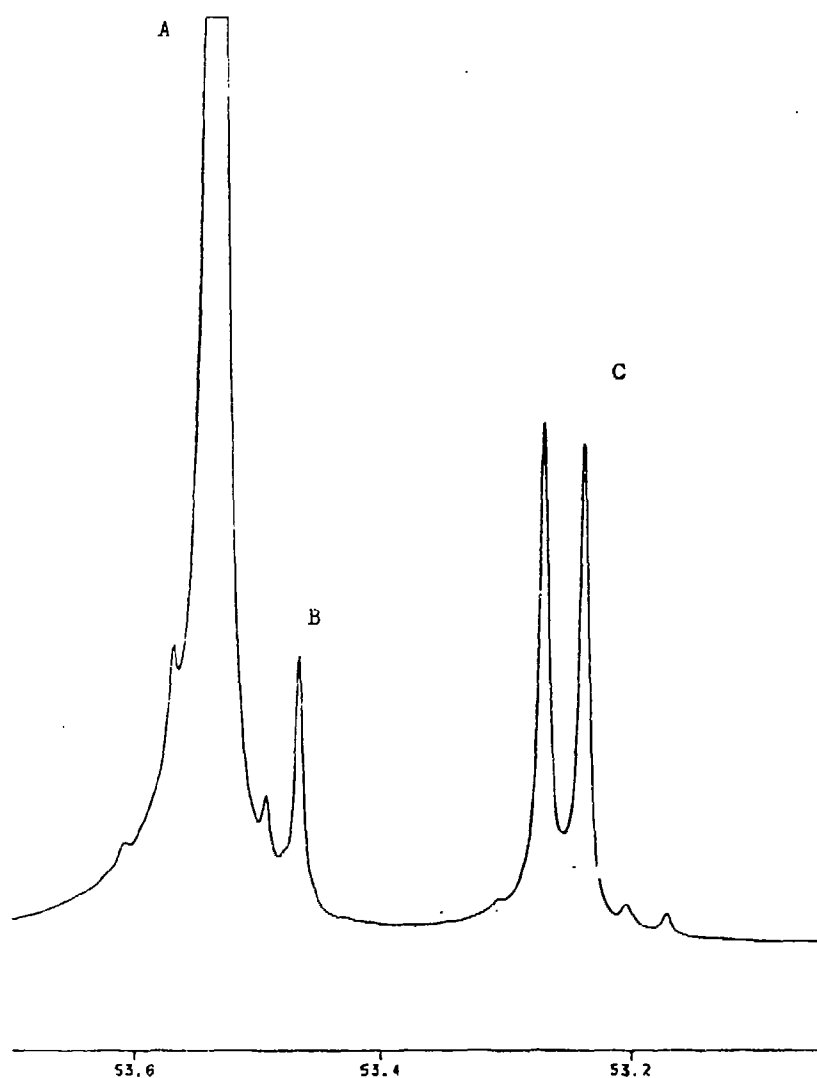
^c F-on-Se(VI) region: $^2J(^{19}F_{ax}-^{19}F_{aq})$, 219 Hz; $^2J(^{77}Se-^{19}F_{aq})$, 1398 Hz;

$^2J(^{77}Se-^{19}F_{ax})$, not resolved.

^d Not applicable.

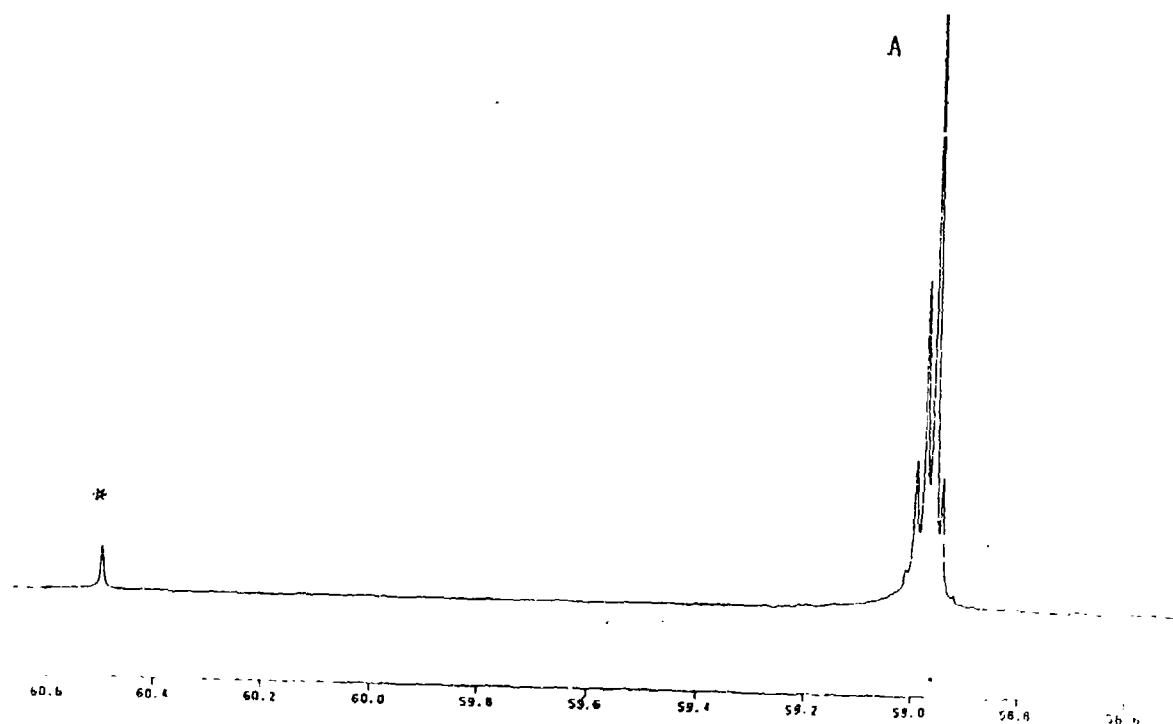
* F-on-Se(VI) region: $^2J(^{19}F_{ax}-^{19}F_{aq})$, 217 Hz; $^2J(^{77}Se-^{19}F_{aq})$, 1392 Hz;

$^2J(^{77}Se-^{19}F_{ax})$, not resolved: $^1\Delta^{19}F(^{34}/^{32}S)$, -0.066 ppm.



$\delta_{19}\text{F}$ (ppm from CFCl_3)

Figure 14. ^{19}F NMR spectrum of $\text{F}_3\text{S}\equiv\text{N}-\text{Xe}-\text{OSeF}_6^+\text{AsF}_6^-$ in BrF_3 solvent at -60°C , F-on-S(VI) region: (A) F-on- ^{32}S (VI), (B) F-on- ^{34}S (VI), (C) F-on-S(VI) of $\text{F}_3\text{S}\equiv\text{N}-\text{Xe}-\text{F}^+\text{AsF}_6^-$.



$\delta_{19\text{F}}$ (ppm from CFCl_3)

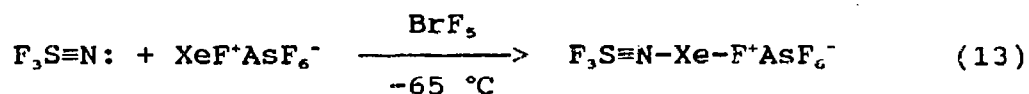
Figure 15. ^{19}F NMR spectrum of $\text{F}_3\text{S}\equiv\text{N}-\text{Xe}-\text{OSeF}_6^+\text{AsF}_6^-$ in BrF_3 solvent at -60°C , F-on-Se(VI) region: SeF_6 decomposition product, SeF_6 : (A) F-on-Se(VI), (*) ^{77}Se satellite.

The F-on-Se(VI) region of the ^{19}F NMR spectrum shown in Figure 16 is an AB₄ spin system. The chemical shifts and coupling constant for the system were calculated using the method of Harris and Packer.²⁹ The observed couplings associated with this second order spin system, $^1J(^{77}\text{Se}-^{19}\text{F}_{ax})$, $^1J(^{77}\text{Se}-^{19}\text{F}_{eq})$ and $^1J(^{19}\text{F}_{ax}-^{19}\text{F}_{eq})$, indicate that the s-character of the bonding molecular orbitals for the SeF_6 group is essentially the same in the precursor and in the adduct cation.¹⁸

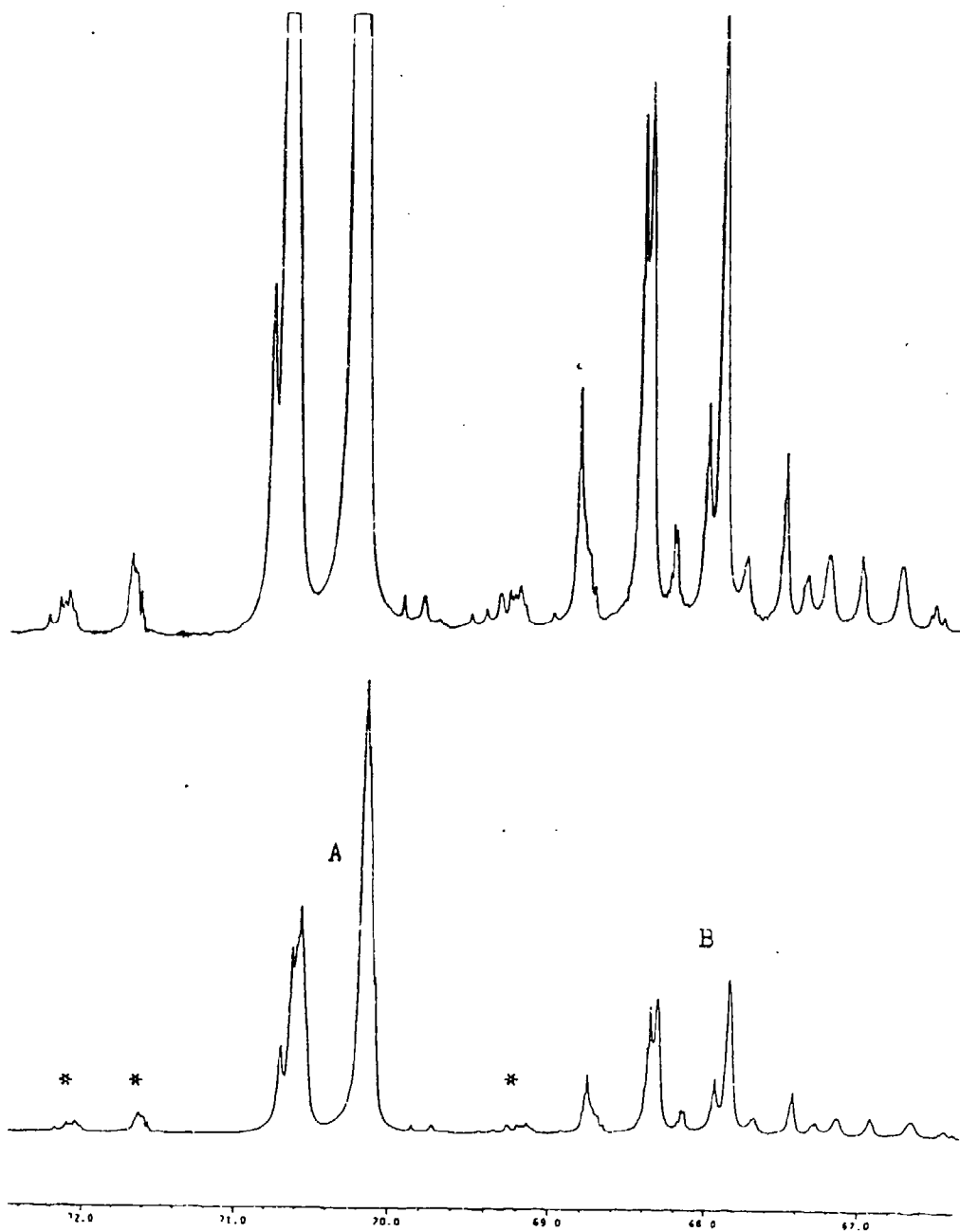
Characterization of $\text{F}_3\text{S}\equiv\text{N}-\text{Xe}-\text{F}^+\text{AsF}_6^-$ in BrF_3 Solvent by ^{19}F and ^{129}Xe NMR Spectroscopy

The $\text{F}_3\text{S}\equiv\text{N}-\text{Xe}-\text{F}^+$ cation was prepared by the reaction of $\text{XeF}^+\text{AsF}_6^-$ with $\text{N}\equiv\text{SF}_3$ in BrF_3 solvent at -60°C , and was characterized at -60°C in BrF_3 by ^{19}F and ^{129}Xe NMR spectroscopy. The NMR parameters are given in Table 13.

The ^{129}Xe NMR spectrum displays a broad doublet at -1661 ppm compared with -869 ppm for XeF^+ in BrF_3 (-52°C). The decrease in $\delta(^{129}\text{Xe})$ relative to that of XeF^+ results from an increase in shielding at xenon attributable to the formation of the Xe-N donor-acceptor bond according to equation (13). Moreover, xenon in $\text{F}_3\text{S}\equiv\text{N}-\text{Xe}-\text{F}^+$ is deshielded by 318 ppm with respect to



$\text{F}_3\text{S}\equiv\text{N}-\text{Xe}-\text{OSeF}_5^+$, which is consistent with the lower electro-negativity of the OSeF_5 group.



$\delta_{19\text{F}}$ (ppm from CFCl_3)

Figure 16. ^{19}F NMR spectrum of $\text{F}_3\text{S}\equiv\text{N}-\text{Xe}-\text{OSeF}_5^+\text{AsF}_6^-$ in BrF_5 solvent at -60°C , F-on-Se(VI) region: (A) F_{eq} -on-Se(VI), (B) F_{ax} -on-Se(VI), (*) ^{77}Se satellites.

Table 13. NMR Parameters for $F_3S=N-Xe-F^+AsF_6^-$ in BrF_5 and HF Solvents

Species	Solvent, T(°C)	Chemical Shift, ppm		
		$\delta(^{129}Xe)$	$\delta(^{19}F)^a$	$\delta(^{19}F)^b$
$Xe-F^+AsF_6^-$ ^c	BrF_5 , -47	-884	d	e
$F_3S=N-Xe-F^+AsF_6^-$ ^f	BrF_5 , -60	-1661	53.3	-180.5
$F_3S=N-Xe-F^+AsF_6^-$ ^g	HF, -20	-1653	51.2	-185.5
$F_4S=N(H)-Xe-F^+AsF_6^-$ ^h	HF, -20	-2672	54.0, F_a 64.2, F_b 110.5, F_c	i
$F_5S=N(H_2)-Xe-F^+AsF_6^-$ ^j	HF, -20	-2886	59.2, F_{ax} 71.9, F_{eq}	i

^a F-on-S(VI) region.

^b F-on-Xe(II) region.

^c G.J. Schrobilgen, unpublished work.

^d Not applicable.

^e $\delta(^{19}F)$, not recorded; $^1J(^{129}Xe-^{19}F)$, 6892 Hz.

^f $^1J(^{129}Xe-^{19}F)$, 6248 Hz; $^4J(^{19}F-^{19}F)$, 15 Hz; $^1J(^{129}Xe-^{14}N)$, not observed;

$^1\Delta^{19}F(^{34/32})S$, -0.066 ppm.

^g $^1J(^{129}Xe-^{19}F)$, 6251 Hz; $^4J(^{19}F-^{19}F)$, not observed; $^1J(^{129}Xe-^{14}N)$, 347 Hz;

$^1\Delta^{19}F(^{34/32})S$, not observed.

^h $^3J(^{129}Xe-^{19}F_b)$, 202 Hz; $^3J(^{129}Xe-^{19}F_c)$, 129 Hz; $^3J(^{129}Xe-^{19}F_a)$, not observed;

$^2J(^{19}F_a-^{19}F_b)$, 207 Hz; $^2J(^{19}F_a-^{19}F_c)$, 206 Hz; $^2J(^{19}F_b-^{19}F_c)$, 18 Hz; $^1\Delta^{19}F_a(^{34/32})S$,

-0.066 ppm.

ⁱ $\delta(^{19}F)$, not observed, see text.

^j $^2J(^{19}F_{ax}-^{19}F_{eq})$, 153 Hz; $^1\Delta^{19}F_a(^{34/32})S$, -0.059 ppm.

The ^{19}F NMR spectrum of the F-on-S(VI) region (Figure 17), displays a doublet at 53.3 ppm (cf., 53.5 ppm for $\text{F}_3\text{S}\equiv\text{N}-\text{Xe}-\text{OSeF}_5^+$) resulting from the $\text{F}_3^{32}\text{S}\equiv\text{N}-\text{XeF}^+$ cation, and a weak doublet resulting from the ^{34}S isotopomer, $\text{F}_3^{34}\text{S}\equiv\text{N}-\text{XeF}^+$, shifted 0.066 ppm to lower frequency (cf., $^1\Delta^{19}\text{F}(^{34}/^{32})\text{S} = -0.066$ ppm for $\text{F}_3\text{S}\equiv\text{N}-\text{Xe}-\text{OSeF}_5^+$). These parameters indicate that the F_3SeOXe^+ cation possesses a Lewis acid strength similar to that of the XeF^+ cation.

The ^{19}F NMR spectrum of the F-on-Xe(II) region (Figure 17) consists of a partly resolved 1:3:3:1 quartet at -180.5 ppm with a pair of ^{129}Xe satellites. The quartet arises from the four-bond coupling ($^4J(^{19}\text{F}-^{19}\text{F}) = 15$ Hz) between the three equivalent fluorines on sulfur and the terminal fluorine on xenon. The ^{129}Xe satellites arise from spin-spin coupling to natural abundance ^{129}Xe (26.44 %) ¹⁸ and do not display the fine structure which is observed on the central quartet. This difference in linewidths is the result of shielding anisotropy (chemical shift anisotropy) relaxation associated with ^{129}Xe in low-symmetry environments. The effect stems from the faster rate of spin-lattice relaxation associated with the $\text{F}_3\text{S}\equiv\text{N}-^{129}\text{XeF}^+$ cation and becomes important at high magnetic field strengths for heavy nuclides with large chemical shift ranges such as ^{129}Xe , i.e., the effect increases with B_0^2 and the mean expectation value of the valence p-orbitals.

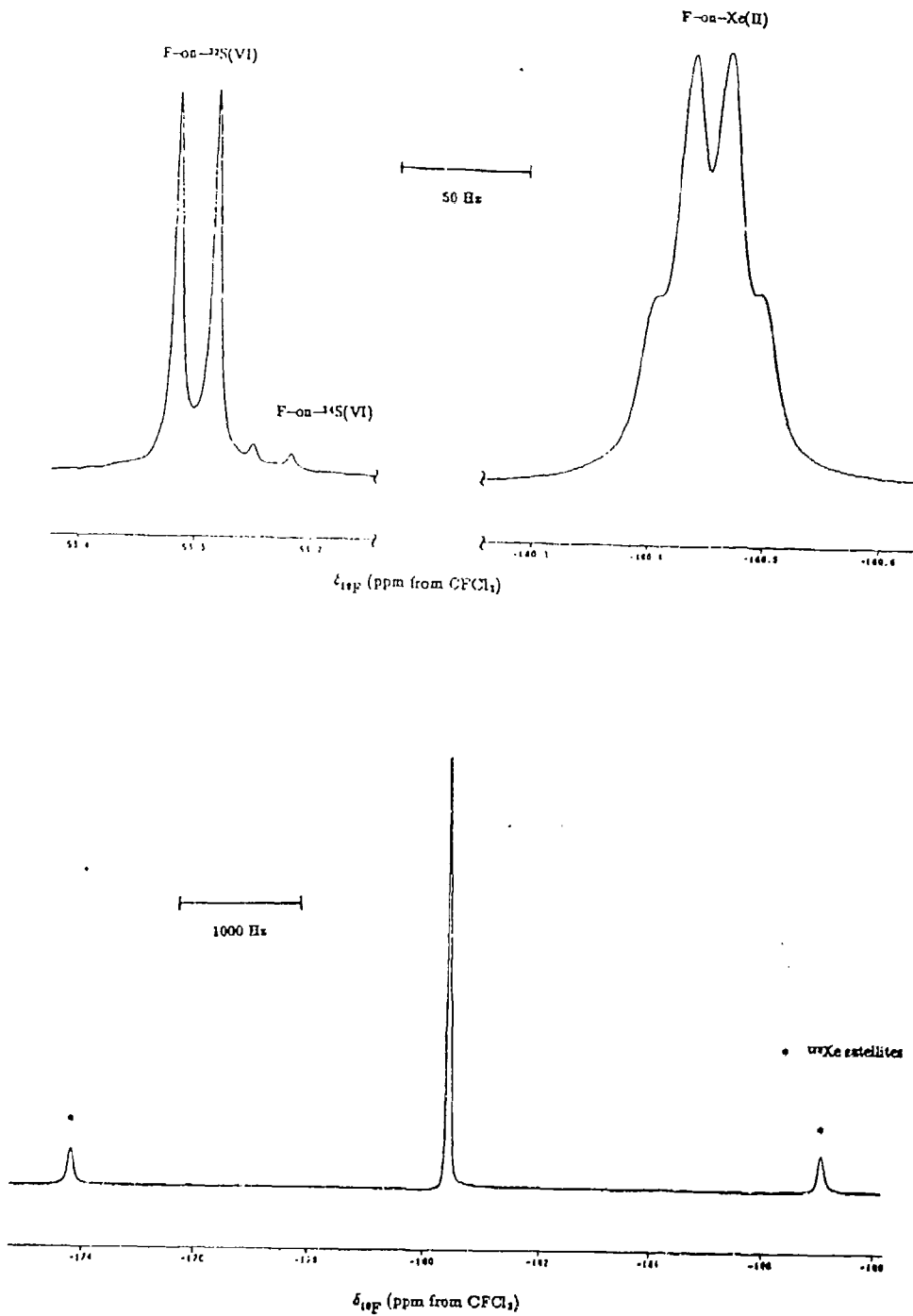


Figure 17. ^{19}F NMR spectrum of $\text{F}_3\text{S}\equiv\text{N}-\text{XeF}^+\text{AsF}_6^-$ in BrF_5 at -60°C .

Characterization of $F_3S\equiv N-Xe-F^+AsF_6^-$ in Anhydrous HF Solvent by ^{19}F and ^{129}Xe NMR Spectroscopy

Samples containing the $F_3S\equiv N-Xe-F^+$ cation in anhydrous HF were prepared by the dissolution of solid $F_3S\equiv N-Xe-F^+AsF_6^-$ in anhydrous HF at $-25^\circ C$. The salt used in the preparation was obtained from a Raman spectroscopy sample prepared in BrF_5 solvent. The bulk of the solvent had been removed by dynamic pumping at $-15^\circ C$ for eight hours, but was shown still to contain a significant amount of BrF_5 by Raman spectroscopy at $-196^\circ C$. A solution of the solvate in anhydrous HF was studied at $-20^\circ C$ using ^{19}F and ^{129}Xe NMR spectroscopy; the NMR parameters are given in Table 13.

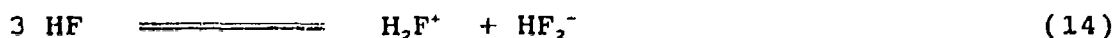
The ^{129}Xe NMR spectrum of $F_3S\equiv N-Xe-F^+AsF_6^-$ in anhydrous HF solvent at $-20^\circ C$ (Figure 18) consists of a broad doublet of triplets centered at -1653 ppm (cf., -1661 ppm for $F_3S\equiv N-Xe-F^+AsF_6^-$ in BrF_5), the doublet splitting (6251 Hz) is assigned to $^1J(^{129}Xe-^{19}F)$, (cf., 6248 Hz for $F_3S\equiv N-Xe-F^+AsF_6^-$ in BrF_5) and a 1:1:1 triplet splitting (347 Hz) is assigned to $^1J(^{129}Xe-^{14}N)$. Again, the decrease in $\delta(^{129}Xe)$ relative to that of the XeF^+ cation in anhydrous HF solvent results from an increase in shielding at xenon attributable to the formation of the Xe-N donor-acceptor bond. Coupling to ^{14}N indicates that the electric field gradient at the nitrogen center is small in the axially-symmetric cation and its observation is made more favorable by the fact that anhydrous HF possesses a low viscosity at this temperature, allowing for rapid tumbling of the cation.¹⁸

In the ^{19}F NMR spectrum, the F-on-Xe(II) region displays a singlet at -185.5 ppm (cf., -180.5 ppm for $F_3S\equiv N-Xe-F^+AsF_6^-$ in BrF_5) with ^{129}Xe satellites. The F-on-S(VI) region displays a singlet at 51.2 ppm (cf., 53.3

ppm for $F_3S\equiv N-Xe-F^+AsF_6^-$ in BrF_5). The isotope shift for the $F_3^{34}S\equiv N-Xe-F^+$ cation was not observed in the anhydrous HF solvent due to the broadening in the F-on-S(VI) region owing to partially quadrupole collapsed $^2J(^{19}F-^{14}N)$, so the broader resonances obscure the ^{34}S isotopic shift.

In order to study the $F_3S\equiv N-Xe-F^+$ cation further, another sample was prepared for ^{129}Xe and ^{14}N NMR spectroscopy. The sample was prepared by dissolution of solid $F_3S\equiv N-Xe-F^+AsF_6^-$ in anhydrous HF at $-78^\circ C$. This latter sample was prepared by the neat reaction of $N\equiv SF_3$ with $XeF^+AsF_6^-$ at $-25^\circ C$, thereby circumventing the use of BrF_5 solvent and the problems encountered with the removal of BrF_5 . However, the ^{129}Xe NMR spectrum of the sample did not show the expected singlet, but a 1:2:1 triplet at -1554 ppm with a coupling constant of 5676 Hz, and is readily assigned to XeF_2 .¹⁹ The ^{14}N NMR spectrum consisted of a sharp singlet at -73.0 ppm and a broad singlet at -278.0 ppm (Figure 19) which could not be assigned since a ^{14}N NMR spectrum of the free $N\equiv SF_3$ was not obtained.

Apparently, BrF_5 , which has a significant fluoride ion acceptor strength,³⁰ acts as a sink for HF_2^- generated in the autoionization of anhydrous HF according to equations (14) and (15). In the absence of BrF_5 , the HF_2^- ion presumably serves as a strong nucleophilic fluorinating agent towards positively charged nitrogen, reacting with the $F_3S\equiv N-XeF^+$ cation to $N\equiv SF_3$ and XeF_2 according to equation (16).



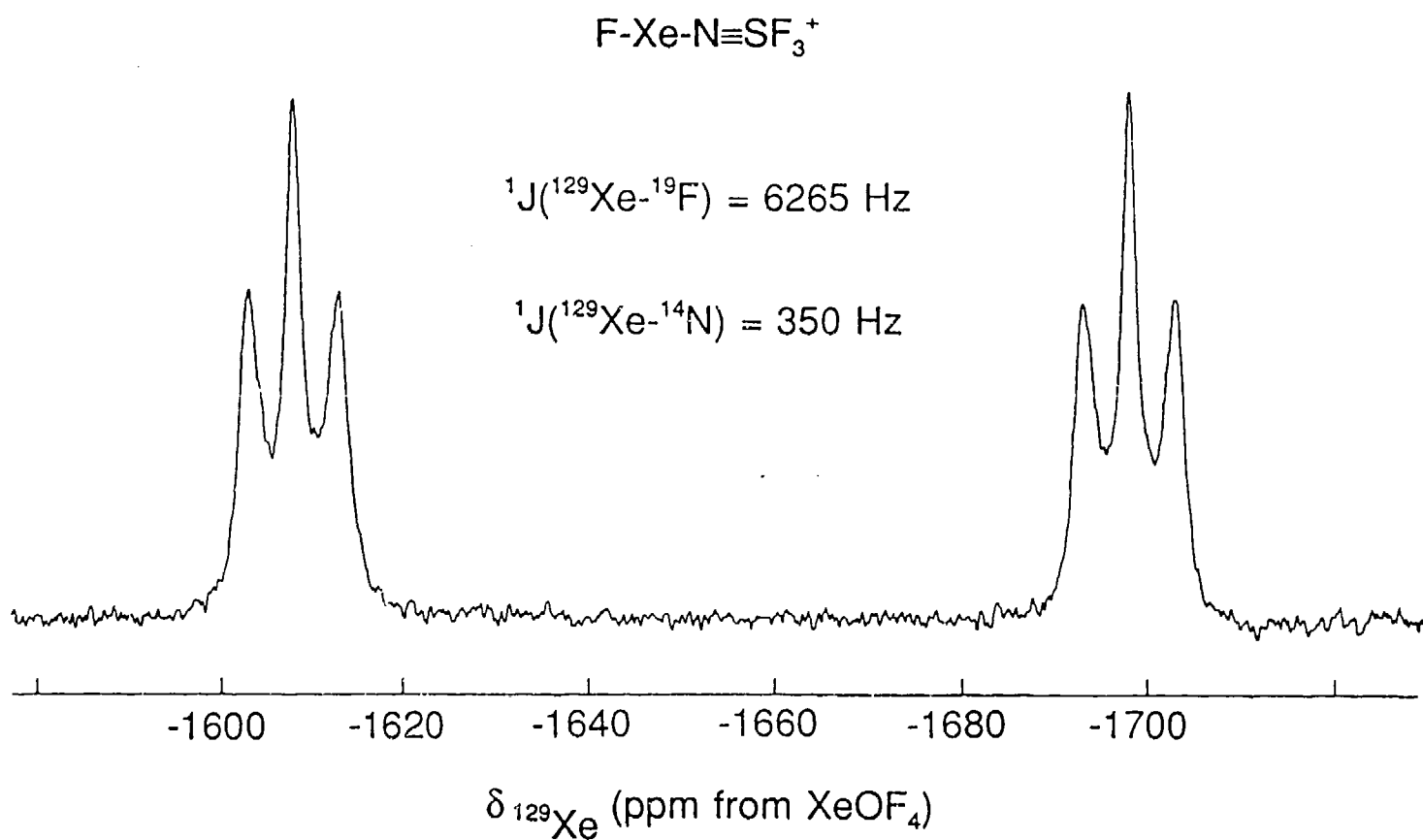
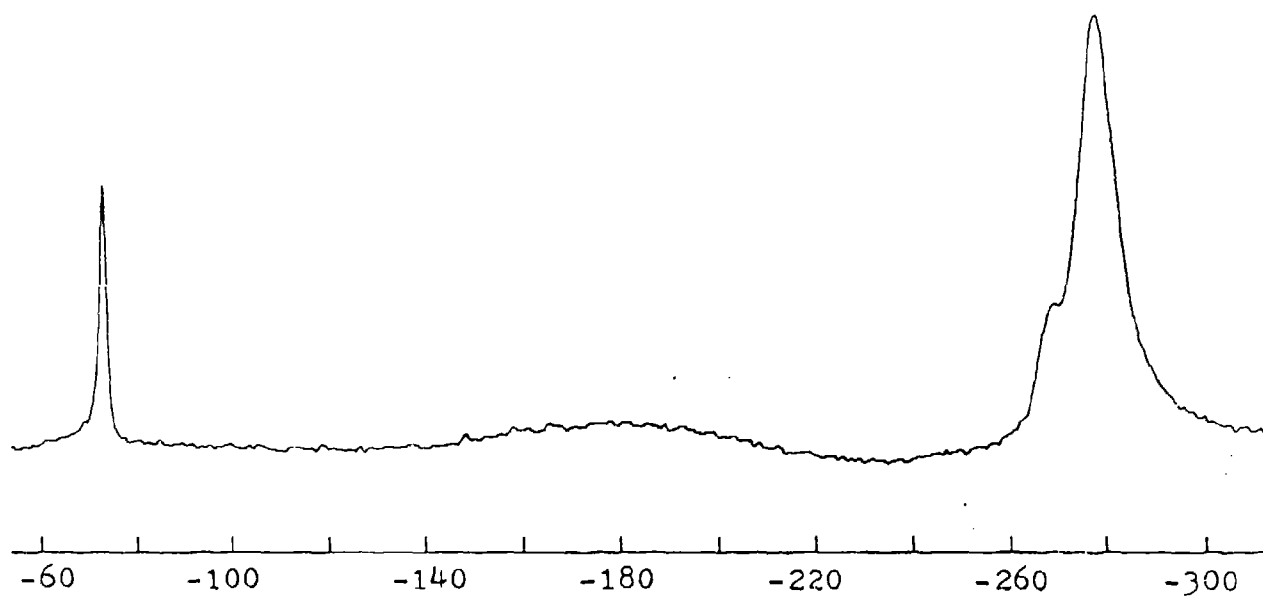


Figure 18. ^{129}Xe spectrum of $\text{F}_3\text{S}\equiv\text{N-Xe-F}^+\text{AsF}_6^-$ in anhydrous HF solvent.



$\delta_{14\text{N}}$ (ppm from CH_3NO_2)

Figure 19. ^{14}N NMR spectrum of $\text{F}_3\text{S}\equiv\text{N}-\text{Xe}-\text{F}^+\text{AsF}_6^-$ (prepared neat) in anhydrous HF solvent at -20°C .

This discovery is important because HF is a preferred solvent for low-temperature NMR spectroscopy owing to its solvent properties and low viscosity. However, the fluorinating strength the pure solvent has limited its usefulness to the study in the present instance. A mixed solvent system consisting of anhydrous HF and several mole percent of BrF_3 exhibits the properties of low viscosity associated with anhydrous HF but has a reduced fluoride ion basicity. It would therefore be worthwhile attempting the analogous experiment using the strong fluoride acceptor AsF_6^- to inhibit reaction (16).

Characterization of the Solvolysis Products of the $\text{F}_3\text{S}\equiv\text{N}-\text{XeF}^+$ Cation in Anhydrous HF Solvent by ^{19}F and ^{129}Xe NMR Spectroscopy; The $\text{F}_3\text{S}=\text{N}(\text{H})-\text{Xe}-\text{F}^+$ and $\text{F}_3\text{S}-\text{N}(\text{H}_2)-\text{Xe}-\text{F}^+$ Cations

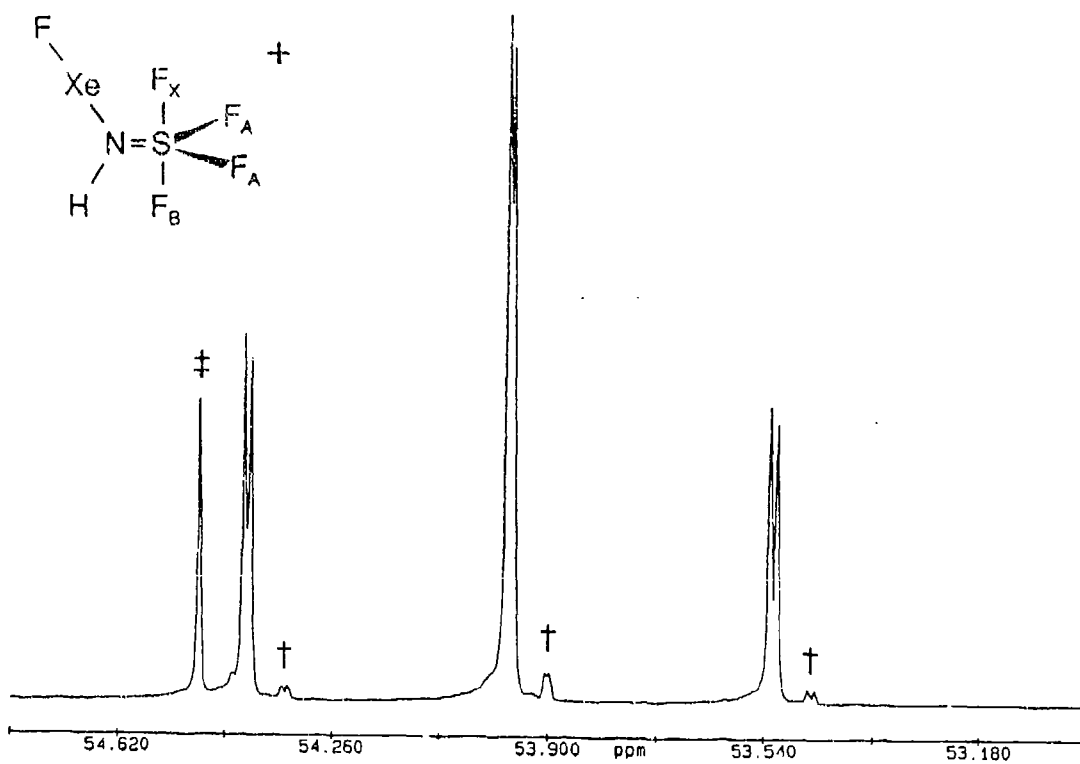
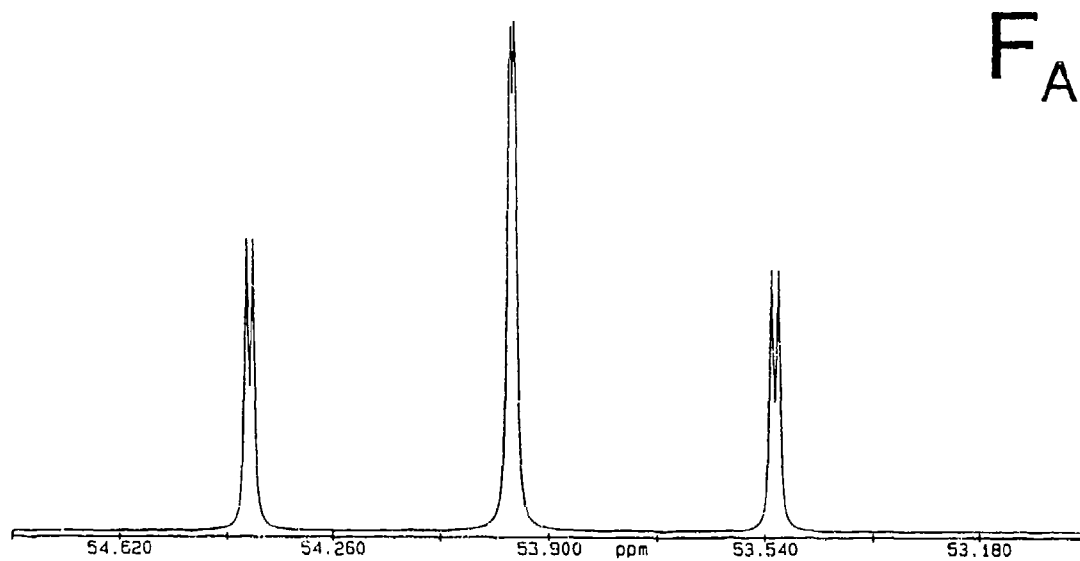
The $\text{F}_3\text{S}\equiv\text{N}-\text{Xe}-\text{F}^+\text{AsF}_6^-$ salt was prepared by the reaction of $\text{XeF}^+\text{AsF}_6^-$ with $\text{N}\equiv\text{SF}_3$ in BrF_3 solvent at -60°C and characterized as indicated in the previous section. The sample was isolated and redissolved in anhydrous HF for use in NMR spectroscopy. After approximately twenty minutes at -20°C in the NMR probe, new resonances grew in the F-on-S(VI) region of the ^{19}F NMR spectrum and in the ^{129}Xe NMR spectrum (Table 13). These new resonances grew in intensity with the concomitant loss of the resonances associated with the $\text{F}_3\text{S}\equiv\text{N}-\text{XeF}^+$ cation, indicating that solvolysis of the $\text{F}_3\text{S}\equiv\text{N}-\text{XeF}^+$ cation had occurred.

In the ^{19}F NMR spectrum, the multiplet at 54.0 ppm (F_a , Figure 20) integrates to twice the intensity of the other, newly observed resonances

(F_b and F_c) and consists of a doublet of doublets exhibiting second order effects where the two coupling constants, ${}^2J({}^{19}\text{F}_a-{}^{19}\text{F}_b)$ and ${}^2J({}^{19}\text{F}_a-{}^{19}\text{F}_c)$, differ by only one Hz, and a ${}^{34}/{}^{32}\text{S}$ isotopic shift was observed on F_a. The multiplet centered at 64.2 ppm consists of a 1:2:1 "triplet" resulting from coupling to the two equivalent F_a nuclei (exhibiting second order effects), which is split into doublets by ${}^2J({}^{19}\text{F}_b-{}^{19}\text{F}_c)$ coupling and displays ${}^{129}\text{Xe}$ satellites (F_b, Figure 21). The third resonance, centered at 110.5 ppm (F_c, Figure 22) consists of a 1:2:1 triplet resulting from coupling to ${}^{19}\text{F}_a$, which is split into doublets by ${}^2J({}^{19}\text{F}_b-{}^{19}\text{F}_c)$ coupling and also displays ${}^{129}\text{Xe}$ satellites.

Due to the complexity of the A₂BX spin system, the ${}^{19}\text{F}$ NMR spectrum was simulated in order to confirm the assignments. Two simulations were carried out using an iterative NMR simulation program for a personal computer.³¹ The first calculation fitted the four fluorines on sulfur (chemical shifts and coupling constants were iterated), the second consisting of the four fluorines on sulfur plus the ${}^{129}\text{Xe}$ couplings and the two simulations were summed to produce the ${}^{19}\text{F}$ NMR spectrum with ${}^{129}\text{Xe}$ satellites (see Appendix). The calculated spectra are shown with the corresponding regions of the recorded ${}^{19}\text{F}$ NMR spectra (Figures 19 to 21) and closely resemble the observed spectra.

In the ${}^{129}\text{Xe}$ NMR spectrum, the new resonance consists of a doublet of doublets centered at -2672 ppm with couplings of 202 and 129 Hz which correspond to ${}^2J({}^{129}\text{Xe}-{}^{19}\text{F}_b)$ and ${}^2J({}^{129}\text{Xe}-{}^{19}\text{F}_c)$, respectively (Figure 23).



δ_{19F} (ppm from CFCl_3)

Figure 20. ^{19}F NMR spectrum of the $\text{F}_x\text{S}=\text{N}(\text{H})-\text{Xe}-\text{F}^+$ cation, F_A -on-S(VI) region:

top; simulation, (line broadening), 7 Hz,

bottom; spectrum, (line broadening), 5 Hz.

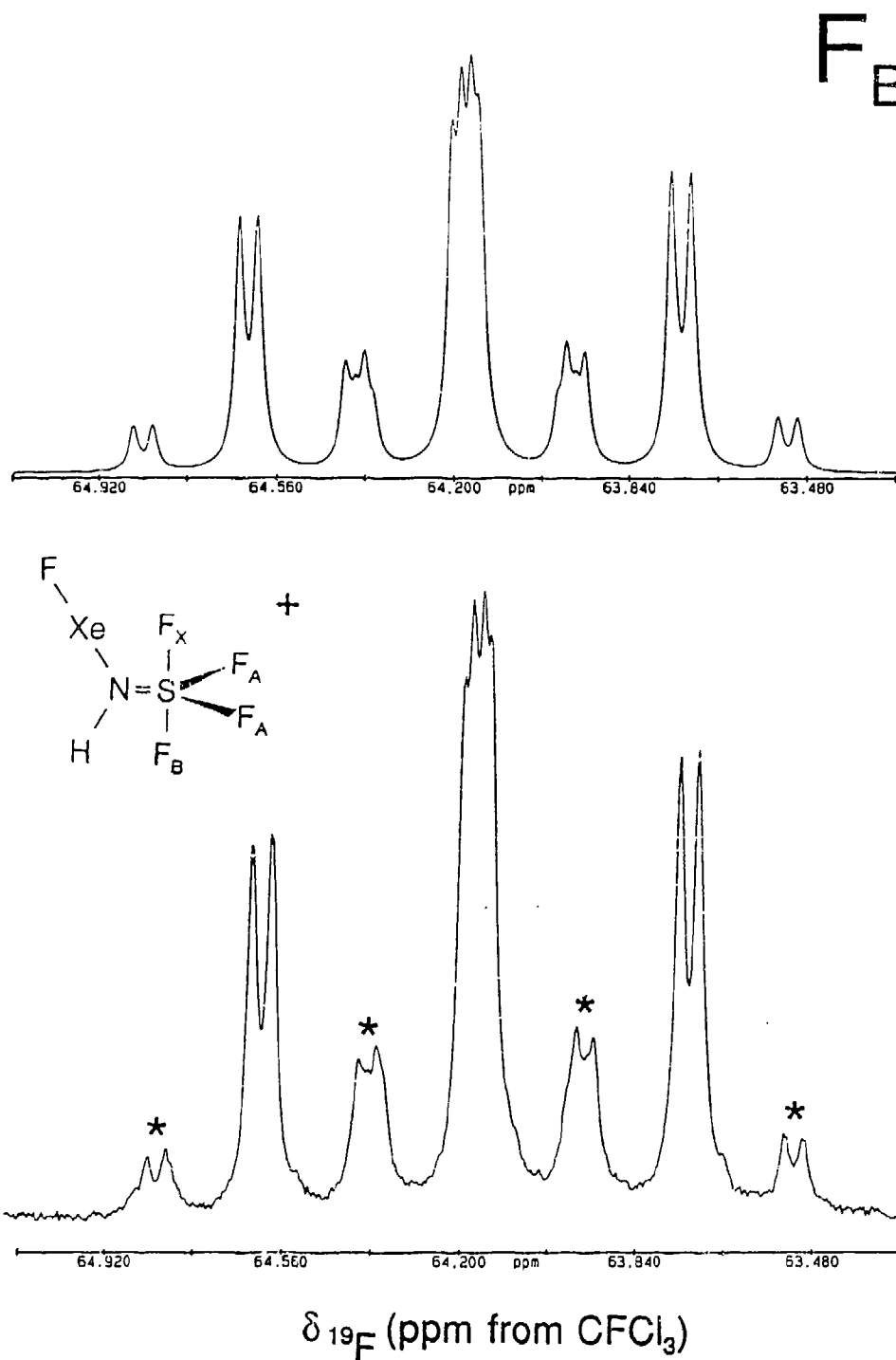


Figure 21. ^{19}F NMR spectrum of the $\text{F}_4\text{S}=\text{N}(\text{H})-\text{Xe}-\text{F}^+$ cation, F_B -on-S(VI) region:
top; simulation, (line broadening), 24 Hz,
bottom; spectrum, (line broadening), 14 Hz.

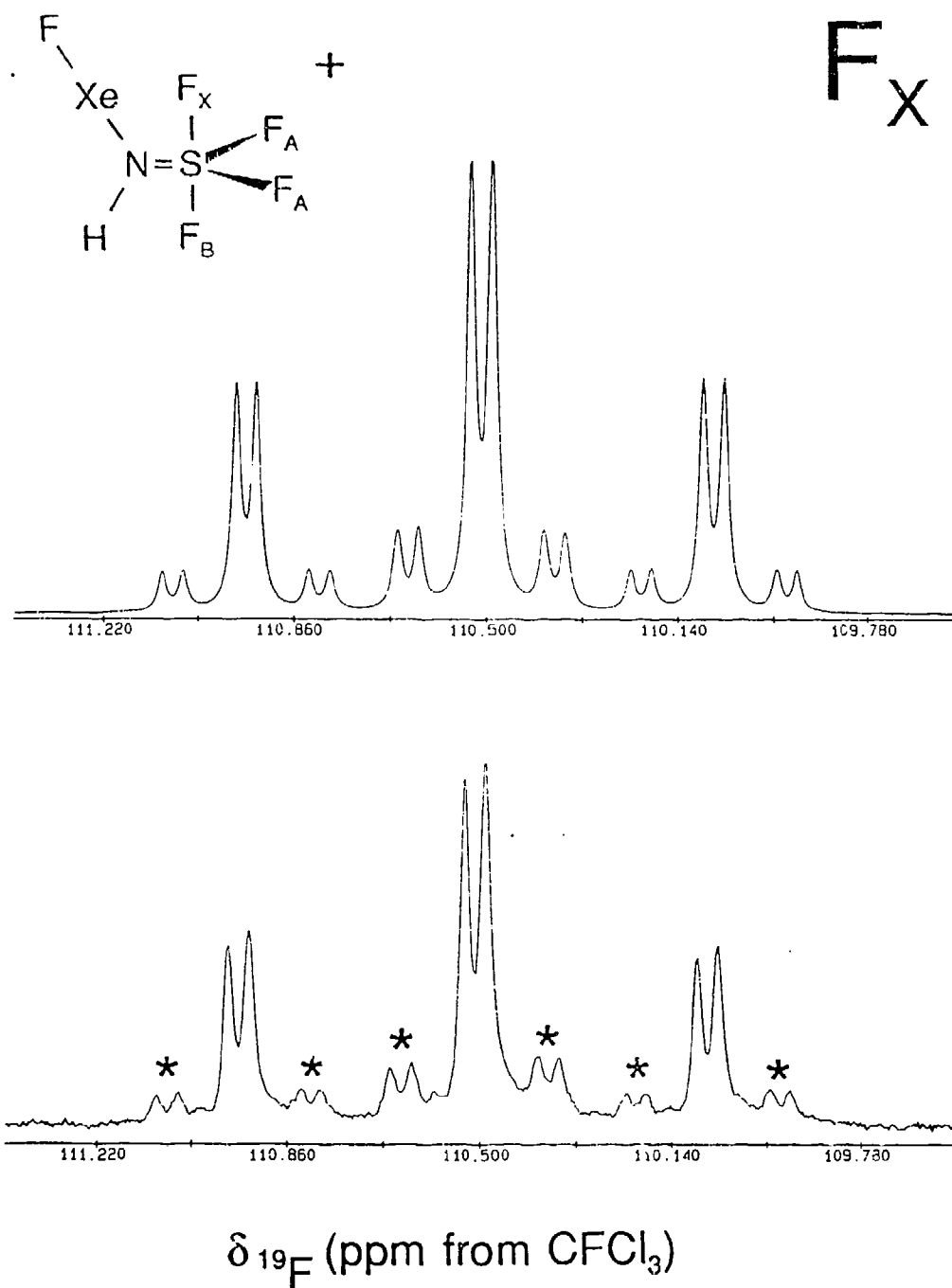


Figure 22. ^{19}F NMR spectrum of the $\text{F}_4\text{S}=\text{N}(\text{H})-\text{Xe}-\text{F}^+$ cation, F_c -on-S(VI) region:
 top; simulation, (line broadening), 20 Hz,
 bottom; spectrum, (line broadening), 11 Hz.

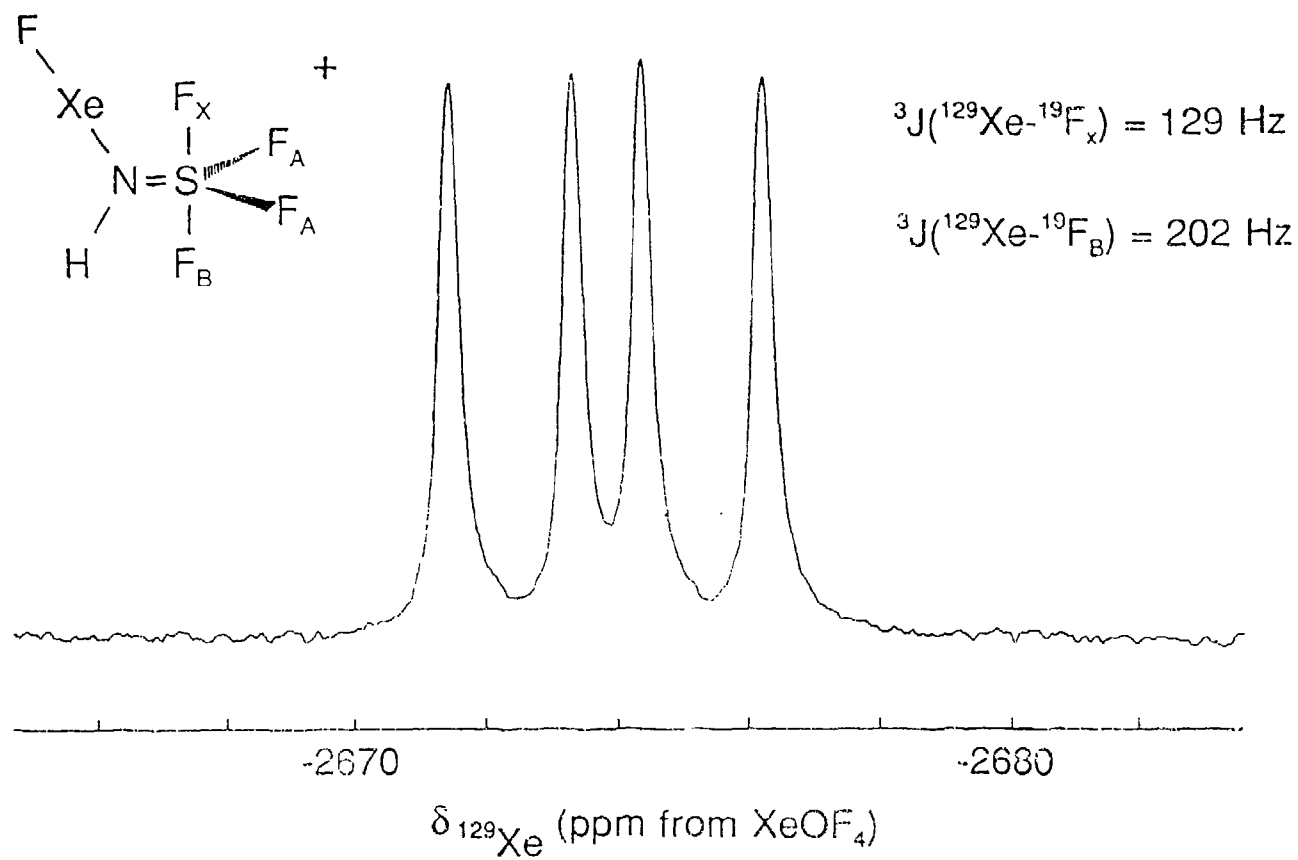
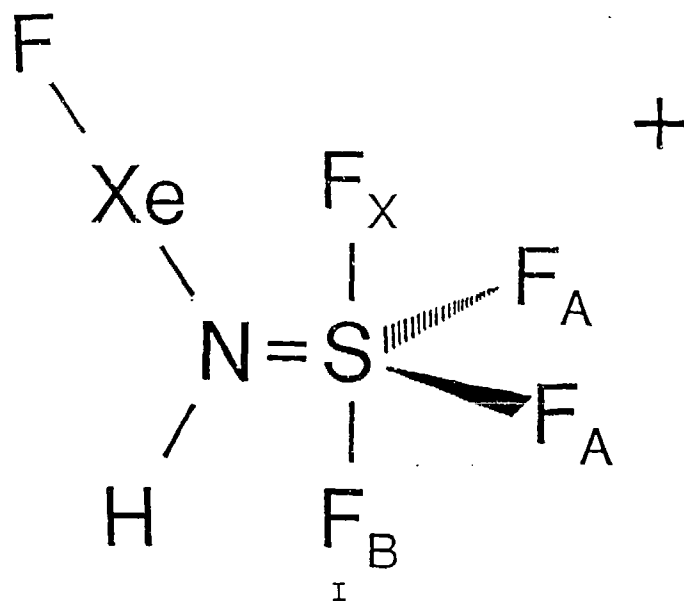
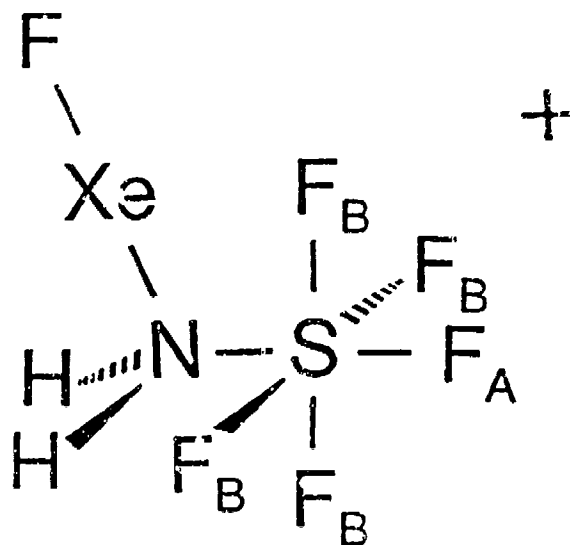


Figure 23. ${}^{129}\text{Xe}$ NMR spectrum of the $\text{F}_4\text{S}=\text{N}(\text{H})-\text{XeF}^+$ cation.

The ^{129}Xe chemical shift indicates a substantial increase in shielding at xenon relative to that of xenon in $\text{F}_3\text{S}=\text{N}-\text{XeF}^+$ and is presumably the result of a decrease in electronegativity anticipated when the nitrogen lone pair hybridization changes from sp to sp^2 upon going from $\text{F}_3\text{S}=\text{N}$ to $\text{F}_4\text{S}=\text{NH}$.³² The expected structure of the $\text{F}_4\text{S}=\text{N}(\text{H})-\text{Xe}-\text{F}^+$ cation deduced from the NMR spectra is depicted in Structure I.

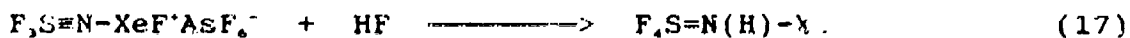


The F-on-Xe(II) resonance in the ^{19}F NMR spectrum was not observed, presumably owing to exchange of this fluorine with the anhydrous HF solvent and this would account for the lack of a $^1J(^{129}\text{Xe}-^{19}\text{F})$ coupling in the ^{129}Xe spectrum and the lack of coupling to the proton in the $\text{F}_4\text{S}=\text{N}(\text{H})-\text{Xe}-\text{F}^+$ cation. Exchange of the fluorine on xenon could presumably be promoted by hydrogen bond formation between the N-H proton and HF in the cyclic intermediate represented by Structure II.



II

The probable mechanism for solvolysis of the $F_5S=N-Xe-F^+$ cation proceeds by addition of HF to the $N=S$ triple bond as has been previously observed for the free $N=SF_5$ in anhydrous HF (ref. 24 and this work). Addition of one molecule of HF across the $S=N$ triple bond would result in the formation of the $F_5S=N(H)-Xe-F^+$ cation in accordance with equation (17). The product resulting



from the addition of HF to $N=SF_5$, namely, $F_5S=NH$, has not been previously observed due to the rapid rate of solvolysis by a second molecule of HF resulting in pentafluorosulfanylamine, F_5S-NH_2 , which has been isolated.²¹

After the sample had been in the NMR tube at $-20^\circ C$ for approximately 45 minutes, the resonances in the ^{19}F and ^{136}Xe NMR spectra associated with the $F_5S=N(H)-Xe-F^+$ cation decreased in intensity while another set of resonances grew in. The ^{19}F NMR spectrum (Figure 24) depicts two AX₄ spin systems, one corresponding to F_5S-NH_2 (the solvolysis product of $N=SF_5$ in anhydrous HF, see Table 11), and the parameters of the other are

given in Table 13. The new F_{ax} -on-S(VI) (quintet, 59.2 ppm) and F_{aq} -on-S(VI) (doublet, 71.9 ppm) resonances occur at higher frequency than those observed for free F_5S-NH_2 in HF at $-56^\circ C$ (51.0 ppm and 71.9 ppm, respectively). The $^{34}/^{32}S$ isotopic shift of -0.059 ppm is essentially the same as the isotopic shift observed for free F_5S-NH_2 in anhydrous HF solvent, indicating that the S-F bond strengths in the free base and the adduct-cation are similar. The newest resonance likely results from pentafluorosulfanylamine (F_5S-NH_2), which remained coordinated to XeF^+ after the addition of a second molecule of HF giving rise to the $F_5S-N(H_2)-Xe-F^+$ cation formed by reaction (18).



Dissociation of this adduct cation results in the formation of free F_5S-NH_2 and $XeF^+AsF_6^-$ in HF solvent according to equilibrium (19).

The ^{129}Xe NMR spectrum displays a singlet at -2886 ppm, and is the most shielded ^{129}Xe environment observed for a xenon-nitrogen bonded species. Moreover, this cation represents the first example of a bond between xenon and an sp^3 -hybridized nitrogen. The ^{129}Xe chemical shift indicates a further increase in shielding at the xenon relative to xenon in $F_5S=N(H)-XeF^+$ and $F_5S=N-XeF^+$. The increase in shielding at ^{129}Xe in this series of closely related cation parallels the decrease in electronegativity anticipated when the nitrogen lone pair hybridization changes from sp to sp^2 to sp^3 along the

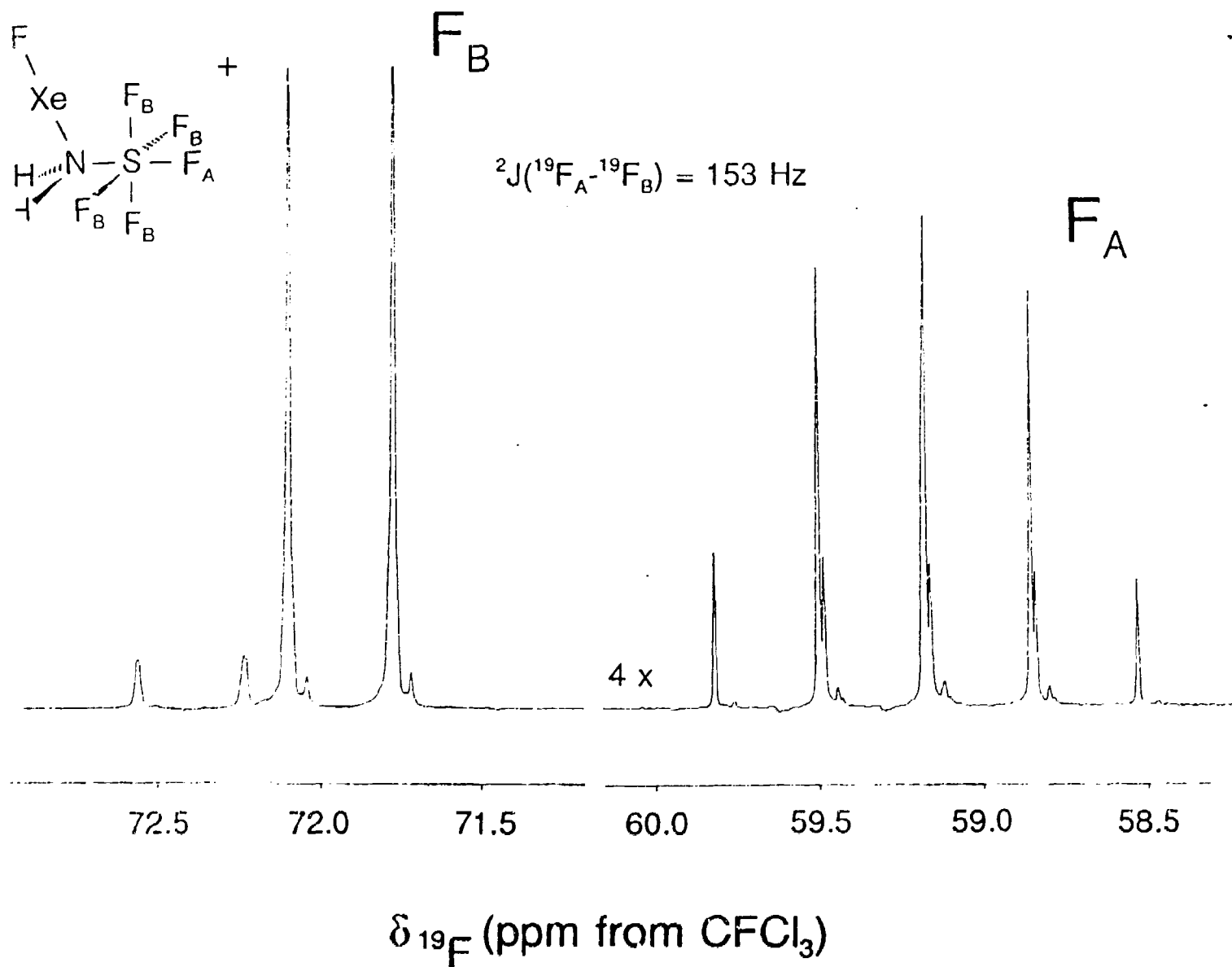


Figure 24. ${}^{19}\text{F}$ NMR spectrum of the SF_6 group of the $\text{F}_5\text{S-N}(\text{H}_2)\text{-Xe-F}^+$ cation recorded in anhydrous HF solution at -20°C .

series $F_3S\equiv N$, $F_4S=NH$, F_5S-NH_2 . The trend in electronegativity in nitrogen is analogous to the accepted increase in carbon electronegativity with increasing s-character of the hybrid orbitals.³²

Characterization of $F_3S\equiv N-XeF^+AsF_6^-$ by Raman Spectroscopy

Solid samples of $F_3S\equiv N-XeF^+AsF_6^-$ used for Raman spectroscopy were initially prepared by the combination of $XeF^+AsF_6^-$ and $N\equiv SF_3$ in BrF_3 solvent at $-60^\circ C$ (equation (13)). Unfortunately, this preparative method proved to be unacceptable for Raman spectroscopy samples owing to the difficulty in removing the BrF_3 solvent after synthesis (see Experimental Section). The amount of BrF_3 present in different samples varied with pumping time and temperature of the sample while the BrF_3 was being removed under dynamic vacuum. To avoid this problem, $F_3S\equiv N-XeF^+AsF_6^-$ was prepared at $-25^\circ C$ by the direct combination of the reactants, $N\equiv SF_3$ and $XeF^+AsF_6^-$, in the absence of a solvent (see Experimental Section). A trace of the low-temperature ($-196^\circ C$) Raman spectrum of the salt is shown in Figure 25 and the observed vibrational frequencies with their tentative assignments are given in Table 14.

The Raman spectra are consistent with the formation of $F_3S\equiv N-XeF^+AsF_6^-$. The $F_3S\equiv N-XeF^+$ cation is expected to give rise to $3N - 6 = 15$ normal modes of vibration belonging to the irreducible representations $5 A_1 + 5 E$ under the point symmetry C_{3v} . All fifteen modes are Raman and infrared active, and consist of five stretching modes, $\nu_1(A_1)$, $S\equiv N$ stretch; $\nu_2(A_1)$, sym $S-F$ stretch; $\nu_4(A_1)$, $Xe=F$ stretch, $\nu_3(A_1)$, $Xe-N$ stretch and $\nu_6(E)$, asym $S-F$ stretch and five bending modes, $\nu_5(A_1)$, sym SF_3 bend;

$\nu_7(E)$, asym SF_3 bend; $\nu_8(E)$, XeNS bend; $\nu_9(E)$, NSF bend and $\nu_{10}(E)$, FXeN bend. Therefore, ten vibrational bands are expected in both the Raman and infrared. In addition, the octahedral AsF_6^- anion is expected to give rise to three Raman-active vibrational bands under O_h symmetry, $\nu_1(a_{1g})$, $\nu_2(e_g)$ and $\nu_3(t_{2g})$. However, 39 bands as opposed to the predicted 18 from a consideration of free ion symmetries are observed in the Raman spectrum of $F_3S\equiv N-XeF^+AsF_6^-$ (Table 14). The disparity between the number of observed bands and the number predicted from a consideration of the free species is attributed to vibrational coupling within the unit cell and/or reduction of the free ion symmetries due to site symmetry effects. In the absence of a crystallographic space group for $F_3S\equiv N-XeF^+AsF_6^-$,³³ no attempt has been made in the ensuing discussion to account for factor-group splittings and their symmetry species in a rigorous manner. In the present discussion, the AsF_6^- anion has been assigned under O_h symmetry, but several of the bands in the spectrum are assigned to the formally Raman forbidden modes which apparently are rendered Raman active as the result of site symmetry lowering in the unit cell. Thus, the inactive mode $\nu_6(t_{2g})$, AsF_6^- and the IR active mode, $\nu_3(t_{1u})$, AsF_6^- , is also assigned along with its factor group splitting.

Vibrational assignments were aided by comparison with $F_3S\equiv N^{17,34}$, $F_3S\equiv N-MF_6$ (where $M = As, Sb$)¹⁷, $XeF^+AsF_6^-$,²¹ and $RC\equiv N-XeF^+AsF_6^-$, ($R = H, CH_3, CH_2F$, etc.).²¹ The fundamental stretching modes $\nu(XeF)$ and $\nu(SN)$ are readily assigned by comparison with the Raman spectra of $XeF^+AsF_6^-$ and other related species which are listed in Table 8, and $N\equiv SF_6$ and several Lewis acid/ $N\equiv SF_6$ adducts.^{17,34} As the Xe-F and S-N stretching modes belong to the totally symmetric representation, A_1 ; their splittings can only be attributed to coupling of vibrational modes within the unit cell.

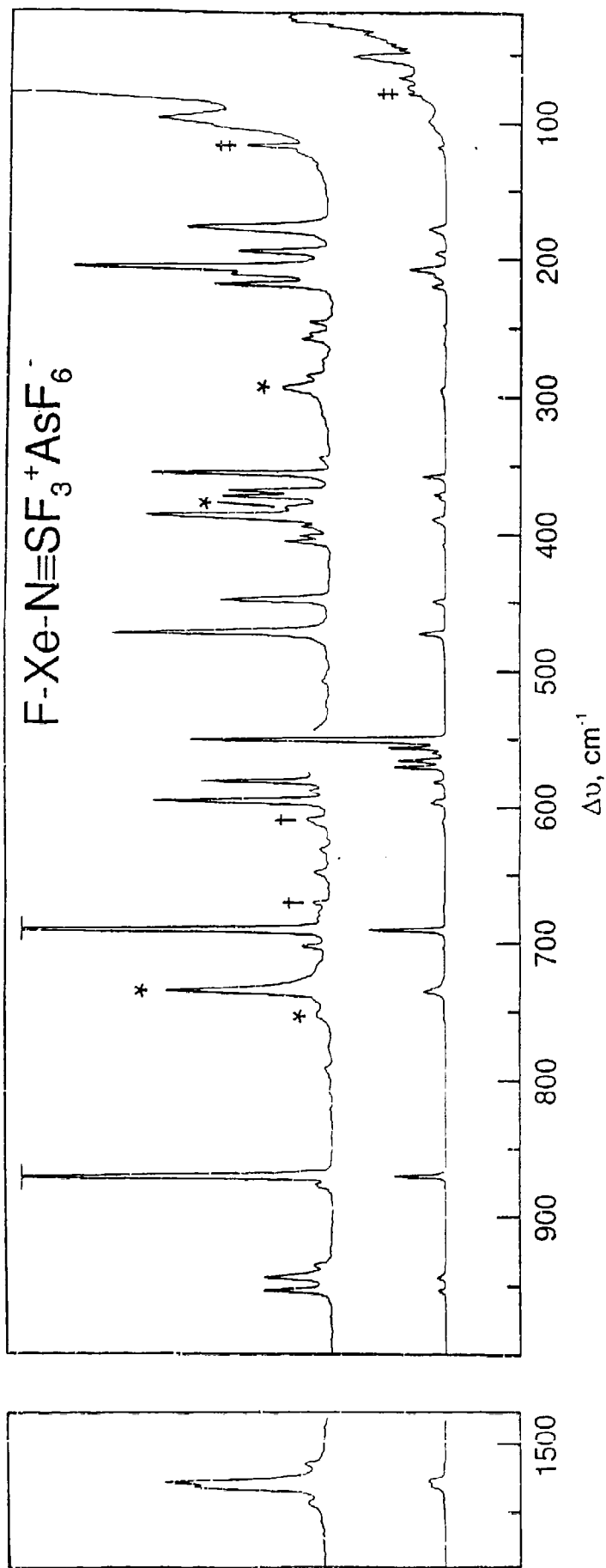


Figure 25. Trace of the Raman spectrum of $F_3S \equiv N - XeF^+ AsF_6^-$ recorded at $-196^\circ C$ in an FEP reaction tube: (*) FEP absorption bands, (+) argon ion laser plasma lines, (+) $XeF^+ AsF_6^-$ impurity bands: $672(1) \text{ cm}^{-1}$, $\nu_1(a_1)$ of AsF_6^- ; $610(1) \text{ cm}^{-1}$, $\nu(Xe-F)$.

Table 14. Raman Frequencies and Tentative Assignments for
 $F_3S\equiv N-XeF^+AsF_6^-$ at $-196^\circ C.$ ^a

<u>Freq. (cm⁻¹)^b</u>	<u>Tent. Assign.</u>	<u>Freq. (cm⁻¹)</u>	<u>Tent. Assign.</u>
1544 (1)	$\nu_1(a_1)$, S \equiv N str	571 (10)	$\nu_3(a_1)$, sym SF ₃ bend
1531 (7)		566 (19)	
1527 (9)		561 (9)	
1515 (1)		556 (23)	$\nu_4(a_1)$, Xe-F str
		551 (100)	
954 (4)	$\nu_6(e)$, asym S-F str		
945 (4)		473 (12)	$\nu_7(e)$, asym SF ₃ bend
936 (1)		449 (6)	
877 (1)	$\nu_2(a_1)$, sym S-F str	407 (2)	$\nu_8(e)$, XeNS bend
871 (21)		404 (2)	
		397 (2)	
792 (.5)	?	390 (10)	
703 (2)	$\nu_3(t_{1u})$, AsF ₆ ⁻	374 (6)	$\nu_5(t_{2g})$, AsF ₆ ⁻
		371 (6)	
691 (30)	$\nu_1(a_{1g})$, AsF ₆ ⁻		
649 (1)	?	358 (10)	$\nu_9(e)$, NSF bend
		261 (2)	$\nu_5(a_1)$, Xe-N str
632 (.5)	?	257 (1)	
597 (10)	$\nu_2(e_g)$, AsF ₆ ⁻	248 (1)	$\nu_6(t_{2g})$, AsF ₆ ⁻
589 (1)			
582 (7)		221 (16)	$\nu_{10}(e)$, FXeN bend
		213 (6), sh	
		208 (14)	
		197 (5)	
		179 (8)	

Continued...

Table 14 (Continued)

Lattice Modes (cm^{-1})^a:

99 (6), 82 (4), 74 (8), 67 (10), 53 (19),
52 (25), 47 (5), 46 (4), 43 (6), 41 (6),
35 (7), 30 (11), 26 (16), 23 (9)

^a Raman spectrum was recorded using FEP sample tubes and 514.5 nm excitation from an argon ion laser. Lines due to the FEP sample have been not been included in this table and are indicated on the spectral trace.

^b Values in parentheses denote intensities; sh denotes a shoulder, str denotes a stretching mode.

The most intense band at 551(100) cm^{-1} and the weaker bands at 556(23) and, tentatively, 561(9) cm^{-1} are assigned to the factor group split XeF stretching frequency of the $\text{F}_3\text{S}\equiv\text{N}-\text{XeF}^+$ cation, and are characteristic of the terminal XeF bond in xenon(II) species of the type L-Xe-F (see Table 8). The Xe-F stretching frequency can be used to assess the covalent nature of the Xe-F bond. The XeF^+ cation has been shown to be weakly coordinated to the anion by means of a fluorine bridge, and the Xe-F stretch has been shown to correlate with the degree of covalent character in the Xe---F bridge bond, decreasing with increasing base strength of the anion. Consequently, the Xe-F stretching frequency is expected to increase as the xenon-nitrogen bond becomes more ionic and the terminal XeF bond becomes more covalent.

The Xe-N stretching frequency of the $\text{F}_3\text{S}\equiv\text{N}-\text{XeF}^+$ cation is tentatively assigned to weak, low-frequency lines at 261(2) and 257(1) cm^{-1} where the splitting is again attributed to vibrational coupling within the unit cell. The Xe-N stretching frequency of $\text{F}_3\text{S}\equiv\text{N}-\text{XeF}^+$ is at lower frequency than that of $\text{FXeN}(\text{SO}_2\text{F})_2$ (422 cm^{-1}).³⁵ This is attributed to the greater covalent character of the Xe-N bonds in the imidodisulfonyl-fluoride derivative, whereas the Xe-N bond of the $\text{F}_3\text{S}\equiv\text{N}-\text{XeF}^+$ cation is one of the most ionic among the Xe-N bonded species presently known. This is corroborated by the high-frequency position of the Xe-F stretch, which is among the highest of any F-Xe-L type species.

The formally doubly degenerate XeNS bending modes are tentatively assigned to weak lines at 407(2), 404(2), 397(2) and 390(10) cm^{-1} . The FXeN bending modes are expected at lower frequencies than $\delta(\text{XeNS})$, and are assigned to bands at 221(16), 213(6)sh, 208(14), 197(5) and 179(8) cm^{-1} . Lines occurring below 99 cm^{-1} have been assigned to lattice modes.

CONCLUSIONS AND DIRECTIONS FOR FURTHER RESEARCH

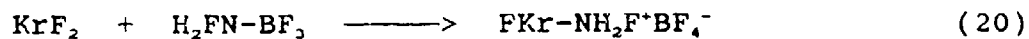
Thiazyl trifluoride was found to be an appropriate Lewis base for adduct formation with the noble-gas cations XeF^+ and XeOSeF_5^+ . It should be possible to extend this work to the XeOTeF_5^+ cation, and possibly to the more strongly oxidizing xenon(IV) cation, XeF_3^+ , and the krypton(II) cation, KrF^+ .

The mixed solvent system consisting of anhydrous HF and several mole percent of BrF_5 was shown to exhibit the properties of low viscosity associated with anhydrous HF but also displayed a reduced fluoride ion basicity which conveniently serves to inhibit nucleophilic attack of positively charged nitrogen in the $\text{F}_3\text{S}=\text{N}-\text{XeF}^+$ cation. Therefore, a strong fluoride acceptor, AsF_5 , would also be expected to inhibit reaction (16) and ought to be attempted.

It was discovered that solvolysis of the $\text{F}_3\text{S}=\text{N}-\text{XeF}^+$ cation took place in the above mentioned mixed solvent system. The addition of HF to the $\text{S}=\text{N}$ triple bond provided the first evidence for the $\text{F}_3\text{S}=\text{NH}$ moiety which has been stabilized as an adduct cation with XeF^+ , namely, $\text{F}_3\text{S}=\text{N}(\text{H})-\text{XeF}^+$. Further solvolysis of $\text{F}_3\text{S}=\text{N}(\text{H})-\text{XeF}^+$ resulted in the addition of HF to the $\text{S}=\text{N}$ double bond to yield the $\text{F}_3\text{S}-\text{N}(\text{H}_2)\text{XeF}^+$ cation, completing this series of novel cations. It is therefore reasonable that the known $\text{RC}\equiv\text{N}-\text{XeF}^+$ cations^{17,19} might undergo solvolysis in HF solvent in which they have been prepared by analogous routes. These would be expected to display the same trends in shielding at xenon related to hybridizational changes from sp to sp^2 to sp^3 as observed in the solvolysis of the $\text{F}_3\text{S}=\text{N}-\text{XeF}^+$ cation if the intermediates can be stabilized.

Using the solvent system mentioned above, the ^{14}N NMR spectrum should be obtained for the solvolysis products of the $\text{F}_3\text{S}\equiv\text{N}-\text{XeF}^+$ cation, completing the characterization of the $\text{F}_4\text{S}=\text{N}(\text{H})-\text{XeF}^+$ and $\text{F}_3\text{S}-\text{N}(\text{H}_2)-\text{XeF}^+$ cations.

There are doubtless other sulfur-nitrogen bases which exhibit Lewis-base characteristics which could be used to form other examples of novel adduct-cations such as $\text{N}\equiv\text{SF}$ and $\text{N}(\text{SF}_2)_3$, which may prove sufficiently stable to redox degradation and solvent attack to form stable adduct cations with the strongly oxidizing noble-gas cations. The present work provides the groundwork for attempting to coordinate XeF^+ and other strong oxidizers such KrF^+ and ClF_2^+ to a more endothermic bases such as NH_2F using the general synthetic approaches given in equations (20) and (21) the low molecular weight of counter anion, BF_4^- .



REFERENCES

1. P.J. MacDougall, G.J. Schrobilgen and R.F.W. Bader, *Inorg. Chem.*, 1989, 28, 763.
2. C.B. Hunt, *Educ. Chem.*, 1983, 20, 177.
3. R.D. LeBlond and D.D. DesMarteau, *J. Chem. Soc. Chem. Commun.*, 1974, 555.
4. J.F. Sawyer, G.J. Schrobilgen and S.J. Sutherland, *Inorg. Chem.*, 1982, 21, 4064.
5. R. Faggiani, D.K. Kennepohl, C.J.L. Lock and G.J. Schrobilgen, *Inorg. Chem.*, 1986, 25, 563.
6. D.D. DesMarteau, R.D. LeBlond, S.F. Hossian and D. Nothe, *J. Am. Chem. Soc.*, 1981, 103, 7734.
7. G.A. Schumacher and G.J. Schrobilgen, *Inorg. Chem.*, 1983, 22, 2178.
8. O. Glemser and H. Richert, *Z. Anorg. Allg. Chem.*, 1961, 307, 313.
9. D.B. Beach, W.L. Jolly, R. Mews and A. Waterfeld, *Inorg. Chem.*, 1984, 23, 4080.
10. A.A.A. Emara and G.J. Schrobilgen, *J. Chem. Soc., Chem. Commun.*, 1988, 257.
11. A.A.A. Emara and G.J. Schrobilgen, *J. Chem. Soc., Chem. Commun.*, 1988, 1644.
12. G.J. Schrobilgen, *J. Chem. Soc., Chem. Commun.*, 1988, 1506.
13. Dibeler, V.H. and Liston, S.K., *J. Chem. Phys.*, 1968, 48, 4765.
14. G.J. Schrobilgen, *J. Chem. Soc., Chem. Commun.*, 1988, 863.
15. A.F. Clifford and C.S. Kobaashi, *Inorg. Chem.*, 1965, 4, 571.
16. R. Mews, K. Keller and O. Glemser, *Inorg. Synth.*, 1986, 24, 12.
17. O. Glemser and W. Koch, *An. Asoc. Quim. Argentina*, 59, 143, (1971).
18. J. Mason, ed., "Multinuclear NMR", Plenum, New York, 1987.

19. G.J. Schrobilgen, J.H. Holloway, P. Granger and C. Brevard, *Inorg. Chem.*, 1978, 17, 980.
20. R.J. Gillespie, A. Netzer and G.J. Schrobilgen, *Inorg. Chem.*, 1974, 13, 1455.
21. R.J. Gillespie and B. Landa, *Inorg. Chem.*, 1973, 12, 1383.
22. J.C.P. Sanders and G.J. Schrobilgen, unpublished work.
23. H. Musso and H. Jungo, *Tetrahedron Lett.*, 1966, 33, 4003.
24. A.F. Clifford and G.C. Duncan, *Inorg. Chem.*, 1966, 5, 692.
25. "Handbook of Chemistry and Physics", CRC Press, Inc., Boca Raton (Florida), 1987, 68th ed.
26. R.G. Kidd, "Quadrupolar and Other Types of Relaxation", 5, in *NMR of Newly Accessible Nuclei*, P. Laszlo (ed), Academic Press Inc., New York, 1983.
27. R. Mews, *Adv. Inorg. Chem. Radiochem.* 1976, 19, 165.
28. E.L. Muetterties and W.D. Phillips, *J. Am. Chem. Soc.*, 1959, 81, 2183.
29. R.K. Harris and K.J. Packer, *J. Chem. Soc.*, 1961, 4736.
30. K.O. Christe and W.W. Wilson, *Inorg. Synth.*, 1989, 28, 3275.
31. M. Clark and J.S. Thrasher, unpublished work.
32. J.E. Huheey, "Inorganic Chemistry", 3rd ed., Harper and Row, New York, 1983, p. 152-155.
33. W.G. Fateley, F.R. Dollish, N.T. McDevitt and F.F. Bentley, *Infrared and Raman Selection Rules for Molecular and Lattice Vibrations: The Correlation Method*, Wiley-Interscience, New York, 1972.
34. A. Müller, A. Ruoff, B. Krebs, O. Glemser and W. Koch, *Spectrochim. Acta*, 1968, 25A, 199.
35. G.A. Schumacher and G.J. Schrobilgen, *Inorg. Chem.*, 1983, 22, 2178.

APPENDIX

Simulation of the ^{19}F NMR Spectrum of the $\text{F}_4\text{S}=\text{N}(\text{H})-\text{XeF}^+$ Cation

The NMR simulation program, LAOCOON PC,²⁸ was used to fit the ^{19}F NMR spectrum of the $\text{F}_4\text{S}=\text{N}(\text{H})-\text{XeF}^+$ cation. Files 1 and 2 contain the calculated transition energies and their intensities generated by the program calculated from the "raw" observed chemical shifts and coupling constants corresponding to the four fluorines on sulfur. File 1 is the .NMR file for the A_2BX spin system where the xenon nucleus is spinless. Only File 1 was iterated, resulting in an RMS of 0.0033 for 24 fitted lines and was used to calculate, without iteration, .SPC Files 2 and 3. File 2 is the .NMR file for the $A_2BX\Omega$ spin system where Ω represents a hypothetical cation having ^{129}Xe in 100 percent abundance. Since this program is not designed to simulate heteronuclear spin systems, the xenon chemical shift was arbitrarily set at -190 ppm in the fluorine spectrum, a value far removed from the F-on-S(VI) region, yet within the range -99,999 to +99,999 Hz allowed by the program.

File 3 is the .SPC file created by the summation of .SPC File 1 corresponding to the A_2BX spin system (fluorine on the spinless xenon isotopes) with .SPC File 2 of the $A_2BX\Omega$ spin system (fluorine spectrum of the ^{129}Xe satellites) after File 2 had been weighted at 17.97% of its original intensity. This weighting factor corresponds to one half the natural abundance of ^{129}Xe divided by the sum of the natural abundances of the other xenon isotopes. The resulting file, File 3, represents the final

fitted transition energies and their intensities for the natural abundance $^{19}\text{F}_4\text{S}=\text{N}(\text{H})-\text{XeF}^+$ cation. File 3 has been plotted using Lorentzian lineshapes in Figures 20 - 22 and is compared with the experimental spectrum.

File 1:

Lacocon PC

UA Version 3.1

Iteration of A_2BX Spin System: $^{19}\text{F}_4\text{S}=\text{N}(\text{H})-\text{Xe}-\text{F}^+$

Number of Nuclei : 4

Minimum Intensity: .010

Spectrometer Frequency: 470.600

Input Values :

Shift (1)	=	53.867 ppm
Shift (2)	=	53.867 ppm
Shift (3)	=	64.175 ppm
Shift (4)	=	110.513 ppm
Coupling (1,2)	=	.000 Hz
Coupling (1,3)	=	210.757 Hz
Coupling (1,4)	=	206.854 Hz
Coupling (2,3)	=	210.757 Hz
Coupling (2,4)	=	206.854 Hz
Coupling (3,4)	=	18.120 Hz

File 1 (continued)

Parameter Sets Fitted:

1	Shift (1)		
	Shift (2)		
2	Shift (3)		
3	Shift (4)		
4	Coupling (1,3)		
	Coupling (2,3)		
5	Coupling (1,4)		
	Coupling (2,4)		
6	Coupling (3,4)		
Iteration	0	RMS Error=	.0600
Iteration	1	RMS Error=	.0033
Iteration	2	RMS Error=	.0033

Calculated values: Iteration of A₂BX Spin System: ¹⁹F,S=N(H)-Xe-F

Shift (1)	=	53.970 ppm
Shift (2)	=	53.970 ppm
Shift (3)	=	64.168 ppm
Shift (4)	=	110.512 ppm
Coupling (1,2)	=	.000 Hz
Coupling (1,3)	=	207.449 Hz
Coupling (1,4)	=	206.456 Hz
Coupling (2,3)	=	207.449 Hz
Coupling (2,4)	=	206.456 Hz
Coupling (3,4)	=	18.051 Hz

Probable Errors of Parameter Sets:

1	.001
2	.001
3	.001
4	.001
5	.001
6	.001

File 1 (continued)

NMR Simulation

Iteration of A₂BX Spin System: ¹⁹F₄S=N(H)-Xe-F*

Line	Expt Freq	Calc Freq	Intensity	Error
55	53.519	53.519	1.898	.000
51	53.530	53.531	1.903	-.001
33	53.961	53.959	1.925	.002
26	53.968	53.962	2.067	.006
18	53.961	53.968	1.929	-.007
42	53.968	53.969	2.071	-.001
1	54.399	54.399	2.101	.000
5	54.410	54.409	2.107	.001
54	63.717	63.717	1.086	.000
29	63.754	63.756	1.092	-.002
48	64.156	64.149	.999	.007
43	64.164	64.167	.995	-.003
13	64.185	64.187	1.001	-.002
6	64.214	64.206	.996	.008
28	64.595	64.598	.917	-.003
3	64.633	64.637	.915	-.004
53	110.054	110.055	1.016	-.001
30	110.093	110.094	1.015	-.001
40	110.494	110.492	1.001	.002
35	110.494	110.495	1.001	-.001
15	110.533	110.531	.999	.002
8	110.533	110.535	.999	-.002
22	110.933	110.932	.986	.001
4	110.972	110.971	.983	.001

24 Lines

32 Lines below minimum intensity.

Execution time: 3 seconds

File 2:

Laocoon PC

UA Version 3.1

A₂BXΩ Spin System (100% ¹²⁹Xe): ¹⁹F₄S=N(H)-¹²⁹Xe-F'

Number of Nuclei : 5

Minimum Intensity: .010

Spectrometer Frequency: 470.599

Input Values :

	Shift (1)	=	53.970 ppm
	Shift (2)	=	53.970 ppm
	Shift (3)	=	64.168 ppm
	Shift (4)	=	110.512 ppm
Arbitrary δ(¹²⁹ Xe)	Shift (5)	=	-190.000 ppm
	Coupling (1,2)	=	.000 Hz
	Coupling (1,3)	=	207.449 Hz
	Coupling (1,4)	=	206.456 Hz
	Coupling (1,5)	=	.000 Hz
	Coupling (2,3)	=	207.449 Hz
	Coupling (2,4)	=	206.456 Hz
	Coupling (2,5)	=	.000 Hz
	Coupling (3,4)	=	18.051 Hz
	Coupling (3,5)	=	202.735 Hz
	Coupling (4,5)	=	129.352 Hz

File 2 (continued)

NMR Simulation

A₂BXΩ Spin System (100% ¹²⁹Xe): ¹⁹F₄S=N(H)-¹²⁹Xe-F⁺

Line	Expt Freq	Calc Freq	Intensity	Error
206		-190.353	.997	Arbitrary δ(¹²⁹ Xe)
175		-190.353	.997	
115		-190.353	.997	
169		-190.353	.997	
82		-190.078	.999	
157		-190.078	.999	
34		-190.078	.999	
71		-190.078	.999	
163		-189.923	1.001	
103		-189.923	1.001	
45		-189.922	1.001	
94		-189.922	1.001	
60		-189.648	1.003	
12		-189.648	1.003	
23		-189.647	1.003	
5		-189.647	1.003	
209		53.519	1.895	
166		53.519	1.899	
108		53.531	1.905	
204		53.531	1.901	
182		53.959	1.922	
66		53.959	1.926	
153		53.962	2.068	
40		53.962	2.065	
27		53.968	1.932	
141		53.968	1.928	
193		53.969	2.073	
97		53.969	2.070	
52		54.398	2.103	
1		54.399	2.099	
120		54.409	2.109	
6		54.409	2.105	
208		63.503	1.090	
177		63.541	1.096	
161		63.933	1.083	
200		63.934	1.001	
194		63.953	.995	
56		63.972	1.089	
132		63.972	1.003	
121		63.997	.997	
89		64.383	.997	
98		64.383	.992	

File 2 (continued)

155	64.384	.917
18	64.403	.999
7	64.422	.994
54	64.422	.915
41	64.814	.917
3	64.853	.916
207	109.918	1.017
178	109.957	1.016
156	110.193	1.015
57	110.232	1.014
190	110.355	1.002
184	110.358	1.002
134	110.394	1.000
123	110.398	1.000
79	110.630	1.000
68	110.633	1.000
19	110.669	.998
10	110.672	.998
145	110.796	.986
55	110.834	.984
31	111.070	.985
4	111.109	.983

64 Lines

146 Lines below minimum intensity.

Execution time: 2 seconds

File 3:

$A_2BX + 0.1797(A_2BX\Omega): {}^{19}\text{F}_4\text{S}=\text{N}(\text{H})-{}^{129}\text{Xe}-\text{F}^+$

ppm 470.59960

-190.353	0.717
-190.078	0.718
-189.922	0.719
-189.647	0.721
53.519	1.898
53.519	0.682
53.531	1.903
53.531	0.684
53.959	1.925
53.959	0.691
53.962	2.067
53.962	0.743
53.968	1.929
53.968	0.694
53.969	2.071
53.969	0.744
54.399	2.101
54.399	0.755
54.409	2.107
54.409	0.757
63.503	0.196
63.541	0.197
63.717	1.086
63.756	1.092
63.934	0.374
63.953	0.179
63.972	0.376
63.992	0.179
64.149	0.999
64.167	0.995
64.187	1.001
64.206	0.996
64.364	0.179
64.383	0.178
64.384	0.165
64.403	0.180
64.422	0.343
64.598	0.917
64.637	0.915
64.814	0.165
64.853	0.165
109.918	0.183
109.957	0.183
110.055	1.016
110.094	1.015

File 3 (contiued)

110.193	0.182
110.232	0.182
110.355	0.180
110.358	0.180
110.394	0.180
110.398	0.180
110.492	1.001
110.495	1.001
110.531	0.999
110.535	0.999
110.630	0.180
110.633	0.180
110.669	0.179
110.672	0.179
110.796	0.177
110.834	0.177
110.932	0.986
110.971	0.983
111.070	0.177
111.109	0.177

Reprinted from *Inorganic Chemistry*, 1990, 29.
Copyright © 1990 by the American Chemical Society and reprinted by permission of the copyright owner.

Contribution from Rocketdyne, A Division of Rockwell International Corporation, Canoga Park, California 91303,
Department of Chemistry, McMaster University, Hamilton, Ontario L8S 4M1, Canada,
and Department of Nuclear Medicine, Chedoke-McMaster Hospitals, Hamilton, Ontario L8N 3Z5, Canada

The Hexafluorochlorate(V) Anion, ClF_6^-

Karl O. Christe,^{*1a} William W. Wilson,^{1a} Raman V. Chirakal,^{1b,c} Jeremy C. P. Sanders,^{1b}
and Gary J. Schrobilgen^{*1b}

Received February 12, 1990

The low-temperature reactions of either $\text{N}(\text{CH}_3)_4\text{F}$ or CsF with ClF_3 in CH_3CN solutions produce white solids, which on the basis of material balances and low-temperature Raman spectra, contain the ClF_6^- anion. The similarity of the Raman spectrum of ClF_6^- to that of the octahedral BrF_6^- ion indicates that ClF_6^- is also octahedral and that the free valence electron pair on chlorine is sterically inactive. The existence of the ClF_6^- anion was further supported by an ^{19}F exchange experiment between ClF_3 and ^{19}F -labeled FNO that showed complete randomization of the ^{19}F isotope among the two molecules. A high-field ^{19}F NMR study of neat ClF_3 and ClF_3 in anhydrous HF solution in the presence and absence of excess CsF has provided accurate measurements of the ClF_3 NMR parameters including, for the first time, both $^{37/35}\text{Cl}$ secondary isotopic ^{19}F NMR shifts. Moreover, the NMR study also supports the existence of ClF_6^- , showing that ClF_3 undergoes slow chemical exchange with excess CsF in anhydrous HF at room temperature.

Introduction

The hexafluorochlorate(V) anions belong to the interesting class of AX_6E compounds,² which possess six X ligands and a free valence electron pair E. Depending on the size of the central atom A, the free valence electron pair E can be either sterically active

or inactive. Thus, a recent study has shown that in IF_6^- the free valence electron pair is sterically active, while in BrF_6^- it is not.³ Whereas the ClF_3 molecule was discovered 27 years ago,⁴ and the BrF_6^- and IF_6^- anions have been known for about as long,^{5,6}

(1) (a) Rocketdyne. (b) McMaster University. (c) Chedoke-McMaster Hospitals.
(2) Gillespie, R. J. *Molecular Geometry*; Van Nostrand Reinhold Co.: London, 1972.

(3) Christe, K. O.; Wilson, W. W. *Inorg. Chem.* 1989, 28, 3275.
(4) Maya, W.; Bauer, H. F. U.S. Pat. 3,354,646, 1967.
(5) Emeleus, H. J.; Sharpe, A. G. *J. Chem. Soc.* 1949, 2206.
(6) Whitney, E. D.; MacLaren, R. O.; Fogle, C. E.; Hurley, T. J. *J. Am. Chem. Soc.* 1964, 86, 2583.

the ClF_6^- anion has so far proven elusive. For example, ClF_5 does not form any stable adducts with alkali-metal fluorides and the only reaction observed is a catalytic decomposition of ClF_3 to ClF_2 and F_2 .⁷ Furthermore, a ^{18}F radiotracer study of the $\text{CsF}-\text{ClF}_5$ system did not provide any evidence for fluorine exchange and, thereby, for the formation of a ClF_6^- intermediate.⁸ The well-established existence of the ClF_6^+ cation^{9,12} and of the ClF_6^\cdot radical,¹³ combined with the recent finding that in BrF_6^- the bromine free valence electron pair is sterically inactive,³ indicated that the weak Lewis acidity of ClF_5 and the low solubilities of CsF and CsClF_6 in ClF_3 are the most likely reasons for the previous failures^{7,8} to isolate the ClF_6^- anion. Our recent success¹⁴ with handling ClF_3 in CH_3CN solution and the surprisingly high thermal stability of $\text{N}(\text{CH}_3)_4\text{ClF}_4^-$ combined with its high solubility in CH_3CN , suggested that similar reaction conditions, i.e., the use of $\text{N}(\text{CH}_3)_4^+$ as a large, stabilizing counterion, of CH_3CN as a solvent, and of low temperature, might provide the long sought after ClF_6^- anion.

Experimental Section

Caution! Mixtures of ClF_3 or ClF_6^- salts with organic materials, such as CH_3CN or $[\text{N}(\text{CH}_3)_4]^+$ salts, are highly explosive and must be handled on a small scale with appropriate safety precautions, such as barricades, face shields, heavy leather gloves, and protective clothing.

Materials. The CH_3CN (Baker, Bio-analyzed, having a water content of 40 ppm) was treated with P_2O_5 and freshly distilled in a flamed-out Pyrex vacuum system prior to use, thereby reducing its water content to ≤ 4 ppm. The CsF (KBI) was dried by fusion in a platinum crucible and ground in the drybox. The ClF_3 (Rocketdyne) was purified by fractional condensation prior to its use. The synthesis of HF_2^- and H_2O -free $\text{N}(\text{CH}_3)_4\text{F}$ is described elsewhere.¹⁵

Apparatus. All reactions were carried out in well-passivated (with ClF_3) Teflon-FEP or Kel-F ampules that were closed by stainless steel valves. The ClF_3 was handled in a stainless steel-Teflon-FEP vacuum line,¹⁶ and the CH_3CN was transferred on a baked-out Pyrex vacuum line equipped with Teflon stopcocks. Nonvolatile materials were handled in the dry N_2 atmosphere of a glovebox.

Fluorine-18 Exchange Reaction between FNO and ClF_3 . A 50-ml. nickel can was heated to red heat four times with 2 atm of H_2 , followed by pumping each time. The procedure was repeated four times with F_2 , followed by treatment with 3 atm of FNO at room temperature for 1 day and pumping for 4 h. Nitric oxide (0.62 mmol) was combined at -196°C in the can with a $\text{Ne}/^{18}\text{F}$ -labeled F_2 mixture, which was accelerator produced under conditions previously described.¹⁷ The Ne was pumped off at -196°C , and F_2 (0.31 mmol) was added to the can. The can was briefly warmed to 20°C , and the resulting ^{18}F -labeled FNO was condensed, for the removal of any HF, at -196°C into a U-tube containing 0.5 g of NaF, followed by warming to -78°C . It was then combined at -196°C in a $1/4$ in. o.d. Teflon-FEP ampule with ClF_3 (0.62 mmol). The resulting mixture was warmed to 20°C for several minutes and then vacuum-distilled through two U-traps kept at -120 and -196°C . The -120°C trap contained the ClF_3 , and the -196°C one, the FNO. Individual activity measurements were corrected for the elapsed time by correcting to zero time of the experiment. At the end of the experiment, the -120°C trap, containing ClF_3 , showed a zero time activity of 71.6 mCi (84.9%), whereas that in the -196°C trap, containing the FNO, was 12.7 mCi (15.1%).

Synthesis of $\text{N}(\text{CH}_3)_4\text{ClF}_6^-$. In a typical experiment, $\text{N}(\text{CH}_3)_4\text{F}$ (150.9 mg, 1.62 mmol) was transferred in the drybox into a prepassivated Teflon-FEP ampule that was closed by a stainless steel valve. Dry CH_3CN (5.96 mL, 4.702 g) was added at -196°C on the Pyrex vacuum line, and the mixture was warmed to room temperature. ClF_3 (1.62

mmol) was added at -196°C on the stainless steel vacuum line, and the mixture was kept at -31°C for 3 h with occasional very careful agitation. All material volatile at -31°C was pumped off and trapped in a -196°C trap and consisted of 4.70 g of CH_3CN . The white solid residue was highly shock sensitive and consistently exploded when either exposed to a laser beam at low temperature or warmed to room temperature.

When the above experiment was repeated at room temperature, gas evolution set in at about 0°C , and after solvent removal at 20°C , a stable white solid was obtained, which, on the basis of its weight and vibrational spectrum, was identified as $\text{N}(\text{CH}_3)_4\text{ClF}_4^-$.¹⁴

When CsF was substituted for $\text{N}(\text{CH}_3)_4\text{F}$ in the reaction with ClF_3 in CH_3CN at -31°C , the volatile materials at -31°C consisted of the CH_3CN and ClF_3 starting materials, and the nonvolatile residue was unreacted CsF .

For the recording of the low-temperature Raman spectrum of CsClF_6 , a solution of ClF_3 in CH_3CN was kept in contact with excess CsF for several hours at -40°C and then slowly cooled to -110°C . The Raman spectrum of the product in the bottom of the tube was recorded at -110°C and indicated the presence of CsClF_6 (see below) and solid CH_3CN .

Nuclear Magnetic Resonance Spectroscopy. The ^{19}F NMR spectra were recorded unlocked (field drift < 0.1 Hz h^{-1}) by using a Bruker WM-250 or AM-500 spectrometer equipped with a 5.8719 or 11.744 T cryomagnet, respectively. On both instruments, spectra were obtained by using 5-mm combination $^1\text{H}/^{19}\text{F}$ probes operating at 235.361 MHz (WM-250) or 470.599 MHz (AM-500).

The 5.8719-T ^{19}F spectra were typically accumulated in a 16K memory. Spectral width settings of 5 and 10 kHz were employed, yielding data point resolutions of 0.62 and 1.22 Hz and acquisition times of 1.638 and 0.819 s, respectively. No relaxation delays were applied. The number of free-induction decays accumulated was typically between 2000 and 10,000 transients.

The 11.744-T ^{19}F spectra were accumulated in a 16K memory. Spectral width settings of 5 and 30 kHz were employed, yielding data point resolutions of 0.61 and 3.59 Hz and acquisition times of 1.638 and 0.278 s, respectively. No relaxation delays were applied. Typically 80–1000 transients were accumulated.

On both instruments the pulse width corresponding to a bulk magnetization tip angle, θ , of approximately 90° was equal to 1 μs . No line-broadening parameters were applied in the exponential multiplication of the free-induction decays prior to Fourier transformation.

The spectra were referenced to neat CFCl_3 . The chemical shift convention used is that a positive (negative) sign signifies a chemical shift to high (low) frequency of the reference compound.

Low-temperature studies were carried out by using Bruker temperature controllers. The temperature was measured with a copper-constantan thermocouple inserted directly into the sample region of the probe and was considered accurate to $\pm 1^\circ\text{C}$.

Fluorine-19 NMR samples were prepared in 25-cm lengths of AWG 9 (ca. 4-mm o.d., 0.8-mm wall) FEP plastic tubing heat sealed at one end with the open end flared (45° SAE) and joined, by means of a compression fitting, to a Kel-F valve. The assembly was seasoned overnight with ca. 1 atm of F_2 gas, evacuated, and weighed. A weighed amount of CsF was transferred into a sample tube in a drybox. Both ClF_3 and HF were distilled into NMR tubes through a metal line fitted with a pressure transducer that had been previously seasoned overnight with ca. 1 atm of ClF_3 vapor. The ClF_3 pressure was measured ($\pm 0.5\%$ accuracy) in a calibrated portion of the metal vacuum line with a pressure transducer (0–1000 Torr range), whose wetted surfaces were Inconel, and condensed at -196°C into the FEP NMR sample tube. The amount of HF solvent used was determined by direct weighing of the tube assembly. The FEP tube was heat sealed under dynamic vacuum with its contents frozen at -196°C . The FEP sample tubes were placed in 5-mm thin-walled precision NMR tubes (Wilmad) in order to run their spectra.

Raman Spectroscopy. Low-temperature Raman spectra were recorded on a Cary Model 83 spectrophotometer using the 488-nm exciting line of an Ar ion laser.

Results and Discussion

Synthesis of ClF_6^- Salts. It was found that the activation energy for the $\text{ClF}_3-\text{CH}_3\text{CN}$ reaction is sufficiently high to permit the judicious handling of ClF_3 in a large excess of dry CH_3CN . Although ClF_5 is a more powerful oxidizer than ClF_3 , its pseudooctahedral structure with five fluorine ligands and one free valence electron pair renders it less reactive than the pseudo-trigonal-bipyramidal ClF_3 .

To take advantage of the high activation energy of the $\text{ClF}_3-\text{CH}_3\text{CN}$ reaction, $\text{N}(\text{CH}_3)_4\text{F}$ was carefully combined with ClF_3 in this solvent at -31°C . Removal of the solvent at -31°C resulted in a white, highly sensitive solid that violently exploded

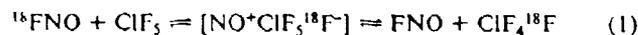
- (7) Christie, K. O.; Wilson, W. W.; Wilson, R. D. *Inorg. Chem.* **1989**, *28*, 675.
- (8) Bougon, R. *Bull. Inf. Sci. Tech., Commis. Energ. At. (Fr.)* **1971**, *161*, 9.
- (9) Christie, K. O. *Inorg. Nucl. Chem. Lett.* **1972**, *8*, 741.
- (10) Roberto, F. Q. *Inorg. Nucl. Chem. Lett.* **1972**, *8*, 737.
- (11) Christie, K. O. *Inorg. Chem.* **1973**, *12*, 1580.
- (12) Christie, K. O.; Wilson, W. W. *Inorg. Chem.* **1983**, *22*, 1950.
- (13) Boate, A. R.; Morton, J. R.; Preston, K. R. *Inorg. Chem.* **1975**, *14*, 3127.
- (14) Wilson, W. W.; Christie, K. O. *Inorg. Chem.* **1989**, *28*, 4172.
- (15) Wilson, W. W.; Christie, K. O.; Feng, J.; Bau, R. To be published.
- (16) Christie, K. O.; Wilson, R. D.; Shaek, C. J. *Inorg. Synth.* **1986**, *24*, 3.
- (17) Chirakal, R.; Firnau, G.; Schrobilgen, G. J.; McKay, J.; Garnett, E. S. *Int. J. Appl. Radiat. Isot.* **1984**, *35*, 401.
- (18) Bougon, R.; Charpin, P.; Soriano, J. C. R. *Hebd. Seances Acad. Sci., Ser. C* **1971**, *272*, 565.

either on exposure to a laser beam at low temperature or on warming to room temperature, thereby preventing its direct identification. It was shown, however, by quantitative material balances that most of the ClF_5 starting material had been retained by the $\text{N}(\text{CH}_3)_4\text{F}$ at -31°C .

When the reaction between $\text{N}(\text{CH}_3)_4\text{F}$ and ClF_5 was carried out at temperatures above -31°C , gas evolution was observed at about 0°C and, after solvent removal at 20°C , a stable, white solid was isolated, which was identified by vibrational spectroscopy as $\text{N}(\text{CH}_3)_4\text{ClF}_4$.¹⁴ Since the latter compound is stable up to 100°C and is not shock sensitive,¹⁴ the explosive material from the -31°C reaction could not have been $\text{N}(\text{CH}_3)_4\text{ClF}_4$ but most likely was $\text{N}(\text{CH}_3)_4\text{ClF}_6$.

To overcome the experimental difficulties associated with the characterization of $\text{N}(\text{CH}_3)_4\text{ClF}_6$, the $\text{N}(\text{CH}_3)_4\text{F}$ starting material in the $\text{N}(\text{CH}_3)_4\text{F}-\text{ClF}_5-\text{CH}_3\text{CN}$ system was substituted by CsF . It was hoped that CsClF_6 would be stable at -31°C , the lowest temperature at which the CH_3CN solvent could be pumped off at a reasonable rate. However, it was found that CsClF_6 is thermally unstable even at -31°C , and all the ClF_5 was pumped off at -31°C , together with the CH_3CN solvent. Since CH_3CN is a much weaker Raman scatterer than the chlorine fluorides,¹⁴ it was possible to record the low-temperature Raman spectrum of CsClF_6 without removal of the CH_3CN and, thereby, to identify the ClF_6^- anion. A detailed discussion of the observed spectrum will be given below.

¹⁸F Radiotracer Study. Further evidence for the formation of the ClF_6^- anion was obtained by an ¹⁸F radiotracer study of the ClF_5 -¹⁸FNO system. It was found that ClF_5 undergoes rapid fluorine exchange with ¹⁸FNO (eq 1). Within several minutes

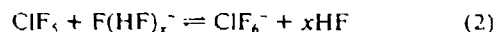


at room temperature, complete randomization of the ¹⁸F isotope had occurred. The measured values of 84.9% for the radioactivity in ClF_5 and 15.1% in FNO are in excellent agreement with the values 83.3 and 16.7% predicted for a random distribution of ¹⁸F involving an unstable $\text{NO}^+\text{ClF}_6^-$ intermediate. The rapid fluorine exchange in the FNO- ClF_5 system is in marked contrast to the results from the previous study of the $\text{CsF}-\text{ClF}_5$ system for which no evidence of exchange was reported.⁸ The lack of exchange in the $\text{CsF}-\text{ClF}_5$ system is probably due to the very low solubility of CsF in ClF_5 and not to the lack of ClF_6^- formation (see below).

¹⁹F NMR Study of Chemical Exchange Behavior between F^- and ClF_5 . Chlorine pentafluoride has previously been shown in two ¹⁹F NMR studies to possess a square-pyramidal (C_{4v}) AX_4E structure in the liquid state^{19,20} as predicted by the VSEPR model.² Alexandre and Rigny²⁰ demonstrated that, unlike the equatorial X_4 part of the ¹⁹F NMR spectrum, which showed a secondary isotopic shift arising from ¹⁹F bonded to ³⁵Cl and ³⁷Cl, the axial A part of the spectrum was broadened significantly and showed no evidence for an isotopic shift.²⁰ This study concluded that chemical exchange between the axial (F_{ax}) and equatorial (F_{eq}) fluorines could be disregarded and that the line broadening of F_{ax} arises from partially quadrupole-collapsed scalar couplings between ¹⁹F_{ax} and the spin- $3/2$ quadrupolar nuclei ³⁵Cl and ³⁷Cl, $1J_{(^{19}\text{F}_{ax}-^{35/37}\text{Cl})}$, which are significantly larger than $1J_{(^{19}\text{F}_{eq}-^{35/37}\text{Cl})}$. Nuclear relaxation time measurements in the same study have confirmed this and have provided estimates of the magnitudes of the scalar couplings ($1J_{(^{19}\text{F}_{ax}-^{35}\text{Cl})} = 192$ and $1J_{(^{19}\text{F}_{eq}-^{35}\text{Cl})} \leq 20$ Hz). The larger value for $1J_{(F_{ax}-^{35}\text{Cl})}$ is in accord with the shorter $F_{ax}-\text{Cl}$ bond observed in this molecule.²¹ The temperature behavior of the ¹⁹F NMR spectrum of liquid ClF_5 was investigated in the previous study,⁸ but it does not report any variations of line widths as a function of temperature. We have recorded the ¹⁹F NMR spectra of neat ClF_5 at 25, -56 , and -90°C (Figure 1). While there is little effect upon the line width of the F_{eq} resonance

on lowering the temperature, a significant narrowing of the F_{ax} resonance line width is observed together with partial resolution of its chlorine isotopic shift. The observed line narrowing for the F_{ax} resonance is attributable to the increased quadrupolar relaxation rates of ³⁵Cl and ³⁷Cl at low temperatures where the isotropic molecular tumbling correlation time (τ_c) for ClF_5 is greater.²² This behavior is consistent with the dominant contribution of scalar relaxation of the second kind, via $1J_{(F_{ax}-^{35/37}\text{Cl})}$, to the spin-spin relaxation time (T_2) of the F_{ax} nuclei, as found in the previous study.²⁰

The ¹⁹F NMR spectra of a solution of ClF_5 (0.536 m) in anhydrous HF and a solution of ClF_5 (0.619 m) in anhydrous HF containing CsF (5.60 m) were investigated. The ¹⁹F NMR spectrum of ClF_5 recorded in HF solvent at 25°C consists of two well-resolved doublets corresponding to equatorial fluorines on ³⁵Cl and ³⁷Cl spin coupled to the axial fluorine environment (Figure 2). The latter environment, as in the neat sample of ClF_5 at 24.4°C , is broadened significantly owing to partial quadrupole collapse of the $1J_{(^{35/37}\text{Cl}-^{19}\text{F})}$ scalar couplings so that resolution of the isotopically shifted quintets (Figure 2; also cf. Figure 1) is precluded. The line broadening on the quintets is again dominated by scalar coupling and not by fluorine exchange, as has been established for neat ClF_5 in the present and earlier studies.²⁰ The addition of F^- to HF solutions of ClF_5 results in pronounced broadening of the doublet resonances at 25°C , preventing resolution of the isotope shift, whereas the appearance of the axial fluorine resonance remains essentially unchanged (Figure 3). The line broadening is consistent with slow intermolecular ¹⁹F exchange arising from equilibrium 2 and the intermediacy of ClF_6^- in the



exchange process. Cooling of the ClF_5-F^- sample to -56°C slowed ¹⁹F chemical exchange sufficiently to allow resolution of the equatorial fluorine doublets (Figure 3) and the axial fluorine quintets. This is the first time the two quintet patterns arising from the ³⁵Cl-³⁷Cl secondary isotope effect have been observed in ClF_5 . The sharpening of the axial fluorine resonance is not, however, attributed to slowing of the ¹⁹F chemical exchange process but is primarily attributed to the dominant effect of the increased quadrupole relaxation rates of the ³⁵Cl and ³⁷Cl nuclei on $1J_{(^{35/37}\text{Cl}-^{19}\text{F})}$ at low temperatures where τ_c for ClF_5 is greater. The addition of CsF presumably increases the viscosity of the solvent medium owing to $\text{F}(\text{HF})_x^-$ formation and hence increases τ_c for ClF_5 , leading to collapse of the $1J_{(^{35/37}\text{Cl}-^{19}\text{F})}$ couplings. In contrast, the ¹⁹F resonances associated with ClF_5 dissolved in HF do not sharpen as significantly, although the quintet pattern clearly possesses a narrower line width than at 25°C (Figure 2). The broader lines can be attributed to the low viscosity of the HF solvent medium, even at -56°C , allowing the partially collapsed $1J_{(^{35/37}\text{Cl}-^{19}\text{F})}$ couplings to persist in the slow chemical exchange limit.

The secondary isotope shifts, $1\Delta^{19}\text{F}_{ax}(^{37/35}\text{Cl}) = -0.189$ ppm and $1\Delta^{19}\text{F}_{eq}(^{37/35}\text{Cl}) = -0.085$ ppm for ClF_5/CsF in HF at -56°C (Figure 3), follow the usual trend and are negative; i.e., the observed NMR nucleus bonded to the heavier of two isotopes has its NMR resonance to lower frequency.²³ They are comparable in magnitude to those for closely related species in the same row of the periodic table; i.e., for ClF_6^+ , $1\Delta^{19}\text{F}(^{37/35}\text{Cl}) = -0.15$ ppm,²⁴ for SF_6 , $1\Delta^{19}\text{F}(^{34/32}\text{S}) = -0.0552$ ppm,²⁵ and for SF_4 , $1\Delta^{19}\text{F}_{ax}(^{34/32}\text{S}) = -0.0690$ ppm and $1\Delta^{19}\text{F}_{eq}(^{34/32}\text{S}) = -0.0330$ ppm²⁵ with the ¹⁹F bonded to the heavier isotope occurring at lower frequency. The relative sizes of isotopic shifts are known to be larger for shorter bonds,²⁶ and this is also true for the secondary isotopic shifts of ClF_5 [$r(\text{Cl}-F_{ax}) = 1.58$, $r(\text{Cl}-F_{eq}) = 1.67$ Å²¹ and $f_{ax,ax} = 3.01$, $f_{eq,eq} = 2.57$ mdyne Å⁻¹]²⁷ and BrF_5 [$r(\text{Br}-F_{ax}) = 1.689$,

(19) Pilipovich, D.; Maya, W.; Lawton, E. A.; Bauer, H. F.; Sheehan, D. F.; Ogimachi, N. N.; Wilson, R. D.; Gunderloy, F. C.; Bedwell, V. E. *Inorg. Chem.* **1967**, *6*, 1918.

(20) Alexandre, M.; Rigny, P. *Can. J. Chem.* **1974**, *52*, 3676.

(21) Goulet, P.; Jurek, R.; Chanussot, J. *J. Phys.* **1976**, *37*, 495.

(22) Boeré, R. T.; Kidd, R. G. *Annu. Rep. NMR Spectrosc.* **1982**, *13*, 320.

(23) Jameson, C. J.; Osten, H. J. *J. Am. Chem. Soc.* **1985**, *107*, 4158.

(24) Christe, K. O.; Hon, J. F.; Pilipovich, D. *Inorg. Chem.* **1973**, *12*, 84.

(25) Gombler, W. *Z. Naturforsch.* **1985**, *40b*, 782.

(26) Jameson, C. J. *J. Chem. Phys.* **1977**, *66*, 4983.

(27) Begun, G. M.; Fletcher, W. H.; Smith, D. F. *J. Chem. Phys.* **1965**, *42*, 2236.

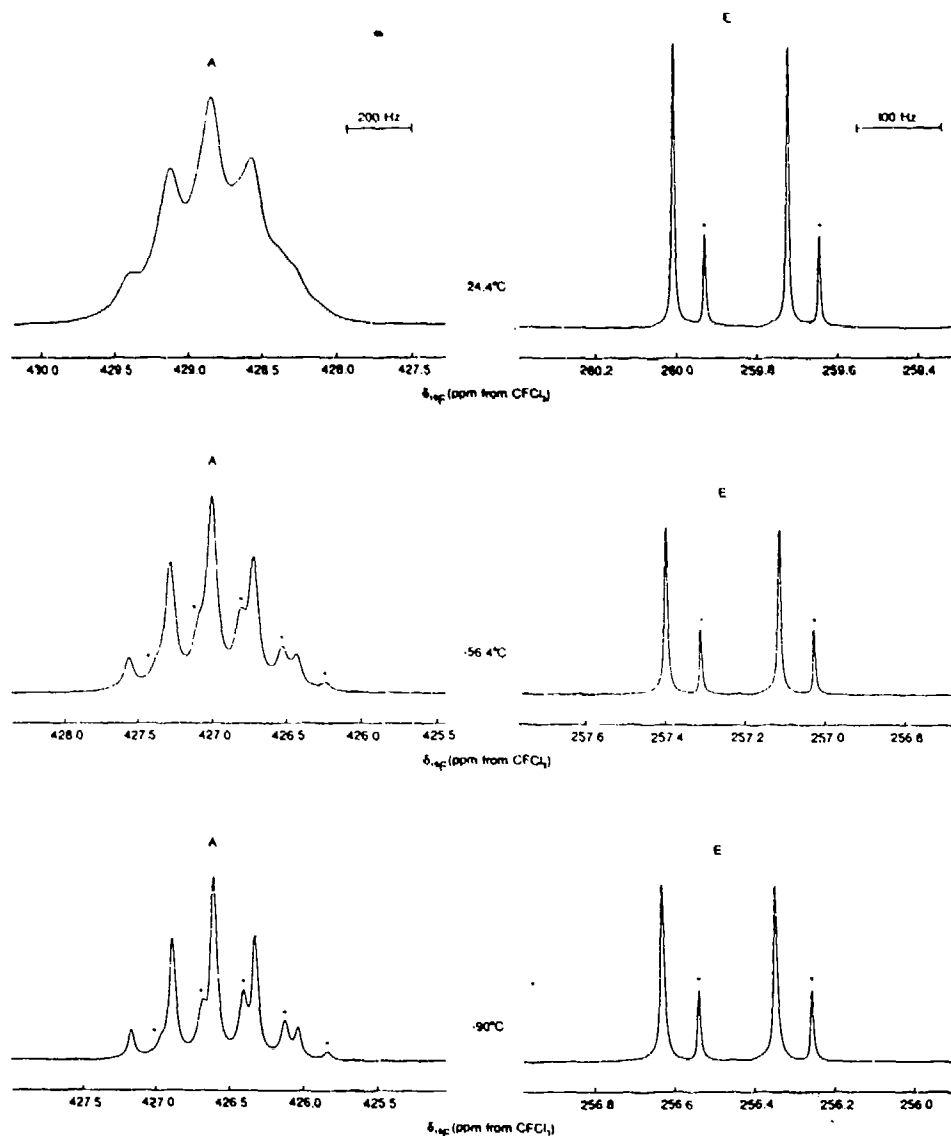


Figure 1. Variable-temperature ^{19}F NMR spectra (470.599 MHz) of neat ClF_3 . A and E denote resonances for the axial and equatorial fluorine environments, respectively; asterisks denote resonances arising from the ^{37}Cl isotopomer.

Table I. ^{19}F NMR Data for Neat ClF_3 and $\text{ClF}_3\text{-HF}$ and $\text{ClF}_3\text{-CsF-HF}$ Solutions

sample compn	T, °C	chem shift δ , ppm ^a		$^2J(\text{F}_{\text{ax}}-\text{F}_{\text{eq}})$, Hz	line width, Hz		secondary isotopic shift ^b $^{19}\text{F}(^{37/35}\text{Cl})$, ppm	
		F_{eq}	F_{ax}		F_{eq}	F_{ax}	F_{eq}	F_{ax}
neat ClF_3	24.4	259.8	428.8	133	3.5	~110	-0.079	e
	-56.4	257.2	426.9	133	4.0	44	-0.088	-0.1977
	-90.0	256.4	426.6	133	5.2	26	-0.091	-0.199
ClF_3 in HF solv ^c	25	256.4	424.6	130	5.7	~140	-0.078	e
	-56.3	253.9	422.6	130	2.5	71	-0.087	e
ClF_3/CsF in HF solv ^d	25	253.6	420.9	123	28	~100	e	e
	-56.3	250.8	418.8	124	6.9	18	-0.085	-0.189

^aSpectra were referenced with respect to external CFCl_3 at 25 °C. ^b $^{19}\text{F}(^{37/35}\text{Cl})/\text{ppm} = \delta(\text{F}(^{37}\text{Cl})) - \delta(\text{F}(^{35}\text{Cl}))$. ^cConcentration of $\text{ClF}_3 = 0.536$ m. ^dConcentration of $\text{ClF}_3 = 0.619$ m, and that of $\text{CsF} = 5.60$ m. ^eIsotopic shift not resolved.

$r(\text{Br}-\text{F}_{\text{eq}}) = 1.774 \text{ \AA}^{28}$ and $f_{\text{Rax}} = 4.07$, $f_{\text{Req}} = 3.19 \text{ mdyne \AA}^{-1}$,²⁷ where $^{19}\text{F}_{\text{ax}}(^{81/79}\text{Br}) = -0.030$ and $^{19}\text{F}_{\text{eq}}(^{81/79}\text{Br}) = -0.015$ ppm.²⁹ Moreover, the ratio $^{19}\text{F}_{\text{ax}}(^{37/35}\text{Cl})/^{19}\text{F}_{\text{eq}}(^{37/35}\text{Cl}) = 2.22$ is remarkably similar to those found for the axial and equatorial secondary isotopic shifts of SF_4 , $^{19}\text{F}_{\text{ax}}(^{34/32}\text{S})/^{19}\text{F}_{\text{eq}}(^{34/32}\text{S}) = 2.09$, and BrF_3 , $^{19}\text{F}_{\text{ax}}(^{81/79}\text{Br})/^{19}\text{F}_{\text{eq}}(^{81/79}\text{Br})$

$= 2.0$.²⁹ NMR data are summarized in Table I.

Raman Spectrum of CsClF_6 . The Raman spectrum of the product from the low-temperature reaction of CsF with ClF_3 in CH_3CN solution was recorded at -110 °C in frozen CH_3CN . In the region of the Cl-F fundamental vibrations, three bands were observed at 525, 384, and 289 cm^{-1} (Figure 4, trace A, which, under the influence of the laser beam, rapidly decayed giving rise to new bands at 507, 418, and 290 cm^{-1} (Figure 4, trace B). These new bands are due to the ClF_4^- anion, as shown by the Raman spectrum of $\text{N}(\text{CH}_3)_4\text{ClF}_4$ in CH_3CN recorded under identical

(28) Robiette, A. G.; Bradley, R. H.; Brier, P. N. *J. Chem. Soc., Chem. Commun.* 1971, 1567.

(29) Sanders, J. C. P.; Schrobilgen, G. J. Unpublished results.

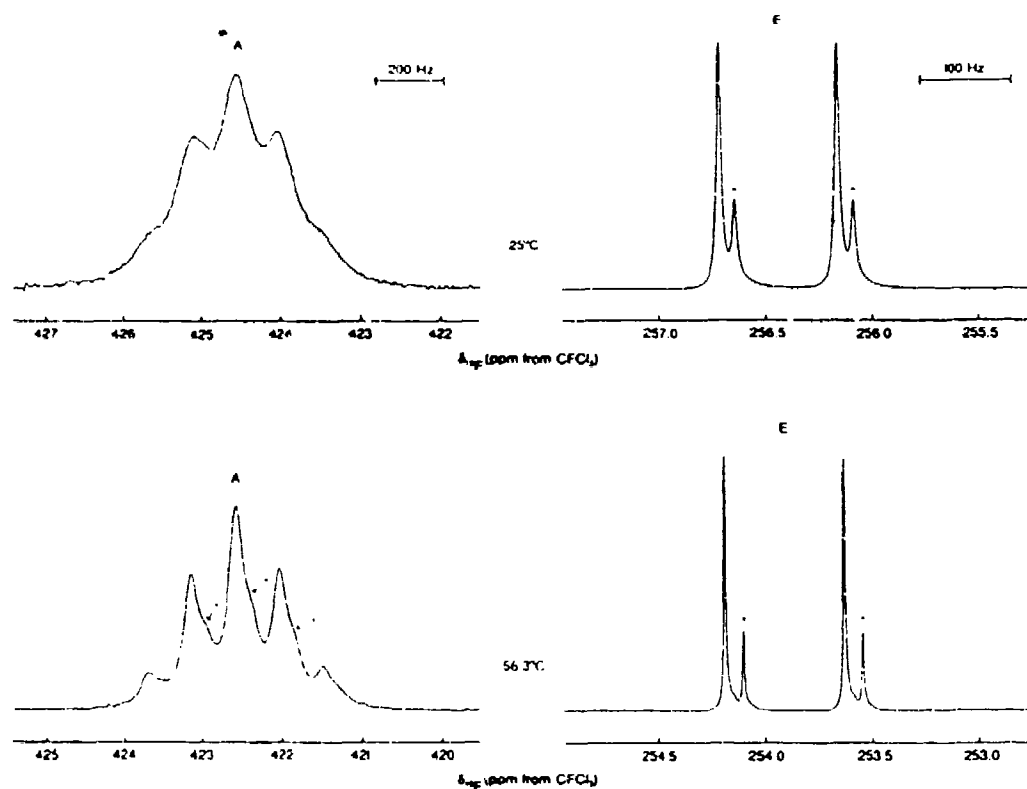


Figure 2. Variable-temperature ^{19}F NMR spectra (235.361 MHz) of ClF_3 (0.536 m) in HF solution. A and E denote resonances for the axial and equatorial fluorine environments, respectively; asterisks denote resonances arising from the ^{37}Cl isotopomer.

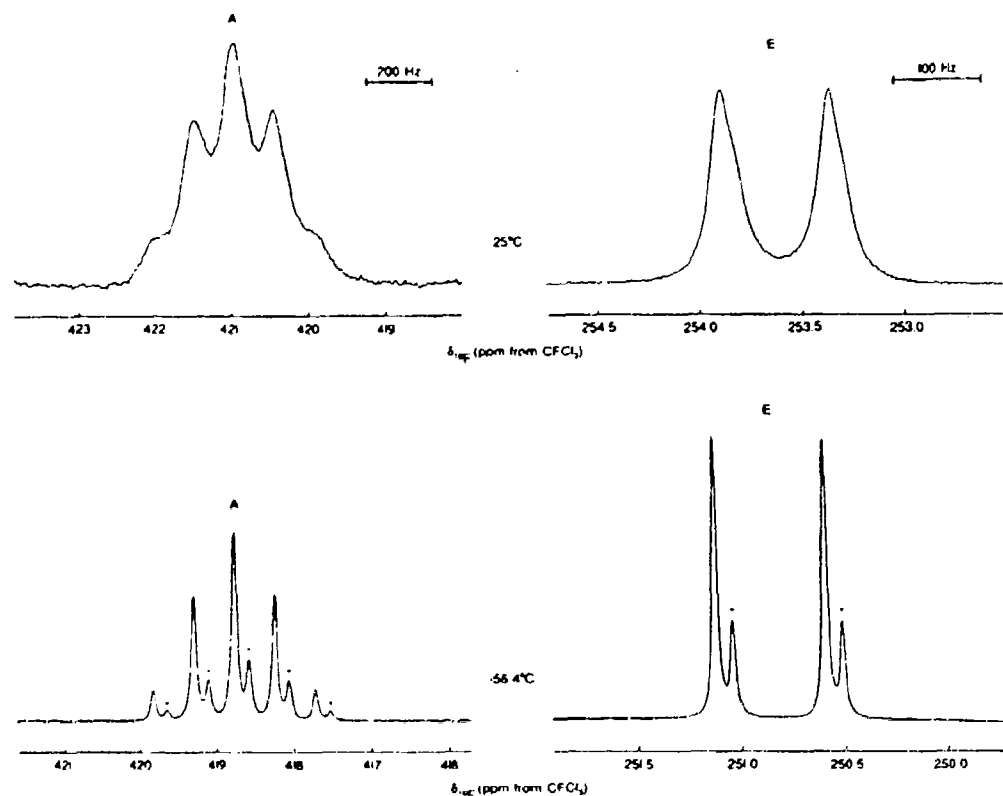


Figure 3. Variable-temperature ^{19}F NMR spectra (235.361 MHz) of ClF_3 (0.619 m)- CsF (5.60 m) in HF solution. A and E denote resonances for the axial and equatorial fluorine environments, respectively; asterisks denote resonances arising from the ^{37}Cl isotopomer.

conditions (Figure 4, trace C). The new set of bands at 525, 384, and 289 cm^{-1} are attributable to ClF_6^- for the following reasons: (i) the bands cannot be assigned to either CH_3CN , ClF_3 , or ClF_4^- ; (ii) they must be due to a species that on photolysis can produce

ClF_4^- ; (iii) the relative intensities of these Raman bands are very similar to those observed for solid $\text{Cs}^+\text{BrF}_6^-$,¹⁸ and (iv) the observed frequencies are in excellent agreement with our expectations for ClF_6^- .

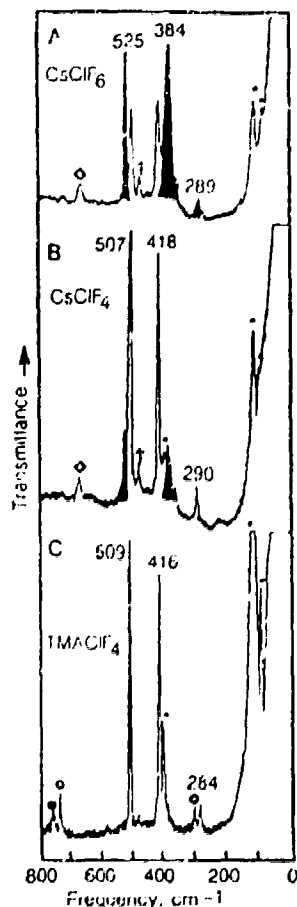


Figure 4. Raman spectra of CsClF_6 (trace A), CsClF_4 (trace B), and $\text{N}(\text{CH}_3)_4\text{ClF}_4$ (trace C) recorded at -110°C for the solids in frozen CH_3CN . The bands assigned to the anions of the title compounds are marked by their frequency values. Bands due to ClF_3 , CH_3CN , Kel-F, Teflon-FEP, and the $\text{N}(\text{CH}_3)_4^+$ cation have been marked by daggers, stars, diamonds, hollow circles, and full circles, respectively. Traces A and B are the first and second scan of the same sample and demonstrate the rapid decay of ClF_6^- (solid peaks) to ClF_4^- (hollow peaks) under the influence of the laser beam.

The last point needs some amplification. By analogy with octahedral BrF_6^{2-} , the ClF_6^- anion, which possesses a smaller central atom than BrF_6^{2-} , should also be octahedral; i.e., the free valence electron pair on chlorine should be sterically inactive. Octahedral ClF_6^- should possess six fundamental vibrations of which only the $\nu_1(\text{A}_1g)$, $\nu_2(\text{E}_g)$, and $\nu_3(\text{F}_2g)$ modes would be Raman active. Since in all the Raman active modes the central Cl atom is at rest, the observed frequencies should depend only on the force constants and should be independent of the mass of the central atom. Furthermore, the F -matrix expressions of these modes contain the same elements as the corresponding modes of the closely related octahedral HalF_6^+ cations and the pseudooctahedral HalF_5 molecules and HalF_4^- anions. Therefore, a plot of the frequencies of the modes should be mass independent and should exhibit smooth trends, with the frequencies decreasing with decreasing oxidation state of the central atom and increasing negative charge on the species. Plots of the sums of the frequencies of the symmetric in-phase and symmetric out-of-phase stretching modes and of those of the scissoring deformation mode for the series BrF_2^{2+} , BrF_6^{2+} , BrF_3^{2+} , BrF_4^{2+} , BrF_5^{2+} , and ClF_4^{2+} , ClF_6^{2+} , ClF_5^{2+} , and ClF_4^{2+} are shown in Figure 5. With the exception of the ClF_4^{2+} values, all the other frequencies had previously been established experimentally. As can be seen from Figure 5, the frequencies observed in this study for ClF_6^- perfectly fit the expected trends and strongly support their assignment to an octahedral ClF_6^- anion.

(30) Christie, K. O.; Schack, C. J. *Inorg. Chem.* 1970, 9, 1852.

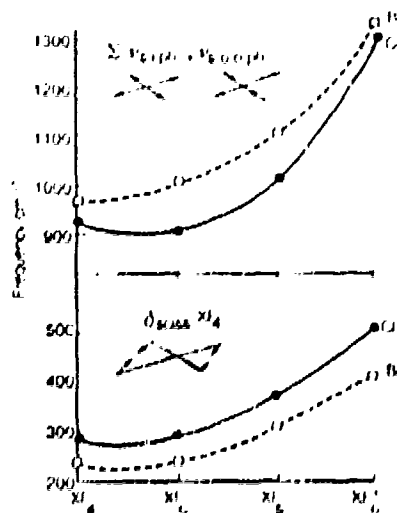


Figure 5. Plots of the sums of the frequencies of the two symmetric stretching modes and of those of the scissoring deformation mode for the different octahedral and pseudooctahedral halogen fluoride ions and molecules. The symmetry coordinates of each mode are depicted by the arrow diagrams.

ClF_6^{2+} , ClF_5^{2+} , and ClF_4^{2+} are shown in Figure 5. With the exception of the ClF_4^{2+} values, all the other frequencies had previously been established experimentally. As can be seen from Figure 5, the frequencies observed in this study for ClF_6^- perfectly fit the expected trends and strongly support their assignment to an octahedral ClF_6^- anion.

Conclusion. The results from this study, i.e., Raman spectroscopy and the ^{35}Cl radiotracer study, provide strong evidence for the existence of the ClF_6^- anion and its octahedral structure. As previously suggested, the past failures¹⁴ to isolate the ClF_6^- anion are due to its thermal and photolytic instability, combined with the low solubility of CsF and CsClF_4 in liquid ClF_3 . These problems were overcome by the use of the larger counterion $\text{N}(\text{CH}_3)_4^+$, which helps to stabilize the ClF_6^- anion and increases the solubility of the resulting salt, the use of CH_3CN as a more effective solvent, and the use of low-temperature spectroscopic techniques. The obvious limitations of this approach are the horrendous incompatibility problems encountered when one works with one of the most powerful known oxidizers in an organic solvent with an organic counterion. In view of our previous work¹ on the structure of BrF_6^{2-} , the steric inactivity of the free valence electron pair on the chlorine atom of ClF_6^- is not surprising and is at variance with the conclusions reached from a theoretical study, which examined the Laplacian of the calculated electronic charge distribution of gaseous ClF_6^- and predicted a fluxional structure having a distorted octahedral (C_{3v}) equilibrium geometry.¹⁷

Acknowledgment. We thank Dr. C. J. Schack and Mr. R. D. Wilson for their help, the U.S. Air Force Astronautics Laboratory, Edwards AFB (K.O.C. and G.J.S.), the U.S. Army Research Office (K.O.C.), and the Natural Sciences and Engineering Research Council of Canada (G.J.S.) for financial support, and Dr. E. S. Garnett for the use of the facilities of the Nuclear Medicine Department, Chedoke-McMaster Hospitals.

- (31) Selig, H.; Holzman, H. *Isr. J. Chem.* 1969, 7, 417.
 (32) Gillespie, R. L.; Schrobilgen, G. *J. Inorg. Chem.* 1974, 13, 1230.
 (33) Christie, K. O.; Wilson, R. D. *Inorg. Chem.* 1975, 14, 694.
 (34) Christie, K. O.; Sawadny, W. *Z. Anorg. Allg. Chem.* 1968, 357, 127.
 (35) Christie, K. O. *Spectrochim. Acta, Part A* 1971, 27a, 631.
 (36) Christie, K. O. *Inorg. Chem.* 1973, 12, 1580.
 (37) MacBungall, P. *J. Inorg. Chem.* 1966, 25, 4709.

The Pentafluoroxenate(IV) Anion, XeF_5^- : The First Example of a Pentagonal Planar AX_5 Species

Karl O. Christe,¹ Earl C. Curtis,¹ David A. Dixon,² H  lene P. Mercier,³
Jeremy C. P. Sanders,³ and Gary J. Schrobilgen^{1,3}

Contribution from Rocketdyne, A Division of Rockwell International, Canoga Park, California 91303, the Department of Chemistry, McMaster University, Hamilton, Ontario L8S 4M1, Canada, and the Central Research and Development Department, E. I. du Pont de Nemours and Company, Inc., Experimental Station, Wilmington, Delaware 19880-0328. Received September 28, 1990

Abstract: Xenon tetrafluoride forms stable 1:1 adducts with $\text{N}(\text{CH}_3)_4\text{F}$, CsF , RbF , KF , and NaF and an unstable 1:1 adduct with FNO . All these adducts are ionic salts containing pentagonal planar XeF_5^- anions as shown by a crystal structure determination of $\text{N}(\text{CH}_3)_4^+\text{XeF}_5^-$, Raman and infrared spectra, and ^{19}F and ^{135}Xe NMR spectroscopy. The X-ray crystal structure of $\text{N}(\text{CH}_3)_4^+\text{XeF}_5^-$ was determined at -86°C . This compound crystallizes in the orthorhombic system, space group $Pm\bar{c}n$, with four molecules in a unit cell of dimensions $a = 6.340$ (2)   , $b = 10.244$ (3)   , and $c = 13.896$ (4)   with $R = 0.0435$ for 638 observed [$I > 3\sigma(I)$] reflections. In addition to four $\text{N}(\text{CH}_3)_4^+$ cations, the structure contains four pentagonal planar XeF_5^- anions per unit cell with D_{3h} symmetry. The Xe-F distances are 1.979 (2)–2.034 (2)   with F-Xe-F angles of 71.5 (4)–72.3 (4) $^\circ$. The D_{3h} structure of the XeF_5^- anion is highly unusual and represents the first example of an AX_5E_2 (E = valence electron lone pair) species in which all six atoms are coplanar. The results from the crystal structure determination and a normal coordinate analysis show that the XeF_5^- plane of XeF_5^- is considerably more rigid than that in the fluxional IF_7 molecule due to the increased repulsion from the xenon free valence electron pairs. Local density functional calculations were carried out for XeF_5^- and XeF_4 with a double-numerical basis set augmented by polarization functions and confirm the experimentally observed geometries and vibrational spectra. It is shown that the bonding in XeF_5^- closely resembles that in XeF_4 . In a valence bond description, it can be visualized as the two axial positions being occupied by two sp-hybridized free valence electron pairs and the equatorial fluorines being bound by two Xe 5p electron pairs through semiionic multicenter four-electron bonds.

Introduction

Recent work in our laboratories has shown that anhydrous $\text{N}(\text{CH}_3)_4\text{F}^+$ holds great potential for the synthesis and characterization of novel, high oxidation state, complex fluoro anions.³⁻⁷ An area of special interest to us is the problem of maximum coordination numbers and their influence on the steric activity of free valence electron pairs. For example, it was shown that nitrogen(V) cannot accommodate five fluorine ligands,⁸ whereas the iodine in IF_6^+ , which had long been thought to have a distorted octahedral structure,^{9,10} has recently been confirmed to possess a sterically active lone valence electron pair.¹⁰ In contrast, the

central atom free valence electron pairs in the smaller ClF_6^- and BrF_6^- anions become sterically inactive due to space limitations, as demonstrated in very recent vibrational^{6,10} and single-crystal X-ray structure studies.¹¹

In this context, the likely structures of the XeF_5^- and XeF_6^{2-} anions posed an interesting problem, since both anions contain two free valence electron pairs on the xenon central atom. Therefore, they are representatives of the novel AX_5E_2 and AX_6E_2 geometries, respectively, where E stands for a free valence electron pair. Whereas no reports have been published on the existence or possible structure of XeF_5^- or any other AX_5E_2 species, Kiselev and co-workers¹²⁻¹⁵ recently reported the synthesis of M_2XeF_6 salts (M = Cs, Rb, K, Na) from XeF_4 and MF. On the basis of vibrational spectra, they surprisingly assigned an octahedral structure to XeF_6^{2-} . However, a closer inspection of their published

(1) Rockwell International, Rocketdyne Division.

(2) E. I. du Pont de Nemours and Company, Inc.

(3) McMaster University.

(4) Christe, K. O.; Wilson, W. W.; Wilson, R. D.; Bau, R.; Feng, J. *J. Am. Chem. Soc.* **1990**, *112*, 7619.

(5) Wilson, W. W.; Christe, K. O. *Inorg. Chem.* **1989**, *28*, 4172.

(6) Christe, K. O.; Wilson, W. W.; Chirakal, R. V.; Sanders, J. C. P.; Schrobilgen, G. J. *Inorg. Chem.* **1990**, *29*, 3506.

(7) Wilson, W. W.; Christe, K. O.; Feng, J.; Bau, R. *Can. J. Chem.* **1989**, *67*, 1988.

(8) Christe, K. O.; Wilson, W. W.; Schrobilgen, G. J.; Chirakal, R. V.; Olah, G. A. *Inorg. Chem.* **1988**, *27*, 789.

(9) Klarum, H.; Meinert, H.; Reich, P.; Witke, P. *Z. Chem.* **1968**, *8*, 469.

(10) Christe, K. O.; Wilson, W. W. *Inorg. Chem.* **1989**, *28*, 3275 and references cited therein.

(11) Mahjoub, A. R.; H  ser, A.; Fuchs, J.; Seppelt, K. *Angew. Chem., Int. Ed. Engl.* **1989**, *28*, 1526.

(12) Reference deleted in proof.

(13) Spitzin, V. I.; Kiselev, Yu. M.; Fadeeva, N. E.; Popov, A. I.; Tchumacvsky, N. A. *Z. Anorg. Allg. Chem.* **1988**, *559*, 171.

(14) Kiselev, Yu. M.; Goryachenkov, S. A.; Martynenko, L. I.; Spitsyn, V. I. *Dokl. Akad. Nauk SSSR* **1984**, *278*, 881.

(15) Kiselev, Yu. M.; Fadeeva, N. E.; Popov, A. I.; Korobov, M. V.; Nikulin, V. V.; Spitsyn, V. I. *Dokl. Akad. Nauk SSSR* **1987**, *295*, 378.

spectra¹³ revealed that both the frequency separations and relative intensities of the observed bands are incompatible with an octahedral species.¹⁶ Furthermore, it was noted that the Raman spectrum attributed to Cs_2XeF_6 was identical with that previously observed during the laser photolysis of CsXeF_7 and tentatively assigned to Cs_2XeF_8 .¹⁷ In view of these discrepancies we decided to investigate the fluoride-acceptor properties of XeF_4 using $\text{N}(\text{CH}_3)_4\text{F}$ as a fluoride ion source and to reinvestigate the XeF_4 -MF systems.

Experimental Section

Apparatus and Materials. Volatile materials were handled in stainless steel-Teflon and Pyrex glass vacuum lines, as previously described.^{18,19} Nonvolatile materials were handled in the dry nitrogen atmosphere of a glovebox.

Literature methods were used for the syntheses of anhydrous $\text{N}(\text{C}_2\text{H}_5)_4\text{F}$,⁴ XeF_4 ,²⁰ and FNO ²¹ and the drying of CH_3CN .^{4,22} The LiF (Research Inorganic Chemicals, Research Organic Chemicals), NaF (Matheson), and BaF_2 (Baker and Adamson) were dried under vacuum at 125 °C prior to their use. The KF (Allied), RbF (American Potash), and CsF (KBI) were dried by fusion in a platinum crucible, followed by transfer of the hot clinkers to the dry nitrogen atmosphere of the glovebox where the fluoride samples were ground prior to use.

Syntheses of M^+XeF_5^- ($\text{M} = \text{Cs, Rb, K, Na}$). The dry, finely powdered alkali metal fluorides (2 mmol) and XeF_4 (4–8 mmol) were loaded inside the drybox into prepassivated (with ClF_3), 10-mL, stainless steel Hoke cylinders that were closed by metal valves. The cylinders were evacuated at –78 °C on the vacuum line and then heated in an oven to 190 °C for 14 h. Unreacted XeF_4 was pumped off at 30 °C and collected in a tared Teflon U-trap at –196 °C until the cylinders reached a constant weight. The combining ratios of MF with XeF_4 were obtained from the observed material balances, i.e., the weights of MF, XeF_4 used, XeF_4 recovered, and the products. Under the above conditions, the following combining ratios were observed: $\text{CsF}:\text{XeF}_4 = 1:0.99$, $\text{RbF}:\text{XeF}_4 = 1:0.95$, $\text{KF}:\text{XeF}_4 = 1:0.65$, and $\text{NaF}:\text{XeF}_4 = 1:0.32$. Additional heating of the $\text{KF}-\text{XeF}_4$ and $\text{NaF}-\text{XeF}_4$ adducts with more XeF_4 to 135 °C for 10 days increased the conversion of KF and NaF to the corresponding XeF_5^- salts to 73% and 36%, respectively.

Synthesis of $\text{NO}^+\text{XeF}_5^-$. In the drybox, XeF_4 (1.03 mmol) was loaded into a prepassivated 0.5-in.-o.d. Teflon-FEP ampule that was closed by a stainless steel valve. On the vacuum line, FNO (6.77 mmol) was added to the ampule at –196 °C. The ampule was allowed to warm to 0 °C and was kept at this temperature for 10 min with agitation, and the unreacted FNO was then pumped off at –78 °C. The white solid residue (265 mg, weight calculated for 1.03 mmol of $\text{NO}^+\text{XeF}_5^- = 264$ mg) had a dissociation pressure of 10 Torr at 0 °C.

Synthesis of $\text{N}(\text{CH}_3)_4^+\text{XeF}_5^-$. In a typical synthesis, $\text{N}(\text{CH}_3)_4\text{F}$ and XeF_4 (2.01 mmol each) were loaded into a Teflon-FEP ampule in a drybox and CH_3CN (3 mL liquid) was vacuum distilled onto the solid at –196 °C. The mixture was warmed to –40 °C for 30 min with agitation and then allowed to warm to room temperature, followed by removal of the solvent in vacuo at this temperature. The white solid residue (605 mg, weight calculated for 2.01 mmol of $\text{N}(\text{CH}_3)_4^+\text{XeF}_5^- = 604$ mg) was identified as $\text{N}(\text{CH}_3)_4^+\text{XeF}_5^-$ by vibrational and NMR spectroscopy and a crystal structure determination. When isolated from CH_3CN solution, the compound is stable indefinitely at room temperature.

Caution! When solutions of $\text{N}(\text{CH}_3)_4^+\text{XeF}_5^-$ in CH_3CN are frozen in liquid nitrogen, they may detonate. Similar, but milder, detonations were also found to occur when XeF_4 solutions were frozen at –196 °C. Exposure of solid samples of $\text{N}(\text{CH}_3)_4^+\text{XeF}_5^-$ to atmospheric moisture for even brief periods has resulted in the violent detonation of bulk samples.

Crystal Structure Determination of $\text{N}(\text{CH}_3)_4^+\text{XeF}_5^-$. Crystal Growing. Single crystals of $\text{N}(\text{CH}_3)_4^+\text{XeF}_5^-$ suitable for X-ray analysis were grown from CH_3CN solution by vacuum distilling ca. 2.5 mL of dry CH_3CN onto ca. 50 mg of $\text{N}(\text{CH}_3)_4^+\text{XeF}_5^-$ in a 1/4-in.-o.d. FEP reaction vessel equipped with a Kel-F valve. The mixture was warmed to 65 °C to effect

Table 1. Summary of Crystal Data and Refinement Results for $[\text{N}(\text{CH}_3)_4]^+[\text{XeF}_5]^-$ *

space group	<i>Pmcn</i> (orthorhombic)
<i>a</i> (Å)	6.340 (2)
<i>b</i> (Å)	10.244 (3)
<i>c</i> (Å)	13.896 (4)
<i>V</i> (Å ³)	902.55
molecules/unit cell	4
molec wt (g mol ⁻¹)	300.44
calcd density (g cm ⁻³)	2.153
<i>T</i> (°C)	–86
color	colorless
cryst decay (%)	0.6
μ (cm ⁻¹)	35.77
wavelength (Å) used for data collectn	0.710 69
sin θ/λ limit (Å ⁻¹)	0.538
total no. of reflns measured	1414
no. of independent reflns	641
no. of reflns used in struct anal. $I > 3\sigma(I)$	638
no. of variable params	83
final agreement factors	$R(F) = 0.0435$ $R(WF) = 0.0435$

* Unit cell parameters obtained at 23 °C were $a = 6.400$ Å, $b = 10.321$ Å, and $c = 14.029$ Å; volume, 926.71 Å³.

dissolution and allowed to cool slowly to room temperature (ca. 5 °C/h). Colorless crystals up to 5 mm in length, having a needle-like morphology, formed overnight. The mother liquor was syringed off the crystals in a dry nitrogen atmosphere and residual solvent was removed under dynamic vacuum. Several crystals were cleaved perpendicular to their long axes to give fragments measuring ca. 0.2 mm × 0.2–0.3 mm and transferred in a drybox to 0.2-mm-o.d. Lindemann glass capillaries (previously dried under dynamic vacuum at 250 °C for 1 day) and sealed under a dry nitrogen atmosphere. The crystals were shown to be identical with the bulk sample prior to recrystallization by obtaining the single-crystal Raman spectrum at room temperature (see Figure 5b) and were found to be stable at room temperature in glass indefinitely.

Collection and Reduction of X-ray Data. Crystals of $\text{N}(\text{CH}_3)_4^+\text{XeF}_5^-$ were centered on a Syntex P₃ diffractometer. Accurate cell dimensions were determined at $T = 23$ °C and at $T = -86$ °C from a least-squares refinement of the setting angles (χ , ϕ , and 2θ) obtained from 15 accurately centered reflections (with $22.14^\circ < 2\theta < 28.11^\circ$) chosen from a variety of points in reciprocal space. At $T = 23$ °C, and after several hours in the X-ray beam, the crystal appeared to be totally decomposed, resulting in an opaque white coloration. Integrated diffraction intensities were collected on a new crystal at $T = -86$ °C using a θ - 2θ scan technique (slowest rate 5.0°/min) with $0 \leq h \leq 10$, $0 \leq k \leq 15$, and $-15 \leq l \leq 15$, using molybdenum radiation monochromatized with a graphite crystal ($\lambda = 0.710 69$ Å). Throughout the data collection, two standard reflections were monitored every 48 reflections; a decay of 0.6% was observed; the intensities were adjusted accordingly. A total of 1414 reflections were collected out of which 641 reflections, satisfying the condition $I > 3\sigma(I)$, were chosen for structure solution. The intensities of these reflections were corrected for Lorentz polarization effects.

Solution and Refinement of the Structure. There were two space groups that were consistent with the reflection pattern: the noncentrosymmetric space group *P21cn* (No. 33) and the centrosymmetric space group *Pmcn* (No. 62). The structure has been solved in both centrosymmetric (*Pmcn*) and noncentrosymmetric (*P21cn*) space groups. The direct method of structure solution in the computer program SHELX-76²³ was used to locate the positions of the Xe atom and the five F atoms. Successive Fourier synthesis yielded all the remaining non-hydrogen atoms. The structure was refined by using the full-matrix least-squares technique with isotropic thermal parameters for individual atoms. In the case of the *Pmcn* space group and after full convergence of the isotropic refinement ($R = 0.1265$), the atoms were assigned anisotropic thermal parameters and further refined by the full-matrix least-squares technique ($R = 0.0714$). The positions of the hydrogen atoms were calculated and the fixed hydrogen atoms were given an isotropic temperature factor of 0.05 Å².²⁴ The *K* factor obtained was 0.0652, with the unit weights. There was significant disagreement between the F_o and F_c values of three reflections, 110, 312, and 413, and these values were consequently omitted in a further refinement. This resulted in a global improvement of the structure and a final value for the *R* factor of 0.0435.

(23) Sheldrick, G. M. *SHELX-76 Program for Crystal Structure Determination*; University of Cambridge: Cambridge, England, 1976.

(24) Hall, S. R.; Stewart, J. H. *XTAL 76 User's Manual*; University of Western Australia and University of Maryland.

(16) Weidlein, J.; Müller, U.; Dehnicke, K. *Schwingungsspektroskopie*; Georg Thieme Verlag: Stuttgart, Germany, 1982.

(17) Christe, K. O.; Wilson, W. W. *Inorg. Chem.* 1982, 21, 4113.

(18) Christe, K. O.; Wilson, R. B.; Schack, C. J. *Inorg. Synth.* 1986, 24, 3.

(19) Syvret, R. G.; Schrobilgen, G. J. *Inorg. Chem.* 1989, 28, 1564.

(20) (a) Bartlett, N.; Sladky, F. O. *J. Am. Chem. Soc.* 1968, 90, 5316. (b) Malm, J. G.; Chernick, C. L. *Inorg. Synth.* 1966, 8, 254.

(21) Christe, K. O. *Inorg. Chem.* 1972, 12, 1580.

(22) Winfield, J. M. *J. Fluorine Chem.* 1984, 25, 91.

Table II. Final Atomic Coordinates for $[N(CH_3)_4]^+[XeF_5^-]$

atom	x	y	z	pop. ^a
Xe1	0.2500	0.1233 (1)	0.0155 (1)	0.5
F1	0.2500	0.1876 (9)	0.1497 (6)	0.5
F2	0.2500	-0.0324 (8)	0.1025 (6)	0.5
F3	0.2500	-0.0399 (8)	-0.0673 (6)	0.5
F4	0.2500	0.1799 (9)	-0.1236 (6)	0.5
F5	0.2500	0.3217 (8)	0.0110 (6)	0.5
N1	0.2500	-0.403 (1)	0.172 (1)	0.5
C1	0.2500	0.628 (2)	0.068 (1)	0.5
C2	0.2500	-0.281 (2)	0.231 (1)	0.5
C3	0.437 (5)	-0.483 (2)	0.196 (1)	1.0

^aThe site occupation factor.

The same procedure was used for the $P2_1cn$ space group, which gave rise to a final R factor of 0.0763. The ratio of agreement factors $R_w(7.63/4.35) = 1.75$ is sufficient by Hamilton's R factor ratio test¹ to state that the correct space group is $Pm\bar{c}n$.

An empirical absorption correction was also applied, but no significant improvement in the refinement was observed; in particular there was no change in the anisotropic thermal parameters.

Details of the data collection parameters and other crystallographic information for the $Pm\bar{c}n$ space group are given in Table I, and the final atomic coordinates are summarized in Table II. The following programs were used: XTAL,²⁴ data reduction; SHELX-76,²⁵ structure refinement; SNOOP,²³ diagrams.

Vibrational Spectroscopy. Raman spectra were recorded on either a Cary Model 83 or a Spex Model 1403 spectrophotometer using a 488-nm exciting line of an Ar ion or the 647.1-nm line of a Kr ion laser, respectively. Baked-out Pyrex melting point capillaries or thin-walled Kel-F tubes were used as sample containers. A previously described²⁶ device was used for recording the low-temperature spectra (at -150 °C). Single-crystal spectra of $N(CH_3)_4^+XeF_5^-$ were recorded at room temperature on a Instruments S.A. Mole S-3000 triple spectrograph system equipped with a microscope for focusing the excitation laser to a one-micrometer spot. The Ar laser line at 514.5 nm was selected for excitation of the sample. Crystals were sealed in Lindemann glass capillaries as described below.

Infrared spectra were recorded by using AgBr disks on a Perkin-Elmer Model 283 spectrophotometer. The finely powdered samples were sandwiched between two thin AgBr disks and pressed together in a Wilks minipress inside the drybox.

Nuclear Magnetic Resonance Spectroscopy. The ^{19}F and ^{129}Xe NMR spectra were recorded unlocked (field drift < 0.1 Hz h^{-1}) with Bruker WM-250 and Bruker AM-500 spectrometers equipped with 5.8719-T and 11.744-T cryomagnets, respectively. Fluorine-19 spectra were obtained by using a 5-mm combination $^1H/^{19}F$ probe operating at 235.36 MHz. The spectra were accumulated in 16K memory. Spectral width settings of 5000 and 30000 Hz were employed, yielding data point resolutions of 0.61 and 3.6 Hz/data point and acquisition times of 1.638 and 0.279 s, respectively. No relaxation delays were applied. Typically 300–7000 transients were accumulated. The pulse width corresponding to a bulk magnetization tip angle, θ , of approximately 90° was equal to 1 μs . No line broadening parameters were applied in the exponential multiplication of the free induction decays prior to Fourier transformation.

Xenon-129 NMR spectra were obtained by using a broad-band VSP probe (tunable over the range 23–202 MHz); spectra were recorded at 139.05 MHz. The spectra were accumulated in a 16K memory. A spectral width setting of 50 kHz was employed, yielding a data point resolution of 6.1 Hz/data point and an acquisition time of 0.164 s. No relaxation delays were applied. Typically 10 000 transients were accumulated. The pulse width corresponding to a bulk magnetization tip angle, θ , of approximately 90° was equal to 18 μs . Line-broadening parameters of 4 Hz were applied in the exponential multiplication of the free induction decays prior to Fourier transformation.

The ^{19}F and ^{129}Xe NMR spectra were referenced to neat external samples of $CFCl_3$ and $XeOF_4$, respectively, at ambient temperature. The chemical shift convention used is that a positive (negative) sign signifies a chemical shift to high (low) frequency of the reference compound.

The ^{129}Xe NMR samples of saturated solutions of $N(CH_3)_4^+XeF_5^-$ in CH_3CN were prepared in 25-cm lengths of $1/8$ -in. o.d., $1/32$ -in. wall FEP plastic tubing that had been reduced to 9-mm o.d. by squeezing in a heated precision brass mold. The FEP tubing was heat sealed at one

end with the open end flared (45° SAE) and joined, by means of compression fittings, to a Kel-F valve. The FEP tubes were heat sealed under dynamic vacuum with their contents frozen at -78 °C. The sealed FEP sample tubes were inserted into 10-mm thin-walled precision NMR tubes (Wilmad) in order to run their spectra.

The ^{19}F NMR samples were prepared in precision 5-mm glass NMR tubes (Wilmad). Solid $N(CH_3)_4^+XeF_5^-$ [or $N(CH_3)_4^+XeF_3^-$ and $N-(CH_3)_4^+F^-$] was loaded into the NMR tube in the drybox and CH_3CN solvent distilled in vacuo into the tube at -78 °C. The tube was flame sealed. On warming to room temperature, a colorless saturated solution resulted containing some solid $N(CH_3)_4^+XeF_5^-$, which was decanted into the top of the tube prior to obtaining the NMR spectrum.

Computational Method. The calculations described below were done by using the local density functional theory^{27–30} with the program system DMol.³¹ DMol employs numerical functions for the atomic basis sets. The atomic basis functions are given numerically as an atom-centered, spherical, polar mesh. The radial portion of the grid is obtained from the solution of the atomic LDF equations by numerical methods. The radial functions are stored as sets of cubic spline coefficients so that the radial functions are piecewise analytic, a necessity for the evaluation of gradients. The use of exact spherical atom results offers certain advantages. Because of the quality of the atomic basis sets, basis set superposition effects should be minimized, correct behavior at the nucleus is obtained, and radial nodal properties of the wave function are present.

Because the basis sets are numerical, the various integrals arising from the expression for the energy need to be evaluated over a grid. The integration points are generated in terms of angular functions and spherical harmonics. The number of radial points N_p is given as

$$N_p = 12 \times 14(Z + 2)^{1/3} \quad (1)$$

where Z is the atomic number. The maximum distance for any function is 12 au. The angular integration points N_θ are generated at the N_p radial points to form shells around each nucleus. The value of N_θ ranges from 14 to 302 depending on the behavior of the density.³¹ The Coulomb potential corresponding to the electron repulsion term could be solved by evaluation of integrals. However, since the method is based on the density, it was found to be more appropriate to determine the Coulomb potential directly from the electron density by solving Poisson's equation

$$-\nabla^2 V_c(r) = 4\pi e^2 \rho(r) \quad (2)$$

In DMol, the form for the exchange-correlation energy of the uniform electron gas is that derived by von Barth and Hedin.³¹

All of the DMol calculations were done with a double-numerical basis set augmented by d polarization functions. This can be thought of in terms of size as a polarized double- ζ basis set. However, because exact numerical solutions are employed for the atom, this basis set is of significantly higher quality than a normal molecular orbital polarized double- ζ basis set. The fitting functions have an angular momentum number one greater than that of the polarization function, resulting in a value of $l = 3$ for the fitting functions.

Geometries were determined by optimization using analytic gradient methods.³² First derivatives in the LDF framework can be calculated efficiently and only take on the order of three to four SCF iterations or 10–25% of an energy evaluation. There are two problems with evaluating gradients in the LDF framework, which are due to the numerical methods that are used. The first is that the energy minimum does not nec-

(27) Parr, R. G.; Yang, W. *Density Functional Theory of Atoms and Molecules*; Oxford University Press: New York, 1989.

(28) Salahub, D. R. In *Ab Initio Methods in Quantum Methods in Quantum Chemistry*, 2nd ed.; Lawley, K. P., Ed.; J. Wiley & Sons: New York, 1987; p 447.

(29) (a) Wimmer, E.; Freeman, A. J.; Fu, C.-L.; Cao, P.-L.; Chou, S.-H.; Delley, B. In *Supercomputer Research in Chemistry and Chemical Engineering*; Jensen, K. F.; Truhlar, D. G., Eds.; ACS Symposium Series: American Chemical Society: Washington, DC, 1987; p 49. (b) Dixon, D. A.; Andrejm, J.; Fitzgerald, G.; Wimmer, E.; Delley, B. In *Science and Engineering on Cray Supercomputers: Proceedings of the Fifth International Symposium*, Cray Research: Minneapolis, MN, 1990; p 285.

(30) Jones, P. O.; Gunnarsson, O. *Rev. Mod. Phys.* 1989, 61, 689.

(31) Delley, B. *J. Chem. Phys.* 1990, 92, 508. DMol is available commercially from BIOSYM Technologies, San Diego, CA.

(32) This grid can be obtained by using the FINE parameter in DMol.

(33) von Barth, U.; Hedin, L. *J. Phys. Chem.* 1972, 76, 1629.

(34) (a) Versluis, L.; Ziegler, T. *J. Chem. Phys.* 1988, 88, 3322. (b) Andrejm, J.; Wimmer, E.; Salahub, D. R. In *The Challenge of d and f Electrons: Theory and Computation*; Salahub, D. P.; Zerner, M. C., Eds.; ACS Symposium Series 394; American Chemical Society: Washington, DC, 1989; p 228. (c) Fournier, R.; Andrejm, J.; Salahub, D. R. *J. Chem. Phys.* 1989, 90, 6311.

(35) Pauling, L. *The Nature of the Chemical Bond*, 3rd ed.; Cornell University Press: Ithaca, NY, 1960; p 260.

(36) Bondi, A. *J. Phys. Chem.* 1964, 68, 441.

(25) Davies, K. *CHEMGRAF Suite*; SNOOP, Chemical Design Ltd Oxford, England, 1981.

(26) Miller, I. A.; Harney, B. M. *Appl. Spectrosc.* 1969, 23, 8.

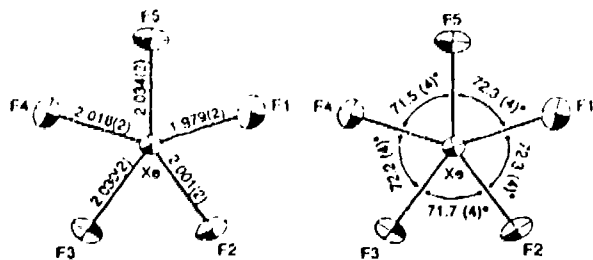


Figure 1. Atom numbering scheme, bond lengths (Å) and angles (deg) for XeF_5^- at -86°C in $[\text{N}(\text{CH}_3)_4]^+[\text{XeF}_5]^-$. Projection of the XeF_5^- anion on (111). Esd's are given in parentheses; thermal ellipsoids are shown at the 50% probability level.

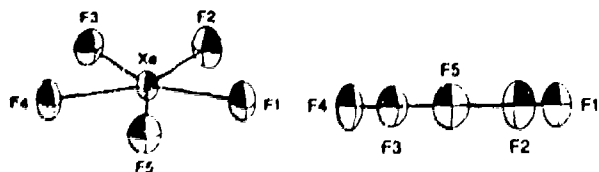


Figure 2. Projections of the XeF_5^- anion on (130) (left) and (010) (right). Thermal ellipsoids are shown at the 50% probability level.

essarily correspond exactly to the point with a zero derivative. The second is that sum of the gradients may not always be zero as required for transitional invariance. These tend to introduce errors on the order of 0.001 Å in the calculation of the coordinates if both a reasonable grid and basis set are used. This gives bond lengths and angles with reasonable error limits. The difference of 0.001 Å is about an order of magnitude smaller than the accuracy of the LDF geometries as compared to experiment.

Results and Discussion

Syntheses and Properties of XeF_5^- Salts. The reactions of the alkali-metal fluorides with XeF_4 were studied under conditions (190°C , 14 h) very similar to those previously reported by Kiselev and co-workers.¹³⁻¹⁵ It was found that XeF_4 combines with either CsF or RbF in a clean 1:1 mole ratio to form the corresponding, previously unidentified XeF_5^- salts. In the case of KF and NaF the same anion was formed; however, the percentage conversion of MF to MXeF_5 decreased with decreasing atomic weight of M ($\text{CsF} = 99\%$, $\text{RbF} = 95\%$, $\text{KF} = 65\%$, and $\text{NaF} = 32\%$) and increased reaction times were required for higher conversions.

The interactions of LiF and BaF_2 with XeF_4 were also examined, but in neither case was evidence for the formation of a stable adduct obtained.

The XeF_5^- salts of Cs^+ , Rb^+ , K^+ , and Na^+ are white, stable solids. Their physical properties, thermal stabilities, etc. are those previously attributed by Kiselev and co-workers to the corresponding M_2XeF_6 salts.¹³⁻¹⁵ As will be shown below, they all contain pentagonal planar XeF_5^- anions.

Attempts to prepare CsXeF_5 from CsF and XeF_4 at room temperature in CH_3CN solutions were unsuccessful because of the very low solubility of CsF in this solvent. However, the highly soluble $\text{N}(\text{CH}_3)_4\text{F}$ readily forms $[\text{N}(\text{CH}_3)_4]^+[\text{XeF}_5]^-$ under these

Table III. Bond Distances (Å) and Bond Angles (deg) in $[\text{N}(\text{CH}_3)_4]^+[\text{XeF}_5]^-$

Bond Lengths			
Xe1-F1	1.979 (2)	N1-C1	1.481 (6)
Xe1-F2	2.001 (2)	N1-C2	1.488 (6)
Xe1-F3	2.030 (2)	N1-C3	1.524 (4)
Xe1-F4	2.018 (2)		
Xe1-F5	2.034 (2)		
Bond Angles			
F2-Xe1-F1	72.3 (4)	C2-N1-C1	110.7 (3)
F3-Xe1-F2	71.7 (4)	C3-N1-C1	108.9 (5)
F4-Xe1-F3	72.2 (4)	C3-N1-C2	109.6 (4)
F5-Xe1-F1	72.3 (4)		
F5-Xe1-F4	71.5 (4)		

conditions. Even with a 2:1 molar ratio of $\text{N}(\text{CH}_3)_4\text{F}:\text{XeF}_4$ in CH_3CN solvent and a large excess of MF in the $\text{XeF}_4\text{-MF}$ systems, only XeF_5^- , and no XeF_6^{2-} , was observed, indicating that XeF_5^- is the favored anion. The $[\text{N}(\text{CH}_3)_4]^+[\text{XeF}_5]^-$ salt is a white, stable solid whose structure was established by a crystal structure determination and vibrational and NMR spectroscopy (see below).

The lack of XeF_6^{2-} formation in these systems was further demonstrated by a study of the FNO-XeF_4 system. Even when a large excess of FNO was used, only $\text{NO}^+\text{XeF}_5^-$, and no $(\text{NO}^+)_2\text{XeF}_6^{2-}$, was formed at temperatures as low as -78°C . The $\text{NO}^+\text{XeF}_5^-$ salt is a white solid having a dissociation pressure of 10 Torr at 0°C . It is ionic, containing NO^+ and XeF_5^- ions as shown by vibrational spectroscopy (see below).

In view of the above results and the structural evidence presented below, it appears quite clear that the salts obtained by the reactions of XeF_4 with fluoride ion sources are XeF_5^- , and not XeF_6^{2-} , salts. The fact that some of the products reported¹³⁻¹⁵ by the Soviet workers gave elemental analyses approaching the M_2XeF_6 composition might be attributed to incomplete conversion of MF to MXeF_5 , thus resulting in $\text{MF} + \text{MXeF}_5$. There is also no doubt that the products observed during the laser photolysis of either CsXeF_7 or NF_4XeF_7 were not XeF_6^{2-} but XeF_5^- salts.¹⁷

X-ray Crystal Structure of $[\text{N}(\text{CH}_3)_4]^+[\text{XeF}_5]^-$. The crystal structure consists of well-separated $[\text{N}(\text{CH}_3)_4]^+$ and XeF_5^- ions. The $[\text{N}(\text{CH}_3)_4]^+$ cation is tetrahedral with the expected bond lengths. Different views of the XeF_5^- anion are shown in Figures 1 and 2, while a stereoview of the packing in the unit cell is given in Figure 3 in which the hydrogen atoms have been omitted in the cation. Important bond lengths and angles are listed in Table III. The xenon and five fluorines of the XeF_5^- anion and the nitrogen and two carbons of the cation are located on special positions that are on the mirror plane, resulting in an anion that is planar by crystal symmetry. The closest anion-cation distance occurs between F2 and C2, which lies in the anion plane, at 3.105 (5) Å, whereas the remaining closest F...C distances occur at 3.237 (5) Å (F5...C1), 3.354 (5) Å (F3...C2), 3.370 (5) Å (F1...C3), and 3.651 (5) Å (F4...C2). The sum of the van der Waals radii of CH_3 (2.00 Å³⁵) and F (1.35³⁵-1.40³⁶ Å) is 3.35-3.40 Å. The F2...C2 distance suggests weak hydrogen bonding between the C2 methyl group and F2 and is somewhat shorter than the shortest F...C

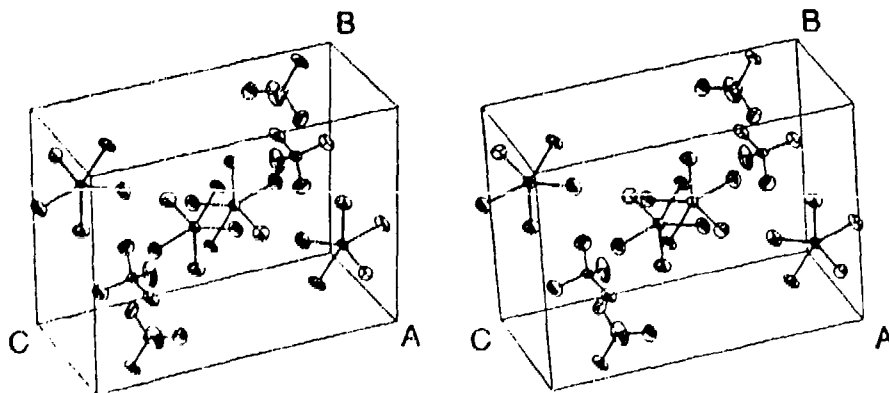


Figure 3. Stereoview [111] of the unit cell of $[\text{N}(\text{CH}_3)_4]^+[\text{XeF}_5]^-$; hydrogen atoms are excluded.

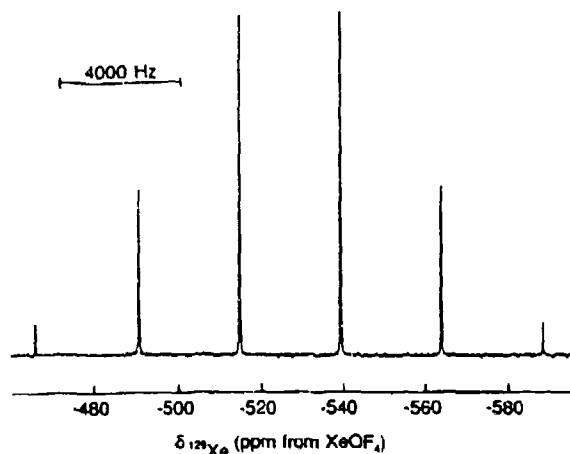


Figure 4. ^{129}Xe NMR spectrum (139.05 MHz) at 24 °C of a saturated solution of $\text{N}(\text{CH}_3)_4^+\text{XeF}_5^-$ in CH_3CN containing a 1 M excess of $\text{N}(\text{CH}_3)_4^+\text{F}^-$.

distance in $\text{N}(\text{CH}_3)_4^+\text{HF}_2^-$ [3.313 (5) Å],⁷ which appears to be at the limit of the van der Waals distance. The short F2...C2 distance appears to account for the greater elongation of the thermal ellipsoid of F2 (in the direction of the C_2 -axis of the anion; Figure 2).

Although the site symmetry of the XeF_5^- anion is C_2 , the five fluorines are clearly equivalently bonded to the xenon, giving a pentagonal planar structure of D_{3h} symmetry. The average F-Xe-F angle of 72.0 (4)° is essentially the ideal angle of 72°. The average Xe-F bond length [2.012 (2) Å] is significantly longer than the average bond length of XeF_4 [1.953 (2) Å]³⁷ and the average equatorial bond length of IF_7 [1.858 (4) Å].³⁸ The nearest-neighbor F...F contacts in the XeF_5^- anion are 2.35–2.38 Å and are substantially less than twice the nominal van der Waals radius for fluorine, i.e., 2.70³⁵–2.80³⁸ Å, indicating that the fluorines of the pentagon are significantly congested and are consistent with the long Xe-F bond length in XeF_5^- . This contrasts with the shorter Xe-F bond length of XeF_4 , where the fluorines in the plane are not contacting, and the intramolecular F...F distances (2.76 Å) are at the limit of the sum of the fluorine van der Waals radii. The short I-F bond lengths for the equatorial belt of five fluorines in IF_7 relative to the Xe-F bond length of XeF_5^- may be attributed to relief of the congestion in the IF_5 belt by means of a 7.5° puckering, which has been deduced from electron diffraction studies³⁹ but not corroborated by an independent study. The fact that XeF_5^- does not relieve its steric congestion by a puckering distortion may be attributed to the presence of the two axial lone pairs of electrons, which exert greater repulsive forces than the two axial fluorines in the IF_7 molecule, thus forcing the XeF_5^- anion to be planar. Moreover, the formal negative charge on XeF_5^- leads to a greater Xe-F bond polarity and elongation of the Xe-F bond, as is evident from a comparison with the Xe-F bond length of XeF_4 , and serves to alleviate some of the steric congestion in the anion plane.

The steric crowding in the XeF_5^- molecular plane is further illustrated by the thermal parameters, which remain essentially unaltered before and after empirical absorption corrections. It is apparent that the principal axes of motion of the fluorine atoms in XeF_5^- and XeF_4 ³⁷ are perpendicular to the bond directions, producing the anticipated polar flattening of the thermal ellipsoids in the Xe-F bond directions. However, the thermal ellipsoids in XeF_5^- are elongated in the direction of the C_2 -axis and flattened in the direction perpendicular to the Xe-F bonds in the molecular plane. In contrast to the fluorine thermal ellipsoids in XeF_5^- , those of XeF_4 are essentially isotropic in the directions perpendicular to the Xe-F bonds and in the molecular plane where the fluorine atoms are apparently not contacting one another to any significant

(37) Burns, J. H.; Agron, P. A.; Levy, H. A. *Science* 1963, 139, 1208.

(38) Adams, W. J.; Thompson, H. B.; Bartell, L. S. *J. Chem. Phys.* 1970, 53, 4040.

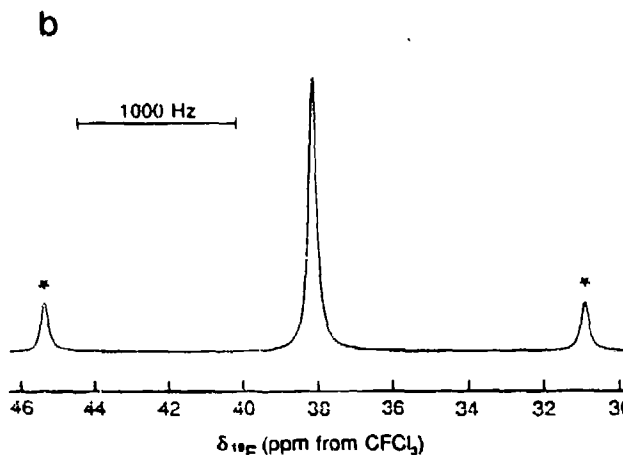
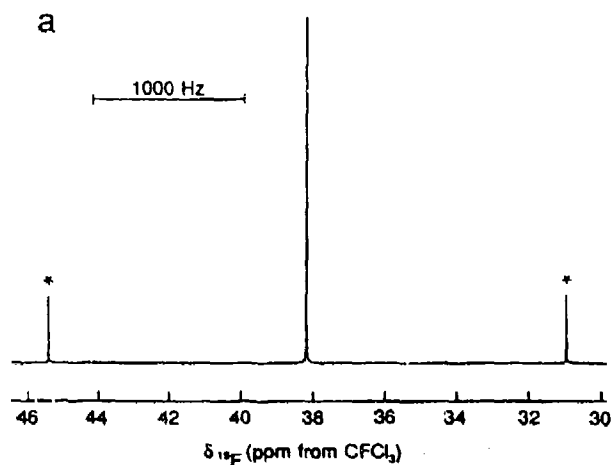


Figure 5. ^{19}F NMR spectrum (235.36 MHz) at 24 °C of (a) a saturated solution of $\text{N}(\text{CH}_3)_4^+\text{XeF}_5^-$ in CH_3CN containing a 1 M excess of $\text{N}(\text{CH}_3)_4^+\text{F}^-$ and (b) a saturated solution of pure $\text{N}(\text{CH}_3)_4^+\text{XeF}_5^-$ in CH_3CN . Asterisks (*) denote ^{129}Xe satellites.

extent. Steric congestion in XeF_5^- is additionally supported by vibrational force constant calculations (see below).

^{129}Xe and ^{19}F NMR Spectra of the XeF_5^- Anion. The ^{129}Xe NMR spectrum of $\text{N}(\text{CH}_3)_4^+\text{XeF}_5^-$ dissolved in CH_3CN containing a 1 M excess of $\text{N}(\text{CH}_3)_4^+\text{F}^-$ at 24 °C (Figure 4) displays a well-resolved binomial sextet ($\Delta\nu_{1/2} = 15$ Hz), consistent with the coupling of the ^{129}Xe nucleus to five chemically equivalent ^{19}F nuclei in the XeF_5^- anion [$\delta(^{129}\text{Xe})$, -527.0 ppm from XeOF_4 ; $^1J(^{129}\text{Xe}-^{19}\text{F})$, 3400 Hz]. The ^{129}Xe chemical shift of XeF_5^- is significantly more shielded (i.e., by -843.9 ppm) than that of XeF_4 in CH_3CN at 24 °C [$\delta(^{129}\text{Xe})$, 316.9 ppm from XeOF_4 ; $^1J(^{129}\text{Xe}-^{19}\text{F})$, 3895 Hz]. This behavior follows the expected trend of increased shielding that accompanies an increase in negative charge.³⁹ The ^{19}F NMR spectrum of a similar sample at 24 °C (Figure 5a) shows a narrow singlet ($\Delta\nu_{1/2} = 2.8$ Hz) flanked by natural abundance (26.44%) ^{129}Xe satellites [$\delta(^{19}\text{F})$, 38.1 ppm from CFCl_3 ; $^1J(^{129}\text{Xe}-^{19}\text{F})$, 3398 Hz]. A resonance due to unreacted fluoride was observed at -75 ppm. Interestingly, the ^{19}F chemical shift of XeF_5^- is deshielded by 56.8 ppm with respect to that of XeF_4 in CH_3CN at 24 °C [$\delta(^{19}\text{F})$, -18.7 ppm from CFCl_3 ; $^1J(^{129}\text{Xe}-^{19}\text{F})$, 3896 Hz]. This result is somewhat surprising in view of the increased ionic character of the Xe-F bonds (i.e., greater bond length and smaller stretching force constant) compared with those in XeF_4 ; the reason for this is not clear but may be related to the congested environment of the fluorine ligands and the rather short nearest-neighbor F...F contact distance. The ^{19}F NMR spectrum of a sample prepared from equimolar

(39) Jameson, C. J.; Mason, J. In *Multinuclear NMR*; Mason, J., Ed.; Plenum Press: New York, 1987; Chapter 3, pp 66–68.

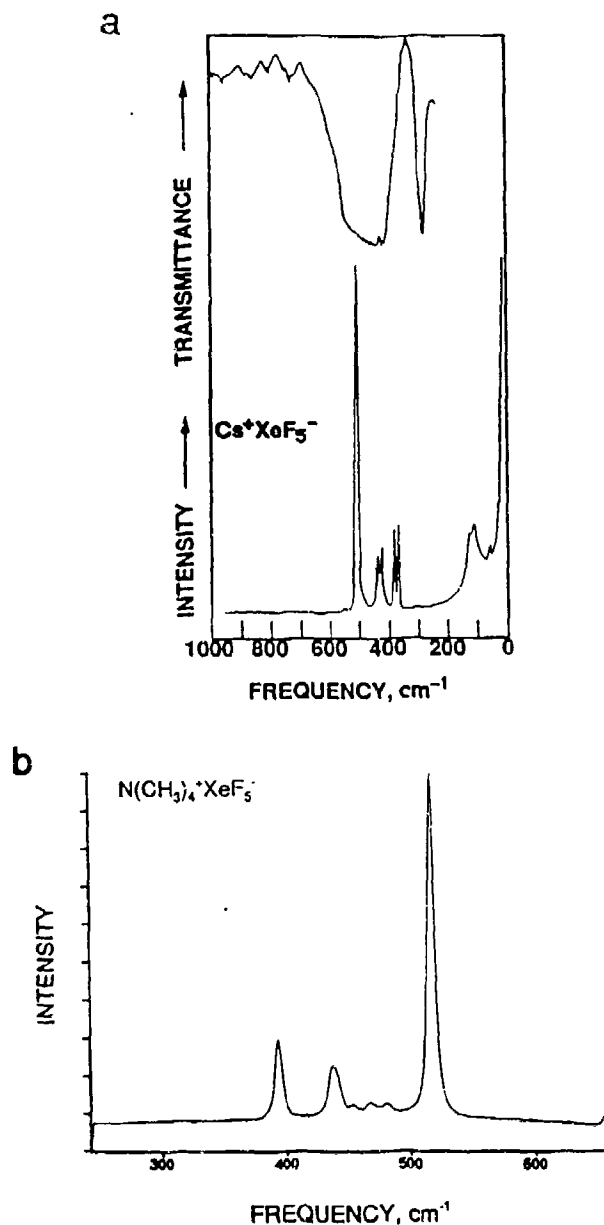


Figure 6. (a) Vibrational spectra of solid $\text{Cs}^+\text{XeF}_5^-$. Upper trace, infrared spectrum recorded at room temperature with an AgBr disk; lower trace; Raman spectrum recorded in a glass capillary at 25 °C with 647.1-nm excitation. (b) Single-crystal Raman spectrum of $\text{N}(\text{CH}_3)_4^+\text{XeF}_5^-$ recorded in a glass capillary at room temperature with 514.5-nm excitation.

quantities of XeF_4 and $\text{N}(\text{CH}_3)_4^+\text{F}^-$ in CH_3CN showed a similar resonance, with accompanying ^{129}Xe satellites, at 38.1 ppm; however, the linewidth was significantly broader, $\Delta\nu_{1/2} = 53$ Hz (Figure 5b). This indicates that XeF_5^- undergoes dissociative fluorine exchange, which can be suppressed by the presence of excess fluoride. There was no evidence for the formation of XeF_6^{2-} at $\text{XeF}_4:\text{N}(\text{CH}_3)_4^+\text{F}^-$ ratios exceeding 1:1, thus casting further doubt on the previous claims¹³⁻¹⁵ for the existence of stable salts of the XeF_6^{2-} anion.

The magnitude of the one-bond $^{129}\text{Xe}-^{19}\text{F}$ coupling constant drops from 3895 Hz in XeF_4 to 3400 Hz in XeF_5^- under the same conditions (i.e., solvent and temperature) of experimental measurement. If it is assumed that the Fermi-contact mechanism provides the dominant coupling contribution,⁴⁰ then the smaller

(40) (a) Jameson, C. J. In *Multinuclear NMR*; Mason, J., Ed.; Plenum Press: New York, 1987; Chapter 4, pp 97-101; Chapter 18. (b) Schrobilgen, G. J. In *NMR and the Periodic Table*; Harris, R. K., Mann, B. E., Eds.; Academic Press: New York, 1978; Chapter 14.

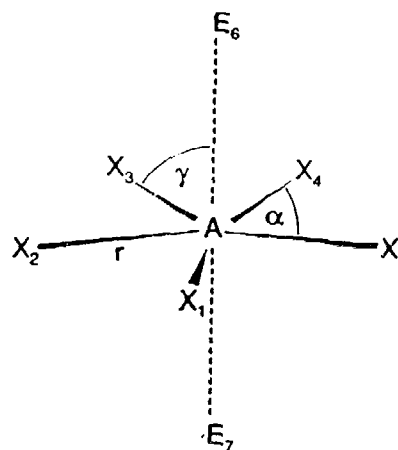


Figure 7. Internal coordinates for pentagonal planar AX_5 .

value of $J(^{129}\text{Xe}-^{19}\text{F})$ in XeF_5^- is in accord with the greater ionic character of the Xe-F bonds in the anion.

In the VSEPR notation, XeF_5^- is a seven-coordinate AX_5E_2 system, and is the first example of this geometry.⁴¹ The solution structure proposed for the anion that is consistent with five equivalent fluorines is a pentagonal planar (D_{5h}) structure having five equivalent equatorial fluorines and two axial lone pairs of electrons. The dynamic behavior for related seven-coordinate geometries is well established in the cases of XeF_6 and IF_7 . In contrast to IF_7 and XeF_5^- , the gas-phase structure of XeF_6 (AX_6E) is based upon a distorted octahedral geometry⁴² in which the valence electron lone pair distorts the octahedral geometry to C_{3v} by occupying triangular faces of the octahedron, passing among adjacent faces via a transition state having intermediate C_i and C_{2v} geometries, with intramolecular exchange dynamics that are distinct from those of IF_7 . The dynamic behavior of IF_7 (AX_7) is also well documented; on the basis of gas-phase electron diffraction measurements it is purported to have a puckered arrangement for the five equatorial fluorines³⁴ in the gas phase and it has been shown by ^{19}F NMR spectroscopy that axial and equatorial fluorine environments of IF_7 undergo rapid intramolecular exchange in solution.⁴³ The single fluorine environment observed in the NMR spectra of XeF_5^- could also be accounted for by assuming that the anion is fluxional. The VSEPR rules postulate that the valence shell lone pairs exert larger repulsive forces on adjacent electron pairs than do bonding pairs, so that, unlike IF_7 , the transition state for exchange of axial lone pair positions with equatorial fluorine positions in XeF_5^- would presumably give rise to prohibitively large repulsive energies when a lone pair or lone pairs occupy an equatorial position, suggesting that XeF_5^- is likely to be rigid in solution.

Vibrational Spectra and Normal Coordinate Analysis of XeF_5^- . The infrared and Raman spectra of CsXeF_5 , RbXeF_5 , KXeF_5 , NaXeF_5 , and $\text{N}(\text{CH}_3)_4^+\text{XeF}_5^-$ and the Raman spectra of NOXeF_5 have been recorded. The observed frequencies and their assignments are summarized in Table IV. Figure 6 shows, as typical examples, the vibrational spectra of CsXeF_5 and $\text{N}(\text{CH}_3)_4^+\text{XeF}_5^-$.

As shown above by the NMR data and the crystal structure determination, the XeF_5^- anion is pentagonal planar and, therefore, belongs to point group D_{5h} . After the removal of translational and rotational degrees of freedom, the irreducible representation of the molecule is

$$\Gamma_{\text{vib}} = 1\text{A}_1'(\text{R}) + 1\text{A}_2''(\text{IR}) + 2\text{E}_1'(\text{IR}) + 2\text{E}_2'(\text{R}) + \text{E}_2''(\text{ia})$$

Since XeF_5^- is the first known example of an AX_5 species of symmetry D_{5h} , it is not surprising that a normal coordinate analysis

(41) Gillespie, R. J. *Molecular Geometry*; Van Nostrand Reinhold Co.: London, 1972.

(42) (a) Bartell, L. S.; Gavin, R. M.; Thompson, H. B. *J. Chem. Phys.* 1965, 43, 2547. (b) Bartell, L. S.; Gavin, R. M. *J. Chem. Phys.* 1968, 48, 2466.

(43) Gillespie, R. J.; Quail, J. W. *Can. J. Chem.* 1964, 42, 2671.

Table V. Symmetry Coordinates and Approximate Mode Descriptions for a Pentagonal Planar XY_5 Molecule

$S_1 = \frac{1}{\sqrt{5}} (\Delta r_1 + \Delta r_2 + \Delta r_3 + \Delta r_4 + \Delta r_5)$		symmetric stretch
$S_2 = \frac{1}{\sqrt{10}} (\Delta \gamma_{16} - \Delta \gamma_{17})$		symmetric out of plane (umbrella) deformation
$S_{3a} = \sqrt{\frac{2}{5}} [\Delta r_1 + \cos \alpha (\Delta r_2 + \Delta r_3) + \cos 2\alpha (\Delta r_3 + \Delta r_4)]$		asymmetric stretch
$S_{3b} = \sqrt{\frac{2}{5}} (\sin \alpha (\Delta r_2 - \Delta r_3) + \sin 2\alpha (\Delta r_3 - \Delta r_4))$		asymmetric stretch
$S_{4a} = \sqrt{\frac{2}{5}} (\Delta \alpha_{34} + \cos \alpha (\Delta \alpha_{45} + \Delta \alpha_{23}) + \cos 2\alpha (\Delta \alpha_{25} + \Delta \alpha_{12}))$		asymmetric in plane deformation
$S_{4b} = \sqrt{\frac{2}{5}} (\sin \alpha (\Delta \alpha_{45} - \Delta \alpha_{23}) + \sin 2\alpha (\Delta \alpha_{25} - \Delta \alpha_{12}))$		asymmetric in plane deformation
$S_{5a} = \sqrt{\frac{2}{5}} [\Delta r_1 + \cos 2\alpha (\Delta r_2 + \Delta r_3) + \cos \alpha (\Delta r_3 + \Delta r_4)]$		asymmetric stretch
$S_{5b} = \sqrt{\frac{2}{5}} (\sin 2\alpha (\Delta r_2 + \Delta r_3) + \sin \alpha (\Delta r_3 + \Delta r_4))$		asymmetric stretch
$S_{6a} = \sqrt{\frac{2}{5}} (\Delta \alpha_{24} + \cos 2\alpha (\Delta \alpha_{45} + \Delta \alpha_{23}) + \cos \alpha (\Delta \alpha_{25} + \Delta \alpha_{12}))$		in plane (scissor) deformation
$S_{6b} = \sqrt{\frac{2}{5}} (\sin 2\alpha (\Delta \alpha_{45} - \Delta \alpha_{23}) - \sin \alpha (\Delta \alpha_{25} - \Delta \alpha_{12}))$		in plane (scissor) deformation
$S_{7a} = \frac{1}{\sqrt{5}} (\Delta \gamma_{16} - \Delta \gamma_{17}) + \cos 2\alpha (\Delta \gamma_{26} - \Delta \gamma_{27} + \Delta \gamma_{56} - \Delta \gamma_{57}) + \cos \alpha (\Delta \gamma_{36} - \Delta \gamma_{37} + \Delta \gamma_{46} - \Delta \gamma_{47})$		asymmetric out of plane deformation
$S_{7b} = \frac{1}{\sqrt{5}} (\sin 2\alpha (\Delta \gamma_{26} - \Delta \gamma_{27} - \Delta \gamma_{56} + \Delta \gamma_{57}) - \sin \alpha (\Delta \gamma_{36} - \Delta \gamma_{37} - \Delta \gamma_{46} + \Delta \gamma_{47}))$		asymmetric out of plane deformation

Table VI G Matrix^a for Pentagonal Planar XeF_5^- of Symmetry D_{5h}

A_1'	$G_{11} = \mu_y = 5.2637 \times 10^{-2}$
A_2''	$G_{22} = (2/r^2)(\mu_y + 5\mu_x) = 4.4802 \times 10^{-2}$
E_1'	$G_{33} = \mu_y + 5\mu_x/2 = 7.1677 \times 10^{-2}$
	$G_{34} = 5(5^{1/2})\mu_x/(4r \sin \alpha) = 1.1123 \times 10^{-2}$
	$G_{44} = (1/r^2)(5\mu_y \sin^2 2\alpha + \mu_x) = 2.4333 \times 10^{-2}$
E_2'	$G_{55} = \mu_y = 5.2637 \times 10^{-2}$
	$G_{56} = 0$
	$G_{66} = (1/r^2)(4\mu_y \sin^2 \alpha) = 4.7026 \times 10^{-2}$
E_2''	$G_{77} = 2\mu_y/r^2 = 2.5995 \times 10^{-2}$

^aThe following geometry was used for the calculation of the G matrix: $r = 2.0124 \text{ \AA}$ and $\alpha = 72^\circ$.

had not previously been carried out for such a species. Force constants were calculated by the Wilson FG matrix method.⁴⁴ Figure 7 shows our choice of internal coordinates to describe the vibrations of such a molecule. Two imaginary ligands, E_6 and E_7 , have been placed in the axial positions to define the angles γ , required for the definition of the out-of-plane deformation modes. The symmetry coordinates and approximate mode descriptions are given in Table V and are derived from those previously reported for the IF_7 molecule after correction for two apparent typographical errors.⁴⁵ The analytical G and F matrices, together with the computed numerical values, are given in Tables VI and VII, respectively. The correctness of our G matrix was verified by an independent calculation of the numerical G matrix by using a computational method that gave identical values.

Vibrational Assignments. In agreement with the above predictions for XeF_5^- of symmetry D_{5h} , three mutually exclusive Raman and two infrared bands were observed in the 200–700- cm^{-1} region expected for the fundamental vibrations. The $\text{N}(\text{CH}_3)_4^+$ salt, containing the largest cation and, hence, the best isolated XeF_5^- anion, shows three narrow Raman lines at 502, 423, and 377 cm^{-1} . On the basis of their relative intensities and frequencies, which are similar to those of the three closely related Raman-active modes of octahedral molecules, the 502-, 423-, and 377- cm^{-1} bands are assigned to the symmetric stretch, $\nu_1(A_1')$, the antisymmetric stretch, $\nu_3(E_2')$, and the symmetric in-plane deformation, $\nu_6(E_2')$, respectively. The rigorous adherence of the observed Raman spectrum to the vibrational selection rules for symmetry D_{5h} and the failure to observe further splittings of the vibrational bands serve to underscore that the vibrational modes of the XeF_5^- anion

Table VII. F Matrix and Force Field for Pentagonal Planar XeF_5^- of Symmetry D_{5h}

assignment	freq, cm^{-1}	symmetry force constants ^a
A_1' ν_1	502	$F_{11} = f_r + 2f_{rr} + 2f_{rr}' = 2.820$
A_2'' ν_2	274	$F_{22} = r^2(f_\gamma + 2f_{\gamma\gamma} \cos \alpha + 2f_{\gamma\gamma}' \cos 2\alpha) = 0.996$
E_1' ν_3	465	$F_{33} = f_r + 2f_{rr} \cos \alpha + 2f_{rr}' \cos 2\alpha = 1.830$
		$F_{34} = r(f_{ra} + 2f_{ra}' \cos \alpha + 2f_{ra}'' \cos 2\alpha) = -0.342$
		$F_{44} = r^2(f_a + 2f_{aa} \cos \alpha + 2f_{aa}' \cos 2\alpha) = 2.212$
E_2' ν_4	290	$F_{55} = f_r + 2f_{rr} \cos 2\alpha + 2f_{rr}' \cos \alpha = 2.003$
		$F_{56} = r(f_{ra} + 2f_{ra}' \cos 2\alpha + 2f_{ra}'' \cos \alpha) = 0$
E_2' ν_5	423	$F_{55} = f_r + 2f_{rr} \cos 2\alpha + 2f_{rr}' \cos \alpha = 2.003$
		$F_{56} = r(f_{ra} + 2f_{ra}' \cos 2\alpha + 2f_{ra}'' \cos \alpha) = 1.797$
E_2'' ν_7	79 ^b	$F_{77} = r^2(f_\gamma + 2f_{\gamma\gamma} \cos 2\alpha + 2f_{\gamma\gamma}' \cos \alpha) = 0.143$

^aStretching constants in $\text{mdyn}/\text{\AA}$, deformation constants in $\text{mdyn}/\text{\AA}/\text{rad}^2$, and stretch-bend interaction constants in mdyn/rad . ^bValue taken from the ab initio calculation.

in its $\text{N}(\text{CH}_3)_4^+$ salt are only very weakly coupled.⁴⁶ It also justifies the use of the assumed free anion symmetry in the subsequent vibrational analysis and force field calculations.

In the salts with smaller cations, stronger coupling of the XeF_5^- motions or slight distortions of the anions can occur, resulting in a splitting of the two E_2' modes into their doubly degenerate components. As expected, the anion-cation interaction is strongest for the NO^+ salt, causing some of the infrared-active modes, such as $\nu_3(E_1')$ and $\nu_4(E_1')$, also to become weakly active in the Raman spectrum.

In the infrared spectra two strong anion bands were observed above 250 cm^{-1} . The first one was a very intense broad band extending from 400 to 550 cm^{-1} , which must be due to the antisymmetric stretching mode $\nu_3(E_1')$. The second one is an intense band at 274 cm^{-1} , which, on the basis of its frequency and relative intensity, must be the symmetric out-of-plane (umbrella) deformation, $\nu_2(A_2'')$.

The third predicted infrared-active mode is the antisymmetric in-plane deformation, $\nu_4(E_1')$. Assuming the F_{66} and F_{44} symmetry force constants to be identical (both modes involve f_{ra} and different combinations of f_{aa} and f_{aa}' , with the latter being small due to the large mass of the xenon central atom), a frequency of 274 cm^{-1} was calculated for $\nu_4(E_1')$. Therefore, $\nu_4(E_1')$, which should be of medium infrared intensity, might either be hidden underneath the intense $\nu_2(A_2'')$ band at 274 cm^{-1} or occur just below the 250- cm^{-1} cutoff frequency of the AgBr windows used for our study. A frequency range 240–290 cm^{-1} for $\nu_4(E_1')$ is also supported by the Raman spectrum of $\text{NO}^+\text{XeF}_5^-$ (see Table IV). In this compound, where the anion-cation interaction is the strongest and the infrared-active modes become also weakly Raman active, two weak Raman bands were observed at 244 and 282 cm^{-1} , respectively. Furthermore, the infrared spectra of RbXeF_5 and CsXeF_5 exhibit a 288- cm^{-1} shoulder on the strong 275- cm^{-1} band, and the Raman spectra of all the alkali-metal XeF_5^- salts show an extremely weak band at about 290 cm^{-1} . Consequently, a frequency of 290 cm^{-1} was chosen by us for $\nu_4(E_1')$ and used for the force field computations. Our choice of 290 cm^{-1} for ν_4 is also supported by ab initio calculations for XeF_5^- (see below) and IF_7 .⁴⁷ Assuming the frequency differences between calculated and observed frequencies to be the same for the two in-plane deformation modes in XeF_5^- , a value of 291 cm^{-1} is predicted for ν_4 . Similarly, the

(46) A factor-group analysis of the vibrational modes of the unit cell was carried out by use of the correlation chart method (Carter, R. L. *J. Chem. Educ.* 1971, 48, 297 and references therein). The free anion symmetry (D_{5h}) was correlated to the site symmetry of the anion (C_2), which, in turn, was correlated to the crystal symmetry (D_{2h}). Assuming complete vibrational coupling occurs in the unit cell of $\text{N}(\text{CH}_3)_4^+\text{XeF}_5^-$, all the vibrational modes of the XeF_5^- anion are found to be Raman- and infrared-active under the crystal symmetry. Moreover, ν_3 , ν_4 , ν_5 , ν_6 , and ν_7 will be split into four and three components in their Raman (A_g , B_{1g} , B_{2g} , B_{3g}) and infrared (B_{1u} , B_{2u} , B_{3u}) spectra, respectively; ν_1 will be split into two components in both the Raman (A_g , B_{1g}) and infrared (B_{1u} , B_{2u}) spectra and ν_2 will not be split in the infrared (B_{3u}) but will be split into two components in the Raman (B_{1g} , B_{2g}) spectrum.

(47) Bartell, L. S.; Rothman, M. J.; Gavezutti, A. *J. Chem. Phys.* 1982, 76, 4136 and references cited therein.

(44) Wilson, E. B. *J. Chem. Phys.* 1941, 9, 76.

(45) Khanna, R. K. *J. Mol. Spectrosc.* 1962, 8, 134.

Table VIII. Internal Force Constants (mdyn/Å) and Bond Length (Å) of XeF₃⁻ Compared with Those of XeF₂, XeF₄, and IF₄⁻

force const	XeF ₂ ^a	XeF ₄ ^b	IF ₄ ^{-b}	XeF ₃ ^{-c}
f_t	2.83	3.055	2.221	2.096
f_{π}	0.14	0.120	0.183	0.143
f_{π}'		0.007	0.466	0.219
$f_a (-f_{aa'})$	0.20	0.193	0.182	0.458
$f (-f')$		0.299	0.257	0.072
$f_{aa} - f_{aa}'$				0.045
$f_a - f_{aa}$				0.413
$f - f'$				0.093
$f - f$				-0.021
r	1.98	1.953		2.012

^aData from ref 53. ^bData from ref 50. The f values in ref 49 have not been properly normalized and must be divided by two to correspond to the values from this work. ^cThis work.

transfer of the computed frequency difference of 102 cm⁻¹ for the two in-plane deformation modes from IF₄⁻ to XeF₃⁻ results in a ν_4 value of 275 cm⁻¹ for XeF₃⁻.

The only missing fundamental vibration is the ring puckering mode, ν_7 (E₂''), which ideally is inactive in both the infrared and Raman spectra. Since no experimental frequency is available for this mode, the frequency of 79 cm⁻¹ obtained by the ab initio calculation (see below) was used.

In addition to the fundamental vibrations, numerous Raman bands were observed in the low-frequency region, which are attributed to lattice vibrations. The infrared spectra exhibit some weak bands above 600 cm⁻¹, which can be readily assigned to different overtones or combination bands of XeF₃⁻ (see Table IV).

In NO⁺XeF₃⁻ and N(CH₃)₄⁺XeF₃⁻, cation bands were also observed (see Table IV) with frequency values that are in excellent agreement with previous literature data.^{4,5,7,48}

Force Constants. The symmetry force constants of XeF₃⁻ are shown in Table VII. Except for the E₁' and E₂' blocks, all of the symmetry force constants are one-dimensional and well determined. In the two-dimensional E₂' block, G₃₆ equals zero (see Table VI), resulting in F₅₆ also becoming zero. Therefore, the only remaining underdetermined problem is the two-dimensional E₁' block. The range of possible solutions for this block was computed by using the extremal conditions reported by Sawodny.⁴⁹ It has previously been pointed out⁴⁹⁻⁵² that in weakly coupled (heavy central atom) systems the values of the general valence force field tend to fall within the range given by F₃₄ = 0 as the lower and F₃₄ = 1/2[F₃₄(max) - F₃₄(min)] as the upper limit with F₄₄ = min being an excellent choice. The latter choice results in an F₃₃ value of 1.830 mdyn/Å with an error limit of about 0.14 mdyn/Å and, therefore, F₃₃ can be considered to be reasonably well determined.

The most important internal force constants of XeF₃⁻, together with the known bond length, are given in Table VIII and are compared with those of the closely related XeF₂⁵³ and XeF₄⁵⁰ molecules and the IF₄⁻ anion.⁵⁰ As can be seen from Table VIII, the force constants well reflect our expectations. Compared with XeF₂ and XeF₄, the increased ⁴⁴Xe-F⁺ polarity of the Xe-F bond in XeF₃⁻, combined with the crowding effect in the equatorial plane, should decrease the Xe-F stretching (f_t), increase the in-plane deformation (f_a), and decrease the out-of-plane deformation (f_{π}) force constants. Furthermore, ($f_{aa} - f_{aa}'$) and ($f_{\pi\pi} - f_{\pi\pi}'$) should exhibit positive signs as expected for adjacent angles interacting more strongly than nonadjacent angles. The excellent agreement between these expectations and the experimental values from Table VIII lends strong support to the above assignments for XeF₃⁻.

(48) Christe, K. O.; Wilson, W. W.; Bougon, R. A. *Inorg. Chem.* 1986, 25, 2163.

(49) Sawodny, W. *J. Mol. Spectrosc.* 1969, 30, 56.

(50) Christe, K. O.; Naumann, D. *Inorg. Chem.* 1973, 12, 59.

(51) Pfeiffer, M. *J. Mol. Spectrosc.* 1969, 21, 181.

(52) Thakur, S. N.; Rai, S. N. *J. Mol. Struct.* 1970, 5, 320.

(53) Siebert, H. *Anwendungen der Schwingungsspektroskopie in der Anorganischen Chemie; Anorganische und Allgemeine Chemie in Einzeldarstellung*, VII; Springer Verlag: Berlin, Germany, 1966.

Table IX. Calculated and Experimental Vibrational Frequencies (cm⁻¹) of XeF₄

assignment	calcd freq	obsd freq ^a	approx mode descriptn
A _{1g} ν_1	532	543	ν_{sym} (in phase)
A _{2u} ν_2	271	291	δ_{sym} (out of plane)
B _{1g} ν_3	498	502	ν_{sym} (out of phase)
B _{2g} ν_4	182	235	δ_{sym} (in plane)
B _{2u} ν_5	156	inactive	δ_{asym} (out of plane)
E _u ν_6	591	586	ν_{asym}
E _u ν_7	143	123	δ_{asym} (in plane)

^aData from ref 55.

Table X. Calculated and Experimental Vibrational Frequencies (cm⁻¹) for XeF₃⁻

assignment	calcd freq			obsd freq	approx mode descriptn
	a	b	c		
A ₁ ' ν_1	467	537	551	502	ν_{sym} (in plane)
A ₂ ' ν_2	270	274	275	274	δ_{sym} (out of plane)
E ₁ ' ν_3	502	574	585	400-550	ν_{asym}
E ₁ ' ν_4	248	255	254	290	δ_{asym} (in plane)
E ₂ ' ν_5	413	477	489	423	ν_{asym}
E ₂ ' ν_6	335	356	361	377	δ_{sym} (in plane)
E ₂ ' ν_7	79	21	28i		δ_{asym} (out of plane)

^aWith the calculated Xe-F bond length of 2.077 Å. ^bWith an assumed Xe-F bond length of 2.022 Å. ^cWith the observed Xe-F bond length of 2.012 Å.

The data in Table VIII demonstrate that the stretching force constants f_t are mainly influenced by the polarity of the Xe-F bonds, with increasing polarity decreasing the force constant. On the other hand, steric crowding has a strong impact on the deformation constants. If this crowding is anisotropic, as in the case of XeF₃⁻ where the crowding is concentrated in the equatorial plane, the deformation constants in the congested plane increase while the deformation constants out of the congested plane decrease significantly. The low value of the out-of-plane deformation constant f_{π} , in combination with a comparable $f_{\pi\pi}$ value, implies a low energy barrier toward puckering of the equatorial plane. When the f_{π} value approaches zero or becomes negative, spontaneous puckering should occur.

Computational Results. For a better understanding of the molecular structure of XeF₃⁻, local density functional calculations were carried out for this ion and for XeF₄. The quality of these calculations for relatively large and heavy molecules was first tested for the well-characterized^{54,55} and closely related XeF₄ molecule. The well-known square-planar (D_{4h}) symmetry and a Xe-F bond length of 1.998 Å (0.045 Å longer than that observed for the solid⁵⁴) were obtained. The calculated vibrational frequencies are in excellent agreement with the experimental values⁵⁵ (Table IX), except for the in-plane deformation modes, where the agreement is only fair.

For XeF₃⁻, the computations confirmed that the pentagonal planar D_{3h} structure is indeed a minimum. Again, the computed bond length (2.077 Å) is slightly longer (0.065 Å) than the observed one (2.012 Å). A comparison between the observed and calculated spectra is given in Table X. As for XeF₄, the agreement between computed and observed frequencies for XeF₃⁻ is quite good, with the largest discrepancies again being found for the in-plane deformation modes. These results confirm the assignments made above for XeF₃⁻.

The influence of the bond length on the vibrational spectrum of XeF₃⁻ was also examined by computing the spectra for two shorter Xe-F bond distances, one at the experimental bond length and one 0.01 Å longer (Table X). As expected, the stretching frequencies are the most sensitive to changes in the bond length except for the equatorial ring puckering mode, ν_7 , which is also

(54) Burns, J. H.; Agron, P. A.; Levy, H. A. *Science* 1963, 139, 1208. Templeton, D. H.; Zalkin, A.; Forrester, J. D.; Williamson, S. M. *J. Am. Chem. Soc.* 1963, 85, 242. Ibers, J. A.; Hamilton, W. C. *Science* 1963, 139, 106.

(55) Claassen, H. H.; Chernick, C. L.; Malm, J. G. *J. Am. Chem. Soc.* 1963, 85, 1927.

Table XI. Valence Molecular Orbitals for XeF_5^-

symmetry	orbital ^a	energy, eV
A_2'	p_y anti on F	3.00
A_1''	p_z anti 0.67 Xe, 0.40 F	3.15
E_1'	p_y on F	3.71
A_1'	0.43 p_z on F, 0.57 s on Xe, anti	4.00
E_2''	p_z on F	4.06
E_1''	p_z on F some Xe d	4.69
E_2'	$p_{x,y}$ on F	4.78
E_2'	$p_{x,y}$ on F	5.72
A_2''	0.77 p_z Xe, 0.21 p_z F	7.38
E_1'	0.56 p_x, p_y Xe, 0.40 p_x on F	9.01
A_1'	0.89 Xe s	16.02

^a $x = \text{Xe-F}$ bond axis, $y =$ orthogonal to Xe-F axis in plane, $z =$ orthogonal to Xe-F axis out of plane.

very sensitive to shortening of the bond length. At the experimental distance, the degenerate deformation frequency becomes imaginary, showing that the molecule would assume a nonplanar structure. As discussed above, increasing congestion in the equatorial ring will result in spontaneous puckering and an imaginary frequency for ν_7 . The calculations at the experimental geometry are far enough from the theoretical minimum that the calculated frequencies should be employed only to show the expected trends, as they do not refer to the minimum energy structure. The data in Table X also indicate that the frequency order of the Xe-F stretching modes is essentially independent of the Xe-F bond length. It should be noted that all the calculated frequencies are harmonic values and were not scaled to include anharmonicity effects, which are usually on the order of 5%.

The Mulliken charges for XeF_5^- are +1.48e for the Xe atom and -0.50e for the F atoms. This differs from the nominal assignments of -1.0e for each F and +4.0e for the Xe. The molecular orbitals (Table XI) provide some insight into the bonding in this molecule. If we consider only the valence p orbitals on F since the 2s orbitals are quite low in energy, the remaining orbitals can be qualitatively summed up as follows: There are 10 electrons in the 2p_y lone pairs on F orthogonal to the Xe-F bond. There are roughly 10 electrons in the 2p_x orbitals on F, which are orthogonal to the molecular plane. The totally symmetric group of these orbitals interacts with the out-of-plane 5p orbital on Xe in a symmetric and antisymmetric way. The 2p_x orbitals on fluorine along the Xe-F bond have about 10e in them. These mix with the 5p_x and 5p_y orbitals on Xe. Although the Xe 5s orbital does mix to some extent with the 2p orbitals on F, it is predominantly a lone pair. The basic description is thus a Xe with a 5s²5p_x² occupancy surrounded by five F⁻ atoms. Delocalization of fluorine electron density into the Xe 5p_x orbitals with only a small participation of the d orbitals on Xe then reduces the charges on the F atoms. The HOMO is the antibonding combination of the in-plane lone pairs on the F atom orthogonal to the Xe-F axis. The NHOMO is almost degenerate in energy with the HOMO and is the antibonding out-of-plane combination of the F 2p_x and the Xe 5p_x orbitals (Figure 8).

Both the orbitals and the bonding in XeF_5^- are quite similar to those of XeF_4 , which were calculated for comparison. In XeF_4 , the Mulliken charges on Xe and F are +1.65e and -0.41e, respectively. The Xe 5s orbital participates in two orbitals, with most of its density in the orbital at 22.02 eV just as in XeF_5^- . The 5p_x orbital of Xe and the out-of-plane 2p_x orbitals on the fluorines interact to give bonding and antibonding molecular orbitals. The orbital configuration at Xe is thus dominated by the 5s²5p_x² configuration just as in the anion. The HOMO in XeF_4 is at 9.15 eV and is the 5p_y antibonding orbital as found in XeF_5^- . Its significantly higher value, compared with that of XeF_5^- , is in agreement with our expectations for an anion and its parent molecule.

It is important to note that the calculations provide a molecular orbital description of the bonding in XeF_5^- and XeF_4 . The orbitals reported above are the canonical orbitals with molecular symmetry. Because of the molecular symmetry, the 5s and 5p_x orbitals cannot mix and thus give separate s² and p² occupancies. In contrast,

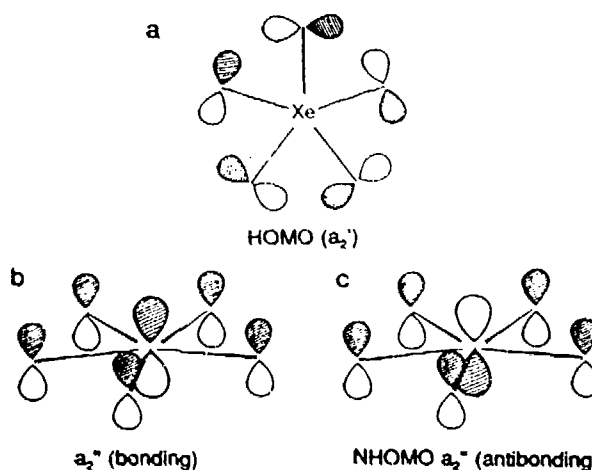


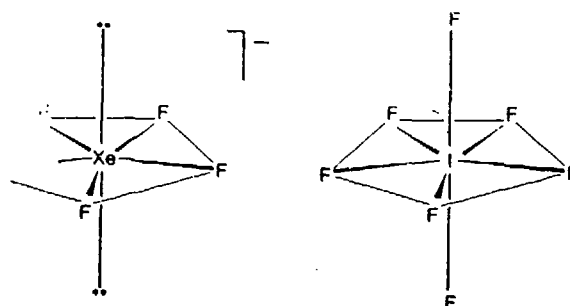
Figure 8. Selected molecular orbitals for XeF_5^- . (a) HOMO, antibonding combination of in-plane p_y 's on F; (b) bonding out-of-plane orbital combination between Xe 5p_x and p_x 's on F; (c) antibonding out-of-plane orbital combination between Xe 5p_x and p_x 's on F.

in the VSEPR model used elsewhere in this work, the valence electron lone pairs may be described as two doubly occupied sp hybrids above and below the plane, but this is not required by the VSEPR model. The two models are equivalent, as the VSEPR model is derived from a localized orbital approach, whereas the calculations are based on a molecular orbital approach. The sum and difference of the 5s² and 5p_x² orbitals will lead to the two sp hybrid lone pairs. However, the total electron density, which is the invariant quantity, is independent of the choice of models used to describe it. (In a formal sense, the wave function is invariant to a unitary transformation.)

Conclusions

Xenon tetrafluoride indeed forms stable adducts with strong Lewis bases, such as tetramethylammonium fluoride and the heavier alkali-metal fluorides. However, contrary to previous reports,¹³⁻¹⁵ these salts do not contain the XeF_6^{2-} dianion, but the XeF_5^- anion.

The XeF_5^- anion has a highly unusual pentagonal planar structure for which no other examples were previously known. It can be derived from that of a pentagonal bipyramid, such as IF_7 ,³⁸ in which the two axial fluorine ligands have been replaced by two sterically active free valence electron pairs. Compared with IF_7 ,



which is a fluxional molecule undergoing with relative ease a dynamic ring-puckering pseudorotation,^{38,47} the equatorial XeF_5 plane of XeF_5^- appears to be considerably more rigid. The increased rigidity of the XF_5 plane in XeF_5^- is attributed to the stabilizing effect of the two free valence electron pairs on xenon. These free pairs are more diffuse and hence more repulsive than the axial I-F bond pairs in IF_7 , thereby offering more resistance toward the puckering of the equatorial XeF_5 plane.

Acknowledgment. We thank C. J. Schack, W. W. Wilson, R. D. Wilson, and S. S. Tsai for their help; F. Adar, Instruments S.A.; Edison, NJ, for recording the single-crystal Raman spectrum of $\text{N}(\text{CH}_3)_4^+\text{XeF}_5^-$; the U.S. Air Force Astronautics Laboratory, Edwards AFB (K.O.C. and G.J.S.); the U.S. Army Research Office (K.O.C.) and the Natural Sciences and Engineering Re-

search Council of Canada (G.J.S.) for financial support; Ministry of Foreign Affairs, France, for a Lavoisier Fellowship (H.P.M.); and C.N.R.S. Laboratoire des Agrégats Moléculaires et Matériaux Inorganiques, Montpellier, France, for granting a leave of absence to H.P.M.

Supplementary Material Available: Tables of anisotropic thermal parameters (Table 1) and hydrogen atomic coordinates (Table 2) (2 pages); tabulation of calculated and observed structure factor amplitudes (Table 3) (13 pages). Ordering information is given on any current masthead page.

PART VIII

THE IF_6O^- , $\text{TeF}_6\text{O}^{2-}$, TeF_7^- , IF_8^- and TeF_8^{2-} ANIONS; NOVEL
EXAMPLES OF AX_7E , AX_7 AND AX_8 VSEPR GEOMETRIES

Chemical Communications

Number 13

1991

High-coordination Number Fluoro- and Oxofluoro-anions; IF_6O^- , $\text{TeF}_6\text{O}^{2-}$, TeF_7^- , IF_8^- and TeF_8^{2-}

Karl O. Christe,^a Jeremy C. P. Sanders,^b Gary J. Schrobilgen^{a,b} and William W. Wilson^a

^a Rocketdyne, a Division of Rockwell International Corporation, Canoga Park, California 91303, USA

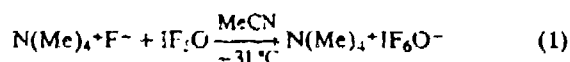
^b The Department of Chemistry, McMaster University, Hamilton, Ontario L8S 4M1, Canada

The novel hypervalent, highly coordinated, high-oxidation state anions IF_6O^- , $\text{TeF}_6\text{O}^{2-}$, TeF_7^- , IF_8^- and TeF_8^{2-} have been synthesized in anhydrous MeCN using anhydrous $\text{N}(\text{Me})_4^+\text{F}^-$ as the fluoride ion source; the anions have been characterized by NMR and vibrational spectroscopy and represent novel examples of seven and eight-coordinate species having symmetries C_{5v} (IF_6O^- , $\text{TeF}_6\text{O}^{2-}$), D_{5h} (TeF_7^-) and D_{4d} (IF_8^- , TeF_8^{2-}).

The study of fluoro-anions having coordination numbers higher than six and, in particular, those involving free valence electron pairs, have recently received considerable attention.¹⁻⁶ To a large extent, these studies have been greatly facilitated by the development of a convenient preparative scale synthesis of anhydrous $\text{N}(\text{Me})_4^+\text{F}^-$ and the realization that this salt is an excellent reagent for the preparation of novel, high-oxidation state complex fluoro- or oxofluoro-anions. Furthermore, the high solubilities of these $\text{N}(\text{Me})_4^+$ salts in solvents such as MeCN or CHF_3 permit the gathering of valuable structure information through NMR and vibrational studies and the growth of single crystals suitable for X-ray structure determinations.

Our recent success with the preparation of the XeF_5^- anion,⁴ the first known example of a pentagonal planar AX_5E_2 (where E stands for a free valence electron pair) species, prompted us to study some closely related iodine and tellurium compounds. In addition, there are relatively few examples of main-group species which allow the applicability of the valence shell electron pair repulsion (VSEPR) rules to coordination numbers exceeding six to be tested.⁸ In this note, we report on the syntheses and structures of the novel IF_6O^- anion and on the $\text{N}(\text{Me})_4^+$ salts of TeF_7^- , TeF_8^{2-} and IF_8^- .

The salt, $\text{N}(\text{Me})_4^+\text{IF}_6\text{O}^-$, was prepared according to eqn. (1) by the reaction of anhydrous $\text{N}(\text{Me})_4^+\text{F}^-$ with a threefold excess of IF_5O in dry MeCN at -31°C for 30 min.



The solvent and unreacted IF_5O were pumped off at -31°C leaving behind $\text{N}(\text{Me})_4^+\text{IF}_6\text{O}^-$ as a colourless crystalline solid in quantitative yield. According to differential scanning calorimetry (DSC) and pyrolysis data, the compound starts to decompose at about 137°C with formation of CF_4 , COF_2 and IF_4O^- as the major products.

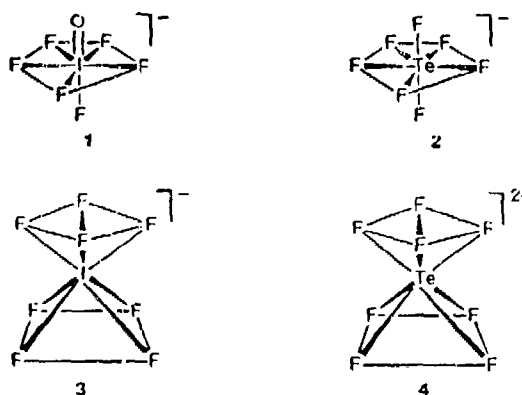
The ^{19}F NMR spectrum of $\text{N}(\text{Me})_4^+\text{IF}_6\text{O}^-$ in MeCN solution recorded at -40°C (Fig. 1) is consistent with the structure predicted by the VSEPR rules, consisting of a pentagonal bipyramidal structure of C_{5v} symmetry (structure 1) in which the oxygen atom occupies an axial position. The spectrum consists of a doublet at δ 166.0, assigned to the

equatorial fluorines, and a 1:5:10:10:5:1 sextet at δ 111.1, assigned to the axial fluorine trans to oxygen. Both resonances are broadened by partially quadrupole-collapsed spin coupling to ^{127}I ($I = 5/2$). The fluorine-fluorine scalar coupling, $^2J(^{19}\text{F}_\text{ax}-\text{F}_\text{eq})$ 205 Hz, is very similar in magnitude to those for IF_5O (271–280 Hz)⁹ and *cis*- IO_2F_4^- (204 Hz in MeCN).¹⁰

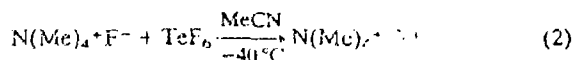
The vibrational spectra of IF_6O^- are also in excellent agreement with symmetry C_{5v} . The assignments were made by comparison with the related IF_7 molecule (see Table 1) and XeF_5^- anion.⁴

The reactions between TeF_6 and alkali metal fluorides have been reported previously, although definitive characterization of the products was never achieved.¹¹ The reactions of TeF_6 with CsF and RbF suspended in C_6F_6 resulted in products approaching the limiting compositions $\text{CsF}\cdot\text{TeF}_6$ and $2\text{RbF}\cdot\text{TeF}_6$, respectively.¹² Vibrational studies on these materials were tentatively interpreted as indicating D_{5h} and D_{4d} structures for TeF_7^- and TeF_8^{2-} , respectively. However, since both compounds decomposed in solution, a fuller characterization of their nature was precluded.

The preparation of $\text{N}(\text{Me})_4^+\text{TeF}_7^-$ was similar to that for the IF_6O^- salt except that a 5% excess of TeF_6 was allowed to



react with $N(\text{Me})_4^+ \text{F}^-$ according to equation (2). The solution and an excess of TeF_6 were pumped off at room temperature, leaving a white solid in quantitative yield:



The room temperature ^{125}Te NMR spectrum of $N(\text{Me})_4^+ \text{TeF}_7^-$ in MeCN consists of a 1:7:21:35:35:21:7:1 octet centred at δ 327.4 (Fig. 2). The octet fine structure arises from the one-bond spin-spin coupling between the central ^{125}Te and the ^{19}F ligands [$1J(^{125}\text{Te}-^{19}\text{F})$ 2876 Hz] and is in accord with a TeF_7^- anion structure in which all seven fluorines are rendered equivalent on the NMR time scale by a facile intramolecular exchange process. The ^{19}F NMR spectrum is also consistent with the TeF_7^- anion undergoing a fluxional process in solution, and consists of a single environment (δ 16.1) and natural abundance satellite spectra arising from $1J(^{125}\text{Te}-^{19}\text{F})$ 2385 and $1J(^{125}\text{Te}-^{19}\text{F})$ 2876 Hz. Under high resolution at an external field strength of 11.744 T, the central line displays the isotopic shift pattern arising from the natural abundance spinless tellurium isotopes corresponding to the fluorines of the ^{130}Te , ^{128}Te , ^{126}Te , ^{124}Te and ^{122}Te isotopomers, with each isotopomer shifted successively to higher frequency of $^{130}\text{TeF}_7^-$, by 0.004 ppm. Earlier NMR studies have shown that the isoelectronic IF_7 molecule also undergoes rapid intramolecular exchange and gives rise to a single fluorine environment in the room temperature ^{19}F NMR spectrum with partially quadrupole-collapsed fine structure arising from $1J(^{127}\text{I}-^{19}\text{F})$.¹³

The vibrational spectra of TeF_7^- have been assigned by analogy with those of the isoelectronic IF_7 molecule (Table 1) and are in agreement with a pentagonal bipyramidal structure of D_{5h} symmetry (structure 2). In general, the TeF_7^- frequencies are shifted to lower frequencies relative to those of IF_7 , in accordance with the formal negative charge of TeF_7^- .

The syntheses of $\text{Cs}^+ \text{IF}_8^-$,¹⁴ $\text{NO}^+ \text{IF}_8^-$,^{14,15} and $\text{NO}_2^+ \text{IF}_8^-$ ¹⁵ have previously been reported, and the ionic nature of these salts was established by the observation of the vibrational bands characteristic for NO^+ and NO_2^+ .^{14,15} Although partial Raman¹⁴ and IR spectra¹⁵ had been reported for IF_8^- , no conclusions could be drawn from these data about the exact structure of this interesting octacoordinated anion. To allow a

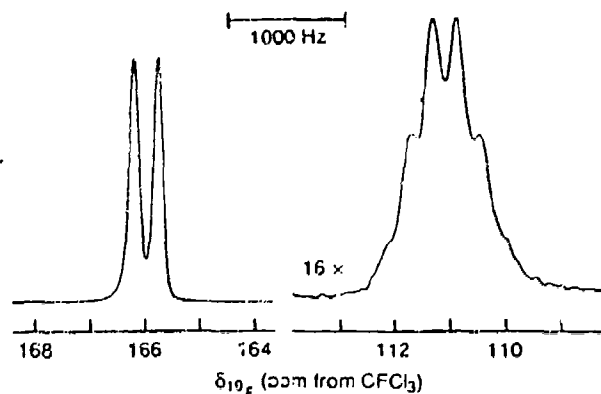


Fig. 1 The ^{19}F NMR spectrum of $N(\text{Me})_4^+ \text{IF}_6\text{O}^-$ recorded at 471.599 MHz in MeCN solvent at -40°C

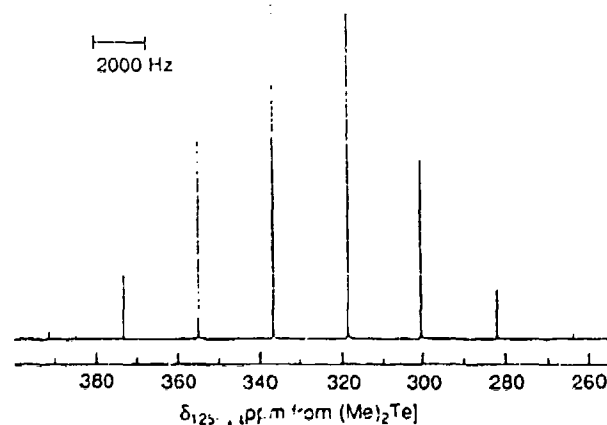


Fig. 2 The ^{125}Te NMR spectrum of $N(\text{Me})_4^+ \text{TeF}_7^-$ recorded at 157.792 MHz in MeCN solvent at 30°C

Table 1 Vibrational frequencies (cm^{-1}) and tentative assignments for IF_6O^- , IF_7 and TeF_7^-

			$\text{IF}_6\text{O}^- (C_{5v})^a$	$\text{IF}_7 (D_{5h})^b$	$\text{TeF}_7^- (D_{5h})^c$
A_1	ν_1	$\nu \text{I}=\text{O}$	873 [vs. IR; 5.3, R (p)]		
	ν_2	$\nu \text{IF ax}$	649 [s. IR; 8.8 R (p)]		
	ν_3	$\nu \text{sym IF}_5$	584 [10, R (p)]		
	ν_4	δ umbrella IF_5	359 (s. IR)		
E_1	ν_5	$\nu \text{asym IF}_5$	585 (vs. IR)		
	ν_6	δ wag $\text{I}=\text{O}$	457 (4.9, R)		
	ν_7	δ wag IF ax	405 (vs. IR)		
	ν_8	δ asym IF_5 in plane	260 (s. IR; 0.2, R)		
E_2	ν_9	$\nu \text{asym IF}_5$	530 (0.4, R)		
	ν_{10}	δ scissoring IF_5 in plane	341 (6.2, R)		
	ν_{11}	δ pucker IF_5			
A_1'	ν_1	$\nu \text{sym MF}_2 \text{ ax}$		675 [2.0, R (p)]	597 (2.6, R)
	ν_2	$\nu \text{sym MF}_4$		629 [10, R (p)]	640 (10, R)
A_2'	ν_3	$\nu \text{asym MF}_2 \text{ ax}$		746 (s. IR)	695 (vs. IR)
	ν_4	δ umbrella MF_5		363 (s. IR)	332 (s. IR)
E_1'	ν_5	$\nu \text{asym MF}_5$		672 (vs. IR)	625 (vs. IR)
	ν_6	δ scissoring $\text{MF}_2 \text{ ax}$		425 (vs. IR)	384 (vs. IR)
	ν_7	δ asym MF_5 in plane		257 (w. IR)	
E_1''	ν_8	δ wag $\text{MF}_2 \text{ ax}$		308 (0.6, R)	299 (0.6, R)
	ν_9	$\nu \text{asym MF}_5$		509 (0.9, R)	458 (1.6, R)
E_2'	ν_{10}	δ scissoring MF_5 in plane		342 (0.6, R)	326 (0.7, R)
	ν_{11}	δ pucker MF_5			

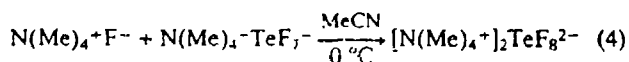
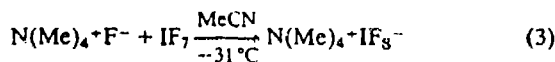
^a Spectra recorded for the $N(\text{Me})_4^+$ salts at 25°C . ^b Frequencies are taken from H. H. Eysel and K. Seppelt, *J. Chem. Phys.*, 1972, 56, 5081. A number of modes have been reassigned so that they are consistent with the corresponding assignments for XeF_6^- (ref. 4), which have been confirmed by a force constant analysis and theoretical calculations. ^c Mode not observed. ^d Inactive in both the IR and Raman spectra.

Table 2 Vibrational frequencies (cm^{-1}) and assignments for IF_8^- in $\text{N}(\text{Me})_4^+\text{IF}_8^-$ and TeF_8^{2-} in $[\text{N}(\text{Me})_4^+]_2\text{TeF}_8^{2-}$ in point group D_{4d}

Raman				IR (solid 25 °C)		Assignment in D_{4d}
IF_8^-		TeF_8^{2-}		IF_8^-	TeF_8^-	
Solid	MeCN sol'n					
25 °C	-142 °C					
660 (0-)	660 (0+)			590 vs, br	558 vs	$\nu_{12}(\text{E}_2)$ $\nu_4(\text{B}_2)$ $\nu_6(\text{E}_1)$
587 (10)	595 (10)	590 (10) p	582 (10)			$\nu_1(\text{A}_1)$
	388 (6.5)					
550 (0.3)	550 (0.5)	550 (0+) dp	490 (0.2), br			$\nu_9(\text{E}_2)$
463 (1.8)	463 (1.9)	462 (0.5) p	408 (1.0)	410 s	375 vs	$\nu_2(\text{A}_1)$ $\nu_5(\text{B}_2)$ $\nu_8(\text{E}_1)$
	419 (0.9)					
411 (0.7)	410 (1.4)	410 sh ^a	388 (1.8)			$\nu_{10}(\text{E}_2)$
	380 (0+) ^b		325 (0.3)			
				314 m	265 w	$\nu_{13}(\text{E}_1)$ $\nu_7(\text{E}_1)$

^a Shoulder on strong MeCN solvent band. ^b This band could possibly be due to the $\text{N}(\text{Me})_4^+$ cation.

better characterization of the IF_8^- anion, we have prepared the new $\text{N}(\text{Me})_4^+\text{IF}_8^-$ salt and its isoelectronic tellurium analogue, TeF_8^{2-} , by the reaction of $\text{N}(\text{Me})_4^+\text{F}^-$ with excess IF_7 and a stoichiometric amount of $\text{N}(\text{Me})_4^+\text{TeF}_7^-$, respectively. For reaction (3) the solvent and unreacted IF_7 were pumped off at -22 and 0 °C, respectively, leaving behind colourless $\text{N}(\text{Me})_4^+\text{IF}_8^-$ in quantitative yield. In the case of reaction (4), $[\text{N}(\text{Me})_4^+]_2\text{TeF}_8^{2-}$ was isolated in admixture with ca. 20-30% $\text{N}(\text{Me})_4^+\text{TeF}_7^-$. The $[\text{N}(\text{Me})_4^+]_2\text{TeF}_8^{2-}$ salt



has a strong tendency to dissociate in MeCN, thus far preventing the preparation of a sample containing only the TeF_8^{2-} anion. At room temperature, dissociation of the insoluble TeF_8^{2-} anion into TeF_7^- and F^- results in rapid solvent attack by F^- and formation of HF_2^- anion. Even in the presence of a fivefold excess of $\text{N}(\text{Me})_4^+\text{F}^-$ at -5 °C, significant amounts of TeF_7^- and F^- were observed in the ^{19}F NMR spectrum, but no resonance attributable to TeF_8^{2-} could be observed. The $\text{N}(\text{Me})_4^+\text{IF}_8^-$ salt is a crystalline solid which, according to DSC data, is stable up to ca. 110 °C where it undergoes exothermic decomposition.

The IF_8^- and TeF_8^{2-} anions possess eight fluorine ligands and no free central atom valence electron pair. Their structures could, therefore, be either a cube of symmetry O_h , which is unlikely owing to steric interactions,⁸ a dodecahedron of symmetry D_{2d} or a square antiprism of symmetry D_{4d} (structures 3 and 4).¹⁷⁻²⁰ Distinction among these three possibilities was made by vibrational spectroscopy. The dodecahedral structure is expected to give rise to two polarized stretching modes and four deformation modes (two polarized; two depolarized) exclusively in the Raman. The IR bands are mutually non-exclusive and comprise four stretching modes and five deformation modes which are all depolarized in the Raman. All Raman and IR bands observed for IF_8^- and TeF_8^{2-} are mutually exclusive, thereby eliminating D_{2d}

symmetry. For the cubic O_h structure, two stretching modes are expected (one polarized; the other depolarized) and two depolarized deformation modes in the Raman, as well as one stretching and one deformation mode in the infrared. All these modes should be mutually exclusive.¹⁸ For the square antiprismatic D_{4d} structure, one polarized and two depolarized stretching modes are expected as well as one polarized and three depolarized deformation modes in the Raman. In the IR spectrum, two stretching and three deformation modes are expected, which again should be mutually exclusive.^{17,19,20} Although the full number of fundamentals for D_{4d} was not observed (see Table 2), probably because of either low relative intensities or coincidences, the observation of a polarized Raman deformation band at 462 cm^{-1} and of at least two IR active deformation modes at 410 and 314 cm^{-1} , respectively, establish the square antiprismatic D_{4d} structure for IF_8^- . It was not possible to obtain polarization data on TeF_8^{2-} owing to the insolubility of the salt and its tendency to dissociate in MeCN. However, the vibrational spectra of TeF_8^{2-} can be assigned by their close analogy to those of IF_8^- (Table 2) and it may be concluded that TeF_8^{2-} also possesses a square antiprismatic structure.

X-Ray crystal structure determinations on these and other closely related anions are underway both in our laboratories and in an independent effort by Dr K. Seppelt and coworkers at the Freie Universität, Berlin.

Note added in proof: The $\text{TeF}_6\text{O}^{2-}$ anion has also been synthesized by the reaction of equimolar amounts of $\text{N}(\text{Me})_4^+\text{F}^-$ and $\text{N}(\text{Me})_4^+\text{TeF}_5\text{O}^-$ at -9 °C in MeCN. The vibrational assignments (ν/cm^{-1}) under C_{3v} establish that $\text{TeF}_6\text{O}^{2-}$ is isostructural with IF_6O^- : ν_1 829 (s, IR; s, R); ν_2 613 (m, IR; vs, R); ν_3 528 (m, R); ν_4 330 (s, IR); ν_5 525 (vs, IR); ν_6 388 (m, R); ν_7 365 (vs, IR); ν_8 245 (not observed, beyond spectrometer limit; w, R); ν_9 not observed; ν_{10} 322 (s, R); ν_{11} (not observed). The ^{19}F NMR spectrum of $\text{N}(\text{Me})_4^+\text{IF}_8^-$ has been obtained at 30 °C (δ 248.6) and is a partially quadrupole collapsed multiplet (saddle-shaped with a 'doublet' separation of 3807 Hz) arising from the ^{127}I - ^{19}F scalar coupling and is consistent with the small electric field gradient at the ^{127}I nucleus that is anticipated for a square antiprismatic AX_8 geometry.

The authors thanks US Air Force Astronautics Laboratory, Edwards AFB, California (K. O. C. and G. J. S.), the US Army Research Office (K. O. C.) and the Natural Sciences and Engineering Research Council of Canada (G. J. S.) for financial support; and Dr K. Seppelt for bringing his X-ray structural studies to our attention.

Received, 21st January 1991; Com. 1100298H

References

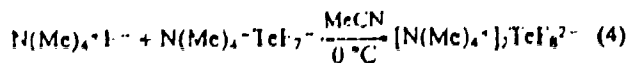
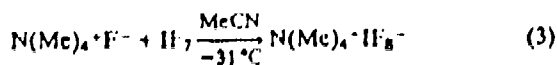
- 1 W. W. Wilson and K. O. Christe. *Inorg. Chem.*, 1989, **28**, 4172.
- 2 K. O. Christe and W. W. Wilson. *Inorg. Chem.*, 1989, **28**, 3275.
- 3 K. O. Christe, W. W. Wilson, R. V. Chirakal, J. C. P. Sanders and G. J. Schrobilgen. *Inorg. Chem.*, 1990, **29**, 3506.
- 4 K. O. Christe, E. C. Curtis, D. A. Dixon, H. P. Mercier, J. C. P. Sanders and G. J. Schrobilgen. *J. Am. Chem. Soc.*, 1991, **113**, 3351.
- 5 A. R. Mahjoub, A. Hoser, J. Fuchs and K. Seppelt. *Angew. Chem., Int. Ed. Engl.*, 1989, **28**, 1526.
- 6 A. R. Mahjoub, B. Nuber and K. Seppelt, personal communication.
- 7 K. O. Christe, W. W. Wilson, R. D. Wilson, R. Bau and J. Feng. *J. Am. Chem. Soc.*, 1990, **112**, 7619.
- 8 R. J. Gillespie and I. Hargittai. *The VSEPR Model of Molecular Geometry*, Allyn and Bacon, Boston, 1991.
- 9 R. J. Gillespie and J. W. Quail. *Proc. Chem. Soc.*, 1963, 278; M. Brownstein, R. J. Gillespie and J. P. Krasznai. *Can. J. Chem.*, 1978, **56**, 2253.
- 10 K. O. Christe, R. D. Wilson and C. J. Schack. *Inorg. Chem.*, 1981, **20**, 2104.
- 11 E. L. Muetterties, *J. Am. Chem. Soc.*, 1957, **79**, 1004.
- 12 H. Selig, S. Sarig and S. Abramowitz. *Inorg. Chem.*, 1974, **13**, 1508.
- 13 R. J. Gillespie and J. W. Quail. *Can. J. Chem.*, 1964, **42**, 2671; E. L. Muetterties and K. J. Packer. *J. Am. Chem. Soc.*, 1964, **86**, 293.
- 14 C. J. Adams. *Inorg. Nucl. Chem. Lett.*, 1974, **10**, 831.
- 15 F. Seel and M. J. Pimpl. *J. Fluorine Chem.*, 1977, **10**, 413.
- 16 K. O. Christe and William W. Wilson. *J. Fluorine Chem.*, 1990, **47**, 117.
- 17 A. Beuter, W. Kuhlmann and A. Sawodny. *J. Fluorine Chem.*, 1975, **6**, 367.
- 18 C. W. F. T. Pistorius. *Bull. Soc. Chim. Belg.*, 1959, **68**, 630.
- 19 H. L. Schläfer and H. F. Wasgestan. *Theoret. Chim. Acta*, 1963, **1**, 369.
- 20 K. O. Hartman and F. A. Miller. *Spectrochim. Acta, Part A*, 1968, **24**, 669.

Table 2 Vibrational frequencies (cm⁻¹) and assignments for IF₆⁻ in N(Me)₄⁺IF₆⁻ and TeF₆²⁻ in [N(Me)₄]₂TeF₆²⁻ in point group D_{3d}

Raman			IR (solid 25 °C)		Assignment in D _{3d}
IF ₆ ⁻		TeF ₆ ²⁻	IF ₆ ⁻	TeF ₆ ²⁻	
Solid	MeCN sol'n				
25 °C	-142 °C				
660 (0-)	660 (0+)			590 vs, br	ν ₁₂ (E _g) ν ₂ (B _{2g}) ν ₆ (E _g)
	595 (10)	590 (10) p	582 (10)		ν ₁ (A _{1g})
587 (10)	588 (6.5)				
550 (0.3)	550 (0.5)	550 (0+) dp	490 (0.2), br		ν ₉ (E _g) ν ₂ (A _{1g})
463 (1.8)	463 (1.9)	462 (0.5) p	408 (1.0)	410 s	ν ₅ (B _{2g}) ν ₈ (E _g)
	419 (0.9)	410 sh ^a	388 (1.8)	375 vs	
411 (0.7)	410 (1.4)				ν ₁₀ (E _g)
	380 (0+) ^b		325 (0.3)		ν ₁₁ (E _g) ν ₇ (E _g)
			314 m	295 w	

^a Shoulder on strong MeCN solvent band. ^b This band could possibly be due to the N(Me)₄⁺ cation

better characterization of the IF₆⁻ anion, we have prepared the new N(Me)₄⁺IF₆⁻ salt and its isoelectronic tellurium analogue, TeF₆²⁻, by the reaction of N(Me)₄⁺F⁻ with excess IF₇ and a stoichiometric amount of N(Me)₄⁺TeF₇⁻, respectively. For reaction (3) the solvent and unreacted IF₇ were pumped off at -22 and 0 °C, respectively, leaving behind colourless N(Me)₄⁺IF₆⁻ in quantitative yield. In the case of reaction (4), [N(Me)₄]₂TeF₆²⁻ was isolated in admixture with ca. 20-30% N(Me)₄⁺TeF₇⁻. The [N(Me)₄]₂TeF₆²⁻ salt



has a strong tendency to dissociate in MeCN, thus far preventing the preparation of a sample containing only the TeF₆²⁻ anion. At room temperature, dissociation of the insoluble TeF₆²⁻ anion into TeF₇⁻ and F⁻ results in rapid solvent attack by F⁻ and formation of HF₂⁻ anion. Even in the presence of a fivefold excess of N(Me)₄⁺F⁻ at -5 °C, significant amounts of TeF₇⁻ and F⁻ were observed in the ¹⁹F NMR spectrum, but no resonance attributable to TeF₆²⁻ could be observed. The N(Me)₄⁺IF₆⁻ salt is a crystalline solid which, according to DSC data, is stable up to ca. 110 °C where it undergoes exothermic decomposition.

The IF₆⁻ and TeF₆²⁻ anions possess eight fluorine ligands and no free central atom valence electron pair. Their structures could, therefore, be either a cube of symmetry O_h, which is unlikely owing to steric interactions,¹⁶ a dodecahedron of symmetry D_{2d} or a square antiprism of symmetry D_{4d} (structures 3 and 4).^{17, 18} Distinction among these three possibilities was made by vibrational spectroscopy. The dodecahedral structure is expected to give rise to two polarized stretching modes and four deformation modes (two polarized, two depolarized) exclusively in the Raman. The IR bands are mutually non-exclusive and comprise four stretching modes and five deformation modes which are all depolarized in the Raman. All Raman and IR bands observed for IF₆⁻ and TeF₆²⁻ are mutually exclusive, thereby eliminating D_{2d}

symmetry. For the cubic O_h structure, two stretching modes are expected (one polarized; the other depolarized) and two depolarized deformation modes in the Raman, as well as one stretching and one deformation mode in the infrared. All these modes should be mutually exclusive.¹⁶ For the square antiprismatic D_{4d} structure, one polarized and two depolarized stretching modes are expected as well as one polarized and three depolarized deformation modes in the Raman. In the IR spectrum, two stretching and three deformation modes are expected, which again should be mutually exclusive.^{17, 19, 20} Although the full number of fundamentals for D_{4d} was not observed (see Table 2), probably because of either low relative intensities or coincidences, the observation of a polarized Raman deformation band at 462 cm⁻¹ and of at least two IR active deformation modes at 410 and 314 cm⁻¹, respectively, establish the square antiprismatic D_{4d} structure for IF₆⁻. It was not possible to obtain polarization data on TeF₆²⁻ owing to the insolubility of the salt and its tendency to dissociate in MeCN. However, the vibrational spectra of TeF₆²⁻ can be assigned by their close analogy to those of IF₆⁻ (Table 2) and it may be concluded that TeF₆²⁻ also possesses a square antiprismatic structure.

X-Ray crystal structure determinations on these and other closely related anions are underway both in our laboratories and in an independent effort by Di K. Seppelt and coworkers at the Freie Universität, Berlin.

Note added in proof: The TeF₆O²⁻ anion has also been synthesized by the reaction of equimolar amounts of N(Me)₄⁺F⁻ and N(Me)₄⁺TeF₅O⁻ at -9 °C in MeCN. The vibrational assignments (ν/cm⁻¹) under C_{3v} establish that TeF₆O²⁻ is isostructural with IF₆O⁻: ν₁ 829 (s, IR; s, R); ν₂ 613 (m, IR; vs, R); ν₃ 528 (m, R); ν₄ 330 (s, IR); ν₅ 525 (vs, IR); ν₆ 388 (m, R); ν₇ 365 (vs, IR); ν₈ 245 (not observed, beyond spectrometer limit; w, R); ν₉ not observed; ν₁₀ 322 (s, R); ν₁₁ (not observed). The ¹⁹F NMR spectrum of N(Me)₄⁺IF₆⁻ has been obtained at 30 °C (δ 248.6) and is a partially quadrupole collapsed multiplet (saddle-shaped with a 'doublet' separation of 3807 Hz) arising from the ¹²⁷I-¹⁹F scalar coupling and is consistent with the small electric field gradient at the ¹²⁷I nucleus that is anticipated for a square antiprismatic AX₆ geometry.

The authors thank US Air Force Astronautics Laboratory, Edwards AFB, California (K. O. C. and G. J. S.), the US Army Research Office (K. O. C.) and the Natural Sciences and Engineering Research Council of Canada (G. J. S.) for financial support; and Dr K. Seppelt for bringing his X-ray structural studies to our attention.

Received, 21st January 1991; Com. 1100298H

References

- 1 W. W. Wilson and K. O. Christe. *Inorg. Chem.*, 1989, **28**, 4172.
- 2 K. O. Christe and W. W. Wilson. *Inorg. Chem.*, 1989, **28**, 3275.
- 3 K. O. Christe, W. W. Wilson, R. V. Chirakal, J. C. P. Sanders and G. J. Schrobilgen. *Inorg. Chem.*, 1990, **29**, 3506.
- 4 K. O. Christe, E. C. Curtis, D. A. Dixon, H. P. Mercier, J. C. P. Sanders and G. J. Schrobilgen. *J. Am. Chem. Soc.*, 1991, **113**, 3351.
- 5 A. R. Mahjoub, A. Hoser, J. Fuchs and K. Seppelt. *Angew. Chem., Int. Ed. Engl.*, 1989, **28**, 1526.
- 6 A. R. Mahjoub, B. Nuber and K. Seppelt. personal communication.
- 7 K. O. Christe, W. W. Wilson, R. D. Wilson, R. Bau and J. Feng. *J. Am. Chem. Soc.*, 1990, **112**, 7619.
- 8 R. J. Gillespie and I. Hargittai. *The VSEPR Model of Molecular Geometry*, Allyn and Bacon, Boston, 1991.
- 9 R. J. Gillespie and J. W. Quail. *Proc. Chem. Soc.*, 1963, 278; M. Brownstein, R. J. Gillespie and J. P. Krasznai, *Can. J. Chem.*, 1978, **56**, 2253.
- 10 K. O. Christe, R. D. Wilson and C. J. Schack. *Inorg. Chem.*, 1981, **20**, 2104.
- 11 E. L. Muetterties, *J. Am. Chem. Soc.*, 1957, **79**, 1004.
- 12 H. Selig, S. Sarig and S. Abramowitz, *Inorg. Chem.*, 1974, **13**, 1508.
- 13 R. J. Gillespie and J. W. Quail. *Can. J. Chem.*, 1964, **42**, 2671; E. L. Muetterties and K. J. Packer, *J. Am. Chem. Soc.*, 1964, **86**, 293.
- 14 C. J. Adams, *Inorg. Nucl. Chem. Lett.*, 1974, **10**, 831.
- 15 F. Seel and M. J. Pimpl. *J. Fluorine Chem.*, 1977, **10**, 413.
- 16 K. O. Christe and William W. Wilson. *J. Fluorine Chem.*, 1990, **47**, 117.
- 17 A. Beuter, W. Kuhlmann and A. Sawodny. *J. Fluorine Chem.*, 1975, **6**, 367.
- 18 C. W. F. T. Pistorius, *Bull. Soc. Chim. Belg.*, 1959, **68**, 630.
- 19 H. L. Schläfer and H. F. Wasgestan. *Theoret. Chim. Acta*, 1963, **1**, 369.
- 20 K. O. Hartman and F. A. Miller. *Spectrochim. Acta, Part A*, 1968, **24**, 669.